



NTNU – Trondheim
Norwegian University of
Science and Technology

Ultimate- and Fatigue Limit State Analysis of a Rigid Offshore Aquaculture Structure

Pål Takle Bore

Pål Alexander Fossan

Marine Technology

Submission date: June 2015

Supervisor: Jørgen Amdahl, IMT

Norwegian University of Science and Technology
Department of Marine Technology

Preface

The following work is a master's thesis in Marine Structures/Hydrodynamics at the Norwegian University of Science and Technology (NTNU) as part of the study program in Marine Technology. The project was carried out during the spring of 2015 as a cooperative effort between NTNU, the marine, offshore and engineering consultancy Global Maritime, and Ocean Farming, a subsidiary of SalMar ASA. The idea came as a result of the previous work done by Mads Fredrik Heiervang and Mats Foss Knutsen (now both Global Maritime) on time domain analyses of fish farms subjected to extreme environmental conditions. This report is confidential, and thus intended for people involved in the Ocean Farming project. However, at a later stage it should be interesting to anyone with extensive knowledge and interest concerning dynamic analysis, the aquaculture industry, and ocean engineering in general.

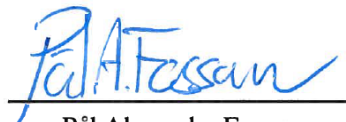
The basis of the thesis was established during the autumn of 2014 through a thorough investigation of the work done by Heiervang and Knutsen. A quick scope into the present state of fish farming, including various concepts, rules and regulations, as well as the challenges facing the industry today was reviewed. Theoretical aspects have been identified beforehand, and simple analysis models for fatigue damage estimation have been tested and verified. The work has been challenging, especially with regards to modelling the structure as correctly and updated as possible in accordance with structural drawings and current weight calculations, while still being able to compare with previous results from simulations and model tests. Ultimate limit state analyses have been based on only one sea state from the 100-year contour line. Fatigue limit state analyses have resulted in a parametric study of stress concentration factors based on a summation of total damage.

Hopefully, by our work, we are able to provide the fish farming industry with new technical insight and help it further out of the shadow from the dominant Norwegian petroleum industry.

Trondheim, June 10, 2015



Pål Takle Bore



Pål Alexander Fossan

Acknowledgements

This work has been carried out under the supervision of Professor Jørgen Amdahl at the Center of Autonomous Marine Operations and Systems (AMOS) and Department of Marine Technology, Norwegian University of Science and Technology. We would like to thank him for his excellent supervision during this study. This work would not have been possible without his continuous guidance, suggestions and motivation, which are most appreciated. Roy Andre Erland, our contact at Global Maritime, also belongs here in the first paragraph due to his more than helpfulness whenever needed.

Gunnar Myrebøe and Arvid Kjønny Hammernes of Ocean Farming have shown their interest in our project and provided us with overall information regarding their concept and possible problems to be addressed. Mads Fredrik Heiervang, and Ole Gunnar Helgøy of Global Maritime have been kind enough to share in their knowledge and data, thus helping us more than we had hoped for. Technical support in USFOS and accompanying software modules from Tore Holmås have also proved invaluable.

Everyone mentioned above have our gratitude.

P.T.B. & P.A.F.

Summary

Ultimate- and fatigue limit state analyses of Ocean Farming’s rigid offshore aquaculture structure have been simulated in USFOS. The cage has been modelled as updated as possible according to current structural drawings and weight calculations provided by Global Maritime, the company in charge of engineering on the project. During the modelling, sound engineering judgement have been critical in order to best represent the real physics while still end up with a well conditioned analysis. That is, choice of element types, modelling of mooring lines, partial filling in pontoons, scaling of the net structure, hydrodynamic properties, damping, as well as distribution of mass from on-board equipment had to be considered.

ULS simulations have been run with waves and current coming from 7 directions inside a quadrant of the model. For each direction, 400 second simulations of 40 seeds on 1.-3. highest waves were performed with a characteristic sea state obtained from the 100-year contour line. Element utilization have been checked according to API-WSD and plotted on a Gumbel probability paper for each direction. By calculating the Gumbel parameters based on the sample, a 90 percent fractile for the highest utilization is as listed in the table below.

| Utilization | Dir 270 | Dir 285 | Dir 300 | Dir 315 | Dir 330 | Dir 345 | Dir 360 |
|-------------|---------|---------|---------|---------|---------|---------|---------|
| $x_{0.9}$ | 0.77 | 0.78 | 0.81 | 0.82 | 0.81 | 0.78 | 0.77 |

All major load effects seems to be properly accounted for. The results from the ULS analyses shows that the Ocean Farming concept is properly designed with respect to structural design criteria and within the requirements in the API-WSD standard. Further verification is however needed on full sea states along the full contour line.

FLS simulations have been run with waves coming from 8 directions around the rig. For each direction, 15 different sea state simulations of 1 hour are run based on blocks in the original scatter diagram, measured and simulated by FUGRO OCEANOR. Total damage for all sea states are summed up and weighted based on directional probability in Frohavet. Lifetime damages have been obtained by assuming a lifetime of 25 years. A parametric study of SCF values on critical members have resulted in the table shown below, where the top three damaged elements are included. SCF_{max} is the limiting value resulting in a Miner sum equal to 1.

| Element | Location | D_{life} | SCF_{max} |
|---------|----------|------------|-------------|
| 154 | CPOS3 | 6.13E-04 | 4.39 |
| 156 | CPOS3 | 3.50E-05 | 4.91 |
| 162 | CPOS3 | 2.31E-04 | 5.34 |

FLS analyses have been performed with some simplifications, introducing uncertainties, and thus affecting the validity of the results. It is in general the intersections between the bottom radial beams and the vertical columns that are most critical with respect to fatigue. Limiting SCFs are within typical values for tubular joints.

Sammendrag (Norwegian)

Bruddgrense- (ULS) og utmattingsgrensetilstand (FLS) har blitt undersøkt på Ocean Farmings eksponerte oppdrettsanlegg. Det ikke-lineære elementprogrammet USFOS har blitt brukt til dette formål. Modellering av merden har hatt som hovedmål å være så oppdatert og korrekt som mulig i henhold til strukturtegnninger og vektregnskap fra Global Maritime, selskapet ansvarlig for ingeniørarbeidet på prosjektet. Modellen skal i tillegg til å ikke være for tung og kjøre, ta hensyn til den reelle fysikken i problemet. En betydelig mengde arbeid har blitt lagt ned i modelleringen for å implementere både ankerliner, skalert nett, reelle hydrodynamiske koeffisienter og demping, delvis fylte pongtonger, samt fordelt masse og dekkslast fra utstyr ombord.

Bruddgrensetilstand har blitt simulert med innkommende bølger og strøm fra 7 retninger innen en kvadrant av modellen. For hver retning, simuleringer på 400 sekunder av den 1.-3. høyeste bølgen har blitt utført. Den valgte sjøtilstanden i ULS er hentet fra 100-års konturen. Utnyttelsen for hvert element har blitt sjekket i henhold til API-WSD for så å plottes på et Gumbel sannsynlighets-papir for hver retning. Ved å finne Gumbel parameterne basert på dette utvalget, har en 90 prosent fraktil for den høyeste utnyttelsen blitt funnet og er listet i tabellen under.

| Utnyttelse | Ret 270 | Ret 285 | Ret 300 | Ret 315 | Ret 330 | Ret 345 | Ret 360 |
|------------|---------|---------|---------|---------|---------|---------|---------|
| $x_{0,9}$ | 0.77 | 0.78 | 0.81 | 0.82 | 0.81 | 0.78 | 0.77 |

Vi har etter beste evne tatt høyde for alle relevante effekter som påvirker anleggets respons. Resultatene viser at Ocean Farmings oppdrettsanlegg er tilstrekkelig designet med tanke på strukturell integritet i henhold til API-WSD standarden. Videre verifikasjon er imidlertid nødvendig, spesielt med tanke på fulle 3-timers simuleringer langs hele konturlinjen, da den vi har sjekket ikke nødvendigvis viser seg å være den verste.

Utmattingsgrensetilstand har blitt sjekket ved å simulere innkommende bølger fra 8 retninger rundt merden. 15 forskjellige sjøtilstander er simulert i 1 time for hver retning basert på blokker i det originale spredningsdiagrammet, målt og simulert av FUGRO OCEANOR. Total skade fra alle sjøtilstandene er summert opp og vektet i henhold til den gitte sannsynligheten for at bølgene kommer fra denne retningen. Total skade er basert på en design livstid på 25 år. Et parameterstudie på stress konsentrasjonsfaktorer av kritiske elementer har resultert i tabellen under. De tre mest utsatte elementene er her oppgitt sammen med total skade og den begrensende konsentrasjonsfaktoren, SCF_{max} , som resulterer i en Miner sum lik 1.

| Element | Posisjon | D_{life} | SCF_{max} |
|---------|----------|------------|-------------|
| 154 | CPOS3 | 6.13E-04 | 4.39 |
| 156 | CPOS3 | 3.50E-05 | 4.91 |
| 162 | CPOS3 | 2.31E-04 | 5.34 |

Utmattingsanalyser har blitt utført med diverse forenklinger som introduserer usikkerheter. De begrensende faktorene er innenfor typiske verdier for rørknutepunkt.

Table of Contents

| | |
|--|--------------|
| Preface | i |
| Acknowledgements | iii |
| Summary | v |
| Sammendrag (Norwegian) | vii |
| Table of Contents | xi |
| List of Tables | xiv |
| List of Figures | xviii |
| Nomenclature | xix |
| 1 Introduction | 1 |
| 1.1 The State of Norwegian Aquaculture | 2 |
| 1.2 Challenges in the Conventional Industry | 6 |
| 1.3 Rules and Regulations | 9 |
| 1.4 The Ocean Farming Concept | 10 |
| 1.5 Problem Definition | 12 |
| 1.6 Outline of the Thesis | 12 |
| 2 Literature Review | 15 |
| 2.1 Fish Farms Subjected to Extreme Environmental Conditions | 15 |
| 2.2 Offshore Cage Design | 16 |
| 2.3 Previous Work on Analysis of Fish Farms | 17 |
| 2.3.1 Current Forces on the Net Structure | 17 |
| 2.4 Fatigue in Offshore Structures | 19 |

| | | |
|----------|--|------------|
| 3 | Primary Theoretical Background | 21 |
| 3.1 | Methods to Calculate the ULS Characteristic Loads and Load Effects . . . | 21 |
| 3.1.1 | Long Term Distribution of Sea States | 22 |
| 3.1.2 | Stochastic Analysis | 25 |
| 3.1.3 | Design Wave Analysis | 28 |
| 3.1.4 | Regular Wave Analysis | 28 |
| 3.2 | Fatigue of Welded Structures | 29 |
| 3.2.1 | Cumulative Damage | 30 |
| 3.2.2 | Fatigue of Tubular Joints | 32 |
| 4 | Modelling and Theoretical Justification | 41 |
| 4.1 | Overview of the Ocean Farming Concept | 41 |
| 4.1.1 | Description of the Design | 43 |
| 4.2 | Wave and Current Loading | 45 |
| 4.2.1 | Determination of Drag and Inertia Coefficients | 47 |
| 4.3 | Important Modelling Considerations | 51 |
| 4.3.1 | Choice of Element Types | 52 |
| 4.3.2 | The Hull Structure | 53 |
| 4.3.3 | The Mooring Lines | 56 |
| 4.3.4 | The Cage Net | 60 |
| 4.3.5 | Hydrodynamic and Structural Damping | 66 |
| 4.3.6 | Distributed and Applied Mass | 69 |
| 4.4 | Model Comparison | 71 |
| 4.5 | Natural Periods | 72 |
| 5 | Limit State Analyses | 77 |
| 5.1 | Ultimate Limit State | 77 |
| 5.1.1 | ULS: Environmental Conditions | 78 |
| 5.1.2 | ULS: Analysis Set-Up | 81 |
| 5.1.3 | Ultimate Limit State Results | 83 |
| 5.2 | Fatigue Limit State | 86 |
| 5.2.1 | FLS: Environmental Conditions | 88 |
| 5.2.2 | FLS: Analysis Set-Up and S-N Curve | 91 |
| 5.2.3 | Fatigue Limit State Results | 97 |
| 6 | Qualitative Comparison and Final Remarks | 101 |
| 6.1 | ULS: Results and Comparison | 101 |
| 6.1.1 | Concluding Remarks | 102 |
| 6.2 | FLS: Results and Discussion | 103 |
| 6.2.1 | Concluding Remarks | 107 |
| 6.3 | Suggestions to Further Work | 108 |
| | References | 111 |
| | Appendix | 115 |
| A | List of Acronyms | 115 |

| | | |
|---|---|-----|
| B | Master Thesis Problem Text | 117 |
| C | Convergence Studies | 121 |
| D | Omitted Results | 125 |
| E | Miscellaneous Figures | 129 |
| F | Source Codes and Script Files | 131 |
| | F.1 Pre-Processing | 131 |
| | F.2 Scripted Analysis | 168 |
| | F.3 Post-Processing | 180 |

List of Tables

| | | |
|------|---|----|
| 3.1 | Combination of environmental actions with expected mean values and annual probability of exceedance 10^{-2} . [46] | 22 |
| 4.1 | The main dimensions of the Ocean Farming concept taken from structural drawings. (Global Maritime [21]) | 44 |
| 4.2 | Proposed values for drag and inertia coefficients for North Sea conditions. [46] | 50 |
| 4.3 | Chosen values of drag and inertia coefficients for the main hull structure on the model, for the rigid fish farm case, all members are considered rough. | 51 |
| 4.4 | Material data chosen for the hull structure elements. | 53 |
| 4.5 | A complete list of dimensions of the structural parts on the hull in our model. | 55 |
| 4.6 | Miscellaneous properties of the mooring lines, supplied by Global Maritime. | 57 |
| 4.7 | Calculated and chosen properties of the modelled mooring lines. | 58 |
| 4.8 | Chosen drag and inertia coefficients for the mooring lines. | 60 |
| 4.9 | EcoNet mesh sizes, with reference to Fig. 4.15. | 61 |
| 4.10 | Modelled properties of the net panels and the net elements. | 66 |
| 4.11 | Directional dependent drag coefficients assigned to the net elements, the coefficients are symmetric about the net panel plane, and α is defined according to Fig. 4.19. | 66 |
| 4.12 | Selected damping levels and proportional damping coefficients used in the analyses. | 68 |
| 4.13 | Weighted elements and their associated nodal masses in the model, based on weight calculations from Global Maritime. | 70 |
| 4.14 | Important parameters related to the mass of the model compared to values from Global Maritime, mooring lines are not included. | 71 |
| 4.15 | Filling ratios in the pontoons compared to values from Global Maritime, designated names are in reference to structural drawings. [21] | 71 |
| 4.16 | Natural periods for the USFOS model with drag and inertia coefficient values as in ULS and FLS, all values are given in seconds. | 73 |

| | | |
|------|---|-----|
| 4.17 | Natural periods of our USFOS model compared to the MARINTEK experiments, all values are given in seconds. | 74 |
| 5.1 | Characteristics of the environmental conditions used in our ULS analyses. | 80 |
| 5.2 | Number of highest utilizations occurring in the given wave order. | 83 |
| 5.3 | Obtained Gumbel parameters and ULS results for all directions. | 86 |
| 5.4 | The 15 sea states to be used in the fatigue analysis, including their probability of occurrence. | 92 |
| 5.5 | Sorted list of the 10 most critical elements in the fatigue analysis. | 98 |
| 6.1 | Characteristic 100-year extreme API-WSD utilizations obtained in the ULS analysis. | 103 |
| 6.2 | Smallest obtained limiting stress concentration factors, including location and calculated lifetime fatigue damage, reference is made to Fig. 5.18. . . | 108 |
| C.1 | The parameters combined for convergence study of the solution procedure. | 121 |

List of Figures

| | | |
|------|---|----|
| 1.1 | A concept illustration of Ocean Farming’s rigid offshore fish farm seen in relatively calm waters accompanied by a wellboat. (Illustration by SalMar/Ocean Farming) | 2 |
| 1.2 | Grow-out production of Atlantic salmon, both quantity and first-hand value for the years 1998-2013. (Directorate of Fisheries [10]) | 3 |
| 1.3 | Total sale of fish from the Norwegian aquaculture industry, both quantity and first-hand value for the years 1998-2013. (Directorate of Fisheries [10]) | 4 |
| 1.4 | Potential for value generation in the marine sector up to the year 2050. Especially of interest is the light-blue segment indicating aquaculture and salmon production, and the grey segment indicating the fish feed and vendor industry. [49] | 4 |
| 1.5 | Several clearly visible salmon louse around the fin of a fish. (Norges Jeger og Fiskerforbund) | 5 |
| 1.6 | Use of veterinary drugs (hydrogen peroxide) in the Norwegian fish farming industry for the years 2009-2013. (Norwegian Institute of Public Health [10]) | 6 |
| 1.7 | A tugboat in the process of saving an aquaculture installation from the pebble after the storm ”Nina” caused failure in the mooring lines, leading the rig adrift in January 2015. (Gunn Berit Wiik Berg, Avisen Strilen) . . | 7 |
| 1.8 | The reported numbers of escaped salmon, both edible and hatchery-produced for the years 2001-2014. (Directorate of Fisheries [10]) | 7 |
| 1.9 | The superstructure of two circular plastic collar fish farms in the Bergen (Norway) area with two workers along the footbridge. (Heiko Junge, Scapix) | 8 |
| 1.10 | A picture taken from the inside of the ”Neptun” concept during construction. The concept is developed by AquaFarm Equipment AS and is seen as an escape-proof solution. (www.aquafarm.no) | 11 |
| 1.11 | A map indicating the location of Frohavet, an area north-west of Trondheim (Norway) more exposed than a conventional aquaculture location, although not entirely ”offshore”. (www.norgeskart.no) | 11 |

| | | |
|------|--|----|
| 3.1 | 10 ($q = 0.1$), 100 ($q = 0.01$) and 10 000 ($q = 0.0001$) year contour lines in the standard Gaussian space from hindcast data on Haltenbanken. [8] | 25 |
| 3.2 | Contour lines in the physical space together with the accompanying hindcast data points from Haltenbanken. [8] | 26 |
| 3.3 | An arbitrary visual example of a S-N curve, Eq. (3.7). | 30 |
| 3.4 | Positional and name definitions on common tubular joints. (DNVGL-RP-0005 [15]) | 33 |
| 3.5 | Definition of hot-spots around the weld connection to be used in superposition of stresses. (DNVGL-RP-0005 [15]) | 35 |
| 3.6 | Linear extrapolation to determine the hot spot stress, based on figure in [16]. | 36 |
| 3.7 | Segments around weld connection for read-out of stresses to be used in derivation of hot spot stress in tubular joints. (DNVGL-RP-0005 [15]) | 37 |
| 3.8 | Crack growth development in both a tubular joint and a planar joint, based on figure in [16]. | 39 |
| | | |
| 4.1 | A graphical representation of the inertia dominated region meant for illustrative purposes only. | 42 |
| 4.2 | An illustration of the concept both in transit (upper) and operation (lower). (Illustration by SalMar/Ocean Farming) | 43 |
| 4.3 | The main dimensions of the Ocean Farming concept illustrated by a cut-out of the general arrangement. (Global Maritime [21]) | 44 |
| 4.4 | Relative importance of mass, viscous drag and diffraction forces on marine structures, based on figure in [18]. | 45 |
| 4.5 | Drag coefficients for a fixed circular cylinder for steady flow in the critical flow regime, for various roughnesses. (DNV-RP-C205 [14]) | 48 |
| 4.6 | Wake amplification factor ψ as a function of KC-number for a smooth ($C_{DS} = 0.65$ - solid line) and rough ($C_{DS} = 1.05$ - dotted line) cylinder. (DNV-RP-C205 [14]) | 49 |
| 4.7 | Added mass coefficient as a function of KC-number for a smooth (solid line) and rough (dotted line) cylinder. (DNV-RP-C205 [14]) | 50 |
| 4.8 | The standard three-dimensional beam element. (USFOS User's Manual [57]) | 52 |
| 4.9 | A screenshot of the model (only the hull) from USFOS's graphical user interface. | 54 |
| 4.10 | Illustration of varying pipe thickness on the hull along various members at an intersection. | 55 |
| 4.11 | The movable bulkhead, modelled as two square non-structural members, is marked with arrows. | 56 |
| 4.12 | An illustration of the difference between a catenary- and a taut leg mooring systems. (Vryhof Anchors [59]) | 57 |
| 4.13 | Comparison between our resulting "pull-up" analysis and catenary profile supplied by Global Maritime. | 59 |
| 4.14 | All 8 resulting mooring lines combined. | 59 |
| 4.15 | Illustration and dimensional explanation of one single mesh in the EcoNet. (www.akvagroup.com) | 61 |
| 4.16 | Illustration of solidity ratio parameters for a square screen/mesh. | 63 |

| | | |
|------|--|-----|
| 4.17 | A screenshot of our modelled net attached to the hull structure. | 63 |
| 4.18 | Illustration of the local coordinate system and the local angle definition, θ , used in USFOS. The local z-axis is defined in the direction of the net panel normal vector, \vec{n} , based on figure in [57]. | 65 |
| 4.19 | Definition of angle of attack, α , for a plane net structure. To obtain correct drag forces, different definitions of α for vertical and horizontal elements must be introduced, based on figure in [20]. | 65 |
| 4.20 | Directional dependent drag coefficients as it appears in USFOS, red indicates maximum drag while blue indicates minimum drag. | 67 |
| 4.21 | Chosen values of proportional damping for the structure and mooring lines used in the analyses are marked as points on the lines. | 69 |
| 4.22 | Plot of the heave motion of the fish farm during a heave decay simulation. | 73 |
| 4.23 | A screenshot taken from USFOS GUI during an ULS analysis, this is the resulting model. | 75 |
| | | |
| 5.1 | Illustration of how an analysis using the SpoolWave option is carried out in USFOS. (USFOS User's Manual [58]) | 78 |
| 5.2 | The 100-year environmental contour line estimated by Global Maritime. | 79 |
| 5.3 | Wave and current directions used in the ULS analyses. | 81 |
| 5.4 | Gumbel probability paper for direction 300. | 84 |
| 5.5 | Gumbel probability paper for direction 315. | 85 |
| 5.6 | Gumbel probability paper for direction 330. | 85 |
| 5.7 | Most utilized members in ULS analyses. | 86 |
| 5.8 | Clock-positions considered in the fatigue analysis, based on figure in [15]. | 88 |
| 5.9 | Numbering of the target positions, the red dots indicate the 20 considered locations, due to wave height limitations, only the locations to the left of the blue line are feasible as final locations. (FUGRO OCEANOR) | 89 |
| 5.10 | The modified scatter diagram, dark-blue figures are chosen values, while light-blue figures are values which they are based on. | 90 |
| 5.11 | The directional probability at location. | 93 |
| 5.12 | Fatigue checked elements is seen highlighted in the total model. | 93 |
| 5.13 | Numbering of the checked elements. | 94 |
| 5.14 | Design S-N curves in DNVGL-RP-0005, showing the transition from in-air to sea water conditions, based on figure in [15]. | 95 |
| 5.15 | Obtained stress in the most utilized element, the plotted stress is taken as the real output minus the mean. | 95 |
| 5.16 | Total damage summed up for all directions and sea states. | 97 |
| 5.17 | The limiting SCF values for 25 years lifetime. | 98 |
| 5.18 | Top ten most damaged elements in the complete model along with directional definitions to be seen in connection with Fig. 5.11. | 99 |
| | | |
| 6.1 | Utilizations found by Heiervang and Knutsen at the direction corresponding to our direction 315, but for an other quadrant (dir 225). [24] | 103 |
| 6.2 | Gumbel probability paper for direction 315. | 104 |
| 6.3 | Fatigue design factors from NORSOK N-004. [47] | 105 |

| | | |
|------|--|-----|
| C.1 | Convergence study related to the Liter command, results are presented in the form of displacement of node 2543 in the y-direction. | 122 |
| C.2 | Convergence study related to the Liter command, results are presented in the form of axial force in element 7757. | 122 |
| C.3 | Convergence study related to the Liter command, results are presented in the form of axial force in element 198. | 123 |
| C.4 | Convergence study related to the Liter command, results are presented in the form of bending moment in element 198. | 123 |
| D.5 | Gumbel probability paper for direction 270. | 125 |
| D.6 | Gumbel probability paper for direction 285. | 126 |
| D.7 | Gumbel probability paper for direction 345. | 126 |
| D.8 | Gumbel probability paper for direction 360. | 127 |
| D.9 | The original scatter diagram measured and simulated on location. | 127 |
| E.10 | Top view of the main deck, note the column names. (Global Maritime [21]) | 129 |
| E.11 | Screenshot of connection 7, 8, and 9, element numbers are in blue and node numbers are in red. | 130 |
| F.12 | A schematic flowchart of the preprocessor used to make the USFOS model file, .m denotes MATLAB-script file, and .fem denotes USFOS input/output. | 131 |
| F.13 | A schematic flowchart of the bash-script used to run several ULS analyses on all threads available, the numbers before the modules assigns the sequence in which the modules is run. | 168 |
| F.14 | A schematic flowchart of the bash-script used to run several FLS analyses on all threads available. | 169 |

Nomenclature

| | |
|----------------------|--|
| α | Angle definition |
| α_1 | Rayleigh damping coefficient 1 |
| α_2 | Rayleigh damping coefficient 2 |
| β | Radius of contour circle in Gaussian space |
| $\ddot{\eta}$ | Normal component of cylinder acceleration |
| ΔK | Range of stress intensity |
| ΔS | Stress range |
| ΔS_0 | Maximum stress range |
| $\Delta S_{eq,real}$ | Real equivalent stress |
| ΔS_{eq} | Equivalent stress range |
| \dot{u}_w | Undisturbed water particle acceleration normal to the cylinder axis due to waves |
| Γ | The complete Gamma function |
| γ | Peak shape parameter (JONSWAP) |
| λ | Mesh size / Wave length |
| B | Damping matrix |
| C | Restoring matrix |
| F | Excitation force |
| M | Mass matrix |
| r | Displacement matrix |
| ν | Poisson's ratio |

| | |
|------------------|--|
| ω | Frequency |
| ω_p | Angular spectral peak frequency |
| $\bar{\lambda}$ | Reduced slenderness parameter |
| $\overline{T_Z}$ | Average zero-up-crossing period |
| \bar{x} | Mean value from sample |
| ϕ_m | Mean wave direction |
| ψ | Wake amplification factor |
| ρ | Density of material/fluid |
| σ | Spectral width parameter (JONSWAP) |
| σ_x | Maximum nominal stress due to axial load |
| σ_y | Yield strength/stress |
| σ_e | Elastic buckling stress / Euler stress |
| σ_{my} | Maximum nominal stress due to in-plane bending |
| σ_{mz} | Maximum nominal stress due to out-of-plane bending |
| θ | Angle definition in USFOS |
| \vec{n} | Net panel normal vector |
| $\hat{\alpha}$ | Gumbel distribution location parameter |
| $\hat{\beta}$ | Gumbel distribution scale parameter |
| A | Area of net panel / Sectional area of member |
| a | Crack length / Amplitude of loading |
| A_{ii} | Diagonal added mass terms |
| C_A | Added mass coefficient |
| C_D | Drag coefficient |
| C_L | Lift coefficient |
| C_M | Inertia coefficient |
| $C_{D,panel}$ | Drag coefficient of the whole net panel |
| C_{DS} | Steady flow drag coefficient |
| C_{ii} | Diagonal restoring terms |
| D | Member diameter / Fatigue damage |
| D_{life} | Lifetime fatigue damage |

| | |
|----------------------------|--|
| E | Modulus of elasticity |
| F | Form function |
| $F_{D,panel}$ | Mean drag forces on a net panel |
| $F_{H_S}(h_s)$ | Cumulative distribution of H_S |
| $f_{H_S T_P}(h_s, t_p)$ | Joint density function of H_S and T_P |
| $f_{H_S}(h_s)$ | Probability density function of H_S |
| $F_{T_P}(t_p h_s)$ | Cumulative conditional probability distribution of $T_P H_S$ |
| $f_{T_P}(t_p h_s)$ | Conditional probability distribution of $T_P H_S$ |
| $F_{X_{3h}}(x h_s, t_p)$ | Short term distribution of X_{3h} |
| $F_{X_{3h}}(x)$ | Long term distribution of 3 hour maximum response |
| h | Weibull shape parameter |
| H_S | Significant wave height |
| $H_{S,100}$ | 100-year value for significant wave height |
| I | Moment of inertia |
| K | Buckling factor |
| k | Roughness height |
| KC | Keulegan-Carpenter number |
| L | Length of member |
| m | S-N curve negative inverse slope parameter |
| M_{ii} | Diagonal inertia/mass terms |
| N | Number of cycles to failure |
| n_0 | Total number of load cycles |
| P_b | Probability of occurrence |
| q | Annual exceedance probability |
| R | Radius of chord |
| r | Radius of brace / Velocity reduction factor |
| Re | Reynold's number |
| s | Standard deviation from sample |
| $S(\omega)$ | Wave spectrum |
| SCF_{AC} | SCF at crown for axial load |

| | |
|------------------|---|
| SCF_{AS} | SCF at saddle for axial load |
| SCF_{max} | Calculated limiting stress concentration factor |
| SCF_{MIP} | SCF for in-plane moment |
| SCF_{MOP} | SCF for out-of-plane moment |
| SCF_{real} | Real stress concentration factor |
| S_n | Solidity ratio |
| $S_{n_{bottom}}$ | Solidity ratio for the modelled bottom net |
| $S_{n_{model}}$ | Solidity ratio for the modelled net |
| $S_{n_{real}}$ | Solidity ratio for the real net |
| $S_{n_{side}}$ | Solidity ratio for the modelled side net |
| T | Thickness of chord / Wave period |
| t | Thickness of brace |
| T_P | Spectral peak period |
| T_Z | Zero-up-crossing period |
| T_{m02} | Zero-up-crossing period |
| T_{ni} | Natural period in degree of freedom i |
| U | Current velocity |
| u | Local current velocity |
| U_C | Current velocity |
| U_W | Maximum wave particle velocity |
| U_∞ | Undisturbed current velocity |
| $U_{C,100}$ | 100-year current velocity |
| u_r | Water particle velocity due to waves and current relative to the cylinder normal to the cylinder axis |
| $x_{0.9}$ | Estimated utilization at 90 percent fractile |

Chapter 1

Introduction

Marine fish farming is in rapid development. Dimensions are expected to increase, and locations are being moved to areas exposed to more energetic waves and stronger currents. This leads to several challenges. Strong currents can cause large net deformations and affect largely the hydroelastic behaviour of the cage. Wave overtopping may occur in extreme waves, so nonlinear effects come into play. Viscous effects are essential for the loading of the net structure, as well as the wake inside the cage. Another issue is the effect of biofouling¹ on the net loading. Waves and currents are of concern for the volume within the fish cage and the design of mooring lines. Operations with a wellboat² moored to the fish farm may become challenging. For example we may have a case where the ship propeller can suck the net, partially breaking it and cause fish escape. Collapse of fish farms, with large scale fish escape to the level experienced in the past, will not be tolerated by the society. New and extreme loading scenarios need to be properly designed for by means of "first principles" methods to meet required safety levels and performance.

Rational design requirements for aquaculture structures must be developed based on simulation of the governing physical phenomena, structural load effects, and structural resistance. That is, the motion of the fish farm in irregular sea states must be simulated along with an accurate assessment of load effects in the load carrying structure. This report looks into one of the promising designs intended to more or less solve many of the challenges facing the industry today. The concept is developed by Ocean Farming, a subsidiary of the Norwegian company SalMar ASA, one of the world's largest and most efficient producers of farmed salmon. A thorough description of the concept will follow in later chapters, but a brief teaser is given in **Fig. 1.1**. This type of rigid steel fish farm is characterized by small water plane area, which implies low natural frequencies in heave, pitch and roll. Buoyancy are mainly obtained from submerged pontoons. The deeply submerged pontoons also makes the structure less exposed to wave excitation loads. Knowledge and

¹accumulation of organisms on wetted surfaces

²live fish carrier

experience from offshore engineering and the oil industry have been utilized in the development of this concept. The focus of our work have been on modelling the structure as correctly as possible according to structural drawings and present weight calculations, conduct extreme response and fatigue limit state analyses, and compare these to previous results from Heiervang and Knutsen [24], Global Maritime, and model experiments carried out by MARINTEK. The concept is still a work in progress, our comparison will therefore be of a qualitative nature due to the continuous change in design.

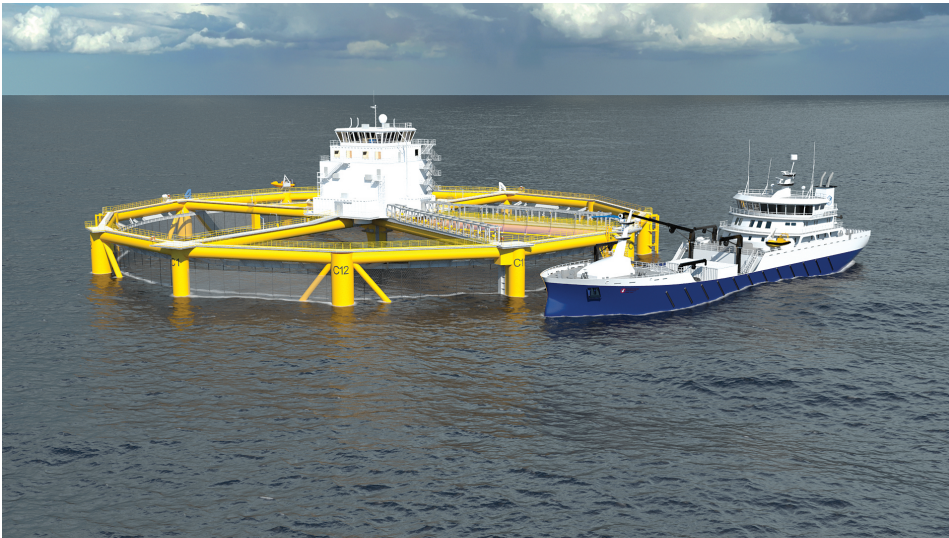


Figure 1.1: A concept illustration of Ocean Farming's rigid offshore fish farm seen in relatively calm waters accompanied by a wellboat. (Illustration by SalMar/Ocean Farming)

1.1 The State of Norwegian Aquaculture

We define aquaculture as the propagation and rearing of freshwater and saltwater organisms in controlled or selected environments. In 2014, the Food and Agriculture Organization of the United Nations (FAO) stated in a comprehensive report on the state of world fisheries and aquaculture, that aquaculture is today the fastest growing form of food production in the world, and global fish production continues to outpace world population growth [19]. If responsibly developed and practised, aquaculture can generate lasting benefits for global food security and economic growth. The produced amounts of especially Atlantic salmon³, the by far most dominant breed in Norwegian fish farming, have had an explosive growth during the last three decades. The growth during the last 15 years can be seen in **Fig. 1.2**. In 2013, the first-hand value of Norwegian fish farming products reached NOK 40 billion, up 35 percent from 2012 according to Statistics Norway [55]. At the same time, the produced quantity was 1.25 million tonnes. The overall development

³Salmo salar

in the industry over the years can be seen in **Fig. 1.3**. The growth is expected to continue, influencing all subgroups involved in the aquaculture industry, ranging from producers of fish feed, to equipment vendors and wellboat operating shipping companies. From the report *Value created from productive oceans in 2050*, prepared in 2012 by a specialist group appointed by the Royal Norwegian Society of Sciences and Letters (DKNVS) and the Norwegian Academy of Technological Sciences (NTVA), **Fig. 1.4** emerged as a summary. This particular figure is frequently present in reports and on conferences where the theme is the future of the aquaculture industry. The figure is unfortunately in Norwegian, seeing as it is taken from the original report [49], but the expected growth is unmistakably visible.

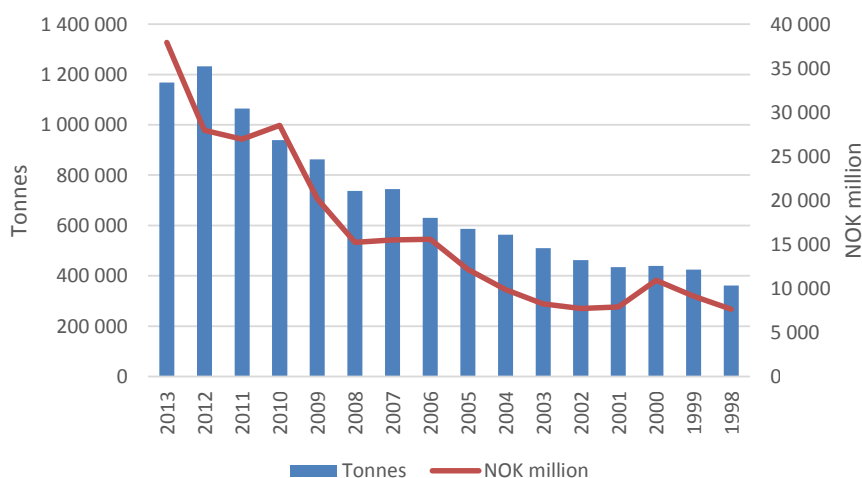


Figure 1.2: Grow-out production of Atlantic salmon, both quantity and first-hand value for the years 1998-2013. (Directorate of Fisheries [10])

The expansive growth of fish farming has led to a lack of new available locations in sheltered waters. It is becoming increasingly difficult to find new mariculture locations without interfering with intended chartered ship traffic routes. Hence, there is a trend that fish farms are installed at more and more exposed locations. Another option would be to convert the industry to a more land-based production. The belief is that at least early in the production phase, alevin⁴ can be grown on land to an adequate size before being moved to a floating facility, thereby decreasing the exposure time to lice, a well known and growing challenge in the industry. Another advantage to land-based production is the possibility of cleansing the water, which is sure to be beneficial in regards to fish health. The land-based option is however not within the scope of this work, and will not be discussed further here. Expansion of the Norwegian fish farming industry has been accompanied by a recent increase in incidents of escapes of various severity and the growing problem of salmon lice⁵, seen in multiple numbers near the fin of a fish in **Fig. 1.5**. Escaped farmed fish

⁴juvenile salmon

⁵*Lepeophtheirus salmonis*

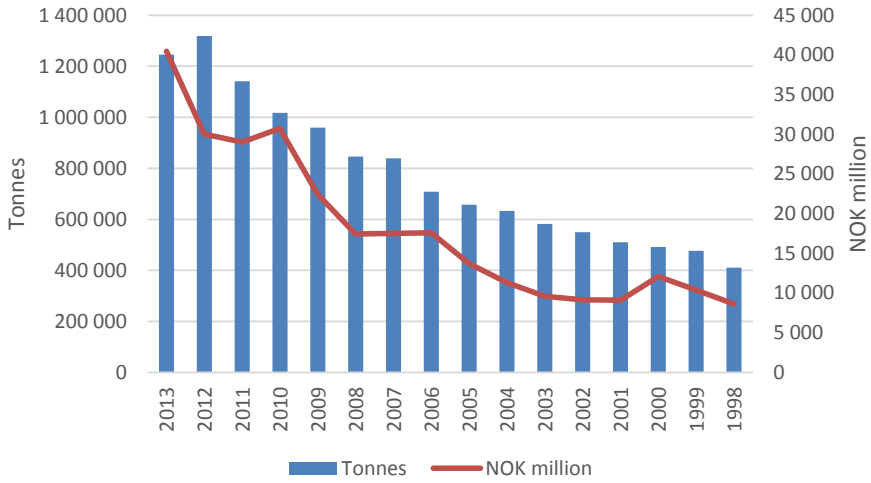


Figure 1.3: Total sale of fish from the Norwegian aquaculture industry, both quantity and first-hand value for the years 1998-2013. (Directorate of Fisheries [10])

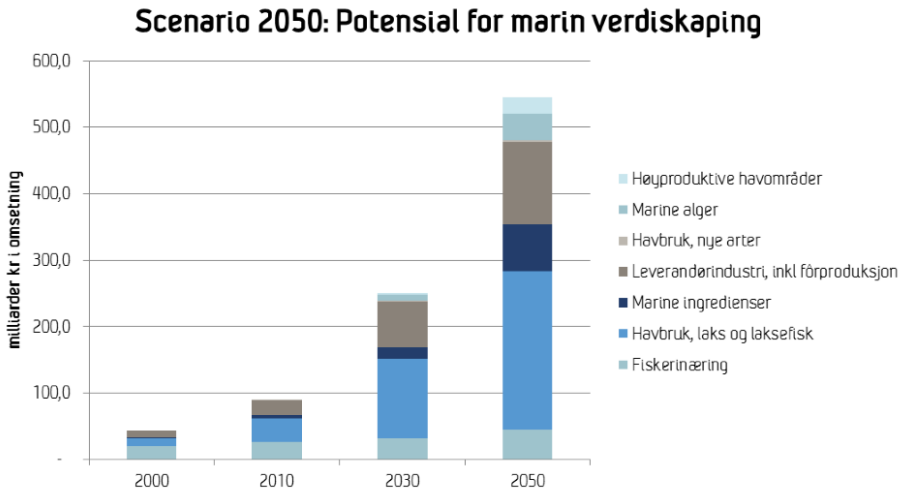


Figure 1.4: Potential for value generation in the marine sector up to the year 2050. Especially of interest is the light-blue segment indicating aquaculture and salmon production, and the grey segment indicating the fish feed and vendor industry. [49]

are considered harmful for the environment, mainly due to the danger of genetic pollution in the wild population that follows from breeding between the farmed and the wild fish that have spent centuries adapting to specific habitats. Salmon lice, a collective term for

parasitic copepods⁶, is a natural player in the ocean environment. Eggs from adult females are released directly into the water mass where they gradually hatch and begin their search for a host. Eggs can travel vast distances, up to several kilometres with the ocean current. The lice will in most cases inflict small, but serious wounds on the fish, causing infections and giving the host trouble with the salt-balance. The number of lice in the fjords will increase with an increasing number of hosts, here farmed salmon. A large concentration of lice in the fjords will be a problem for the wild salmon only present here at certain seasons, especially emigrating⁷ alevin, which have a lower tolerance to lice. Heavily infected wild salmon may return to the rivers earlier than normal, and it is believed that this reduced time in the open ocean will most likely reduce the salmon's potential for reproduction [53].

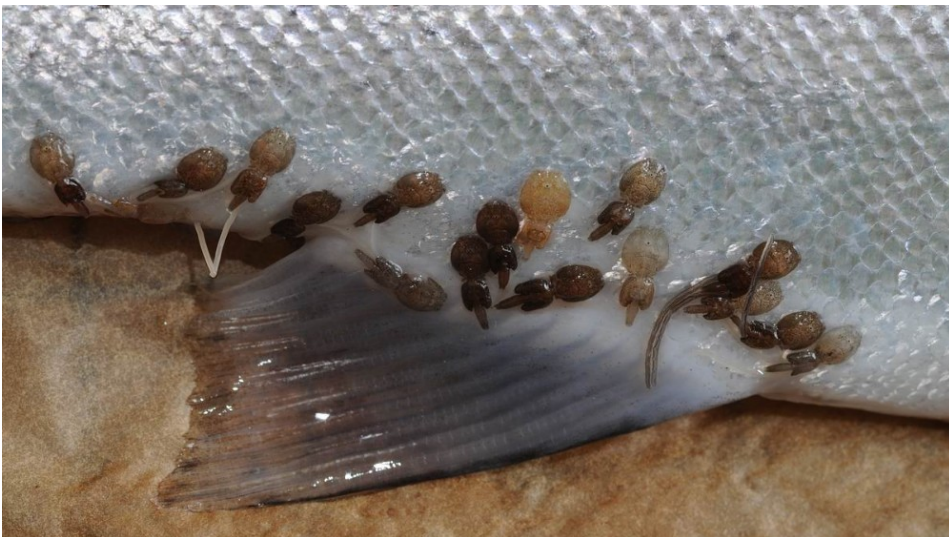


Figure 1.5: Several clearly visible salmon louse around the fin of a fish. (Norges Jeger og Fiskerforbund)

The most used "cure" for salmon lice is medication in the form of showering the fish with hydrogen peroxide. This form of treatment is however not without consequences. It is believed that the corrosive medication is harmful to the fish (The Norwegian Medicines Control Authority), and that the refuse that lands on the seabed below is damaging to the various shellfish like crabs and shrimps living in the proximity. It should be defined precisely that the danger to the shellfish is caused by nerve toxins like flubenzurons⁸ destroying the growth of shell in these species (The Norwegian Institute for Water Research). The rapidly increasing use of medication as seen in **Fig. 1.6**, have given new ammunition to the many environmental opponents of the fish farming industry. Other more ecologically friendly options than medical treatment are currently being investigated. Researchers have, and are currently working on the use of lumpfish⁹ as a sort of biological delousing

⁶ minute marine crustaceans

⁷ from hatching up-river

⁸ diflu- and teflubenzuron

⁹ *Cyclopterus lumpus*

agent. Studies have shown that lumpfish is a suitable cold-water option for delousing [25]. Other possible treatments include; mechanical removal of lice, fish feed dozed in medication, and introducing fallow intervals in the farms after slaughter.

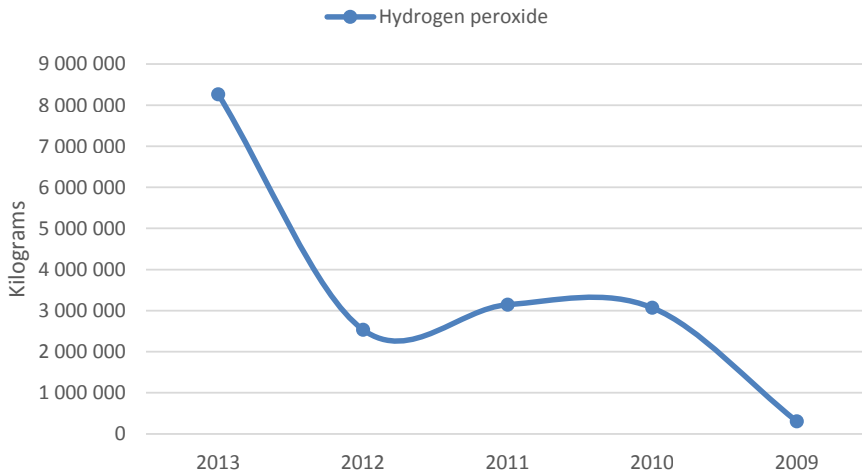


Figure 1.6: Use of veterinary drugs (hydrogen peroxide) in the Norwegian fish farming industry for the years 2009-2013. (Norwegian Institute of Public Health [10])

Exposed locations puts stronger demands on the fish farm structure’s ability to withstand the environmental loads. As many fish farmers have recently experienced, the North-Atlantic ocean has a rather harsh weather climate, especially in the winter season. In mid January 2015, the storm “Nina” hit the south-western part of Norway, causing large amounts of fish escapes in the Hordaland area. The Directorate of Fisheries reported that about 127 000 fish escaped as a consequence of net tearing and damage to the cage. **Fig. 1.7** shows a tugboat in the process of saving a fish farm belonging to Eide Fjordbruk that came adrift and nearly hit land as a results of the unusually strong winds causing mooring line failure during this storm. Although the fish farming industry in Norway has become more mature now since its beginning in the early 1980-ies, the problem of fish escape is still not resolved. The statistics on reported escaped salmon are shown in **Fig. 1.8**, there is in addition a high grade of dark figures not represented here, so the true number of escapes is believed to be significantly higher.

1.2 Challenges in the Conventional Industry

Open cage fish farms are the most common type of plants used for farming today. The open cage fish farm is characterized by a slender floating structure which forms circular or rectangular cages. Each cage is equipped with a net-pen, where sinkers are used to



Figure 1.7: A tugboat in the process of saving an aquaculture installation from the pebble after the storm "Nina" caused failure in the mooring lines, leading the rig adrift in January 2015. (Gunn Berit Wiik Berg, Avisen Strilen)

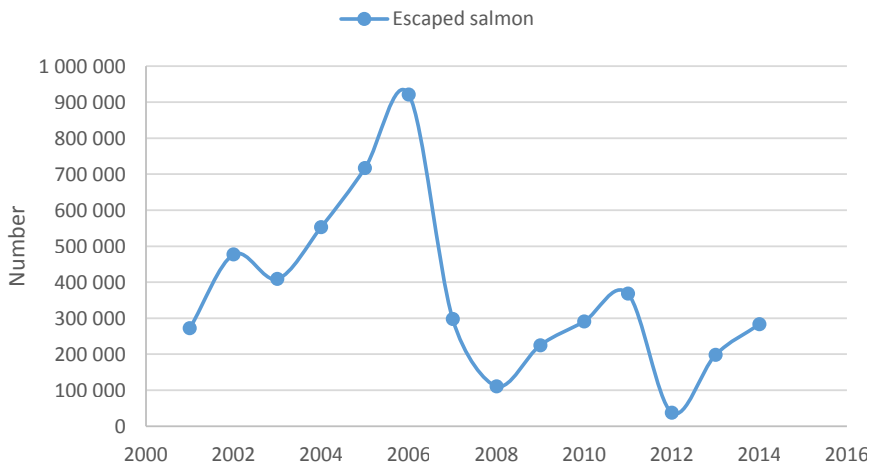


Figure 1.8: The reported numbers of escaped salmon, both edible and hatchery-produced for the years 2001-2014. (Directorate of Fisheries [10])

splay the net-cage. The buoyancy is obtained by distributed pontoons or by floating collars. A spread mooring system composed of a larger number of pre-tensioned mooring lines is used to keep the structure on its location. Other concepts like single point mooring

of plants have been tested, but rarely used. A fence facing the fish and a footbridge is mounted on the floating collar to enable workers to move around the net cage as seen in **Fig. 1.9**. Usually, open cage fish farms are equipped with a feeding system, often including a feeding barge. The structural design has been modified and improved during the years, often on the basis of trial and error. Today, fish farms structures are usually made of steel, aluminium, or high density polyethylene (HDPE) plastic. The circular plastic collar farm, a cheap and easy to install design, is today the most dominant concept in the Norwegian aquaculture industry. It is also possible to set up several cages in close proximity, increasing the operating margins by benefiting from economies of scale. Due to the flexibility and low stiffness of the floating collar and the closing net, disadvantages primarily relates to large motions and net deformations, giving raise to cage volume reductions, even for moderate weather. Full scale measurements performed by SINTEF Fisheries and Aquaculture on commercial farms showed that for a current velocity of 0.35 meters per second, a 40 percent cage volume reduction factor was observed. Substantial net deformation and cage volume reductions may have significant implications for both fish production and welfare [30]. This restricts the environmental conditions in which such fish farms can operate. Although the most common fish farm concepts used by the Norwegian fish farming industry is the circular plastic collar fish farm and the interconnected hinged steel fish farm, other mentionable concepts include; catamaran steel fish farm, rigid steel fish farm, and submersible fish farm.



Figure 1.9: The superstructure of two circular plastic collar fish farms in the Bergen (Norway) area with two workers along the footbridge. (Heiko Junge, Scanpix)

Besides the previously mentioned challenges related the continuously increasing problem with salmon lice, the problem with fish escapes can be seen in connection with the conventional structure's ability to withstand the extreme environmental loads that occur on a more severe and frequent basis. Damage are often caused by breaking of the mooring lines due to wave and current loads. A conventional rig have many mooring lines attached to ensure redundancy and station keeping. A single line break however may cause a redistribution of the mooring line forces, transient motions and a new equilibrium position. If all the lines should fail, the rig may come adrift, hitting the shore and tearing the net (which the farm in Fig. 1.7 came dangerously close to achieve). Fatigue from continuous wave

loading is another aspect to consider. This is a problem that arises in the joints of hinged or rigidly connected steel concepts where the members are more or less elastic (like the Ocean Farming design). Oscillations at higher natural frequencies are effectively damped by structural damping, so the lower natural frequencies are more important from a fatigue point of view, Kristiansen [28]. The concept of fatigue will be thoroughly discussed in section 3.2 in the theoretical part of this report, chapter 3. Heiervang and Knutsen [24] carried out extreme response analyses on a conventional circular plastic collar fish farm. The focus of their work was however more in terms of software utilization and correct modelling. Conventional farms are not the focus of our work, but the challenges with this solution are however important to discuss in order to understand the need for a paradigm shift in the aquaculture industry.

1.3 Rules and Regulations

Compared to the offshore industry, there are not nearly as many rules and regulations to follow when constructing a fish farm structure. This may be because there has not yet been any major accidents with structural failure and collapse leading to loss of human life. If one looks beyond occasional episodes of fish escape of varying scale, locations within sheltered waters seems fairly safe. The Norwegian Standard NS-9415 [48], introduced in 2003, is the overall recommended practice when it comes to marine fish farming. The purpose of this standard is to reduce the risk of fish escape following technical failure, misuse, and human errors. Although it provides some guidelines for design of the main components, the standard is somewhat inadequate from an engineering point of view.

With the industry moving towards harsher conditions, design and planning should be based on the well proven standards and practices from the offshore industry. The most relevant would be DNV-RP-C205 [14] concerning environmental conditions and loads, NORSOK regulations, especially N-001 [45] (integrity of offshore structures), N-003 [46] (actions and actions effects), and N-004 [47] (design of steel structures). Another important one is the NYTEK regulations [40]. RP-C205 gives guidance for modelling, analysis and prediction of environmental conditions as well as guidance for calculating environmental loads acting on structures. Originally indented for offshore oil and gas installations, it may also be used for offshore aquaculture structures since the environment can easily be compared and transformed. One must however recognize the difference between a structure intended for drilling and production of petroleum, and a structure containing a large mass of live fish within a permeable net.

NORSOK and NYTEK are legislative bodies by law. Regulations are governing and above recommended practices (RP) in the hierarchy. They are in place to ensure that the guidelines given in standards and recommended practices are followed. NORSOK is developed by the Norwegian petroleum industry and NYTEK is developed by the Norwegian Directorate of Fisheries, giving technical standards for floating aquaculture farms. All the above can be used when designing an offshore aquaculture structure, but since there are no clear set of rules for offshore farms like the one proposed by Ocean Farming, inspiration must be taken from other offshore industries. The structure must be within the governing regu-

lations, or new instructions must be established from cooperative efforts of the government and the industry.

1.4 The Ocean Farming Concept

Nearly all cages in use can be classified as "gravity" type cages according to the classification scheme proposed by Loverich and Gace [37]. These cages have as previously described, a surface collar structure from which a net is hung into the water column. Loverich and Gace defined in 1997, four sea cage classes:

1. Gravity cage, which rely on buoyancy and weight to hold the cage shape and volume against externally applied forces.
2. Anchored tensioned cage, rely on anchor tension to hold their shape.
3. Self tensioned and self supporting cages, such as a sea station.
4. Characterized by rigid, self supporting structures made up of jointed beams.

With this historical flashback in mind, it is clear that the idea of a rigid steel fish farms is indeed not a new one, but never has one been closer to put a fully sized, functional fish farm of this dimension into operation. The Ocean Farming concept (Fig. 1.1) is a result of the combined knowledge from the Norwegian fish farming and offshore industry. The project has been recognized both at home and abroad, and Ocean Farming are highly optimistic of their design. Many studies has been done in cooperation with various partners; Global Maritime, DNV GL, and MARINTEK, to investigate various properties of the concept, like stability, risk of escape, and fish welfare among others [44]. From our point of view, the interesting properties is the basis of low water plane stiffness, implying inertia domination and reduced motions. This particular design was one of the focus areas in the work by Heiervang and Knutsen [24].

Because of the shear dimensions of the steel concept cage, a massive mass of fish must be farmed in order for it to be economically profitable [6]. Ocean Farming applied for a so-called "green licence", an opportunity to test out their concept in full scale. They were unfortunately denied because the environmental damage at a possible fish escape situation would be unacceptable with this many fish [11]. Another reason for the rejection is that the group assigned to assess the applications felt that only closed farm concepts, essentially a giant bathtub, were able to solve the environmental challenges facing the industry [42]. An example of such a construction can be seen in **Fig. 1.10**. If granted, Ocean Farming wish to place their rig in Frohavet just outside of Trondheim, Norway, see **Fig. 1.11**. This location is believed to be a good recipient with respect to current (high rate of water circulation), temperature, and other environmental factors [44].

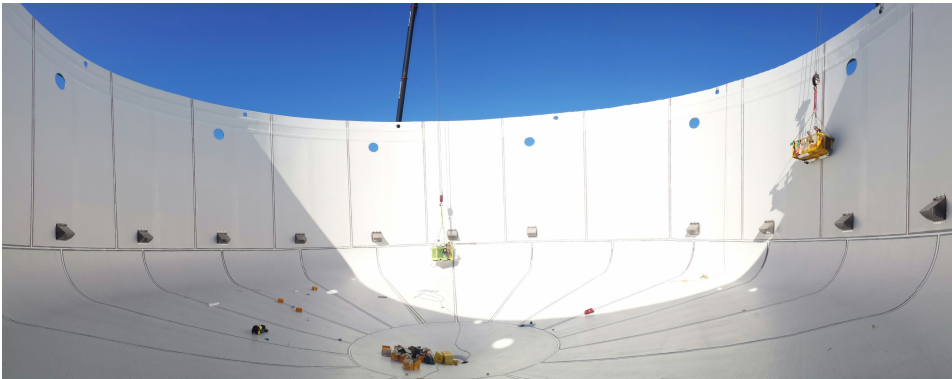


Figure 1.10: A picture taken from the inside of the "Neptun" concept during construction. The concept is developed by AquaFarm Equipment AS and is seen as an escape-proof solution. (www.aquafarm.no)



Figure 1.11: A map indicating the location of Frohavet, an area north-west of Trondheim (Norway) more exposed than a conventional aquaculture location, although not entirely "offshore". (www.norgeskart.no)

1.5 Problem Definition

The work done in this thesis is based on the problem text written by our supervisor, Professor Jørgen Amdahl, reference is made to appendix B. From our understanding, the points listed in the problem text are more suggestions than commands. Thus, some points have been given more attention than others. We feel it is necessary to specify what has been done, and what has been left to further work. So with reference to the enumerated points in the problem text:

1. The most comprehensive point in this thesis. It turned out to be difficult to modify the model made by Heiervang and Knutsen, so we made a new and improved model based on current design from scratch. The immense amount of time invested in modelling was returned in terms of easy completion of the analyses.
2. A qualitative comparison, especially focused on natural periods, have been made.
3. We were not able to obtain stress concentration factors for the critical joints considered. A parametric study of SCF factors have thus been made based on summing up the total fatigue damage on the most critical members and connections.
4. Is included with one sea state along the contour. Mooring lines are not included as the used API-WSD code check is only applicable for steel structures.
5. Simplified methods for ULS were investigated by Heiervang and Knutsen. The chosen FLS method is somewhat simplified.
6. Left for further work.
7. Included as is.

1.6 Outline of the Thesis

This thesis is organized as follows. First, a thorough review of related previous work summarized as a motivational background is described in chapter 2. An overview of the theory needed to conduct the ultimate- (ULS) and fatigue limit state (FLS) analyses is presented in chapter 3. These two chapters are more or less taken directly from our pre-project conducted during the autumn of 2014 [7]. With the basic theory in place, the modelling procedure together with theoretical justification are presented in chapter 4. Thereafter follows the analysis setup, complete with choice of control parameters and scripting procedure in chapter 5. To conclude in chapter 6, the obtained results are discussed in a thorough manner, identifying uncertainties in the analysis method. For the ULS results, a comparison is made with Heiervang and Knutsen [24]. Recommendations for further work concludes the thesis.

In the modelling part especially, sound engineering judgement have been crucial to model the cage as correctly as possible. The intended design taken from structural drawing and current weight calculations has been simplified in order to get a well conditioned analysis.

Simplifications should however not compromise the performance of the model. All this is thoroughly described in the following. It should be mentioned that throughout this report, several terms are used for the Ocean Farming design; this includes the rigid fish farm, Global Maritime model, Ocean Farming concept, rig, offshore fish farm, steel concept cage, etcetera. The reason being that the concept has yet to be given a designated single name.

Chapter 2

Literature Review

Seeing as our thesis is a continuation of the work done by Heiervang and Knutsen [24], a complete review of their thesis would be a natural starting point. In our literature search, a narrowed section concerning offshore aquaculture was difficult to find. We therefore focused our search on a few selected aspects and segments one has to consider when moving aquaculture further offshore. Literature study has been a continued process during our work. The sections mentioned in this chapter is meant to give a brief and historic overall motivational background for our choice of methodological approach to the Ocean Farming rig.

2.1 Fish Farms Subjected to Extreme Environmental Conditions

In their thesis, Heiervang and Knutsen used the nonlinear finite element program USFOS to study two different models of aquaculture structures in the time domain. USFOS is primarily made for static and dynamic analysis of space framed structures such as a jacket. In addition to calculating global response of the models, the work was also founded in investigating if USFOS was suitable for this purpose, that is, analysis of floaters. The two concepts considered were one conventional fish farm and one simplified model of the Ocean Farming design (Fig. 1.1). The response output were compared to simulated results from Global Maritime and results from model tests conducted by MARINTEK. Their focus was to establish good and reliable models and results for maximum response rather than a sensitivity analysis of various parameters.

The Ocean Farming rig is the first of its kind. Its motion characteristics and structural properties will thus differ from conventional fish farm structures. An example is the net, made of ethylene terephthalate (PET), the same kind of material used in landslide safety

nets. Finite element modelling of net structures are uncommon in offshore context. A finite element model was chosen with conventional beam elements, rising the question if such elements were suitable for simulating the behaviour of such a structure, where particularly the flexible net introduced challenges. The steel construction (the designated term for the Ocean Farming rig in their thesis) agreed well with the model tests in comparison. The same could not be said for the conventional design. Not surprisingly, they struggled with the nonlinear properties of the materials and large deformations in the net. Accidental analysis and fatigue were not investigated at this stage.

The response analyses were conducted with three different methods to assess ultimate limit strength (ULS); stochastic analysis, design wave analysis, and regular wave analysis. A limited set of environmental conditions and headings were investigated. The result therefore represents only a selection of the possible extreme responses. The results suggest that a static design wave approach is not necessarily conservative for the rigid structure, but uncertainties makes it difficult to draw any final conclusions. The results differ somewhat from the results presented by Global Maritime. The authors argues that this may be because of slamming loads in the upper part of the structure and they recommend investigating the air gap in the simulations of extreme sea states.

The conventional fish farm was difficult to model with USFOS. Partial good compliance with experiments is observed, in particular the accelerations of the floating collar. The results indicate that the simplified regular wave analysis is conservative for the selected sea states. A better approximation of the loads may be obtained by applying the theory of net panels to fully capture the shielding effects during deformation.

There is no doubt that there is still much work to be done on analysis of both conventional and new types of aquaculture structures. For the rigid offshore fish farm, the subject of our thesis, analysis with respect to fatigue (FLS) and accidental loads (ALS) comes as a natural step after a structural strength assessment. For the conventional fish farm, further work consists of developing a better numerical model to reduce divergence in calculations and get a better accordance with model-test data.

2.2 Offshore Cage Design

There is an overwhelming support to move aquaculture cages into offshore waters. A paper by Shainee et al. [52] looks into the current offshore cage designing concepts in order to propose an optimum design concept by using a set of requirements derived earlier by the authors. By a set of experts, each representing various disciplines important to fish farm development, the assessment points towards a single point mooring cage. This conclusion is derived from studying the relation between the total horizontal forces and the vertical force components acting on the cage as it submerges. The paper also proposes an alternative classification of cages, that is, systems that are intended to resist and dissipate environmental forces, and systems that are designed to avoid environmental forces.

As described in another article by Shainee et al. [51] on this subject, moving further offshore could provide a better return of investment through various factors such as reduced

mortality, better growth rates, less disease, and net fouling. Currently there is a race towards an optimum cage design for the offshore environment. This paper attempts to apply a holistic¹ and theoretical approach to fish cage designing. The authors argue that instead of trying to extend the onshore and near-shore fish farm designs and technology to adapt to offshore sites, ideas should be borrowed from more developed and advanced knowledge from offshore and marine industry.

2.3 Previous Work on Analysis of Fish Farms

Due to the simple nature of the classical conventional fish farms and the relatively sheltered locations in which they are anchored, analysis of global response and other possible structural failure modes is a relatively new issue in the world of aquaculture. With the industry moving towards harsher conditions and new definitions of "extreme weather" following climate change, this segment will become more important. Previous work relates to work done on conventional concepts including hydrodynamic effects on net structures and floater elements.

Much like most floating structures, fish farms are exposed to waves, current and wind. Wind is however a small part of the total loading because of the relatively small superstructures. In conventional designs, the superstructure is almost negligible, and wind is therefore a factor often disregarded. Waves and current however are highly important. Theoretical models and experiments for assessing both steady and unsteady hydrodynamic forces on fish farms and trawls² have been presented in the past decades. However, more work, both experimental and theoretical, is needed to establish well validated computational tools, Kristiansen and Faltinsen [29]. Hydrodynamic loads can be separated into three main categories; current forces on the net, combined wave and current force on the structure, and forces on the floating collar. Our focus have been on elements both seen on the conventional type of fish farms and the Ocean Farming rigid structure, which primarily is ways of modelling the net.

2.3.1 Current Forces on the Net Structure

In order to analyse a net in current, one needs a structural model and a hydrodynamic model. A direct computational fluid dynamics (CFD) simulation of a fish farm is unrealistic since the number of twines may be in the order of ten millions. A CFD analysis would be too computationally demanding, and thus efficient rational methods are needed. Kristiansen and Faltinsen [29] have investigated two methods for estimating the hydrodynamic forces acting on a net structure; the widely used Morison type of force models, and a screen/net panel type model. Both have been shown to be equally effective, but the Morison model significantly over-estimates forces for highly deformed nets. Both methods are discussed in the following.

¹everything in nature is seen as being connected in some way

²fishing vessel where a submerged net is pulled through the water

In the Morison model, the net is represented by an equivalent system of twines, or equivalent trusses. The equivalent twine is given a certain length and diameter such that it has the same projected area as the physical net represents. *Morison's equation* (thoroughly discussed in section 4.2) is applied to calculate the cross-flow force on each equivalent twine based on the cross-flow principle. The Morison approach assumes that there is no interaction between individual twines, implying that the net can be modelled by individual cylinders [29]. As stated by Kristiansen and Faltinsen, two objections arise from this approach:

1. When the inflow angle between current velocity and the net is large, the Morison model clearly overestimates drag force acting on the net. At for instance a 90 degree inflow angle, the Morison model predicts that the total drag force is approximately half the value of inflow at zero degrees. In reality, it should be close to zero.
2. Interaction effects including shading and local speed up between individual twines are not accounted for. Local speed up can be compensated for by adjusting the drag coefficient, while the shading effect is hard to take into account.

Attempts to improve the calculations with regards to these two obstacles have been made. "Only the action of external forces can bring an infinitely flexible structure like a net into a definite shape. When considering supple nets in immersed fluid, these external forces themselves depend on the net geometry." This was the basis of the work by Le Bris and Marichal [35] who proposed a numerical model to solve this coupled problem and tried, with good results, to validate the model by measuring the hydrodynamic forces on a plane panel of netting spread across a transverse current. Moe et al. [41] modelled the net cage using truss elements that represented several parallel twines, that is, a Morison force model. By using experimental drag coefficients from Fredheim [20] in their calculations, the authors conclude, not surprisingly, that it must be assumed that drag loads can be over predicted for large displacements if the potential shadow effects are not included.

In the screen type model, the net is divided into a number of net panels and the hydrodynamic force is decomposed into a normal and tangential force component. The model proposed by Kristiansen and Faltinsen is in principle a generalization of the screen model suggested by Løland [36]. It is assumed that there is an interaction between the individual twines. The approach was first proposed by Løland as an empirical model for drag force of individual screens, summarized in the widely used *Løland's formula*, Eq. (2.1). Løland also suggested an empirical formula for the lift coefficient Eq. (2.2), however not seen as important as the drag when considering fish nets. Both coefficients are calculated as a function of the angle between net normal and flow direction α , and the solidity ratio Eq. (2.3), defined as the ratio between the area covered by the threads in the screen and the total area of the screen, where λ is the mesh size, and D is the twine diameter.

$$C_D = 0.04 + (-0.04 + 0.33Sn + 6.54Sn^2 - 4.88Sn^3) \cos \alpha \quad (2.1)$$

$$C_L = (-0.05Sn + 2.3Sn^2 - 1.76Sn^3) \sin(2\alpha) \quad (2.2)$$

$$S_n = \frac{2D}{\lambda} - \left(\frac{D}{\lambda}\right)^2 \quad (2.3)$$

Løland's formula yield the best results for inflow angles less than 45 degrees, in addition, it under predicts the results for Reynold's numbers (Re) less than 500. This has a direct influence on validation of numerical results against model experiments were Re may be as low as 30. The model proposed by Kristiansen and Faltinsen [29] is a more general version of Løland's formula, valid for attack angles greater than 45 degrees. In addition to the dependency of inflow angle and solidity ratio, Re is also taken into consideration.

Calculation of drag force on a net cage is complicated due to the porous nature of the net, geometry, and flexibility of the system. Adding to the complexity is the wake effect, or reduced velocity, behind each individual twine which will have a significant effect on the forces and deformations of the net cage. This wake effect will result in reduced inflow velocity on parts of the net being downstream.

Endresen et al. [17]

Based on empirical experiments, Løland suggests to model this velocity reduction, r , as in Eq. (2.4) [36].

$$r = 1.0 - 0.46C_D \quad (2.4)$$

2.4 Fatigue in Offshore Structures

Traditional frequency domain analysis can hardly properly handle nonlinear effects induced from many sources. Junbo Jia presents in his paper [26] a general calculation procedure for wave induced fatigue damage of a typical jacket structure based on time domain analyses. The nonlinear dynamic analysis method presented in the paper has been successfully applied in several industry projects for the lifetime extension of offshore installations subjected to wave and wind loads. Although this paper looks into the case of a typical jacket structure, we feel that the general calculation procedure may also be applied on an offshore fish farm consisting of tubular members like the Ocean Farming rigid structure.

Fatigue life is one of the major concerns for the offshore installations since the utilization of tubular members gives rise to significantly high stress concentrations in the joints. Fatigue analysis based on a time domain response calculation is normally performed with the following procedure [26]:

1. Calculate the stress variations during the lifetime.
2. Count the stress amplitudes using certain counting methods.

3. Calculate the fatigue damage for each stress amplitude range according to the material data (S-N curves).
4. Sum them up to estimate the total fatigue damage during the structures entire fatigue life.

Jia used USFOS to carry out the dynamic analysis in the time domain. In each step, the hydrodynamic forces are recalculated according to the updated structural deformation. The subroutine FATAL³ is adopted to count the stress amplitude cycle and calculate the fatigue damage. FATAL can according to Jia also be used to calculate the stress concentration factor at each joint, we were however not successful in utilizing this feature in our pre-project fatigue analysis models [7].

³USFOS utility tool for fatigue estimation

Chapter 3

Primary Theoretical Background

The following is a walk-through of the theoretical aspects involved in our response and fatigue analyses. The text in section 3.1 and 3.2 is more or less taken from our pre-study conducted during the autumn of 2014 [7].

3.1 Methods to Calculate the ULS Characteristic Loads and Load Effects

The Ocean Farming concept can in many ways be compared to a semi-submersible platform with catenary mooring, and just as a semi-submersible, the characteristic global behaviour can be described by 6 free degrees of freedom sorted in translations¹ and rotations². The action effect analyses of the Ocean Farming fish farm can therefore be based on the same kind of procedures as for a semi-submersible. Thus, it is necessary to perform a global wave motion analysis (global response/motion analysis) to find the characteristic ULS (ultimate limit state) loads and load effects. This is in contrast to a fixed structure, where a wave-structure-foundation analysis must be performed.

The purpose of a motion analysis of structures with at least one free mode, is to determine displacements, accelerations, velocities and hydrodynamic pressure relevant for the action on the hull, superstructure, riser and mooring system, as well as relative motions (in free modes) needed to assess airgap and green water requirements. Excitation by waves, current and wind should be considered.

NORSOK N-003 [46]

¹heave, sway, and surge

²pitch, roll, and yaw

To find the ULS loads, extreme environmental actions, corresponding to an annual exceedance probability of 10^{-2} (100-year return period), must be applied on the structure. An offshore structure will be exposed to a combination of environmental actions. To assume that all the individual 100-year environmental actions will occur at the same time is highly conservative. N-003 therefore suggests the combination of environmental actions shown in **Tab. 3.1** to be used in the ultimate limit state consideration.

Table 3.1: Combination of environmental actions with expected mean values and annual probability of exceedance 10^{-2} . [46]

| ULS case | Wind | Waves | Current | Ice | Snow | Earthquake | Sea level |
|----------|-----------|-----------|-----------|-----------|-----------|------------|-----------|
| 1 | 10^{-2} | 10^{-2} | 10^{-1} | - | - | - | 10^{-2} |
| 2 | 10^{-1} | 10^{-1} | 10^{-2} | - | - | - | 10^{-2} |
| 3 | 10^{-1} | 10^{-1} | 10^{-1} | 10^{-2} | - | - | mean |
| 4 | - | - | - | - | 10^{-2} | - | mean |
| 5 | - | - | - | - | - | 10^{-2} | mean |

For the Ocean Farming fish farm, the loading from the waves are believed to be by far the most important action with respect to extreme loads and responses. Thus, only the first ULS condition will be checked. In addition, the exposed area of the topside is relatively small, meaning that the wind loads are neglected. Since we are dealing with a floating structure, it is obvious that the sea level will not have any influence on the loads. Here we will have a look at different methods for determining the characteristic ULS loads and responses. We will, as stated above, mainly focus on the environmental actions from the waves. When waves are governing the design, there are in general three main methods used for determining the extreme loads and response on an offshore structure:

- Stochastic analysis
- Design wave analysis
- Regular wave analysis

All the analyses listed above rely on a long term distribution of the sea states. We will therefore start with a brief statistical description of the long term distribution of waves.

3.1.1 Long Term Distribution of Sea States

A sea state is a short term description of the sea surface process at a given location, mainly described by the slowly varying parameters H_S (significant wave height) and T_P (spectral peak period). The waves will also have a mean direction, ϕ_m . Within the duration of the sea state, usually taken to be 3 hours, the sea surface process is assumed to be a stationary stochastic process. This means that the sea state characteristics are independent of absolute time, that is, the mean and the variance of the process are constant within the duration of the sea state. In a longer span, the process will be of a varying severity, meaning that it is of a non-stationary nature.

However, the variation in the severity regarding the characteristics, significant wave height and, say, spectral peak period is much lower than the variation on the surface process itself. For this reason, one can for practical purposes consider a long term period of the sea surface process as a sequence of piecewise stationary processes.

Haver [23]

The long term distribution of the sea surface can thus be described by a long term distribution of sea states.

The long term distribution of sea states are usually based on site measurements, often presented in term of scatter diagrams. Since we are interested in estimating long term extremes (100-year sea states for ULS), the measurements must have been performed over a long period of the time for the estimated long term extremes to be statistically significant. For oil and gas location, measurements have been made over several years, making it possible to predict long term extremes with a reasonable good accuracy. For most aquaculture locations, this is however not the case, and predictions of long term extremes, often only based on expert opinions, will be associated with large uncertainties. This also applies for the proposed location of the Ocean Farming fish farm (Fig. 1.11). To take into account the directionality of the waves in a good manner is in any case not possible. Haver [23] actually suggests that a minimum of 50 years of data should be available before directional distributions are to be established for design. The omni-directional wave climate should thus be used (as is the case in the analyses performed by Heiervang and Knutsen [24]). The long term variability of the wave conditions can then be described by the joint density function of H_S and T_P , disregarding ϕ_m . This joint density function is conveniently given in Eq. (3.1).

$$f_{H_S T_P}(h_s, t_p) = f_{H_S}(h_s) f_{T_P|H_S}(t_p | h_s) \quad (3.1)$$

The marginal probability distribution of H_S , $f_{H_S}(h_s)$ (often Weibull distributed), and the conditional probability distribution of $T_P | H_S$, $f_{T_P|H_S}(t_p | h_s)$ (often log-normal distributed), can quite easily be obtained from available data.

Contour line method

Haver [23] describes the contour line method as a short term approach for estimating long term extremes. Basically this implies that instead of performing a full stochastic long term response analysis, we only perform a stochastic short term response analysis. This means that we restrict ourselves to consider a rather limited number of environmental conditions. The idea is that we can estimate the q-probability response by primarily studying the short term response for the most unfavourable sea state along the q-probability contour line. The contour lines are curves indicating values for H_S and T_P corresponding to a constant given annual exceedance probability, q . The distributions from Eq. (3.1) are used as a basis for this. Below we will have a quick look on how environmental contour lines can

be obtained. The example figures, **Fig. 3.1, 3.2**, presented are based on hindcast data from the Haltenbanken (Norway) area from the year 1958 to 2008 [8].

To make the contour lines we use a simplified method where we transform the parameters in question into standard Gaussian variables using a first order reliability method (FORM). The key feature of this transformation is that it conserves probability. The transformations are given by

$$\begin{aligned}\Phi(u1) &= F_{H_S}(h_s) \\ \Phi(u2) &= F_{T_P|H_S}(t_p | h_s)\end{aligned}\tag{3.2}$$

Where $F_{H_S}(h_s)$ and $F_{T_P|H_S}(t_p | h_s)$ are known. This means that

$$\begin{aligned}u1 &= \Phi^{-1}(F_{H_S}(h_s)) \\ u2 &= \Phi^{-1}(F_{T_P|H_S}(t_p | h_s))\end{aligned}\tag{3.3}$$

The gain obtained by the transformation is that the iso-probability lines (contour lines) in the transformed space, u-space, are circles with center in the origin. This is because both variables are standard Gaussian variables. All points along this circle can be found when knowing the radius of the circle. This radius is determined by the target annual exceedance probability q we are looking at. The radius, β , is therefore given by

$$\begin{aligned}\beta &= -\Phi^{-1}(q_{3h}) \\ q_{3h} &= \frac{q}{2920}\end{aligned}\tag{3.4}$$

The 10-, 100-, and 10 000-year contour lines from the Haltenbanken area in the Gaussian space are shown in **Fig. 3.1**.

Since we now have all the points on the contour lines in the Gaussian space, all we have to do is to transform these points back to the physical space to get the real contour lines. These contour lines together with the hindcast data are shown in **Fig. 3.2**. For ULS, it is the 100-year contour line that is of interest (meaning q equal to 0.01).

When the desired contour line is obtained, we can search along this contour line to find the combination of H_S and T_P that gives the largest response. For structures demonstrating a dynamic behaviour this is particularly important, as the largest wave not necessarily will give the largest response. It should still be said that unless we are dealing with a very special structure, the largest response is expected to be excited in a sea state found near the top of the contour. This means that for most structures, it is sufficient to do global response analyses in sea states obtained from the top-region of the contour.

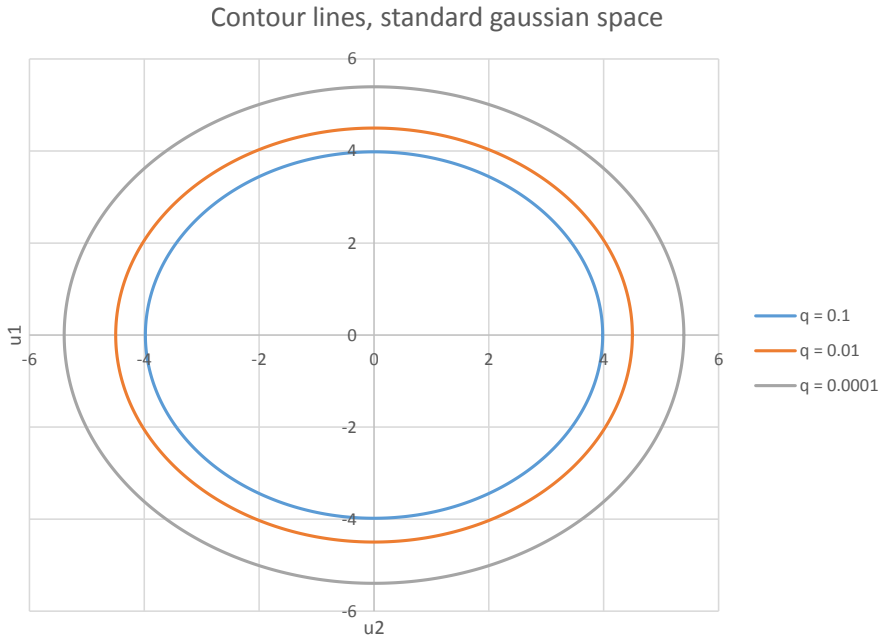


Figure 3.1: 10 ($q = 0.1$), 100 ($q = 0.01$) and 10 000 ($q = 0.0001$) year contour lines in the standard Gaussian space from hindcast data on Haltenbanken. [8]

3.1.2 Stochastic Analysis

The stochastic analysis applies the statistical distributions of the waves for calculation of short term and long term responses. This can be done either in the frequency domain or in the time domain. The basis for the calculations is sea states found from the long term distribution of the waves. The contour line method is a convenient method for selecting sea states relevant for the ultimate limit state. The short term distribution of the selected sea states can further be described by different wave spectra. Relevant wave spectra and their properties can be found in DNV-RP-C205 [14].

A frequency domain analysis implies establishing transfer functions and using the relationship between the wave spectrum and the transfer functions in order to obtain a response spectrum. Having established the response spectrum, the various statistical properties of the response, such as probability distribution of response amplitudes and maximum probable response, can be calculated. If the response quantities in question are close to linearly related to the wave process, a full long term response analysis can be found without being very time consuming. If we are considering sea states with a duration of 3 hours, this means finding the long term distribution of the 3-hour maximum response, X_{3h} given in Eq. (3.5).

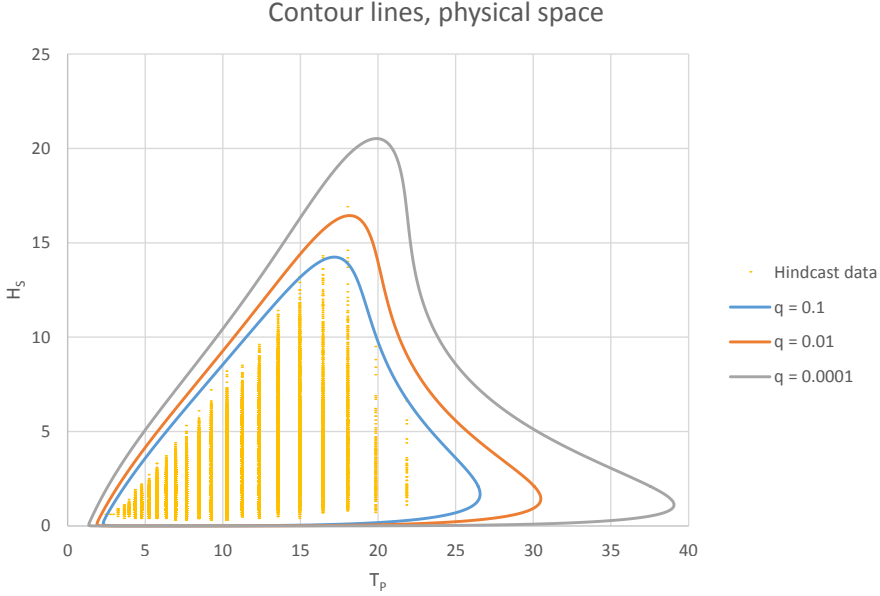


Figure 3.2: Contour lines in the physical space together with the accompanying hindcast data points from Haltenbanken. [8]

$$F_{X_{3h}}(x) = \int_{h_s} \int_{t_p} F_{X_{3h}|H_S,T_P}(x | h_s, t_p) f_{H_S T_P}(h_s, t_p) dt_p dh_s \quad (3.5)$$

where $f_{H_S T_P}(h_s, t_p)$ is given by Eq. (3.1), and $F_{X_{3h}|H_S,T_P}(x | h_s, t_p)$ is the short term distribution of X_{3h} given the sea state characteristics.

Time domain analysis implies solving the equation of motion for the structure in time domain when being exposed to environmental actions. This is done for the chosen sea states, where each sea state is given a duration, usually 3 hours. As stated above, each sea state is represented by an adequate wave spectrum. A difference between a frequency- and a time domain analysis is that in a frequency domain analysis, the wave spectrum is used directly as the wave spectrum is given in the frequency domain. Here, all the statistical properties of the surface elevation is completely described by the wave spectrum (given a Gaussian surface elevation). In a time domain analysis however, a realization of the wave spectrum must be obtained, usually by utilizing inverse fast Fourier transform (FFT). The realization will be associated with inherent variability as it is only a realization out of an infinite number of realizations, Haver [23]. Several simulations of each sea state should therefore be conducted in order to reduce the risk of the individual simulation not being representative for the sea state. This also allows a short term extreme value distribution for

the response to be established. According to Haver, the following steps are usually applied when performing a time domain analysis:

1. Simulate a possible realization of the surface elevation field of an adequate duration, often taken to be 3 hours. This could be a Gaussian random field or it could be a second order random field.
2. Calculate the corresponding kinematics in the fluid covering the load exposed structural members with sufficient accuracy. Generally, one needs to account for kinematics to the exact surface.
3. Calculate the load vector of the submerged part of the structure at each time step during the period covered by the simulated sea surface process.
4. Solve the equation of motion for the given load vector history. This is typically quick if the structural motions are small, that is, the left side of the equation can be considered as a linear mechanical problem. If stiffness and/or damping need to be updated for each or some few time steps, the time domain solution may become rather time consuming.
5. As a result of step number 4, time histories of duration d hours for all nodal displacements are available. From these time histories one can establish the distribution function for all "global" maxima (which is the largest maximum between up-crossings of the mean level). If we rather focus on the d -hour maximum, one can identify an estimate for the d -hour maximum for each response per simulation. If we have simulated M time histories, we have M estimates for the d -hour extreme value. From these estimates we can establish a proper d -hour extreme value distribution (often following a Gumbel distribution).
6. In combination with the environmental contour line method for selecting adequate short term sea states for design purposes, a proper estimate for the q -probability value is obtained by determining the α -percentile of the extreme value distribution. If the sea state considered is taken as the worst (in term of the problem under consideration) along the q -probability contour line, a proper estimate is often found using $\alpha = 90$.

Regarding the number of simulations to be performed, it is common to only run a few simulations (say five) for each sea state selected from the contour line. Based on this, it should be possible to identify the worst sea state. When the worst sea state is found, additional simulations based on this sea state should be performed in order to reduce the uncertainty of the estimated parameters in the extreme value distribution. According to Haver, 20 observations (meaning 20 simulations) is the absolute minimum in order to get acceptable results when fitting observed values to a given distribution. Monte Carlo³ simulations can be performed if one wants to investigate the uncertainty of the estimated distribution based on the given sample size.

³repeated random sampling to obtain numerical results, generation of draws from a probability distribution

3.1.3 Design Wave Analysis

The design wave analysis is another method to determine the characteristic ULS loads on a structure. The major difference between this method and the stochastic analysis is that instead of aiming at the sea state that gives the largest response, we want to determine the properties of the individual wave that gives the largest response. This wave is called the *design wave*. For ULS, this wave should in general correspond to a 100-year wave, meaning that it has wave characteristics that will occur with an annual probability of 10^{-2} . If this method is to be used, the structural response should be linearly related to the wave process. The main issue for this analysis is determining the design wave characteristics. There are multiple ways of doing this, and the various methods are often suited for specific types of offshore structures.

In the "manual" by Haver [23], a standard method for determining the characteristic design wave on fixed offshore structures, like a jacket, is described. Basically it involves determining the 100-year extreme wave height and use this together with a 90 percentile confidence band for the corresponding wave period. A Stokes 5th order wave profile is then adopted based on these characteristics.

For semi-submersibles, a more common approach is the method described in DNV-RP-C103 [13]. This method is performed in the frequency domain, and thus applies the properties and relations of the wave spectrum and the transfer functions of the structure in order to decide the properties of the design wave. This method is quite involved, and in reality we are almost solving the entire response problem in order to arrive at the correct design wave. Since USFOS⁴ only conduct analyses in the time domain, we will not discuss this particular approach further.

3.1.4 Regular Wave Analysis

Regular wave analysis implies exposing the structure to regular waves with a given wave height and period. This can be conducted both in the frequency domain and in the time domain. In accordance with the governing standard for fish farms in Norway, NS-9415 [48], the parameters given in Eq. (3.6) shall be used for the regular waves.

$$\begin{aligned}H_{REG} &= 1.9H_S \\T_{REG} &= T_P\end{aligned}\tag{3.6}$$

Regular waves implies Airy waves, and are described by linear wave theory. This procedure is not common within the Norwegian oil and gas industry. For conventional fish farms, however, it is used extensively. For ULS, it is actually stated in NS-9415 to use the 50-year return period significant wave height. As the Ocean Farming fish farm is to be

⁴non-linear dynamic analysis software

located on a more exposed location than the ones typically described in NS-9415, we however consider it better to use the 100-year value for significant wave height, in accordance with for example NORSOK. This means inserting the value of $H_{S,100}$ for H_S in Eq. (3.6).

3.2 Fatigue of Welded Structures

Fatigue is caused by cyclic loads, in most cases loads less than yield stress of a given material, and is a cycle by cycle process of damage accumulation, Berge [5]. It is thus important for structures subjected to a large degree of dynamic loading. Offshore structures will fall into this category, mainly due to the cyclic nature of the waves that they will be exposed to. This is reflected in the design codes for offshore structures, where in addition to for instance the accidental- (ALS) and the ultimate limit state (ULS), also the fatigue limit state (FLS) should be considered.

Fatigue history can be separated into three stages; initiation, crack growth, and final fracture. In welded structures, fatigue cracks almost always start at a weld defect, and the crack growth period accounts for more than 90 percent of the fatigue life. Fatigue capacity of welded joints are therefore of particular interest. The crack growth depends on the stress conditions at the crack tip (geometry), and the crack grows when opened by tensile stresses. This is due to plastic strains at the notch/crack tip. For compressive loading, the two surfaces may be forced into contact and can then transmit forces without activating the notch at the crack tip. Fatigue damage is thus avoided. In welded joints, that have not undergone post-weld heat treatment⁵, residual stresses will be present. These are commonly assumed to be tensile and of yield magnitude. For a welded member subjected to cyclic loading, the stresses in the welds thus always tends to be tensile (at least for a one dimensional stress condition). The whole stress range, ΔS , of each cycle will thus contribute to fatigue damage, Moan [1].

Fatigue crack growth follows different laws depending upon the magnitude of the cyclic stress. Because of this, we distinguish between high cycle and low cycle fatigue. The high cycle range of fatigue life is approximately above 10^4 - 10^5 cycles. For marine structures, fatigue stresses are mainly in the high cycle range. We will thus focus on this. In the high cycle range of fatigue, stresses are essentially elastic. S-N data in this range tends to follow a log-linear relationship, the *S-N curve*, Eq. (3.7).

$$N(\Delta S)^m = \text{constant} \quad (3.7)$$

In this context, N denotes the number of cycles to failure and ΔS is the constant amplitude stress range. Plotted on log-log scale, Eq. (3.7) becomes a straight line with the slope $-1/m$. A fatigue limit may also be defined, below which there are no fatigue damage. A graphical example of the equation is shown in **Fig. 3.3**.

⁵method for reducing and redistributing the residual stresses in the material

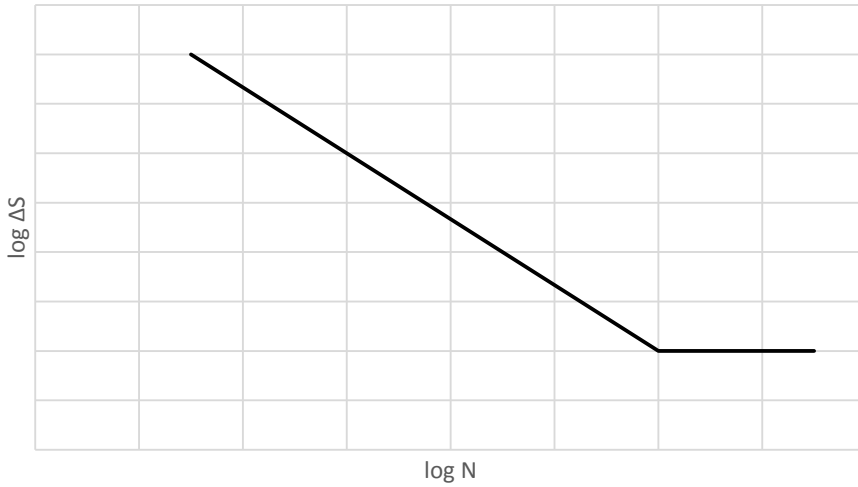


Figure 3.3: An arbitrary visual example of a S-N curve, Eq. (3.7).

The fatigue capacity of welded joints subjected to constant amplitude uni-axial loading is expressed in terms of S-N diagrams. A convenient feature for welded structures is that the S-N curve is essentially independent of the yield strength of the material. The crack growth depends on the local cyclic stress at the crack tip. Hence, fatigue is governed by the geometry, especially any change in geometry that introduces stress concentrations. Geometrical effects associated with the weld profile and inevitable weld defects are normally accounted for in the S-N data. Other geometrical effects should however be considered in the calculation of local stress ranges according to Moan [1].

3.2.1 Cumulative Damage

As previously mentioned, fatigue design of welded structures is based on constant amplitude S-N data. A marine structure however, will experience a load history of a stochastic nature due to the environmental conditions. The development of fatigue damage under stochastic or random loading is in general termed cumulative damage. The main procedure for calculating cumulative damage by use of S-N data is based on the *Miner summation*. It can be shown that the Miner summation conforms with a fracture mechanics approach to crack growth, but this will not be further discussed. The basic assumption of the Miner summation method is that the "damage" induced on the structure per load cycle is constant at a given stress range, and equal to

$$D = \frac{1}{N} \quad (3.8)$$

where N is the number of cycles until failure at the given stress range. For a stress history consisting of several stress ranges, ΔS_i , the total damage is thus given by

$$D = \sum_i \frac{n_i}{N_i} \quad (3.9)$$

where n_i is the number of cycles at stress range ΔS_i , and N_i is the corresponding number of cycles until failure.

If we measure the stresses at a joint for a marine structure that is exposed to environmental actions for some time, we obtain a stress-time history. This stress history can be quite complex. In cumulative damage analyses, the stress-time history is broken down into individual cycles which are summed up to a distribution of stress ranges. The most recognised counting method seems to be a *rainflow counting* algorithm, especially for broad-band loading. Each peak is imagined as a source of water that "drips" down a pagoda⁶ where the number of half-cycles is counted by looking for terminations in the occurring flow. This counting algorithm was first proposed by Matsuishi and Endo in 1968 [38]. Some care should however be taken with this counting procedure. Unless the load history is rearranged to start with its most positive peak or its most negative trough, a rainflow count will give a number of unpaired half cycles which are difficult to handle in cumulative analyses. Moreover, rainflow counting loses its physical significance when applied to cracked specimens where crack closure may occur under compressive loading, Berge [1].

If we are in possession of long term statistics for the environmental actions, it is possible to obtain statistics for the long term stress range distribution. There are different methods for arriving at a long term distribution of stress ranges, for example by use of a deterministic analysis or a stochastic analysis. Fines [1] list the following steps when conducting a stochastic approach:

1. Selection of major wave directions.

A few directions, typically 8, are selected for the analysis. The total number of waves is distributed between these major wave directions. Major wave propagation directions should be included, as well as directions causing high stresses in major structural elements.

2. For each direction, select a number of sea states which adequately describes the long term distribution of waves. Associate a duration to each sea state.
3. For each sea state, calculate the short-term distribution of stress ranges. This can be done either in the frequency domain or in the time domain.
4. Combine the results for all sea states in order to find the long term distribution of stress ranges.

One can then obtain an exceedance diagram of stress ranges for the desired lifetime, often called the stress spectrum. The total lifetime fatigue damage can then be calculated based

⁶tall, ornately decorated building, popular in Asia for religious purposes

on the stress spectrum in combination with an appropriate S-N curve. In many cases, the stress spectrum can be approximated by a two-parameter Weibull distribution, making cumulative damage calculations particularly convenient.

For fatigue design analysis based on time domain response calculation it is however not common to find the long term distribution of stress ranges before calculating the total fatigue damage. Here, one usually calculates the fatigue damage for each sea state based on the stress-time history by applying rainflow counting and Miner summation (and an appropriate S-N curve). The total damage is then found by summing the individual contributions from all the sea states.

For cumulative damage, it is important to be aware that the Miner rule does not take into account stress interaction effects [1]. The state of stress and strain in the damage area is a result of the preceding stress-strain history. This means that the fatigue damage from one cycle is not a function of the stress range alone, but also of the previous cycles. Interaction, or stress memory effects will thus be present, leading to large uncertainties in fatigue damage calculations. For the typical random load history experienced by offshore structures, interaction effects tends to give failure at a Miner sum less than unity according to Berge [1]. For this reason, design fatigue factors are applied. A table of these can for instance be found in NORSOK N-001 [45].

3.2.2 Fatigue of Tubular Joints

Frame work made of tubular members are widely used in offshore structures. The most common example is the piled jacket structure, but there are a lot of other examples. The bracing of semi-submersibles can be viewed as tubular structures, although with more complex joints. According to Berge [16], there are three main reasons to why tubes are preferred as structural members in offshore structures:

1. The drag coefficient for tubes is relatively low, and comparatively small forces are generated from waves and currents.
2. The strength properties of tubes are well suited for structures which are designed to withstand loading from the offshore environment. The cross section is uniform and symmetrical, with small stress concentration factors and excellent buckling and torsional strength. Strength properties are insensitive to lateral load direction. This is important for offshore structures, which may experience loads from any direction.
3. Compared to other cross sectional shapes, cost of maintenance, surface treatment, and corrosion protection are reduced, due to relatively small areas of exposed steel, and a less complicated external geometry. The relatively small outer area also gives a larger inherent fire resistance.

The drawback of tubular structures is that the joints tend to be complicated and that connections and joints, which for offshore structures usually are welded, represent structural discontinuities which give rise to very high stress concentrations in the intersection area. This is in particular detrimental to fatigue strength. Thus, lowered fatigue strength due to

high stress concentrations at the weld toes of the connecting welds is a major problem in welded tubular joints, Gibstein and Moe [1].

A tubular joint is commonly a joint between a main load carrying member and one or more secondary members, all being tubes. The main member, with the larger diameter, is denoted *chord* while the secondary member/members are denoted *brace*. Reference is made to **Fig. 3.4**. The typical situation is that the chord is subjected to essentially static loads while the brace is dynamically loaded from environmental forces. In fatigue assessments of tubular joints, the stresses in the chord are neglected. We thus only consider the dynamic loading from the braces, following the "stress range" thinking of fatigue design, Berge [16].

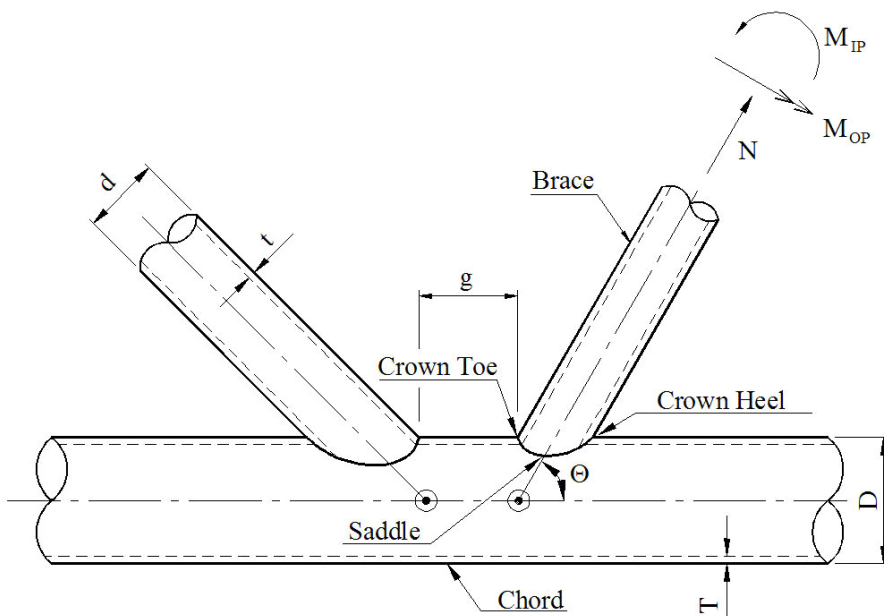


Figure 3.4: Positional and name definitions on common tubular joints. (DNVGL-RP-0005 [15])

As mentioned above, large stress concentrations will be present in tubular joints. Fatigue design of these joints are therefore highly dependant on finding these stress concentration factors (SCF) at the connection between the brace and the chord. The location of maximum stress tends to be located at the *saddle* or the *crown* of the intersection, depending on the mode of loading and on the joint geometry, but according to Berge [16], this is not true in all cases. When determining the SCF it is important to remember that the stress concentration (or notch factor) due to the weld profile and inevitable weld defects already are included in the S-N curve. We are therefore only interested in the stress concentration factor due to the overall (nominal) shape of the joint, often termed *geometric* or *global* stress concentrations. The stress associated with this SCF is often called the *hot spot stress*.

Stress concentration factors for simple tubular joints

For simple tubular joints it is possible to find parametric formulas for the stress concentration factors. In RP-C203 [15], one can obtain stress concentration factors for simple tubular joints of joint type T, Y, X, K, and KT. However, these are given separately for axial loading in-plane bending and out-of plane bending. Superposition is therefore required in order to find the hot spot stress due to the above mentioned actions. The procedure for superposition of stresses in tubular joints, according to RP-C203, is given in the following.

The stresses are calculated at the crown and the saddle points, see **Fig. 3.4**. Then the hot spot stress at these points is derived by summation of the single stress components from axial, in-plane and out-of-plane action. As mentioned earlier, the hot spot stress may be higher for the intermediate points between the saddle and the crown. The hot spot stress at these points is derived by a linear interpolation of the stress due to the axial action at the crown and saddle, and a sinusoidal variation of the bending stress resulting from in-plane and out-of-plane bending. Based on this it is concluded that the hot spot stress should be evaluated at 8 spots around the circumference of the intersection, see **Fig. 3.5**. The equation set (3.10) gives the hot spot stresses at these 8 locations.

$$\begin{aligned}
 \sigma_1 &= SCF_{AC}\sigma_x + SCF_{MIP}\sigma_{my} \\
 \sigma_2 &= \frac{1}{2}(SCF_{AC} + SCF_{AS})\sigma_x + \frac{1}{2}\sqrt{2}SCF_{MIP}\sigma_{my} - \frac{1}{2}\sqrt{2}SCF_{MOP}\sigma_{mz} \\
 \sigma_3 &= SCF_{AS}\sigma_x - SCF_{MOP}\sigma_{mz} \\
 \sigma_4 &= \frac{1}{2}(SCF_{AC} + SCF_{AS})\sigma_x - \frac{1}{2}\sqrt{2}SCF_{MIP}\sigma_{my} - \frac{1}{2}\sqrt{2}SCF_{MOP}\sigma_{mz} \\
 \sigma_5 &= SCF_{AC}\sigma_x - SCF_{MIP}\sigma_{my} \\
 \sigma_6 &= \frac{1}{2}(SCF_{AC} + SCF_{AS})\sigma_x - \frac{1}{2}\sqrt{2}SCF_{MIP}\sigma_{my} + \frac{1}{2}\sqrt{2}SCF_{MOP}\sigma_{mz} \\
 \sigma_7 &= SCF_{AS}\sigma_x + SCF_{MOP}\sigma_{mz} \\
 \sigma_8 &= \frac{1}{2}(SCF_{AC} + SCF_{AS})\sigma_x + \frac{1}{2}\sqrt{2}SCF_{MIP}\sigma_{my} + \frac{1}{2}\sqrt{2}SCF_{MOP}\sigma_{mz}
 \end{aligned} \tag{3.10}$$

Here, σ_x , σ_{my} and σ_{mz} are the maximum nominal stresses due to axial load and bending in-plane and out-of-plane respectively. SCF_{AS} is the stress concentration factor at the saddle for axial load, and SCF_{AC} is the stress concentration factor at the crown. SCF_{MIP} is the stress concentration factor for in-plane moment, and SCF_{MOP} is the stress concentration factor for out-of-plane moment.

For fatigue damage calculations, the stress range at the hot spot should be combined with the *T-curve* (S-N curve for tubular joints).

Calculation of hot spot stress by finite element analysis

For more complex tubular joints, the hot spot stresses are often determined based on a finite element analysis. If one has performed a detailed finite element analysis of a structure, it can be hard to evaluate what the "nominal stress" to be used together with the S-N curves

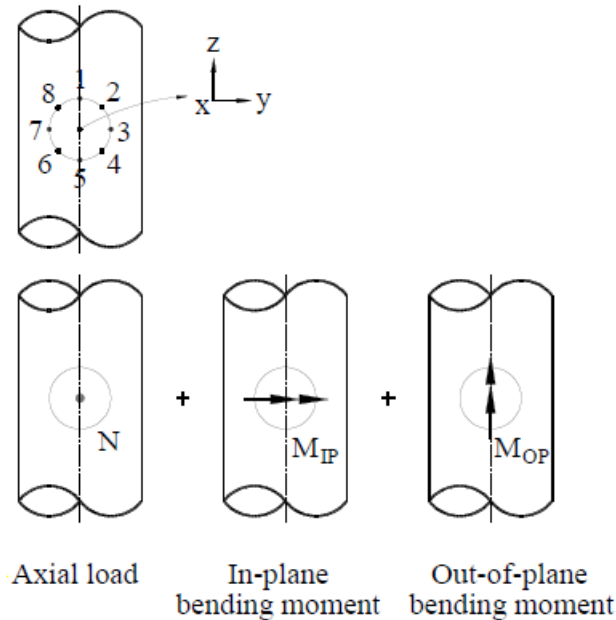


Figure 3.5: Definition of hot-spots around the weld connection to be used in superposition of stresses. (DNVGL-RP-0005 [15])

is. As previously mentioned, this is because some of the local stress due to the detail is accounted for in the S-N curve. Simplified methods have therefore been developed for assessment of the hot spot stress, and are based on extrapolation of the stresses. A schematic visualization of the extrapolation procedure is given in **Fig. 3.6**.

The standard procedure for determining the hot spot stress is by a linear extrapolation of the stresses obtained from a finite element analysis (FEA) at positions a and b from the weld toe. In RP-C203 [15] these distances are given for extrapolation along the brace and chord at the crown and saddle positions. Reference is made to **Fig. 3.7**. They are given in Eq. (3.11), (3.12), and (3.13).

For extrapolation of stress along the brace surface normal to the weld toe

$$\begin{aligned} a &= 0.2\sqrt{rt} \\ b &= 0.65\sqrt{rt} \end{aligned} \quad (3.11)$$

For extrapolation of stress along the chord surface normal to the weld toe at the crown position

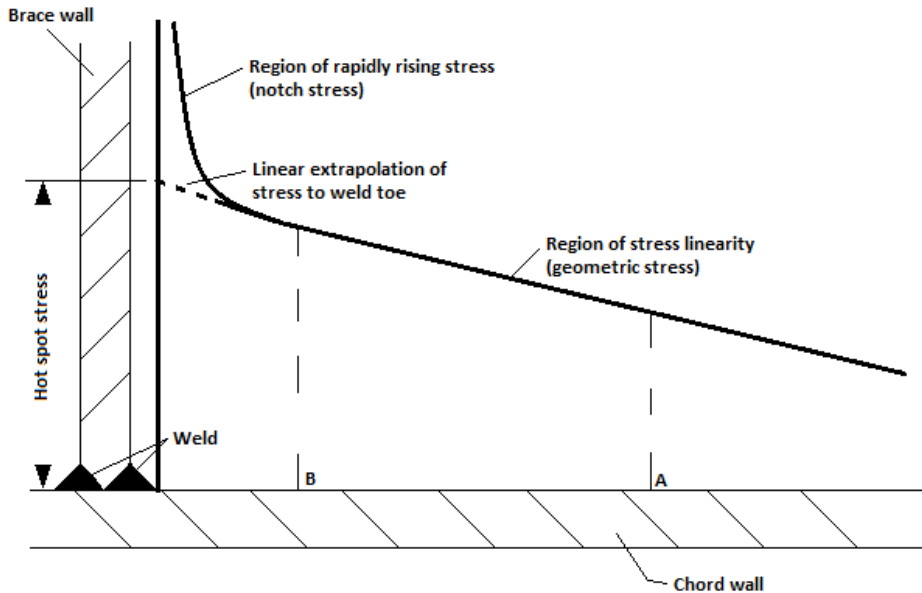


Figure 3.6: Linear extrapolation to determine the hot spot stress, based on figure in [16].

$$\begin{aligned}
 a &= 0.2\sqrt{rt} \\
 b &= 0.4\sqrt[4]{rtRT}
 \end{aligned}
 \tag{3.12}$$

For extrapolation of the stress along the chord surface normal to the weld toe at the saddle position

$$\begin{aligned}
 a &= 0.2\sqrt{rt} \\
 b &= 2\pi R \frac{5}{360} = \frac{\pi R}{36}
 \end{aligned}
 \tag{3.13}$$

In RP-C203 [15], there is also briefly described another approach for determining the hot spot stress from a FE analysis where the extrapolation procedure is avoided. For this alternative approach one can use the stresses at the Gaussian points (integration points) if these are placed a distance $0.1\sqrt{rt}$ from the weld toe (r equals the radius of considered tubular and t equals the thickness). The stress at this point may be used directly in the fatigue assessment. Regarding the FE analysis, it is most common to model the joint using thin-shell elements. This does however not allow modelling of the weld geometry. According to for instance *Fatigue Handbook* [1] and *Fatigue in Offshore Structures* [16],

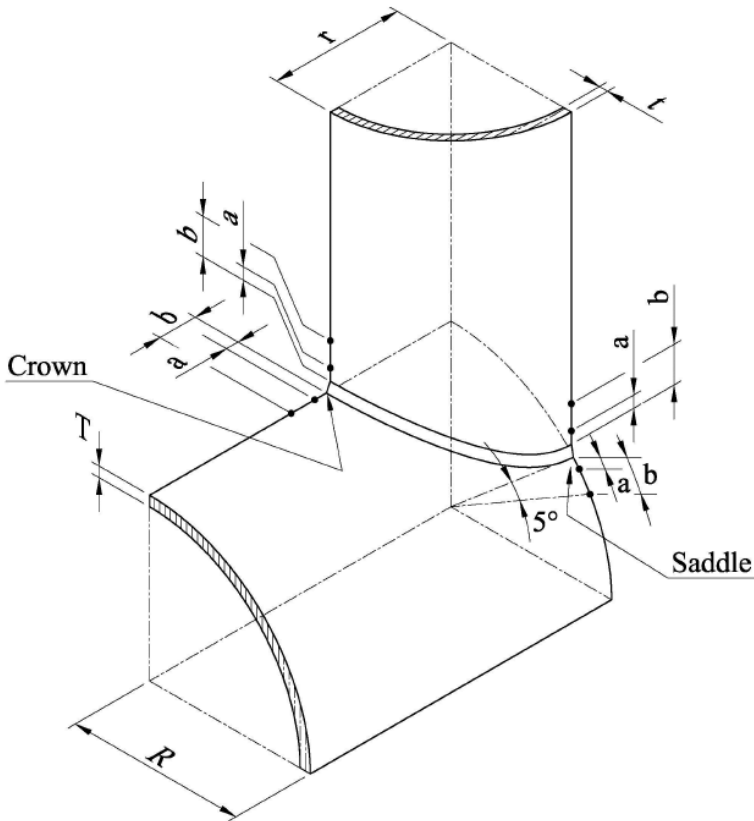


Figure 3.7: Segments around weld connection for read-out of stresses to be used in derivation of hot spot stress in tubular joints. (DNVGL-RP-0005 [15])

more reliable results can be obtained by including the weld geometry in the model. This implies the use of three-dimensional elements. Thick shell elements in combination with solid elements for modelling of the weld are generally to be recommended [16].

Hot spot stress for fatigue assessment of tubular joints

Here we will give the main physical reasons for why determination of the hot spot stress is sufficient for fatigue assessment of almost any kind of tubular joint. The reasoning is heavily based on information found in Stig Berge's chapter in *Fatigue Handbook: Offshore Steel Structures* [1].

In general, for fatigue assessment of welded joints, two types of stress concentrations need to be considered:

- Stress concentrations due to the overall (nominal) shape of the joint, often termed *geometric* or *global* stress concentrations (gives the hot spot stress).
- Local stress concentrations due to the shape of the weldment, often termed *notch* or *peak* stresses.

The role of these two stress components in fatigue may be illustrated by referring to typical crack growth behaviour. **Fig. 3.8** shows the growth development of semi-elliptical cracks from geometrically similar welds in a tubular joint and a flat plate respectively. As seen, in the flat plate weld, the initial growth is very slow, until the growth rate accelerates towards the end of the fatigue life. This behaviour reflects the characteristics of a growth rate proportional to $(\Delta K)^3$ where

$$\Delta K = \Delta S \sqrt{\pi a} F \quad (3.14)$$

and

- ΔK range of stress intensity
- ΔS stress range
- a crack length
- F form function

In the tubular joint however, we see that the growth is nearly constant for a relatively large part of the life.

The main reason for the difference in behaviour is the three-dimensional character of the stress field of tubular joints and the effect of load shedding. In a flat plate, the stress acting over the cross section is a remote stress which is relatively unaffected by the crack. For a tubular joint, the growth of a crack through the hot spot cross section causes gross load redistribution and a significant decrease in the driving force for crack growth. Thus, Eq. (3.14) with F derived from flat plate solutions gives very conservative results, and are not applicable to a fracture mechanics analysis of tubular joints.

Again with reference to **Fig. 3.8**, the fatigue life for a planar joint is dominated by the growth of a small crack from the weld toe. In this phase the stress at the crack, and thus the crack growth rate, is strongly affected by the local geometry of the weld. Because of this, with respect to fatigue design, planar joints are allocated to weld classes with different design curves, depending on the weld geometry and other technological factors. For tubular joints, however, the fatigue life is largely determined by the growth of a crack in a region where the peak/notch stress from the weld geometry is of minor significance. For this reason, the so-called hot spot stress (or geometric stress) has been taken as the characteristic stress for fatigue design of tubular joints. By assuming this, S-N data for tubular joints within a large range of geometries and load cases fall within a common scatter band, giving rise to the so-called *T-curve*.

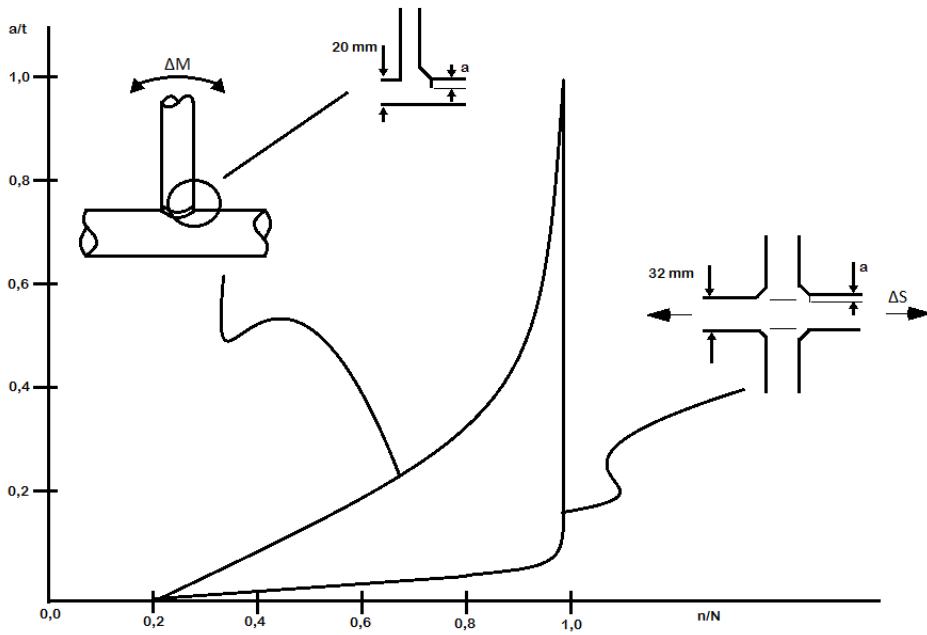


Figure 3.8: Crack growth development in both a tubular joint and a planar joint, based on figure in [16].

Chapter 4

Modelling and Theoretical Justification

Chapter 4 is a thorough description of the modelling process and underlying concepts suggesting the appropriate action in ways of choices. The main focus has been to further develop and improve the model made by Heiervang and Knutsen [24]. Due to difficulties with implementing changes in their existing model/source code, we have been forced to model the structure from scratch. The fish farm has been modelled by a MATLAB-script¹, producing a model.fem file to be read by USFOS with an accompanying control file. All analyses will at a later stage be simulated in USFOS. A significant amount of project time have been invested in modelling, thus the detailed process is described in the following.

4.1 Overview of the Ocean Farming Concept

The idea behind the Ocean Farming concept is to introduce a design robust enough to be safely installed and operated on exposed coastal sites. Through industrialized construction and improvements in the efficiency of operations, that is, by a higher degree of automation, the aim is to achieve competitive costs of production. Due to industry wide challenges, preventing fish escapes and reducing the danger of lice infection, both for farmed and wild salmon, have been particularly emphasized.

The Ocean Farming steel cage has been designed by combining knowledge from both the Norwegian petroleum and aquaculture industry. In stead of a traditional "gravity" type cage, using a flexible floating collar and clump weights to support the net, the Ocean Farming concept consist of a rigid frame supporting the net and a superstructure/wheel-house containing living quarters and rig controls. In many ways, the design has similarities

¹high-level technical computing language

to a semi-submersible platform. Just as a semi-submersible, the concept is based on having a high mass relative to the water plane stiffness. As seen in Eq. (4.1) [18], this implies large natural periods.

$$T_{ni} = 2\pi\sqrt{\frac{M_{ii} + A_{ii}}{C_{ii}}} \quad (4.1)$$

When exposed to waves, the structure will thus behave as an inertia dominated system. In an inertia dominated system, the structure under consideration is exposed to cyclic excitation forces with a substantially lower period than its natural period. Due to the large inertia of the structure, and the relatively low-period loads, the displacements will be too small for activation of any significant stiffness forces. In accordance with the dynamic equilibrium equation, Eq. (4.2), the excitation forces is then primarily balanced by inertia forces.

$$M\ddot{\mathbf{r}} + B\dot{\mathbf{r}} + C\mathbf{r} = \mathbf{F}(t) \quad (4.2)$$

In the inertia dominated region, dynamics gives favourable motion characteristics. This is visualized in **Fig. 4.1**, which is an illustration of the dynamic amplification versus the excitation load period normalized with respect to the natural period.

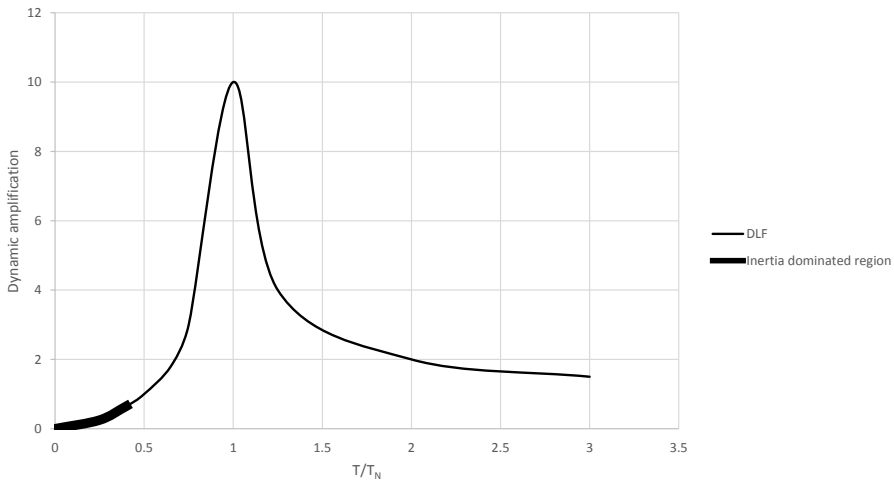


Figure 4.1: A graphical representation of the inertia dominated region meant for illustrative purposes only.

Favourable motion characteristics together with sufficient stability is the main key to ensure safe operation. When considering an aquaculture structure, one can also mention that this is important with regards to fish welfare.

4.1.1 Description of the Design

The Ocean Farming concept consists of a twelve-sided, cylindrically shaped frame with a net attached to (stretched over) the sides and bottom. This makes up the hull and the fish cage. The hull is designed to withstand environmental forces, support the superstructure and the net, ensure sufficient stability and, as described previously, minimize motions. To avoid drifting off, the structure is kept in place by eight mooring lines. Seven pontoons are located at the lowest part of the structure, six at the periphery and one in the middle. An illustration of the concept both in transit and operation is given in **Fig. 4.2**.



Figure 4.2: An illustration of the concept both in transit (upper) and operation (lower). (Illustration by SalMar/Ocean Farming)

The frame of the structure consists of several circular beams of different diameter and thickness. As mentioned in section 3.2, a circular cross-section is preferred in this situation seeing as it has a relatively low drag coefficient and favourable strength properties regarding its ability to withstand forces from the offshore environment. A selection of the concept's main dimensions are listed in **Tab. 4.1**, and should be seen in connection with **Fig. 4.3**.

The dimensions are relatively large compared to a conventional single cage fish farm. For

Table 4.1: The main dimensions of the Ocean Farming concept taken from structural drawings. (Global Maritime [21])

| Dimension | Value | Unit |
|---------------------------------------|---------|-------------------|
| Diameter | 110.0 | [m] |
| Circumference | 341.6 | [m] |
| Overall height (excl. superstructure) | 50.8 | [m] |
| Height vertical side columns | 33.0 | [m] |
| Height periphery pontoons | 13.0 | [m] |
| Height centre pontoon | 7.0 | [m] |
| Diameter periphery pontoons | 12.0 | [m] |
| Diameter centre pontoon | 17.0 | [m] |
| Operation draft | 43.0 | [m] |
| Transit draft | 8.8 | [m] |
| Volume net (approx.) | 245 000 | [m ³] |

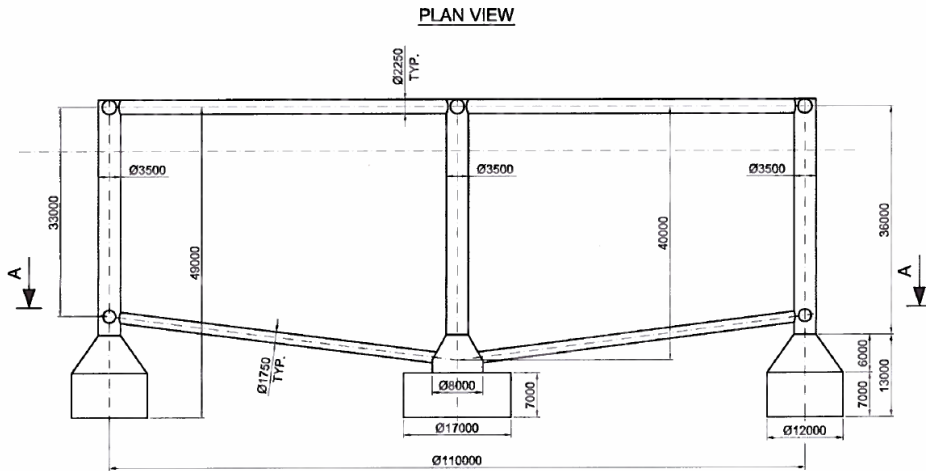


Figure 4.3: The main dimensions of the Ocean Farming concept illustrated by a cut-out of the general arrangement. (Global Maritime [21])

instance, the Ocean Farming concept has approximately twice the diameter of a typical conventional net cage. The basis for farming a huge number of fish is thus in place. This is reflected in the capacity of the concept, which is around 1.6 million salmon. However, for the concept to utilize its potential, changes in the regulations are needed. As of today, the maximum number of fish allowed in a net cage is set to 200 000 [39].

4.2 Wave and Current Loading

In our analyses, the Ocean Farming concept will be exposed to both wave and current loading. The main difference between these two types of loading is that the wave loads are dynamic forces, arising from both oscillating water particle accelerations and velocities, while the current loading is more or less a static force, arising from a constant flow of water passing through the structure. Thus, both viscous effects and potential flow effects (including wave diffraction and radiation) may be important in determining the wave-induced motions and loads on the structure, while only the viscous effects matter for the current loading, Faltinsen [18]. The latter is a consequence of the irrotational flow approximation in the potential flow theory, and applies to any non-lifting body of any shape immersed in a uniform stream (D'Alembert's paradox), Çengel and Cimbala [9].

The Ocean Farming concept mainly consists of circular, cylindrical structural members. All surface-piercing members have a small diameter, D , relative to the expected wave length, λ , of incoming waves (in ULS, a typical λ/D ratio will be around 60). Reflection and diffraction will thus be of minor importance, and *Morison's equation* can therefore be used to estimate the wave loading on the structure. The general requirement for this to be true is that the λ/D ratio is greater than 5, Pettersen [50]. This limit is seen in **Fig. 4.4** as well as the relative importance of mass, viscous drag, and diffraction forces on marine structures exposed to waves.

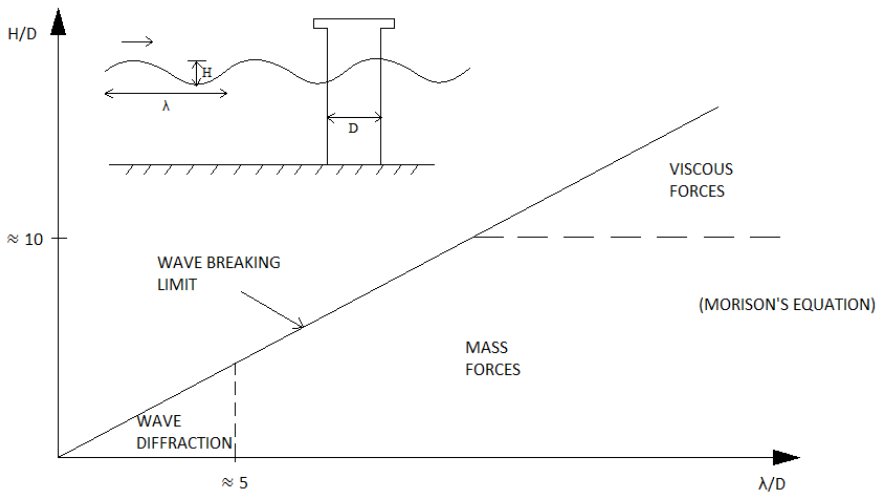


Figure 4.4: Relative importance of mass, viscous drag and diffraction forces on marine structures, based on figure in [18].

The origin of the well-known *Morison's equation* is the work of among others, J.E. Morison, a graduate student at the University of California at the time. He wanted to predict wave forces on an exposed vertical pile, see Morison et al. [43] for the complete theory. To

do this, he simply superimposed the linear inertia force (from potential theory and oscillating flows) and the adapted quadratic drag force (from real flows and constant currents) to get the following resultant force (per unit length) [27]

$$F(t) = F_{inertia}(t) + F_{drag}(t) \quad (4.3)$$

or

$$F(t) = \rho C_M \frac{\pi D^2}{4} \dot{u}(t) + \frac{1}{2} C_D D u(t) |u(t)| \quad (4.4)$$

The first term in Eq. (4.4) is the inertia force and the second term represents the drag force.

Eq. (4.4) is only valid for a fixed circular cylinder, and is therefore not applicable for calculating the hydrodynamic forces on a moving structure such as the Ocean Farming concept. It is however possible to modify Morison's equation so that it can be used on moving structures as well. For a moving circular cylinder exposed to waves and current, the Morison's equation then takes the form shown in Eq. (4.5) below (force per unit length) [18].

$$F = \rho C_M \frac{\pi D^2}{4} \dot{u}_w - \rho(C_M - 1) \frac{\pi D^2}{4} \ddot{\eta} + \frac{1}{2} C_D D u_r |u_r| \quad (4.5)$$

where

- C_M inertia coefficient
- C_D drag coefficient
- D cylinder diameter
- ρ density of water
- \dot{u}_w undisturbed water particle acceleration normal to cylinder axis due to waves
- $\ddot{\eta}$ normal component of cylinder acceleration
- u_r water part. vel. due to waves and current rel. to the cyl. normal to the cyl. axis

It should be precisely defined that the inertia coefficient, C_M , consists both of a contribution of magnitude 1 from the ambient pressure field, the Froude-Krylov force², and the coefficient of added mass, C_A , that arises due to the cylinders disturbance of the flow pattern, see Eq. (4.6).

$$C_M = 1 + C_A \quad (4.6)$$

It is important to notice that Morison's equation can not predict at all the oscillatory forces due to the effect of vortex shedding. These forces are however in general small, and

²the force introduced by the unsteady pressure field generated by undisturbed waves

tends to cancel each other out if we look at the global force acting on the whole structure. Neglecting these forces is not assumed to influence the results of our analyses in any significant way. If resonant vortex induced vibrations (VIV) were expected to occur in some structural members, this assumption would not hold.

VIV will contribute to fatigue damage accumulation, but the oscillations will also lead to an increase of drag forces, which means that the static (or average) deformation will be influenced by VIV.

Larsen [32]

For the Ocean Farming concept, VIV due to waves and current is not considered an issue.

4.2.1 Determination of Drag and Inertia Coefficients

When determining the hydrodynamic forces on a cylinder by using Morison's equation, the challenging part is determining the values of the drag coefficient, C_D , and the inertia coefficient, C_M . The values of these coefficients depends on multiple factors that influences the flow past the cylinder. The most important according to Pettersen [50] are:

1. Reynold's number, $Re = \frac{UD}{\nu}$
2. Keulegan-Carpenter number, $KC = \frac{U_W T}{D}$
3. Roughness number, $\frac{k}{D}$

When exposed to both waves and current, the relative current number, U_C/U_W , will also be important. U_C denotes current velocity and U_W denotes maximum wave particle velocity. This definition of the relative current number is only valid when the current velocity is in the same direction as waves. This will be the case in our ULS and FLS analyses.

These main factors influences the flow past the cylinder. The effect of varying Reynold's number³ and roughness ratio on the drag coefficient, C_D , is seen in **Fig. 4.5**. We see a distinct drop in the drag coefficient at certain Reynold's numbers for the different roughness ratios. If our Reynold's number is to the right (higher) of this drop, the flow is said to be in the supercritical regime. This will generally be the case for our analyses. It is observed that the roughness ratio reduces the required Reynold's number for the flow to be supercritical. For higher Reynolds numbers, the roughness generally increases the drag.

The Keulegan-Carpenter number is used as the main parameter to classify the effects of an oscillating flow past a cylinder. The difference between an oscillating flow and a steady flow past a cylinder is mainly related to effects from the oscillating wake. In RP-C205 [14], the effects of an oscillating flow on C_D is taken into account by use of an *wake amplification factor*, ψ , that is dependent upon the KC-number. This amplification factor is to be multiplied by the steady flow drag coefficient, C_{DS} , found for the flow characteristic Reynold's number and roughness ratio, see Eq. (4.7).

³ratio of inertial forces to viscous forces

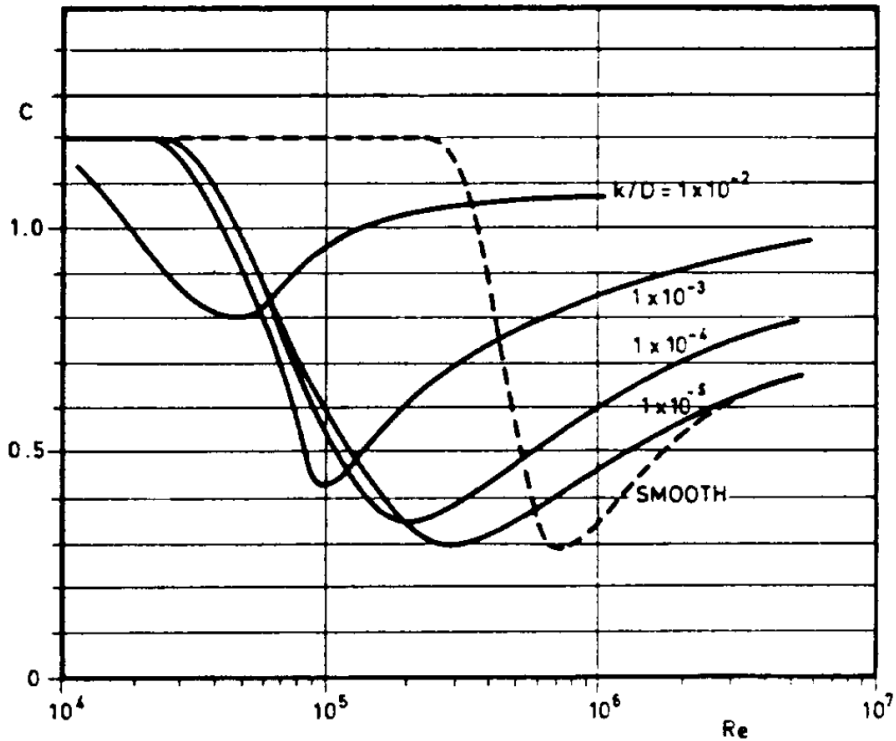


Figure 4.5: Drag coefficients for a fixed circular cylinder for steady flow in the critical flow regime, for various roughnesses. (DNV-RP-C205 [14])

$$C_D = C_{DS}\psi \quad (4.7)$$

For C_{DS} values valid in the supercritical flow regime, the effect of an oscillating flow on the drag coefficient for different KC -numbers is seen in **Fig. 4.6**.

For combined wave and in-line current action, the increase in the KC -number due to the current may according to RP-C205 [14] be taken into account by modifying the formula for KC

$$KC^* = \frac{(U_W + U_C)T}{D} \quad (4.8)$$

When $U_C > 0.4U_W$, one can, according to RP-C205, take C_D to equal C_{DS} . This will be the general case for our ULS analyses.

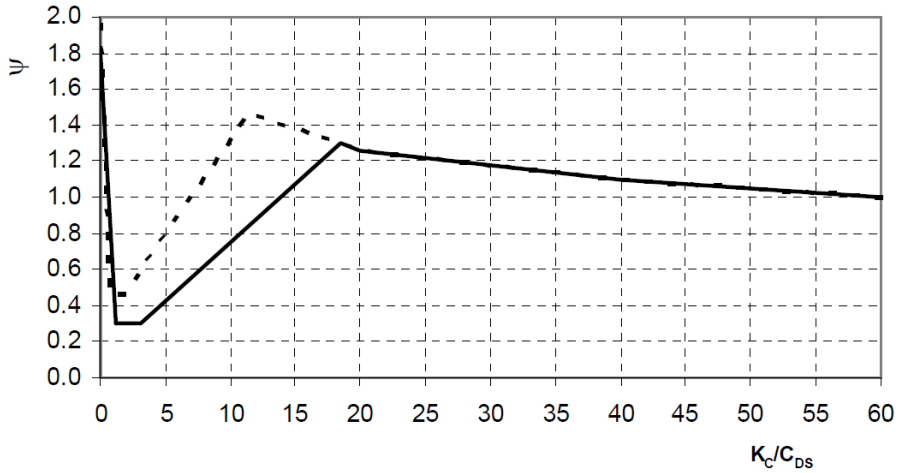


Figure 4.6: Wake amplification factor ψ as a function of KC-number for a smooth ($C_{DS} = 0.65$ - solid line) and rough ($C_{DS} = 1.05$ - dotted line) cylinder. (DNV-RP-C205 [14])

The effects on the inertia coefficient, C_M , are related to changes in the added mass coefficient, C_A , which is strongly dependent on the frequency of oscillation. In RP-C205, the added mass coefficient is given as a function of the Keulegan-Carpenter number, see **Fig 4.7**. It is observed that C_A is reduced for increasing KC-numbers until an asymptotic value is reached.

The values of C_D and C_M must be empirically determined, and are as seen above, dependent on many parameters [18]. A lot of experimental results exists in the literature, giving values for these coefficients for different Reynold's number, Keulegan-Carpenter number, roughness ratio, etcetera, see for example *Sea loads on ships and offshore structures* by Faltinsen [18]. A problem is that various parts of the structure are exposed to different flow conditions. This means that one in principle should assign different C_D and C_M values for various members to comply with the local flow conditions. For a time domain simulation, exposing the structure to an irregular sea surface generated from a wave spectrum, we complicate the problem even further as the wave heights and periods will be of a stochastic, random nature. The associated local flow conditions, and thus the *true* values of C_D and C_M , will then also be of random nature. For practical purposes, it is not possible to take this into account, and C_D and C_M must be determined based on some main wave and current characteristics. For ULS we are interested in the largest response, which typically is generated by the largest waves. Here it would be logical to base the choice of C_D and C_M on the flow characteristics of these extreme events. For fatigue (FLS), however, it is the lower and more frequent occurring sea states that are important for the fatigue accumulation, and C_D and C_M should thus be determined accordingly. This is reflected in the governing codes for marine structures, where different values for C_D and C_M are suggested for ULS and FLS. For time domain simulations, modelling the

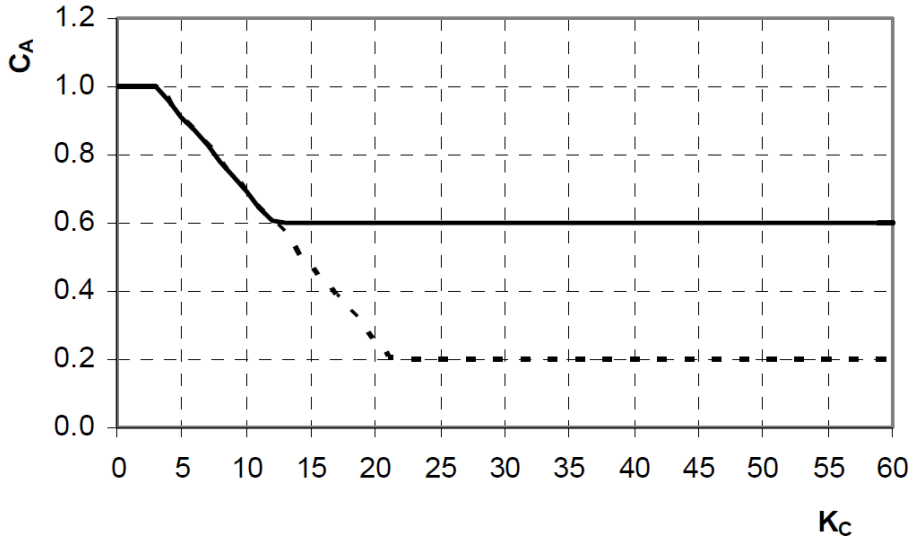


Figure 4.7: Added mass coefficient as a function of KC-number for a smooth (solid line) and rough (dotted line) cylinder. (DNV-RP-C205 [14])

sea surface elevation as a Gaussian process, NORSOK N-003 [46] states:

If the sea surface is modelled as a Gaussian process, the hydrodynamic coefficients should be calibrated to give a reasonable quasi-static load level in view of the purpose of the simulation. If extremes are under consideration, a reasonable load level should be obtained for the largest waves of the most severe sea state, while for fatigue a reasonable level for the most important fatigue accumulating waves, should be ensured.

For both the ULS and FLS, our analyses will be conducted in time domain, modelling the sea surface as a Gaussian process. For North Sea conditions, NORSOK N-003 proposes the coefficients listed in **Tab. 4.2** for slender tubular members.

Table 4.2: Proposed values for drag and inertia coefficients for North Sea conditions. [46]

| State | C_D (smooth) | C_D (rough) | C_M (smooth) | C_M (rough) |
|-------|----------------|---------------|----------------|---------------|
| ULS | 1.15 | 1.15 | 1.60 | 1.20 |
| FLS | 0.65 | 0.80 | 2.00 | 2.00 |

A member is considered smooth if it is located more than 2 meters above the free surface. The reason why the drag coefficient has the proposed value of 1.15 is to compensate for the simplified surface elevation and kinematics of the Gaussian process. This is in particular important for drag dominated structures exposed to extreme waves of the magnitudes

found in the North Sea. For calmer sea states, the error of modelling the sea surface as Gaussian is reduced, and an increase in the drag coefficient is not needed.

The Ocean Farming concept is designed to operate in far calmer waters than found in the North Sea. The basic ULS condition in which the concept is designed to operate in is described by

- $H_S = 5$ meters
- $T_P = 11$ seconds
- $U_C = 0.75$ meters per second

A characteristic diameter of a structural member is taken to be $D = 2$ meters. For these conditions the flow is in the supercritical regime and the typical relative current number, U_C/U_W is approximately 0.5. As stated earlier, since $U_C > 0.4U_W$, we will have that $C_D = C_{DS}$. This also means that the value of the added mass coefficient, C_A , can be chosen according to the asymptotic values found in **Fig. 4.7**. In the fatigue limit state however, we will apply a significantly lower current velocity and also, in general, smaller waves. This will result in a small KC-number. The values from **Tab. 4.2** for FLS therefore seems reasonable. For the main structure (not the net and the mooring lines), our choice of drag and inertia coefficients will therefore be as listed in **Tab. 4.3**.

Table 4.3: Chosen values of drag and inertia coefficients for the main hull structure on the model, for the rigid fish farm case, all members are considered rough.

| State | C_D (smooth) | C_D (rough) | C_M (smooth) | C_M (rough) |
|-------|----------------|---------------|----------------|---------------|
| ULS | 0.65 | 1.05 | 1.60 | 1.20 |
| FLS | 0.65 | 0.80 | 2.00 | 2.00 |

The drag coefficient of the net will be modelled according to net panel theory, and will be discussed later in this chapter. For the mooring lines, proposed values of C_D are found in DNV-OS-E301 [12]. This will also be discussed more in detail later. Due to the small diameter of both the mooring lines and the net, it is obvious that they will be drag dominated. For simplicity, the inertia coefficient, C_M , for these will thus be set equal to the C_M values for the ultimate limit state in **Tab. 4.3** both for ULS and FLS.

4.3 Important Modelling Considerations

In the following, important considerations regarding the build-up of our model will be discussed. The main focus is how the different parts is uniquely modelled with regards to material and hydrodynamic properties. In addition, some basic global properties of the structure will be mentioned.

4.3.1 Choice of Element Types

The USFOS analysis module is a finite element program based on an updated Lagrangian formulation.

USFOS User's Manual [57]

An updated Lagrangian formulation means that the discrete equations are formulated in the *current* structural configuration. This is in contrast to the total Lagrangian formulation, where the discrete equations are formulated with respect to the *initial* structural configuration.

The standard element in USFOS is the three-dimensional beam element, and as described above, it is based on an updated Lagrangian formulation. The element has two nodes with 6 degrees-of-freedom per node, and can transmit an axial force, two shear forces, two bending moments, and a torque. See **Fig. 4.8** for an illustration. For more detailed information about the updated Lagrangian formulation of the three-dimensional beam element, and the underlying continuum mechanics theory, reference is made to for example Bathe and Bolourchi [4].

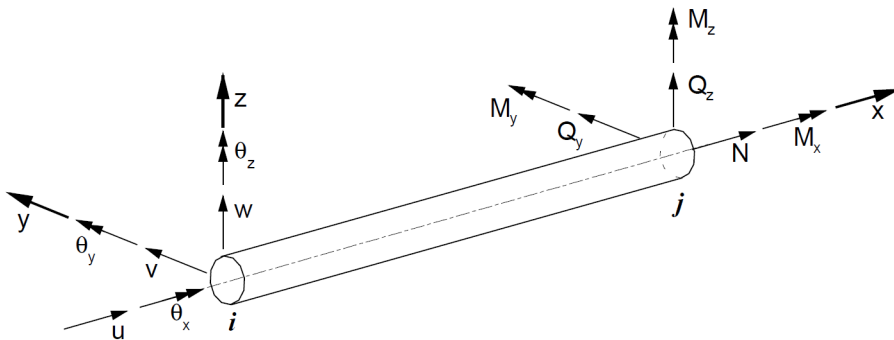


Figure 4.8: The standard three-dimensional beam element. (USFOS User's Manual [57])

In USFOS, the beam element is used to model an entire structural member; beams as well as beam columns. As a consequence of this, large structural systems can be modelled by means of a relatively small number of elements. This is a great advantage as it significantly reduces the computational resources required for analysing large structures. In USFOS one also have the option between choosing different types of beam elements. The two main options are *jacket* and *riser* elements. The jacket elements should be chosen if ultimate strength is important, while the riser⁴ elements are better for elements experiencing large elastic rotations and displacements (like a typical riser will do). As ultimate strength is not an issue (based on the work by Heiervang and Knutsen [24]), and because large elastic displacements and rotations will be present, the riser elements have been found suitable. Investigations of the structural behaviour, and correspondence with Tore Holmås (technical

⁴extension of a subsea oil well to a surface facility

support, USFOS) have also suggested that the riser elements are the best choice for our floating structure.

USFOS also offers the possibility of using shell elements. This is primarily an option for performing detailed modelling of joints and other structural discontinuities, and offers the opportunity of accounting for local effect such as dents/local buckling, surface cracks, etcetera. These components may be modelled as shell element based substructures in a global model based on beam-column theory [54]. In our model, the focus has been placed on the overall global performance, hence detailed modelling by use of shell elements have been omitted.

All members on the Ocean Farming steel cage have thus been modelled by use of the standard three-dimensional beam element, see **Fig. 4.8**. For the net and mooring lines, this will cause an unrealistically large compression and bending stiffness. However, this is not expected to cause any errors of significance seen from a global perspective. As the main load-carrying structure have similar geometries as to a jacket, beam elements is believed to be a good choice for these members. According to for example Amdahl [2], jackets are usually modelled using beam elements.

Regarding the fatigue analysis, detailed modelling of the tubular joints using shell elements could have been performed if we had not been pressed for time. This is however very time consuming work and requires detailed drawings of the joints. The advantage is, as mentioned in section 3.2, that the local stress ranges which governs the fatigue life, are found directly, without the use of stress concentration factors. We will however base the fatigue analysis on multiplying the forces/moments found from the global beam model by appropriate stress concentration factors.

4.3.2 The Hull Structure

The entire hull is modelled as tubular beams. The construction material is NV-36 steel with basic mechanical properties listed in **Tab. 4.4**. By *the hull* we mean all columns, braces, and beams in addition the pontoons. An illustration of the modelled hull is seen in **Fig. 4.9**.

Table 4.4: Material data chosen for the hull structure elements.

| Property | Symbol | Value | Unit |
|-----------------------|------------|-------|----------------------|
| Modulus of elasticity | E | 210 | [GPa] |
| Yield strength | σ_y | 355 | [MPa] |
| Poisson's ratio | ν | 0.3 | [-] |
| Density | ρ | 7850 | [kg/m ³] |

Our focus have been on modelling the structure as correctly as possible in accordance with information and structural drawings received from Global Maritime. To be able to attach the net to the hull, all main beams, columns, and braces have been divided into 10 elements. When modelling the hull, the following principal points have been kept in mind:

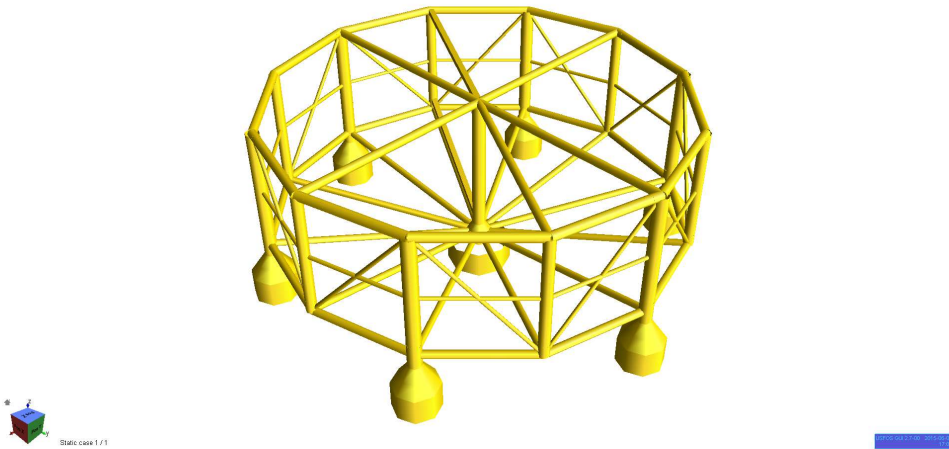


Figure 4.9: A screenshot of the model (only the hull) from USFOS’s graphical user interface.

1. The diameter, thickness, and weight of the members should be modelled as correctly as possible, especially for critical parts. Simplifications could be introduced to less critical parts as long as the overall performance is considered acceptable.
2. The diameter and thickness of members facing joints should be 100 percent in accordance with the structural drawings to ensure correct stresses in these regions. This is in particular important for the FLS analyses.
3. If the midspan of a beam is divided into sections with different thicknesses, an equivalent thickness is introduced, giving the correct weight.
4. Ring stiffeners are present. These are modelled as “smeared” and included in the equivalent thickness at the midspan of the beams to get the correct weight.
5. The concept of introducing an equivalent thickness giving the desired total weight also applies for the modelling of the pontoons as they consists of a lot of internal bulkheads and stiffeners.

Based on the above, a typical configuration of the pipe thickness of a construction detail is as shown in **Fig. 4.10**. The colors indicate the varying thickness along the members.

As seen from **Fig. 4.10**, the thickness of the member endings facing the joints have been assigned the *real thickness*, corresponding to the thickness in the structural drawings, while the midspan of the beams have been assigned an *equivalent thickness* to get the correct total weight. As all beams, columns, and braces have been split into 10 individual elements/sections, the typical situation is thus that the two end elements have the correct properties, while for the eight mid-elements some minor simplifications have been introduced. For some members, the end elements also have a slightly different diameter. A complete list

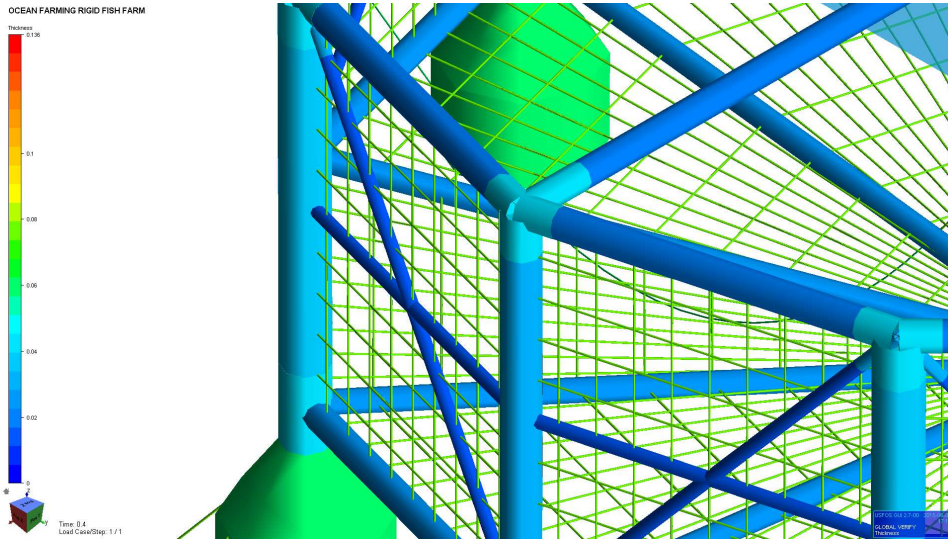


Figure 4.10: Illustration of varying pipe thickness on the hull along various members at an intersection.

of the dimensions of the different parts on the hull is listed in **Tab. 4.5**.

Table 4.5: A complete list of dimensions of the structural parts on the hull in our model.

| Segment | D_{mid} | D_{end} | t_{mid} | t_{end} | L |
|----------------------------|-------------|-------------------|-----------------|-----------------|------|
| Centre column | 3.56 | 3.58 ¹ | 32 | 40 ¹ | 37.0 |
| Vert. columns above pont. | 3.56 | 3.58 | 34 | 40 | 33.0 |
| Vert. intermediate columns | 2.80 | 2.83 | 30 | 40 | 33.0 |
| Bot. radial beams | 1.75 | 1.75 | 23 | 23 | 55.4 |
| Bot. outer ring beams | 2.05 | 2.05 | 24 | 24 | 28.5 |
| Top outer ring beams | 2.29 | 2.33 | 18 | 40 | 28.5 |
| Top cross beams | 2.05 | 2.08 | 18 | 40 | 55.0 |
| Mid. outer ring beams | 1.00 | 1.00 | 15 | 15 | 28.5 |
| Outer diag. supports | 1.00 | 1.00 | 15 ² | 30 ² | 43.6 |
| Centre pont. | 17.0 | 17.0 | 137 | 137 | 7.0 |
| Centre pont. cone/joint | 8.0 – 3.56 | 8.0 – 3.56 | 137 | 137 | 5.0 |
| Side pont. cylinder part | 12.0 | 12.0 | 62 | 62 | 7.0 |
| Side pont. cone part | 12.0 – 3.58 | 12.0 – 3.58 | 62 | 62 | 6.0 |
| Dimension | [m] | [m] | [mm] | [mm] | [m] |

¹ only at top end

² deviates slightly from updated drawings

Moveable bulkhead

The Ocean Farming concept is equipped with a moveable bulkhead which can be used for different purposes. Examples are forcing the fish into closed quarters, making it easy for a wellboat to extract the fish for slaughter, and cleaning of the net. The moveable bulkhead constitutes a quite significant weight, and will in addition to attract loads from the environment, give a buoyancy contribution. As it is not fixed, it is reasonable to believe that the global stiffness contribution from the bulkhead will be limited. It should thus be modelled so that it's weight and load contributions are included, while it's global stiffness contribution is kept low. The solution is to use the NONSTRU-command in USFOS. This record is used to specify non-structural beam elements (passive elements). Such elements are excluded from the global stiffness formulation, while the attracted loads are kept. For simplicity, the moveable bulkhead is modelled as two beams with a quadratic box geometry with a width and height of 1.5 meters. The thickness is taken so that the total weight is conserved. See **Fig. 4.11** for an illustration.

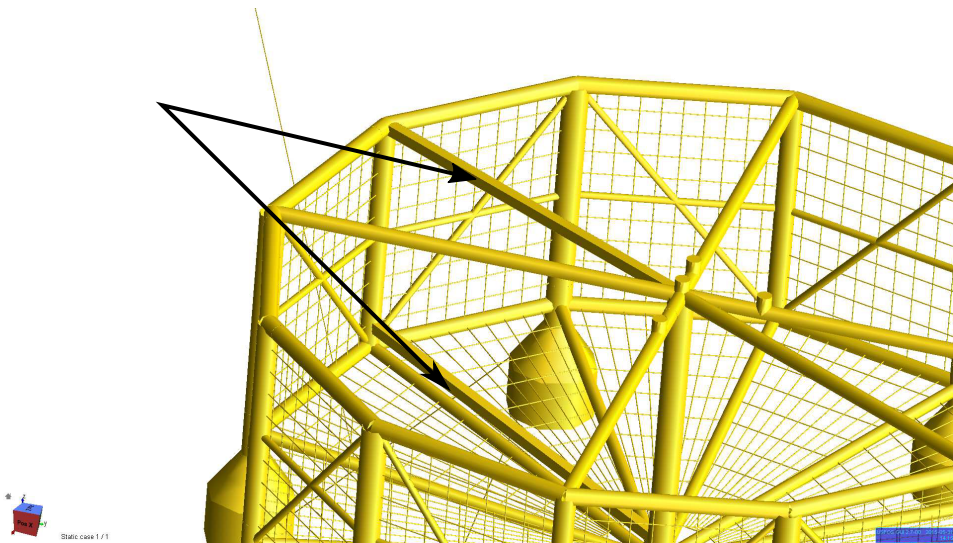


Figure 4.11: The moveable bulkhead, modelled as two square non-structural members, is marked with arrows.

4.3.3 The Mooring Lines

To avoid drifting off, a permanent spread mooring system will be attached to the structure. The two most typical spread mooring systems are catenary line mooring and taut line mooring. Catenary mooring lines are usually made up of chain or steel wire, while taut mooring lines are made up of light weight fibre ropes. For the line profiles, the main difference between a catenary mooring and a taut leg mooring, is that where the catenary mooring touches down at the seabed horizontally, the taut leg mooring arrives at the seabed

at an angle. This means that in a taut leg mooring system, the anchor point has to be capable of resisting both horizontal and vertical forces, while in a catenary mooring system the anchor point is only subjected to horizontal forces [59]. An illustration of both concepts is seen in **Fig. 4.12**. The main task of the mooring lines is to reduce the horizontal offset of the floating structure to an acceptable limit by providing restoring forces. In a catenary mooring system, most of the restoring forces are provided by the *geometric stiffness* of the line. This geometric stiffness is generated by the weight (or buoyancy) of the mooring line. In a taut leg mooring system, the restoring forces are mainly provided by the *elastic stiffness* due to axial line elongation.

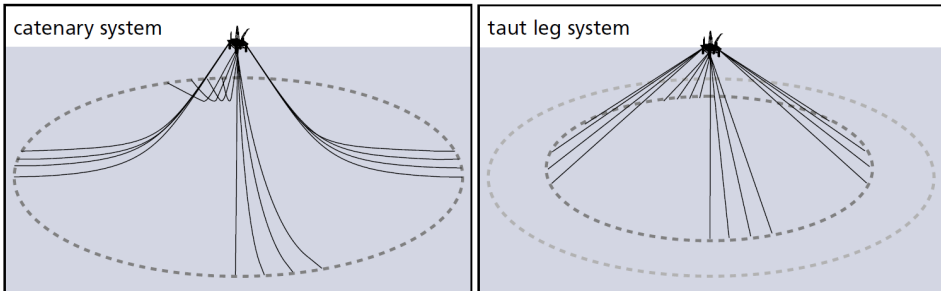


Figure 4.12: An illustration of the difference between a catenary- and a taut leg mooring systems. (Vryhof Anchors [59])

The Ocean Farming concept will be held in place by eight mooring lines, forming a symmetric spread with a 45 degree angle between each line. All eight mooring lines have the same properties. The chosen mooring type is a catenary chain concept with a fibre rope insert at the top. This means that a single mooring line consists of two parts, one part made of 88 mm steel chain and one part made of 160 mm fibre rope. Such multi-component lines give an optimal combination of stiffness and total weight [27]. The total length of each mooring line is 1100 meters. The properties of the mooring lines, including information on top tension and site specific water depth, is shown in **Tab. 4.6**. This information have been provided by Global Maritime.

Table 4.6: Miscellaneous properties of the mooring lines, supplied by Global Maritime.

| Property | Chain | Fibre | Dimension |
|----------------------------|--------|--------|-----------|
| Length | 1000 | 100 | [m] |
| Diameter | 88 | 160 | [mm] |
| Axial stiffness, EA | 680.81 | 235.44 | [MN] |
| Minimum breaking load, MBL | 7051.4 | 8122.7 | [kN] |
| Submerged weight | 147.0 | 4.0 | [kg/m] |
| Top tension | 196.2 | | [kN] |
| Water depth at site | 150 | | [m] |

As USFOS originally is intended for analyses of fixed offshore structures, there is no built-

in option for easy modelling of mooring lines. Due to this, the lines have been modelled in a simplified manner by application of tubular beam elements. The geometry and mechanical properties of these beam elements were chosen to best match the properties of the real mooring lines (Tab. 4.6). For the chain part of the mooring line, an equivalent diameter was used, giving the same cross-sectional area as the typical chain cross-section. Since the mooring lines are modelled as tubular beams, a thickness must also be given. The density is calculated so that the lines will have the same submerged weight as specified in **Tab. 4.6**, and the yield strength is taken as the axial stress over the cross-section area giving the specified minimum breaking load (MBL). The mooring line properties used in our analyses is given in **Tab. 4.7**.

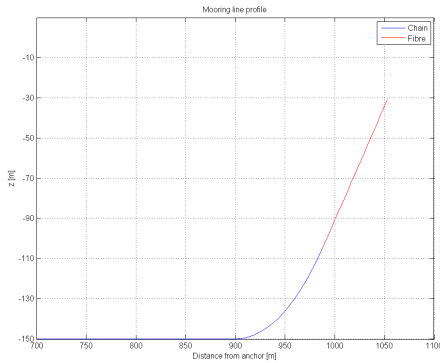
Table 4.7: Calculated and chosen properties of the modelled mooring lines.

| Property | Chain | Fibre | Dimension |
|-----------------------|--------|-------|----------------------|
| Total length | 1000 | 100 | [m] |
| Element type | beam | beam | |
| Geometry | pipe | pipe | |
| Element length | 5 | 5 | [m] |
| Number of elements | 200 | 20 | |
| Diameter | 124.5 | 160.0 | [mm] |
| Thickness | 61.2 | 79.0 | [mm] |
| Modulus of elasticity | 60.0 | 11.7 | [GPa] |
| Yield strength | 580 | 404 | [MPa] |
| Density | 13 110 | 1224 | [kg/m ³] |

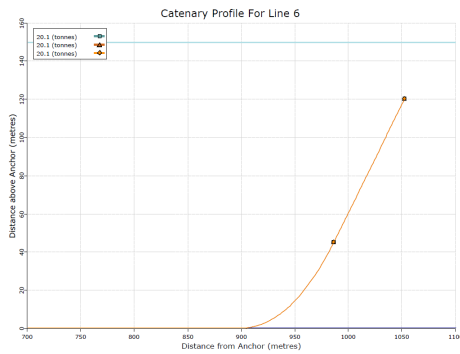
Another problem related to the modelling of the mooring lines, is that the initial catenary profile, giving line equilibrium, is not known in advance. This equilibrium is governed by the initial top tension, the water depth, the line length, the axial stiffness of the line, and the weight (kg/m) of the line. To solve this problem we first had to model the mooring line by laying it flat on the sea bed. Compression springs were used to model the sea bottom, and the line element length was set according to **Tab. 4.7**. We then did an analysis where the correct top tension was applied at the top node of the mooring line. The line was then pulled up during the analysis, forming the catenary profile giving line equilibrium. The coordinates of all the nodes were dumped to a file at the end of the analysis for further input in the complete modeller⁵. As the mooring spread is symmetric with equal line properties, this profile was used as a basis for the modelling of all the eighth mooring lines in the total model. An illustration of our obtained catenary profile compared to the catenary profile received from Global Maritime is found in **Fig. 4.13a** and **4.13b**. If one looks closely at the axes, it can be seen that the catenary profile obtained from USFOS is approximately identical to the one from Global Maritime. This indicates that our simplified way of modelling the mooring lines in USFOS is sufficient for this purpose.

As mentioned, the catenary profile from **Fig. 4.13a** has been used as the basis for modelling all the eight mooring lines in the total model. This was done by translating and

⁵model-writing script



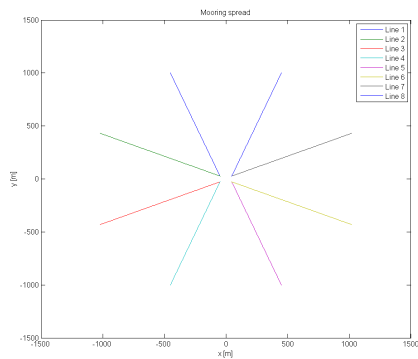
(a) From our analysis.



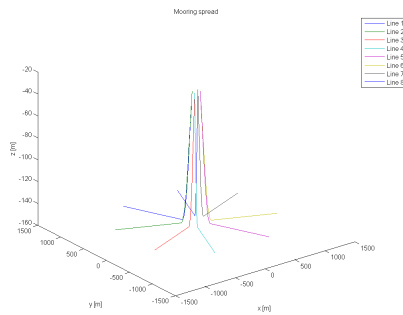
(b) Catenary profile from GM.

Figure 4.13: Comparison between our resulting "pull-up" analysis and catenary profile supplied by Global Maritime.

rotating this profile, in and to the desired directions and positions. The mooring lines are attached to the hull in pairs at the top of four of the side pontoons. A top view of the resulting mooring spread is seen in **Fig. 4.14a**, and a three-dimensional plot is found in **Fig. 4.14b**.



(a) Top view.



(b) Three dimensional view.

Figure 4.14: All 8 resulting mooring lines combined.

Modelling of the sea floor is obviously important for doing a realistic simulation. However, no easy way of specifying a sea floor exists in USFOS. This has been solved by attaching springs with special properties to all mooring line nodes. For the mooring line elements initially laying on the sea bottom, a combination of *compression* and *friction springs* have been used. The compression springs holds the lines in place when vertical compression forces are present, but gives no resistance for line up-lift, while the friction springs provide

frictional resistance in the horizontal plane when normal forces between the seabed and the mooring lines exists. The friction coefficient is set to 0.7 (chain) in accordance with the modelling "manual" by Vryhof Anchors [59], and should give a reasonable representation of the frictional resistance of the part of the mooring line that is laying on the seabed. For the part of the mooring lines that initially is above the seabed, another modelling strategy had to be carried out. The challenge here is to model the seabed touchdown of the lines, occurring on the leeside of the mooring system when the structure is exposed to current. This has been solved by attaching custom compression springs to these line nodes that only activates if the node reaches the seabed. In practice this means that a unique spring has been assigned to each of these nodes.

The drag coefficient of the fibre and chain part the mooring lines has been set according to specified values in DNV-OS-E301 [12]. The inertia coefficients have been set equal to the coefficient used for the hull members in the ultimate limit state. Values are found in **Tab. 4.8**.

Table 4.8: Chosen drag and inertia coefficients for the mooring lines.

| Property | Symbol | Chain | Fibre |
|---------------------|--------|-------|-------|
| Drag coefficient | C_D | 2.4 | 1.6 |
| Inertia coefficient | C_M | 1.2 | 1.2 |

4.3.4 The Cage Net

As the net is the only barrier keeping the farmed fish inside, and predators outside, it is the most critical piece of equipment on a cage farm that prevents fish escapes and other fish losses. Fish escapes is most unwanted, both seen from an economic and an environmental perspective, so the net should be of high quality. For conventional fish farms, the net is usually made of some sort of fibre material, such as nylon. For the Ocean Farming concept, the chosen net type is called *EcoNet*. The *EcoNet* is made of ethylene terephthalate (PET), offering both good mechanical properties as well as low weight, and has an expected lifetime of 20 years. As PET is stiffer than conventional fibre nets, the deformation of the net due to environmental actions becomes significantly reduced. In addition, the shape of the *EcoNet* wire mesh is designed with redundancy in mind, intended to remain intact if a single wire is cut. An illustration of the *EcoNet* mesh is shown in **Fig. 4.15**.

The net comes in two different sizes, *small* and *large*. For the Ocean Farming concept, the small net size has been chosen. The values of the lengths referred to in **Fig. 4.15** for both mesh sizes are found in **Tab. 4.9**.

The net consists of millions of individual threads and twines. Correct modelling of this means a huge amount of elements. For the global response analysis, this is not feasible due to the enormous computational time and resources such a model would have required. A simplified model of the net with a much coarser mesh has thus been applied to keep the computational time within reason. As this coarse mesh will reduce the viscous forces

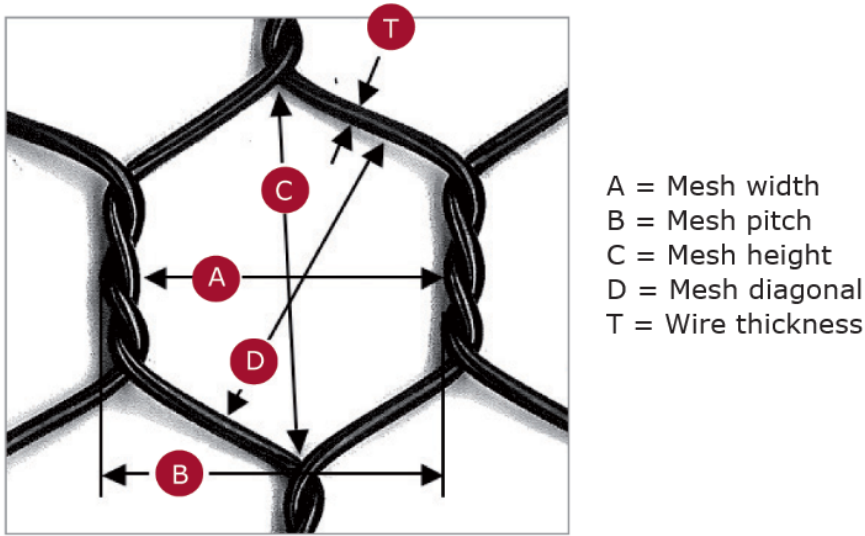


Figure 4.15: Illustration and dimensional explanation of one single mesh in the EcoNet. (www.akvagroup.com)

Table 4.9: EcoNet mesh sizes, with reference to Fig. 4.15.

| Mesh size | T [mm] | A [mm] | B [mm] | C [mm] | D [mm] | Weight [g/m ²] |
|-----------|--------|--------|--------|--------|--------|----------------------------|
| Large | 3.0 | 45 | 50 | 71 | 59 | 590 |
| Small | 2.5 | 35 | 40 | 43 | 37 | 570 |

acting on the net, a scaled drag coefficient is necessary to compensate for this reduction. An important effect we have been trying to model, is the change in total drag force on a net panel relative to the angle of incoming current velocity. It is quite easy to understand that such an effect is present if one imagine holding a net panel *normal* to a current and a net *parallel* to the current. It is obvious that the net panel parallel to the flow will be exposed to significantly lower forces than the net facing the current. In the following some theoretical background regarding forces on net panels will be addressed. Further on, our way of modelling the net will be discussed.

The *current force model* developed by Løland [36], briefly described in section 2.3.1, have been used as a basis for determination of the drag coefficients of our modelled net. The main assumption in this method is that the net cage can be divided into several *net panels*, and the method aims to provide a good estimate for the total force acting on each of these net panels. Based on the structural layout, the way the net have been attached to the structure, and the semi-rigid net type (EcoNet), this is seen as a reasonable assumption. The method looks at both drag and lift forces acting on the net panels. The lift forces have however been neglected, seeing as they will be of minor importance relative to the drag

forces, and will not be discussed further.

The *current force model* is based upon the assumption that the mean drag forces on a net panel can be written as

$$F_{D,panel} = \frac{1}{2}\rho C_{D,panel}(\alpha)AU^2 \quad (4.9)$$

where

| | |
|---------------|---|
| $C_{D,panel}$ | drag coeff. whole net panel as a func. of angle bet. net normal and flow dir. |
| A | area of the net panel |
| U | current velocity |
| ρ | density of water |
| α | angle bet. the flow dir. and the net normal vector in the dir. of the flow |

It is important to not mix the net panel drag coefficient, $C_{D,panel}$, with the element drag coefficient used in Morrison's equation (Eq. 4.4).

The drag coefficient is a function of the solidity ratio, Sn , mesh type, and the Reynold's number, Re . So it is not possible to find a general expression for C_D as a function of Sn and Re valid for all combinations of these parameters.

Løland [36]

Based on model experiments, the solidity ratio has been seen as the most important parameter describing the drag coefficient of a net panel. Løland has thus estimated the following functional relationship for determination of the drag coefficient, known as *Løland's formula*

$$C_{D,panel} = 0.04 + (-0.04 + 0.33Sn + 6.54Sn^2 - 4.88Sn^3) \cos \alpha \quad (4.10)$$

The factor 0.04 was introduced to take into account the drag on a net panel parallel to the flow. As seen, directional dependent drag coefficients for the net panel can be obtained by use of this formula. The solidity ratio is defined as the ratio between the area covered by the threads in the screen and the total area of the screen, see **Fig. 4.16** for an illustration. For a square screen/mesh with diameter D and mesh size λ , the solidity ratio takes the following form

$$Sn = \frac{A_{threads}}{A_{screen}} = \frac{2D}{\lambda} - \left(\frac{D}{\lambda}\right)^2 \quad (4.11)$$

An additional effect that must be accounted for when looking at the whole net cage, is the shielding effect from the net panels upstream, facing the current. This leads to a reduced incident current velocity for the net panels downstream. Løland [36] has suggested the following formula for this velocity reduction factor, r

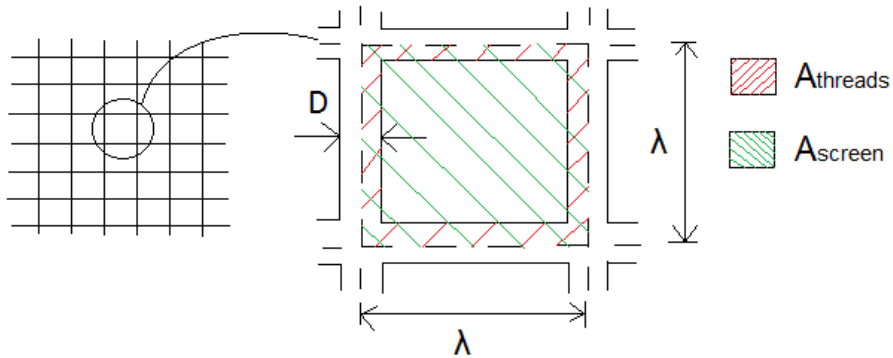


Figure 4.16: Illustration of solidity ratio parameters for a square screen/mesh.

$$r = \frac{u}{U_\infty} = 1.0 - 0.46C_{D,panel} \quad (4.12)$$

For our model, we have divided the net into a total of 24 net panels. This follows from the 12 sided cylindrical shape of the structure, giving 12 net panels on the sides, and 12 for the bottom. See **Fig. 4.17** for an illustration of the model with the net structure included.

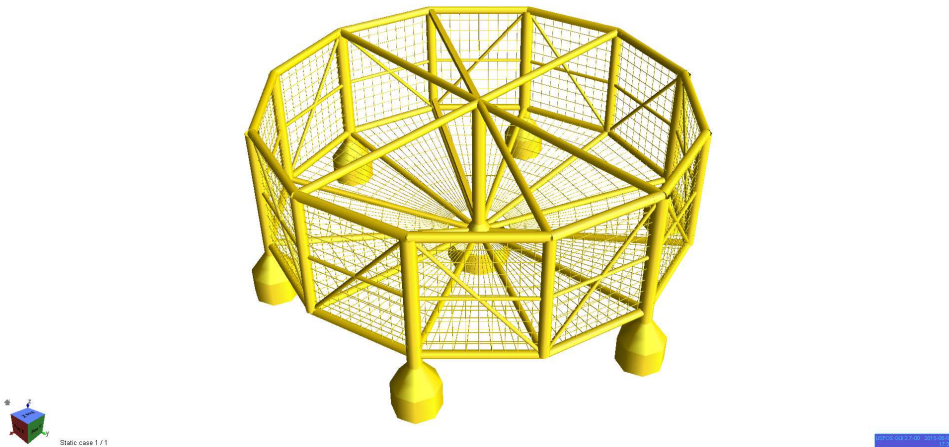


Figure 4.17: A screenshot of our modelled net attached to the hull structure.

The current force model gives us global directional dependent drag coefficients for a net panel in accordance with Eq. (4.9). As USFOS uses a Morison model for calculation

of hydrodynamic forces, these global drag coefficients must be converted into equivalent drag coefficients on an element level, giving the same total drag force on the net panel. The procedure used for assigning directional dependent drag coefficients to the modelled net elements in USFOS is described by the following points:

1. Directional dependent drag coefficients are assigned with respect to the element's local coordinate system, following a right hand system where the local x-axis always goes from node 1 to node 2. For consistent modelling, the direction of the local z-axis must be defined for each net element. By assuming small deflections in the net, the local z-axis is defined as the normal vector of the net panel, and assigned to all net elements forming the given panel. The y-axis then follows from the x- and z-axis. Reference is made to **Fig. 4.18**.
2. By using Eq. (4.10), the drag coefficient for the real net panels, $C_{D,panel}$, is calculated for different flow angles, α , (see Fig. 4.19) based on the given solidity ratio for the real net, $Sn_{real} = 0.157$. For $\alpha = 0$ we get $C_{D,panel} = 0.194$.
3. The solidity ratio for the modelled net, Sn_{model} , must be calculated based on the hydrodynamic diameter of the modelled net elements. As the layout of the modelled side and bottom net is different, we get one solidity ratio for the side net and one for the bottom net, called Sn_{side} and Sn_{bottom} respectively.
4. The directional dependent drag coefficient to be used in Morison's equation for a net element located at a given net panel is then calculated as

$$C_{D,element}(\alpha) = \frac{C_{D,panel}(\alpha)}{Sn_{model}} \quad (4.13)$$

5. The directional dependent drag coefficients must be converted to match the local angle definition in USFOS. USFOS defines the angle, θ , as shown in **Fig. 4.18**. $\theta = 0$ represents a current flowing towards the local y-axis.
6. A current blockage factor is assigned to all elements affected by shielding according to Eq. (4.12). This gives a current blockage factor of approximately 0.9.

The net elements are modelled as tubular beam elements. Due to the large drag coefficient assigned to these elements from the procedure described above, these elements have to be modelled with severely increased strength properties relative to the threads in the real net to avoid too large incremental rotations in the USFOS simulations (leads to numerical instability, causing abortion in the analysis). This means that the net elements have been modelled with an increased *structural* diameter, an increased E-modulus, and increased yield strength. This will introduce additional stiffness to the global model. However, as both the structural diameter and the E-modulus of the modelled net elements are significantly smaller than for the hull members, this contribution is considered negligible. The *hydrodynamic* diameter of the modelled net, used in connection with drag- and mass forces according to Morison's equation, is on the other hand defined in accordance with the real net diameter. Information about the modelled net and the properties of the net elements are found in **Tab. 4.10**. The calculated solidity ratios are based upon the hydrodynamic diameter of the net elements.

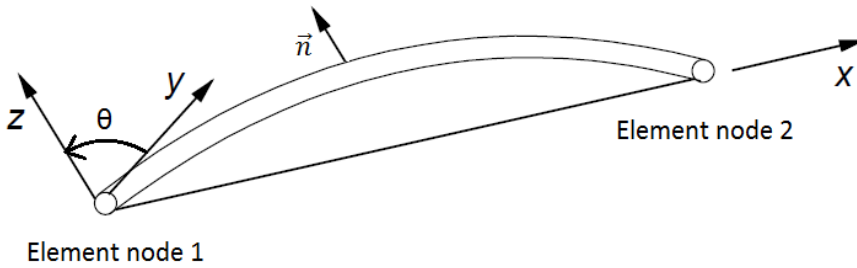


Figure 4.18: Illustration of the local coordinate system and the local angle definition, θ , used in USFOS. The local z-axis is defined in the direction of the net panel normal vector, \vec{n} , based on figure in [57].

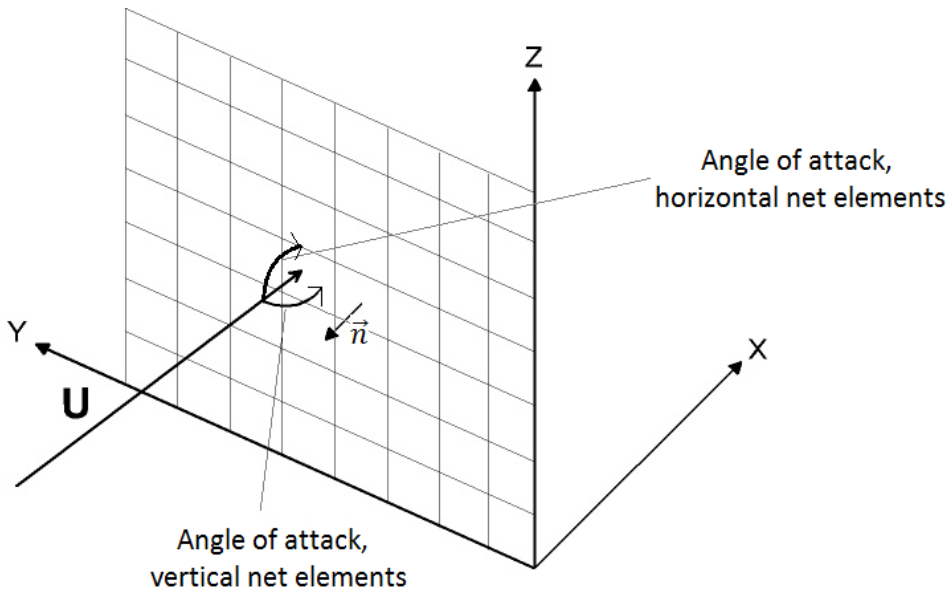


Figure 4.19: Definition of angle of attack, α , for a plane net structure. To obtain correct drag forces, different definitions of α for vertical and horizontal elements must be introduced, based on figure in [20].

The thermal expansion coefficient have been defined seeing as all net elements have been exposed to a temperature field, reducing the element temperature by 1 degree Celsius. This shrinks the elements to 0.1 percent of their original size, introducing a pre-tension in the net. This has been done to avoid compression forces in the net elements as the threads in the real net have negligible compression strength. The directional dependent drag coefficients assigned to the net elements at the side and the bottom of the net is found in **Tab. 4.11**. The angle of attack, α , is defined according to **Fig. 4.19**. The inertia

Table 4.10: Modelled properties of the net panels and the net elements.

| Property | Value | Unit |
|---------------------------------|---------|----------------------|
| Mesh size side net panel | 10 x 10 | [-] |
| Mesh size bottom net panel | 10 x 10 | [-] |
| Solidity ratio side net panel | 0.0019 | [-] |
| Solidity ratio bottom net panel | 0.0019 | [-] |
| Structural diameter | 150 | [mm] |
| Hydrodynamic diameter | 2.5 | [mm] |
| Thickness | 74 | [mm] |
| E-modulus | 40 | [GPa] |
| Density | 1025 | [kg/m ³] |
| Yield strength | 3550 | [MPa] |
| Thermal expansion coefficient | 0.001 | [1/K] |

coefficient, C_M , have been set equal to 1.2 for all elements.

Table 4.11: Directional dependent drag coefficients assigned to the net elements, the coefficients are symmetric about the net panel plane, and α is defined according to Fig. 4.19.

| Angle of attack, α [deg] | $C_{D,side}$ | $C_{D,bottom}$ |
|---------------------------------|--------------|----------------|
| -90 | 26.7 | 21.1 |
| -75 | 53.3 | 42.1 |
| -60 | 78.0 | 61.7 |
| -45 | 99.3 | 78.5 |
| -30 | 115.7 | 91.4 |
| -15 | 125.9 | 99.5 |
| 0 | 129.4 | 102.3 |
| 15 | 125.9 | 99.5 |
| 30 | 115.7 | 91.4 |
| 45 | 99.3 | 78.5 |
| 60 | 78.0 | 61.7 |
| 75 | 53.3 | 42.1 |
| 90 | 26.7 | 21.1 |

A screen dump from USFOS, illustrating the directional dependent drag coefficient on a part of the side net of the model is seen in **Fig. 4.20**.

4.3.5 Hydrodynamic and Structural Damping

Damping designates the ability of a structure to dissipate kinetic energy, that is, to transform it into other types of energy such as heat or radiation (of water

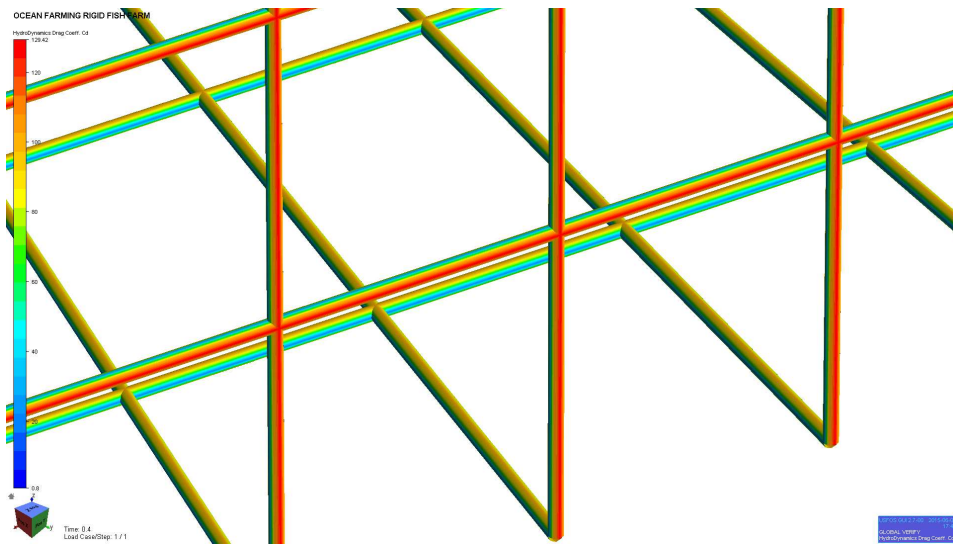


Figure 4.20: Directional dependent drag coefficients as it appears in USFOS, red indicates maximum drag while blue indicates minimum drag.

waves, sound waves, etcetera). For a real vibration system, there will always be damping present so that the kinetic energy of the system will decrease if no external energy is supplied.

Langen [31]

Finding the correct damping is a well known problem in dynamic analyses of structures. A number of different types of damping may be present, and correct modelling of this damping is in general difficult. Due to this, simplified models are therefore introduced, which for many applications yields satisfactory solutions [31].

For a structure exposed to current and waves, the effective damping consists of a combination of hydrodynamic and structural damping. Hydrodynamic damping arises from the part of the pressure *from* the fluid *on* the structure in-phase with the velocity of the structure [31]. This damping is usually assumed to be composed of two parts. One linear part caused by some of the kinetic energy being transformed into wave energy, and one nonlinear part, the so-called *drag damping*, arising due to viscous effects. The structural damping refers to the damping of the structural material itself and damping in connections/intersections between the elements in the structure. In our case, drag damping and structural damping will be of particular interest. The drag damping enters the equation system in USFOS directly through the drag part of Morison's equation, while the structural damping is included as a proportional damping (Rayleigh damping). For a stiff floating structure like the Ocean Farming concept, it is important to realize that it is mainly the hydrodynamic damping that affects the global response, while the structural damping mainly affects the local response of an individual member.

The model tests performed by MARINTEK proved that significant damping was present. Free decay tests showed relative damping levels of roughly 30 percent in surge and sway and about 10-15 percent in heave, roll and pitch. Further, two surge decay tests were performed with current. These showed that the fish farm was over-critically damped in current of 0.25 and 0.50 meters per second. The drag damping from the mooring lines and the net is assumed to be the main contributions to these high damping levels. Free decay tests performed in USFOS have also indicated high damping levels.

As mentioned, a proportional damping relation has been used to model the structural damping. In the proportional damping model, frequently referred to as *Rayleigh damping*, the structural damping is assumed to be proportional to the mass- and stiffness matrix of the system, see Eq. (4.14).

$$\mathbf{C} = \alpha_1 \mathbf{M} + \alpha_2 \mathbf{K} \quad (4.14)$$

If we know the damping ratio for two frequencies, in the response domain of interest, α_1 and α_2 can be determined according to Eq. (4.15) and (4.16).

$$\alpha_1 = \frac{2\omega_1\omega_2}{\omega_2^2 - \omega_1^2}(\lambda_1\omega_2 - \lambda_2\omega_1) \quad (4.15)$$

$$\alpha_2 = \frac{2(\omega_2\lambda_2 - \omega_1\lambda_1)}{\omega_2^2 - \omega_1^2} \quad (4.16)$$

As we did not know the real structural damping ratio for any frequencies, typical values for steel structures had to be selected. For the mooring lines, higher damping values than for the rest of the structure were assigned. The arguments for this is that additional frictional resistance between the individual links in the chain will be present in addition to a different material behaviour for the fibre part. The damping levels were selected at periods 3.3 and 100 seconds. See **Tab. 4.12** for detailed information.

Table 4.12: Selected damping levels and proportional damping coefficients used in the analyses.

| Property | Structure | Mooring lines |
|-------------|-----------|---------------|
| ω_1 | 0.063 | 0.063 |
| ω_2 | 1.885 | 1.885 |
| λ_1 | 0.05 | 0.05 |
| λ_2 | 0.02 | 0.05 |
| α_1 | 0.0062 | 0.0061 |
| α_2 | 0.0195 | 0.0513 |

The resulting Rayleigh damping used in the analyses is found in **Fig. 4.21**. It is seen that for the structure, the relative damping is between 1-2 percent in the wave period regime (3-20 seconds), while for the mooring lines a somewhat higher damping is seen in this region, ranging from 2-5 percent. Both are seen as conservative estimates.

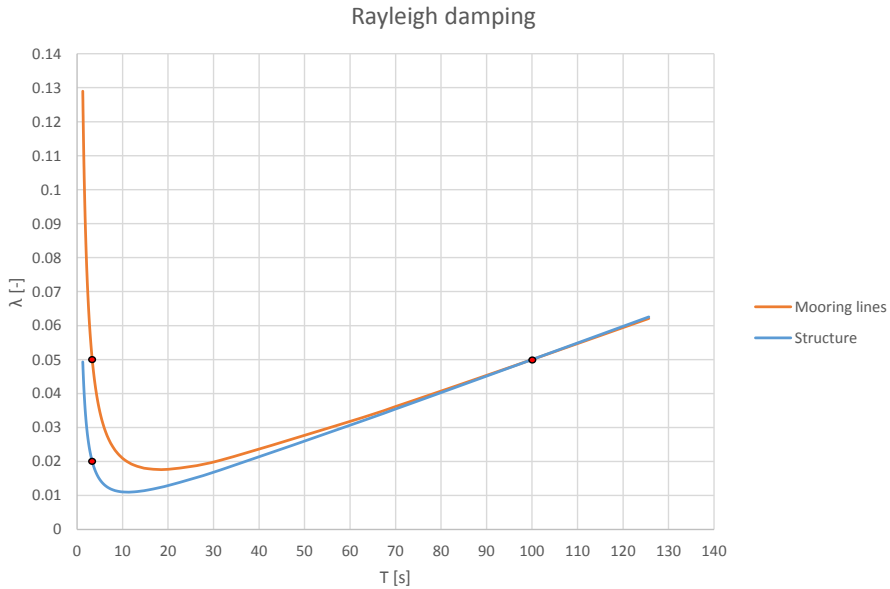


Figure 4.21: Chosen values of proportional damping for the structure and mooring lines used in the analyses are marked as points on the lines.

Analyses of the natural periods of the structure, investigating the effect of different structural damping levels, have been performed. The results showed that the structural damping had little to no effect on the natural periods. This is as expected, seeing as it is mainly the hydrodynamic damping that has influence on these periods. As a final remark it should be said that the damping is in particular important for reduction of resonant motions, Larsen [33].

4.3.6 Distributed and Applied Mass

The mass is one of the governing parameters regarding a floating structure's motion characteristics and stability. A correct representation of the mass of the structure is therefore important to ensure realistic behaviour of the model in our analyses.

Global Maritime operates with several different load cases for the Ocean Farming concept. The differences primarily relates to changes in the vertical center of gravity (VCG) and the draught of the structure. We have chosen to use "Load case 1" as the basis for our mod-

elling. Load case 1 is chosen as it is the in-operation condition with the highest vertical centre of gravity due to full fish feed tanks. As an increase in vertical centre of gravity generally leads to reduced stability, it is expected to be the in-operation load case where the largest responses are seen. Since only the main structure of the fish farm has been modelled in USFOS, all mass contributions from equipment, superstructure, tanks, etcetera, have been modelled as nodal masses applied on the hull. These masses have been roughly distributed according to information provided by Global Maritime. We would like emphasize that deviations related to the distribution of masses is present in our model, however, the overall performance of the model is believed to be good. The different contributions to the applied nodal masses are listed in **Tab. 4.13**.

Table 4.13: Weighted elements and their associated nodal masses in the model, based on weight calculations from Global Maritime.

| Contribution | Weight [kg] |
|---|------------------|
| Fish feed | 600 000 |
| Marine growth | 50 000 |
| Ice/Snow | 109 000 |
| Superstructure/Main deck | 350 496 |
| Aquaculture equipment | 151 141 |
| Marine systems and equipment | 140 163 |
| Walkways, handrails and ladders | 150 870 |
| Foundations | 129 961 |
| Deck plates and bulkheads | 72 138 |
| Brackets | 100 000 |
| Anodes | 15 000 |
| Paint, welds, and corrosion allowance | 329 856 |
| Fixed bulkheads | 172 001 |
| Structure in connection with movable bulkhead | 195 706 |
| Oil, water, ensile, and fuel oil tanks | 93 600 |
| Total | 2 687 794 |

As mentioned in section 4.3.2, the hull structure has been modelled with a focus on maintaining the correct weight. The mass distribution of the hull is thus considered to be correct. This also applies for the mooring lines. Some simplifications have been introduced for the net with respect to the weight, but this is assumed to be of minor importance. The fill ratio of ballast water in the pontoons is also of great importance for the total weight and location of the center of gravity (CoG). Due to deviations in the longitudinal and transverse CoG for the modelled structure, the specified fill ratios for the ballast water from Global Maritime could not be directly used in our model. Somewhat different filling ratios have therefore been applied in order to avoid an initial heel angle. The total amount of ballast water is however approximately the same as specified by Global Maritime. Important parameters related to the total mass of the model compared to values from Global Maritime are found in **Tab. 4.14**. The weight of the mooring lines is not included. Some of the properties are not directly comparable, and have thus been left blank. Filling ratios of the

different pontoons are found in **Tab. 4.15**, where the referred column names can be seen in **Fig. E.10**. Note that the fill ratios for the USFOS model are specified somewhat different than the ones from Global Maritime.

Table 4.14: Important parameters related to the mass of the model compared to values from Global Maritime, mooring lines are not included.

| Property | USFOS model | Global Maritime | Unit |
|---------------------------|-------------|-----------------|---------|
| Node mass | 2 688 | - | [tonne] |
| Element mass | 5 702 | - | [tonne] |
| Total structural mass | 8 390 | - | [tonne] |
| Weight of ballast water | 7 416 | - | [tonne] |
| Total weight/Displacement | 15 807 | 16 325 | [tonne] |
| VCG (from bottom and up) | 17.59 | 17.94 | [m] |

Table 4.15: Filling ratios in the pontoons compared to values from Global Maritime, designated names are in reference to structural drawings. [21]

| Tank/Pontoon | USFOS model [%] | Global Maritime [%] |
|----------------------------|-----------------|---------------------|
| Peripheral pontoons | | |
| C2, C4, C6 cylinder part | 100 | 88.6 |
| C2, C4, C6 cone part | 59.8 | |
| C8 cylinder part | 100 | 89.2 |
| C8 cone part | 61.7 | |
| C10 cylinder part | 100 | 82.9 |
| C10 cone part | 53.5 | |
| C12 cylinder part | 100 | 83.9 |
| C12 cone part | 53.5 | |
| Center pontoon | | |
| C13 | 52.8 | 37.7 |

4.4 Model Comparison

We find it appropriate to mention a few of the differences in the current model compared to the one made by Heiervang and Knutsen [24] so that this is kept in mind when the results are presented before the discussion. Design of the fish cage is a persisting process, and our model is an improved and optimized version. Heiervang and Knutsen observed a vertical drift during the simulations, and argued that the most probable cause for this was the very simplified manner in which the mooring lines were modelled. Multiple sets of non-linear springs were used, whereas we have used regular beam elements to get a realistic catenary profile and hopefully avoid this error. The bottom net of the cage were not modelled in their work, but is included in the current model, the degree of influence it

may have is however not known, but will most likely increase the hydrodynamic damping. Other main differences include the moveable bulkhead, omitted in the previous model, directional dependent drag coefficients which is accounted for this time, a new set of drag and inertia coefficients, and also minor differences in element geometry.

4.5 Natural Periods

When designing a structure, the natural periods are some of the essential parameters to consider. If possible, these periods should be placed outside the range of the expected excitation periods to avoid resonance. A semi-submersible is designed to avoid resonance [18], and as the Ocean Farming concept is based on the same principles, so is the case for this structure. For a floating construction exposed to waves, it can in most cases be said that resonance in the wave frequency regime is avoided if the natural period in heave is larger than 20 seconds.

From the model tests performed by MARINTEK, the values of the natural periods on the Ocean Farming concept were obtained. However, changes in the design have been made since these tests were performed, and as our model is based upon the updated design, deviations are expected. We have found the natural periods of our model based on decay simulations in USFOS. The simulations involves the structure being subjected to an impulse load in the desired degree of freedom. Natural periods are then found by plotting the motion of the structure in the respective degree of freedom, averaging the resulting oscillation period. A plot of the heave motion from a heave decay simulation is seen in **Fig. 4.22**. As indicated in the figure, the first period of oscillation have not been considered when determining the natural period to avoid transient effects affecting the results.

In section 4.2.1, it was argued that different drag and inertia coefficients for the hull elements should be used in ULS and FLS respectively. The choice of these coefficients, especially C_M , have a great influence on the resulting natural periods determined from the decay simulations. In ULS we have used $C_M = 1.2$ and $C_D = 1.05$ while in FLS, $C_M = 2.0$ and $C_D = 0.8$ have been used. Decay tests using both the ULS and FLS values have been performed, and the results can be found in **Tab. 4.16**. As seen, quite significant variations are present, particularly for surge, sway and yaw. All periods are however outside the wave period regime (taken as 3-20 seconds in our analyses).

It is not obvious what values of C_M and C_D that is correct to use in the decay tests. However, it is possible to consider the flow around the members as an oscillating flow with a period equal to the natural period for the given degree of freedom. For best comparison with the model tests performed by MARINTEK, the choice of C_D and C_M should arise from an equal roughness ratio. The following considerations are thus made:

- For estimation of the natural periods, a correct value of C_M is more critical than a correct value of C_D (the relative importance of C_M is greater).
- The flow around the members are considered as an oscillating flow with a period equal to the natural period in the given degree of freedom.

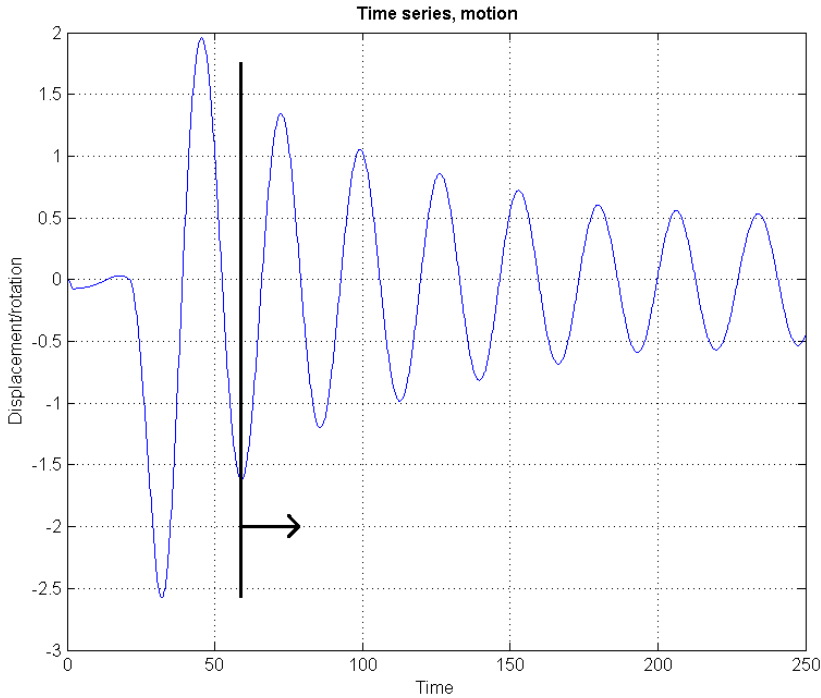


Figure 4.22: Plot of the heave motion of the fish farm during a heave decay simulation.

Table 4.16: Natural periods for the USFOS model with drag and inertia coefficient values as in ULS and FLS, all values are given in seconds.

| | Model ULS | Model FLS |
|-------|-----------|-----------|
| Surge | 166.7 | 228.6 |
| Sway | 160.0 | 222.6 |
| Heave | 24.1 | 26.9 |
| Roll | 33.2 | 37.9 |
| Pitch | 31.5 | 36.2 |
| Yaw | 137.0 | 193.1 |

- The Reynold's number is assumed to be in the supercritical regime.
- The Keulegan-Carpenter number, $KC = \frac{UT}{D}$, should be found by estimating an adequate value of the velocity U by considering the time derivative of the decay plots (structure velocity) and taking T as the natural period. The typical diameter is set to be 2.5 meters.
- In the model experiment, smooth structural members were used. C_D and C_M should

be based upon this.

- Determination of a suitable KC-number for the rotational degrees of freedom is not straight forward. For simplicity, a reasonable KC-number in roll and pitch is taken as KC_{heave} and the KC-number in yaw is taken as KC_{surge} .

Based on the above considerations, the characteristic KC-number in heave, roll and pitch is found to be approximately 3.0, while for surge, sway and yaw it is found to be approximately 8.0. **Fig. 4.7** in section 4.2.1 then gives us $C_M = 2.0$ for heave, roll and pitch, and $C_M = 1.8$ for surge, sway and yaw. A reasonable value for the drag coefficient is found to be $C_D = 0.65$ for all degrees of freedom. This is equal to the steady flow drag coefficient for a smooth circular cylinder. The corresponding natural periods compared with the experimental values determined by MARINTEK are found in **Tab. 4.17**.

Table 4.17: Natural periods of our USFOS model compared to the MARINTEK experiments, all values are given in seconds.

| | USFOS model | MARINTEK experiments |
|-------|-------------|----------------------|
| Surge | 209.2 | 175.0 |
| Sway | 204.0 | 175.0 |
| Heave | 26.8 | 25.5 |
| Roll | 37.8 | 29.0 |
| Pitch | 36.3 | 30.8 |
| Yaw | 180.2 | - |

The natural periods of our model is seen to be higher in all degrees of freedom. The main explanation of this is that the *current* design, which the model is based upon, have increased pontoon dimensions and approximately 13 percent larger displacement than what was the case in the experiments. In addition, our model have a larger radii of gyration in roll, pitch and yaw. All periods are however comparable, and our results are seen as accurate enough.

As mentioned previously, the wave period regime is assumed to be between 3-20 seconds. All natural periods are above this range, meaning that resonance from 1st order wave forces is avoided. Sum-frequency effects are obviously not an issue. The natural periods in surge, sway and yaw are however seen to be within a range where difference-frequency wave loads (wave drift loads) and wind gust loads can cause resonance, Larsen [34]. As no wind is present in our analyses, and because 2nd order wave loads are not captured by USFOS (requires a second order surface process), these effects will not be considered in our analyses.

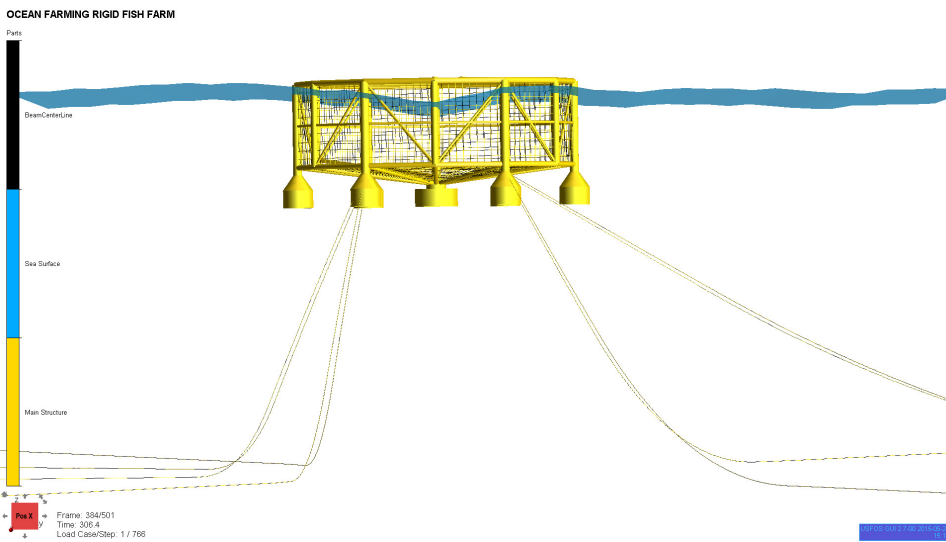


Figure 4.23: A screenshot taken from USFOS GUI during an ULS analysis, this is the resulting model.

Limit State Analyses

Two types of analyses have been executed. One investigating the ultimate limit state (ULS), and the other looking at the fatigue limit state (FLS). All analyses have been run in the time domain, using the nonlinear finite element program USFOS. In the following, the set-up of the analyses are explained and the results will be presented. A reasonable number of simulations have been completed, yielding satisfactory and trustworthy results.

5.1 Ultimate Limit State

Global response analyses, investigating the ultimate limit state, have been carried out in USFOS. A stochastic description of the wave climate have been used in the analyses. The results are thus comparable with what were obtained in the *stochastic ULS analyses* of the Ocean Farming concept performed by Heiervang and Knutsen in their thesis [24].

The initial goal was to conduct 3-hour time domain simulations, exposing the modelled fish farm to ULS environmental actions. Further, post-processing of the results should be performed in the built-in USFOS module CodChk, checking the utilization of all structural elements at all time steps based on the API-WSD standard. Due to the large number of elements in our model and the demand for a reasonable small time step in the analyses, it was found out that CodChk was not able to process simulations of more than 400 seconds. This left us with quite significant limitations regarding how the analyses could be carried out. The solution to this was to apply the *SpoolWave* option in USFOS. When using SpoolWave, USFOS simulates an irregular wave field of specified duration based on a given wave spectrum, and then searches for the 1st, 2nd, 3rd, etcetera, highest wave crest, depending on what is specified as "order" by the user. We have used order 1, 2, and 3 in our analyses (1st, 2nd, 3rd highest wave crest). The analysis time $t = 0$ will be moved forward to the specified "time before peak" as shown in **Fig. 5.1**. As quite significant transient effects will be present after start-up of our ULS analyses due to drift caused by the applied

current, the "time before peak" have been set to 300 seconds (the transient effects last for almost 200 seconds). The total analysis time was set to 400 seconds. Uncertainties will however be present when using the SpoolWave option since we assume that the *highest* waves will give the largest utilization. The results have however indicated that in most cases, this is true.

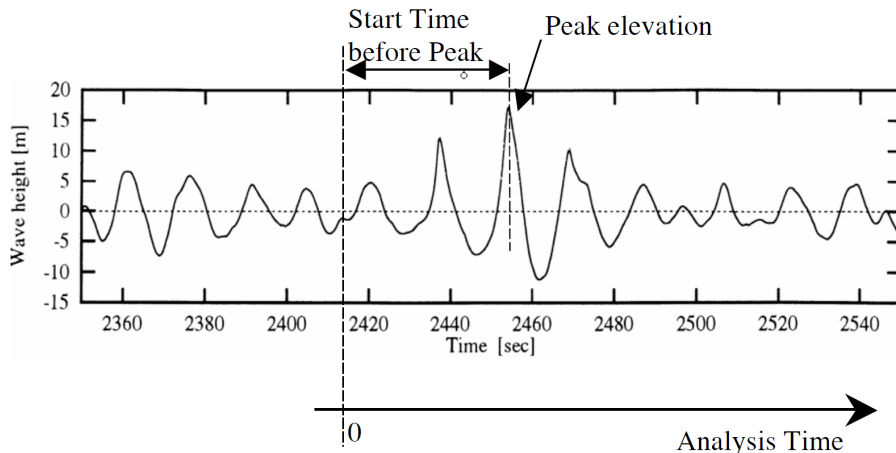


Figure 5.1: Illustration of how an analysis using the SpoolWave option is carried out in USFOS. (USFOS User's Manual [58])

5.1.1 ULS: Environmental Conditions

The environmental conditions at the proposed location in Frohavet have been evaluated by Global Maritime based on limited site data and expert opinions. The result of this is an estimate of the 100-year current velocity, $U_{C,100} = 0.75$ meters per second, and a 100-year environmental contour line, describing combinations of the average zero-up-crossing period, T_Z , and the significant wave height, H_S , with an estimated annual probability of occurrence of $q = 0.01$, see **Fig. 5.2**. The highest significant wave height on the contour is $H_S = 5$ meters, and is seen as the design 100-year significant wave height. Since the exact location of the fish farm have not yet been set, the uncertainty in the estimated long term extreme environmental conditions is not seen as particularly problematic. The argument for this is that the estimated extremes are seen as upper limits for the feasibility of the project. The final choice of location will thus be limited by this. At a late stage in this project, 16 years of simulated wave data for different locations in Frohavet was received from Global Maritime, which could have been used as a basis for our analyses. However, the main point of these data was to determine possible locations where $H_{S,100}$ was less or equal to the design 100-year significant wave height. Due to this, our ULS analyses have been carried out based on previously estimated upper extremes.

As mentioned in section 3.1.1, one should in general consider several of the most severe

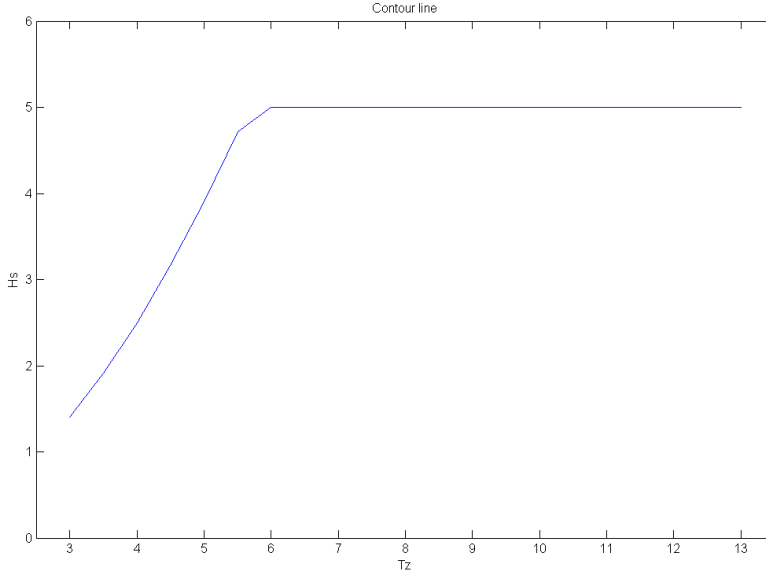


Figure 5.2: The 100-year environmental contour line estimated by Global Maritime.

sea states along the contour when estimating long term extremes based on the contour line method. Due to time limitations, our analyses is however restricted to *one* sea state. This is the same sea state considered by Heiervang and Knutsen [24]. In addition, experimental results exists for this particular sea state from the model tests performed by MARINTEK. This sea state is described by $H_S = 5$ meters and $T_P = 11$ seconds. The 100-year current velocity, $U_C = 0.75$ meters per second, have also been included in these analyses/experiments.

As the chosen sea state is only characterized by a peak period and a significant wave height, an appropriate short term wave description must be adapted in order to describe the individual waves in the sea state. It is common to describe a short term stationary irregular sea state by a wave spectrum; that is, the power spectral density function of the vertical sea surface displacement. We have used the JONSWAP spectrum, which is widely used in connection with stochastic analyses on structures on the Norwegian continental shelf. The spectrum is based on the work carried out during the *Joint North Sea Wave Project* (JONSWAP), Hasselmann et al. [22], and is an analytical expression describing the spectral shape of sea states from measurements performed in the Danish part of the North Sea. The spectrum is defined in Eq. (5.1), and is suitable for wind seas, including fetch limited seas.

$$S_J(\omega) = A_\gamma \frac{5}{16} \cdot H_S^2 \omega_p^4 \cdot \omega^{-5} \exp\left(-\frac{5}{4} \left(\frac{\omega}{\omega_p}\right)^{-4}\right) \cdot \gamma^{\exp\left(-0.5 \left(\frac{\omega - \omega_p}{\sigma \omega_p}\right)^2\right)} \quad (5.1)$$

where

$$A_\gamma = 1 - 0.287 \ln(\gamma)$$

γ is a non-dimensional peak shape parameter and σ is a spectral width parameter described as

$$\sigma = \begin{cases} \sigma_a & \text{for } \omega \leq \omega_p \\ \sigma_b & \text{for } \omega > \omega_p \end{cases}$$

If no particular values are given for the peak shape parameter, γ , DNV-RP-C205 [14] recommends using

$$\gamma = \begin{cases} 5 & \text{for } \frac{T_P}{\sqrt{H_S}} \leq 3.6 \\ \exp(5.75 - 1.15 \frac{T_P}{\sqrt{H_S}}) & \text{for } 3.6 < \frac{T_P}{\sqrt{H_S}} < 5.0 \\ 1 & \text{for } \frac{T_P}{\sqrt{H_S}} \geq 5.0 \end{cases} \quad (5.2)$$

Average values from the JONSWAP experimental data are $\gamma = 3.3$, $\sigma_a = 0.07$, and $\sigma_b = 0.09$ [22]. For $\gamma = 1$, the JONSWAP reduces to the Pierson-Moskowitz (PM) spectrum, describing fully developed wind seas. The characteristics of the sea state used in our analyses are listed in **Tab. 5.1** in addition to the current velocity. The value of the peak shape parameter, γ , is calculated according to Eq. (5.2).

Table 5.1: Characteristics of the environmental conditions used in our ULS analyses.

| Wave spectrum | H_S [m] | T_P [s] | γ | U_C [m/s] |
|---------------|-----------|-----------|----------|-------------|
| JONSWAP | 5.0 | 11.0 | 1.1 | 0.75 |

As mentioned in section 3.1.2, all statistical properties of the surface elevation is completely described by the wave spectrum (given a Gaussian surface elevation). As our analyses are performed in the time domain, a realization of the wave spectrum must be obtained. The realization will be associated with inherent variability as it is only a realization out of an infinite number of possible realizations, Haver [23]. Several simulations of a sea state should therefore be conducted in order to reduce the risk of the individual simulations not being representative for the sea state. This also allows a short term extreme value distribution of the response to be established. For our analyses, each short term extreme value distribution is based on 40 different sea state realizations.

5.1.2 ULS: Analysis Set-Up

As previously mentioned, the *SpoolWave* option in USFOS have been used in connection with the analyses. The duration of the simulated sea states, where USFOS searches for the highest wave crests, have been set to three hours, and are based on the environmental conditions listen in **Tab. 5.1**. The combined wave and current directions have been restricted to one quadrant due to symmetry. More specifically, directions from 270 to 360 degrees have been considered with an angle step of 15 degrees, giving a total of 7 different directions. This is illustrated in **Fig. 5.3**.

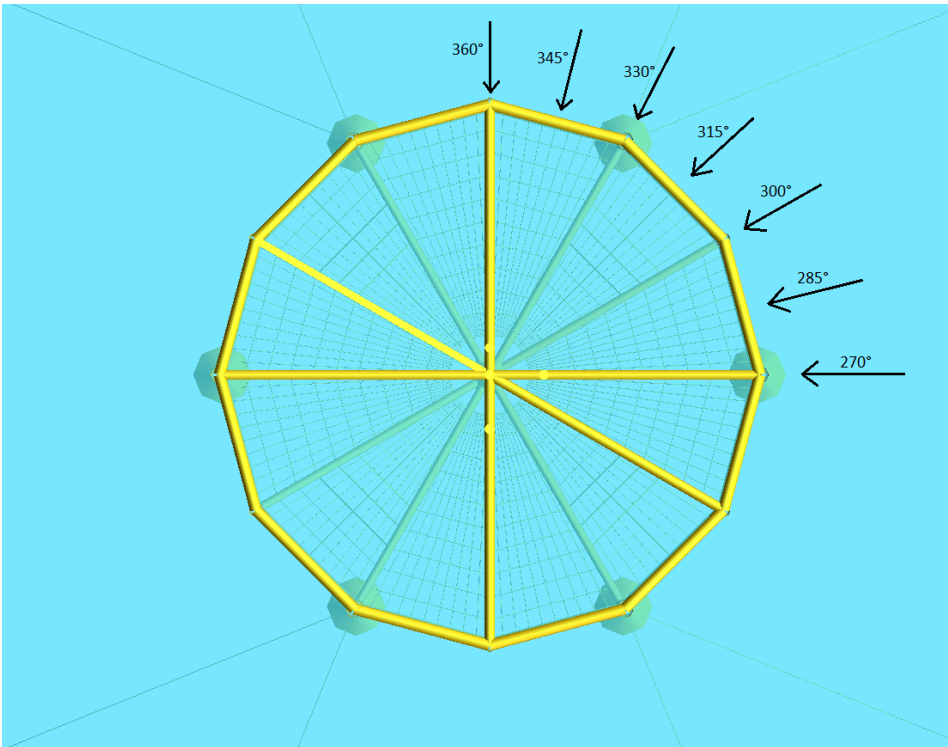


Figure 5.3: Wave and current directions used in the ULS analyses.

For each of the directions, 40 simulations of different wave spectrum realizations (seeds) on the 1st – 3rd highest waves (defined as order 1, 2, and 3) have been run. This means 120 simulations for each of the 7 directions, summing up to 840 analyses in total. All analyses have been performed with "time before peak" set to 300 seconds, a total analysis time of 400 seconds and a timestep of 0.4 seconds. The drag and inertia coefficients are set according to specified values for ULS found in chapter 4.

Post-processing of the USFOS analyses are performed in the CodChk utility tool. Here, the utilization of all hull elements are checked according to the API-WSD standard. The API-WSD standard is a recommended practice for designing and constructing fixed offshore

structures, such as jackets. As the slender tubular beams on the Ocean Farming concept is similar to those found on jackets, this standard is found to be applicable for the utilization check. In the check, the different stress contributions from axial tension/compression, bending, shear, and hydrostatic pressure is calculated and checked against allowable stress levels for cylindrical members defined in the standard [3]. In addition, the combined stresses are considered. This check is performed for all elements based on the calculated stresses at each timestep of the analyses. Due to the large D/t ratio (greater than 60) of the members, local buckling may also be relevant in the utilization check.

As described in section 4.3.2, all members making up the hull (except the pontoons) have been subdivided into smaller elements in order to attach the net to the hull. Due to the attached net elements, the total original length of these members are not accounted for in the elastic buckling check. This means that the elastic buckling stress (Euler stress) will be overestimated in accordance with Eq. (5.3) where K denotes the buckling factor.

$$\sigma_e = \frac{\pi^2 EI}{A(KL)^2} \quad (5.3)$$

Overestimation of the elastic buckling stress is only critical if global elastic column buckling due to axial compression is expected to be the governing failure mode. This is not the case for the Ocean Farming concept. One of the arguments for this is the low value of the reduced slenderness parameter, $\bar{\lambda}$, for all structural members. $\bar{\lambda}$ is defined in Eq. (5.4), and for all members the reduced slenderness is less than one. This means that the allowable axial compression stress will be high (close to the yield stress), Amdahl [2]. However, as no user manual exists for the CodChk module, there have been some confusion related to if this overestimation really have any influence on the final obtained utilization values. Even though CodChk prints out an overestimated value of the Euler stress, the computed *allowable axial stress* seems to be unaffected by the member subdivision. Additional analyses performed on similar columns exposed to a combination of axial compression and bending have also indicated that the overestimation of the elastic buckling stress have no influence on the final utilization values obtained from CodChk.

$$\bar{\lambda} = \sqrt{\frac{\sigma_y}{\sigma_e}} \quad (5.4)$$

As mentioned, we have been running analyses exposing the model to the 1st, 2nd, and 3rd largest wave from the same surface realization. The largest utilization obtained from these analyses is kept as a result. The reason for doing multiple analyses within the same sea state realization is that it is not necessarily the highest wave that will give the largest response. This is particularly important to investigate for new concepts where dynamics are expected to be of importance. Performing full sea state analyses will always be preferable for such structures. This means that in general, using the SpoolWave option to find the response from the three largest waves, is not sufficient for doing the ULS analyses on the

Ocean Farming concept. If the CodChk module is improved so that it can handle larger amount of data, running full 3-hour sea state analyses is thus recommended for further work. Our results indicates however that in most cases, the largest utilizations are seen for the largest wave. The trend is shown in **Tab. 5.2**.

Table 5.2: Number of highest utilizations occurring in the given wave order.

| Order | Dir 270 | Dir 285 | Dir 300 | Dir 315 | Dir 330 | Dir 345 | Dir 360 |
|-------|---------|---------|---------|---------|---------|---------|---------|
| 1 | 39 | 33 | 28 | 25 | 27 | 27 | 30 |
| 2 | 1 | 3 | 6 | 8 | 7 | 6 | 6 |
| 3 | 0 | 4 | 6 | 7 | 6 | 7 | 4 |
| Sum | 40 | 40 | 40 | 40 | 40 | 40 | 40 |

5.1.3 Ultimate Limit State Results

The results are based on the utilizations obtained from the CodChk module. The utilization is the ratio between the computed stress from the USFOS analyses and the allowable stress defined in the API-WSD standard, and should thus be below 1.0 if the structure is properly designed. Since multiple analyses (40) have been performed for each current and wave direction, a short term extreme value distribution can be obtained for each direction. According to NORSOK N-003 [46], a proper estimate for the extreme value can be found by going up to the 90 percent fractile of the short term extreme value distribution.

The short term extremes are expected to follow the Gumbel distribution as they are the largest out of many. The cumulative distribution function of the Gumbel distribution is given in Eq. (5.5).

$$F_X(x) = \exp \left\{ - \exp \left\{ - \frac{x - \alpha}{\beta} \right\} \right\} \quad (5.5)$$

Our results have been plotted on Gumbel probability papers. The property of a probability paper for a given distribution is that the axes are scaled so that the cumulative distribution will appear as a straight line in the paper. For the Gumbel case, this means manipulating Eq. (5.5) so that we get

$$- \ln(- \ln(F_X(x))) = \frac{x - \alpha}{\beta} \quad (5.6)$$

It is seen from Eq. (5.6) that the scaled cumulative distribution function is now linearly dependent on x .

Based on the maximum utilizations for the different directions, the Gumbel parameters α and β can be estimated from samples. By using the moment principle, α and β can be estimated from the mean, \bar{x} , and the standard deviation, s , of the samples according to Eq. (5.7).

$$\begin{aligned}\hat{\beta} &= 0.7797s \\ \hat{\alpha} &= \bar{x} - 0.57722\hat{\beta}\end{aligned}\tag{5.7}$$

Based on the calculated values of $\hat{\alpha}$ and $\hat{\beta}$, extreme value distributions are obtained, making it possible to estimate the values corresponding to the 90 percent fractile.

The results from the combined wave and current headings of 300, 315, and 330 degrees are presented in **Fig. 5.4**, **5.5**, and **5.6** as these are seen to be the most severe directions. Results from the other directions can be found in appendix D. The plots are based on the values of the highest utilized element obtained from each of the 40 different sea state realizations for the given direction. The API-WSD utilization is denoted x in the plots. It should be mentioned that it *looks* like the plots are based on relatively few observations. However, each point in the plot can potentially represent several observations as equal maximum utilization values were obtained for many of the analyses. This is taken into account when estimating the cumulative probabilities. It is observed that good agreement with the Gumbel distribution is achieved, the points lies more or less along the regression line.

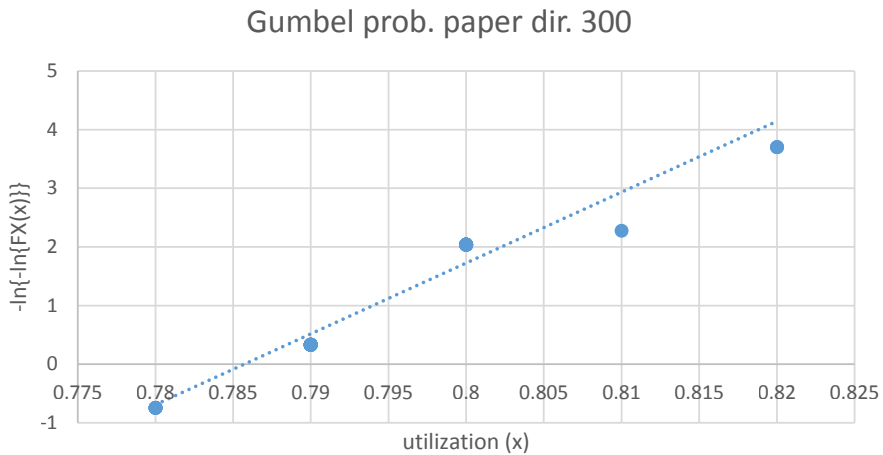


Figure 5.4: Gumbel probability paper for direction 300.

The results shows that it is waves and current coming from direction 315 that gives the largest utilization. This is as expected considering the structural layout, and is also in

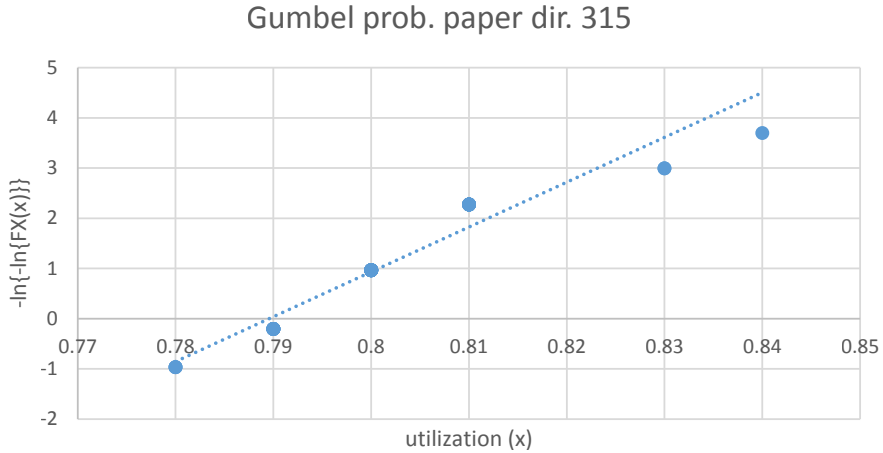


Figure 5.5: Gumbel probability paper for direction 315.

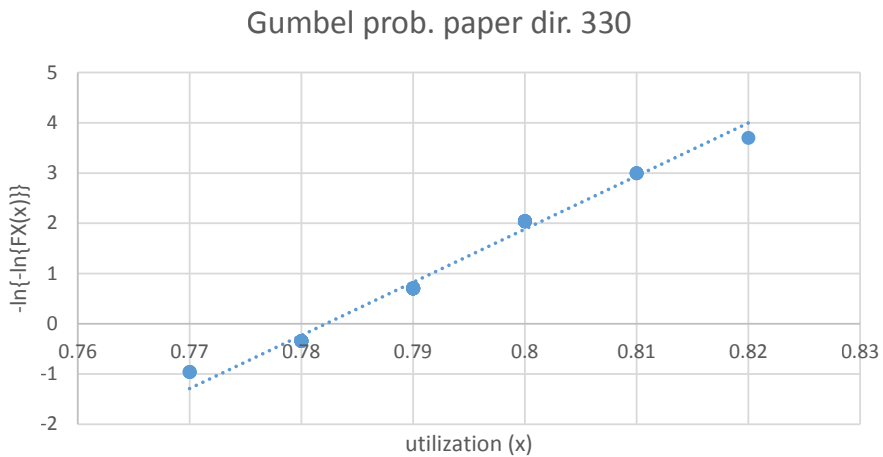


Figure 5.6: Gumbel probability paper for direction 330.

agreement with what was found in the thesis by Heiervang and Knutsen [24]. The values of the API-WSD utilizations is however much lower than found by Heiervang and Knutsen. The reason for this is probably the improvement of the fish farm design, and due to their overestimation of inertia forces on the net from the increase net diameter used in their analyses. Further comparison of the results will be discussed in chapter 6.

As seen in **Fig. 5.5**, the highest utilization during the analyses is 0.84, and is thus within

the requirements in the API-WSD standard. The characteristic extreme value is however, as previously mentioned, determined as the value corresponding to the 90 percent fractile of the obtained extreme value distributions. When seen in connection with the Gumbel papers, the 90 percent fractile is at 2.25 on the vertical axis ($-\ln(-\ln(0.9))$). The results for every direction is presented in **Tab. 5.3**.

Table 5.3: Obtained Gumbel parameters and ULS results for all directions.

| Parameter | Dir 270 | Dir 285 | Dir 300 | Dir 315 | Dir 330 | Dir 345 | Dir 360 |
|----------------|---------|---------|---------|---------|---------|---------|---------|
| \bar{x} | 0.762 | 0.777 | 0.796 | 0.801 | 0.792 | 0.771 | 0.761 |
| s | 0.0036 | 0.0061 | 0.0101 | 0.0128 | 0.0113 | 0.0072 | 0.0069 |
| $\hat{\beta}$ | 0.0028 | 0.0047 | 0.0079 | 0.0100 | 0.0088 | 0.0056 | 0.0054 |
| $\hat{\alpha}$ | 0.760 | 0.774 | 0.791 | 0.795 | 0.787 | 0.768 | 0.758 |
| $x_{0.9}$ | 0.77 | 0.78 | 0.81 | 0.82 | 0.81 | 0.78 | 0.77 |

An illustration of the highest utilized members in the ULS analyses is found in **Fig. 5.7**.

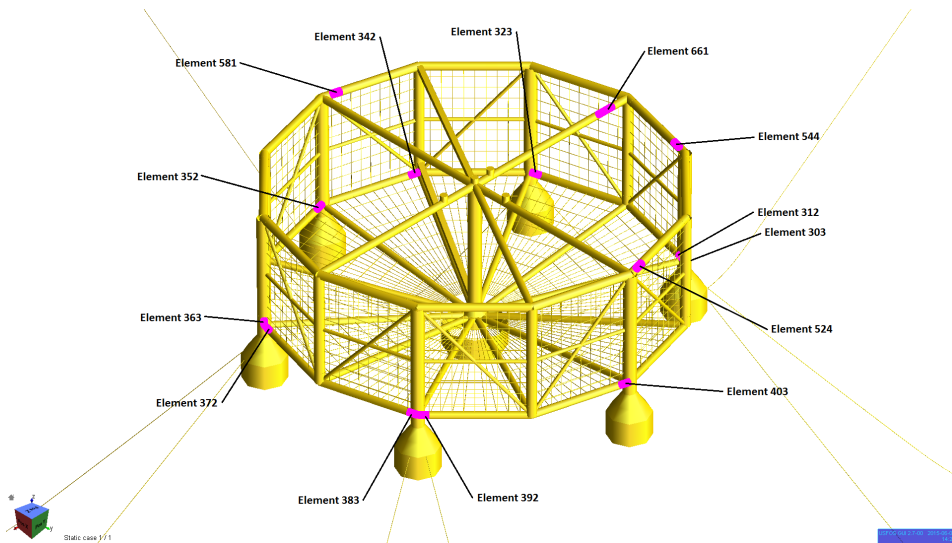


Figure 5.7: Most utilized members in ULS analyses.

5.2 Fatigue Limit State

A simplified dynamic fatigue limit state analysis, based on a stochastic approach, has been carried out on the Ocean Farming concept, looking at the most critical joints. All analyses have been performed in the time domain in USFOS. The results have been post-processed by the fatigue utility module FATAL, counting the stress cycles and calculating the fatigue

damage. The performance of FATAL has been tested and validated for different simple tubular joints in the pre-project [7] to this thesis, yielding satisfactory results. The analysis method used is partly based on the procedure described by Jia [26].

The FATAL control file requires input for SCF values around the connection. Values that must be defined for single or all connections are:

- Axial force SCF for saddle point
- Axial force SCF for crown point
- In-plane bending SCF for crown point
- Out-of-plane bending SCF for saddle point

No stress concentration factors (SCF) have been produced for the tubular joints of the Ocean Farming concept. Parametric formulas for stress concentration factors of simple tubular joints exists, and can be found in for example DNVGL-RP-0005 [15]. The critical joints on the Ocean Farming concept are however more complex, and the parametric SCF formulas are thus not applicable. Hence, finding the SCFs will be a very time consuming procedure as it requires detailed finite element modelling of the joints in question. This is outside the scope of this thesis. The analyses is thus run setting all SCFs equal to 1.0. The following points can summarize the thinking behind the analyses:

- Representative sea states are identified and given a specific probability of occurrence based on site specific scatter diagrams. These sea states are used as a basis for the analyses. Directional dependency is accounted for.
- The fatigue damage for each of these sea states are calculated at 4 clock-positions (see Fig. 5.8) at both the chord and brace side of the considered intersections using stress concentration factors equal to 1.0 and an appropriate S-N curve.
- The individual fatigue damages are multiplied with the specific expected number of sea state occurrences during the lifetime of the fish farm (25 years). The total lifetime fatigue damage is found by summing up all these contributions.
- Based on the calculated total fatigue damages, one can estimate a limiting, upper value of the stress concentration factor at each location that gives a Miner sum equal to 1 (estimating the lowest SCF that gives fatigue failure). This is done using the applied S-N curve as a basis.
- The result is thus a limiting stress concentration factor, denoted SCF_{max} , for each considered location. These are seen as upper values of what the *real* SCFs can be, giving the criteria SCF_{real} must be lower than SCF_{max} .

A more detailed description and argumentation of our choices will be given in the following. It should be noted that if the real stress concentration factors are obtained at a later stage, the full analysis can easily be run again, implementing these stress concentration factors in the FATAL control file enclosed in the electronic appendix to this thesis.

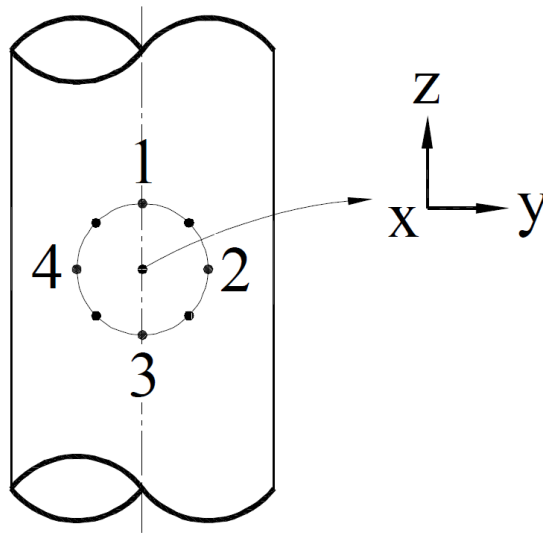


Figure 5.8: Clock-positions considered in the fatigue analysis, based on figure in [15].

5.2.1 FLS: Environmental Conditions

Site specific wave data have been provided by Global Maritime. These data have been produced by FUGRO OCEANOR, and are based on numerical simulations (the SWAN shallow water model) calibrated against satellite altimeter measurements and a wave measuring buoy on site. According to FUGRO OCEANOR, SWAN account for the following physics:

- Wave propagation in time and space, including the effect of shoaling, refraction due to current and depth, frequency shifting due to currents and the effect of non-stationary depth.
- Wave generation by wind.
- Triad and quadruplet non-linear wave-wave interactions.
- White capping, bottom friction, and depth-induced breaking.
- Wave induced setup.
- Transmission through and reflection from obstacles.

Using SWAN, the wave conditions from 01.01.1999 - 31.12.2014 have been simulated and recorded at 20 different locations in Frohavet. The reason for recording at different points is that the exact location of the fish farm have yet to be decided. We thus had to base our environmental conditions on one of these records. One of the criteria for the final location is that the 100-year significant wave height is below 5.0 meters. Our choice of wave record is thus limited to the locations to the left of the blue line in **Fig. 5.9**.

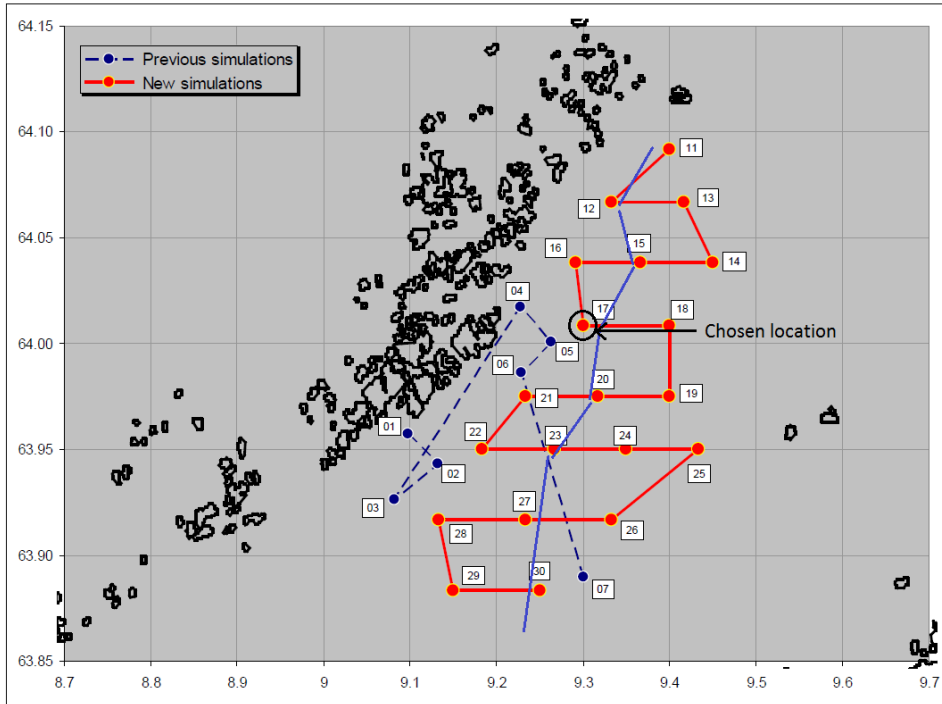


Figure 5.9: Numbering of the target positions, the red dots indicate the 20 considered locations, due to wave height limitations, only the locations to the left of the blue line are feasible as final locations. (FUGRO OCEANOR)

We have chosen location 17, as indicated in **Fig. 5.9**. This is because it has one of the highest estimated $H_{S,100}$ values under 5 meters (4.85), and is thus one of the possible locations where one will expect the most severe wave conditions.

Based on the received omni-directional scatter diagram for location 17 (see Fig. D.9 in the appendix), important sea states to be used in the fatigue analysis have been identified. 15 different sea states have been chosen from the original scatter diagram, and the structure will be exposed to these sea states from 8 different directions. The total number of load cases is then $15 \cdot 8 = 120$. Each chosen sea state is based on a *block* of the scatter diagram. The zero-up-crossing period, significant wave height and probability of occurrence are calculated for each block as expressed in Eq. (5.8), (5.9) and (5.10).

$$T_{m02,j} = \frac{\sum_i m_i \cdot T_{m02,i}}{\sum_i m_i} \quad (5.8)$$

$$H_{S,j} = \frac{\sum_i m_i \cdot H_{S,i}}{\sum_i m_i} \tag{5.9}$$

$$P_{b,j} = \frac{\sum_i m_i}{m_{total}} \tag{5.10}$$

where

- i sea states in block j
- m number of occurrences
- m_{total} total number of occurrences

The scatter diagram, divided into blocks, along with the 15 chosen sea states are found in **Fig. 5.10**. The light blue indicates values in the original scatter diagram while darker blue indicates the chosen sea states.

| H_{m0} [m] \ T_{m02} [s] | 1 | 2 | 3 | 4 | 5 | 6 | 7 | 8 | 9 | 10 | 11 | 12 | 13 | 14 | 15 | Sum |
|------------------------------|----|-------------|-------------|-------------|-------------|-------------|-------------|-------------|-----|-----|----|----|----|----|----|-------|
| 0.50 | 18 | 2937 | 2346 | 1011 | 968 | 1000 | 764 | 595 | 314 | 135 | 26 | 3 | 2 | 1 | 0 | 10120 |
| 0.50 | | 2.69 | | | 6.30 | | | 9.43 | | | | | | | | |
| 1.00 | 0 | 106 | 6960 | 1251 | 319 | 266 | 217 | 184 | 64 | 22 | 6 | 0 | 0 | 0 | 0 | 9395 |
| 1.00 | | 3.14 | | | 6.27 | | | 9.37 | | | | | | | | |
| 1.50 | 0 | 0 | 369 | 2431 | 235 | 50 | 12 | 14 | 6 | 3 | 2 | 0 | 0 | 0 | 0 | 3122 |
| 1.50 | | | 3.96 | | 6.53 | | 9.64 | | | | | | | | | |
| 2.00 | 0 | 0 | 0 | 503 | 89 | 20 | 0 | 1 | 0 | 0 | 0 | 0 | 0 | 0 | 0 | 613 |
| 2.00 | | | | 4.15 | | 6.10 | | | | | | | | | | |
| 2.50 | 0 | 0 | 0 | 35 | 53 | 7 | 1 | 0 | 0 | 0 | 0 | 0 | 0 | 0 | 0 | 96 |
| 2.50 | | | | 4.60 | | 6.13 | | | | | | | | | | |
| 3.00 | 0 | 0 | 0 | 0 | 18 | 5 | 1 | 0 | 0 | 0 | 0 | 0 | 0 | 0 | 0 | 24 |
| 3.00 | | | | | 5.29 | | | | | | | | | | | |
| 3.50 | 0 | 0 | 0 | 0 | 3 | 2 | 0 | 0 | 0 | 0 | 0 | 0 | 0 | 0 | 0 | 5 |
| 4.00 | 0 | 0 | 0 | 0 | 0 | 0 | 0 | 0 | 0 | 0 | 0 | 0 | 0 | 0 | 0 | 0 |
| 4.50 | 0 | 0 | 0 | 0 | 0 | 0 | 1 | 0 | 0 | 0 | 0 | 0 | 0 | 0 | 0 | 1 |
| 3.67 | | | | | 5.67 | | | | | | | | | | | |
| 5 | 0 | 0 | 0 | 0 | 0 | 0 | 0 | 0 | 0 | 0 | 0 | 0 | 0 | 0 | 0 | 0 |
| | | | | | | | | | | | | | | | | 23376 |

Figure 5.10: The modified scatter diagram, dark-blue figures are chosen values, while light-blue figures are values which they are based on.

The sea states will be simulated by the JONSWAP wave spectrum. As the sea states in reality are expected to be composed of both wind sea and swell, the two peak *Thorsethau-gen* spectrum would probably be better suited. This spectrum is however not implemented in USFOS, leaving JONSWAP as the best choice due to the fetch limited sea area considered. As seen, the scatter diagram in **Fig. 5.10** is given for the zero-up-crossing period,

T_{m02} . The JONSWAP spectrum however, requires the peak period, T_P , as an input parameter. The relationship between T_{m02} and T_P depends on the peak shape parameter, γ , in the JONSWAP spectrum as seen in the approximate relationship in Eq. (5.11) where $T_Z = T_{m02}$.

$$\frac{T_Z}{T_P} = 0.6673 + 0.05037\gamma - 0.006230\gamma^2 + 0.0003341\gamma^3 \quad (5.11)$$

As γ is not known, some simplifications had to be made in order to convert the zero-upcrossing periods into peak periods. Based on Eq. (5.11), the recommended formula for γ found in Eq. (5.2), and the average value of γ from the JONSWAP experimental data, $\gamma = 3.3$, the relationship is determined as

$$\begin{aligned} \text{If } \frac{T_P(\gamma = 3.3)}{\sqrt{H_S}} &\geq 5 &\Rightarrow \gamma = 1.0 &\& T_P = 1.4049T_{m02} \\ \text{If } 3.6 < \frac{T_P(\gamma = 3.3)}{\sqrt{H_S}} < 5 &&\Rightarrow \gamma = 3.3 &\& T_P = 1.2859T_{m02} \\ \text{If } \frac{T_P(\gamma = 3.3)}{\sqrt{H_S}} &\leq 3.6 &\Rightarrow \gamma = 5.0 &\& T_P = 1.2420T_{m02} \end{aligned} \quad (5.12)$$

The obtained sea states from Eq. (5.12) to be used in the analysis, describing the JONSWAP spectrum, in addition the probability of occurrence are found in **Tab. 5.4**.

The directional probability of the waves must also be included in the analysis. As scatter diagrams for 8 different directions have been produced by FUGRO OCEANOR, the directional probability is simply obtained by dividing the number of sea states seen for a given direction by the total number of sea states during the entire period. The result is illustrated in **Fig. 5.11**. These probabilities are to be multiplied with the sea state probabilities in **Tab. 5.4**. It is seen that waves coming from north-east is dominating, and to some extent, waves coming from south-west. This is as expected, considering the bathymetry¹ and topography in and around Frohavet.

5.2.2 FLS: Analysis Set-Up and S-N Curve

A total of 30 elements, facing 7 of the most critical joints, have been analysed. More specifically, it is the fatigue damage at the joints above all the 7 pontoons that have been assessed. This is illustrated in **Fig. 5.12** and **5.13**. At all joints, the vertical column has been taken as the chord, while the other members facing the joint is considered as braces. The fatigue damage is calculated at 4 clock-positions (crown and saddle points, reference is made to Fig. E.11, and 3.4 in section 3.2.2) at both the brace and chord side of the intersection. These points have been chosen as the location of maximum stress tends to be

¹underwater equivalent to topography

Table 5.4: The 15 sea states to be used in the fatigue analysis, including their probability of occurrence.

| Block | H_S [m] | T_P [s] | γ | P_b |
|-------|-----------|-----------|----------|--------|
| 1 | 0.5 | 3.5 | 3.3 | 0.2700 |
| 2 | 0.5 | 8.8 | 1.0 | 0.1423 |
| 3 | 0.5 | 13.3 | 1.0 | 0.0206 |
| 4 | 1.0 | 4.0 | 3.3 | 0.3558 |
| 5 | 1.0 | 8.8 | 1.0 | 0.0422 |
| 6 | 1.0 | 13.2 | 1.0 | 0.0039 |
| 7 | 1.5 | 5.1 | 3.3 | 0.1298 |
| 8 | 1.5 | 9.2 | 1.0 | 0.0033 |
| 9 | 1.5 | 13.5 | 1.0 | 0.0005 |
| 10 | 2.0 | 5.3 | 3.3 | 0.0253 |
| 11 | 2.0 | 8.6 | 1.0 | 0.0009 |
| 12 | 2.5 | 5.9 | 3.3 | 0.0038 |
| 13 | 2.5 | 7.9 | 3.3 | 0.0003 |
| 14 | 3.0 | 6.8 | 3.3 | 0.0010 |
| 15 | 3.7 | 7.3 | 3.3 | 0.0003 |
| Sum | | | | 1.0000 |

located at the saddle or the crown of the intersection, depending on the mode of loading, Berge [1]. The reason why only 7 joints have been considered is because FATAL requires that the chord member must go *through* the joint, meaning that the chord cannot end at the joint. As seen in **Fig. 5.12**, this is the case for most of the top-ring joints. By inserting dummy-beams, giving the chord a length on both sides of the joint, this limitation could have been bypassed. This was however discovered in the late phase of this project, and have due to time limitations not been implemented.

The choice of S-N curve has a great influence on the calculated fatigue damage. As all considered joints are tubular, it is the so-called *T-curve* that should be used. Three main types of this curve exist. One for members in air, one for members with cathodic protection exposed to sea water, and one for members without cathodic protection exposed to sea water (free corrosion). The different curves are illustrated in **Fig. 5.14**. As seen, the seawater curves are essentially equal for high stress ranges. For lower stress ranges, a transition to the in-air curve is seen for the "sea water with cathodic protection" curve. One should note that the inverse negative slope, m , of the in-air and cathodic protection S-N curves changes from 3.0 to 5.0 for N greater than 10^7 to account for the so-called fatigue limit, while it is constantly equal to 3.0 for the free corrosion case.

Since our fatigue damages are calculated using SCF equal to 1.0 in all connections, and that we further aim at estimating limiting values for the stress concentration factor, a S-N curve with a constant slope would be preferable to use. This is because the fatigue damage is proportional to $(\Delta S)^m$, or $(SCF \cdot \Delta S_{nom})^m$, and if m is constant, the total damage for all recorded stress ranges is also proportional to $(\Delta S)^m$. The limiting SCFs will then be

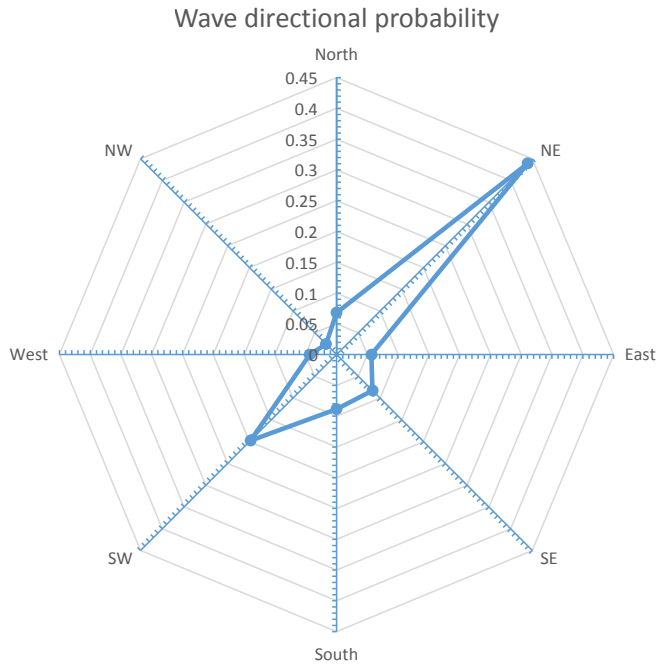


Figure 5.11: The directional probability at location.

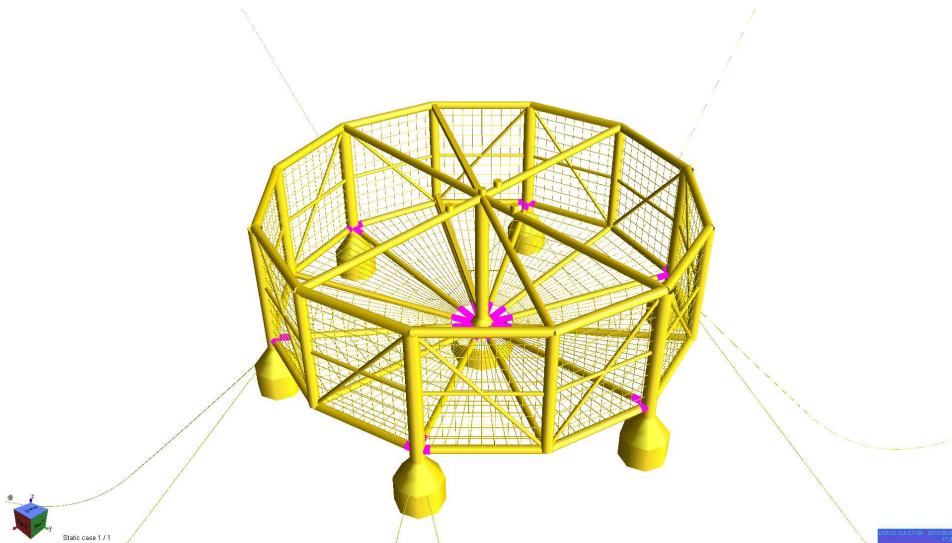


Figure 5.12: Fatigue checked elements is seen highlighted in the total model.

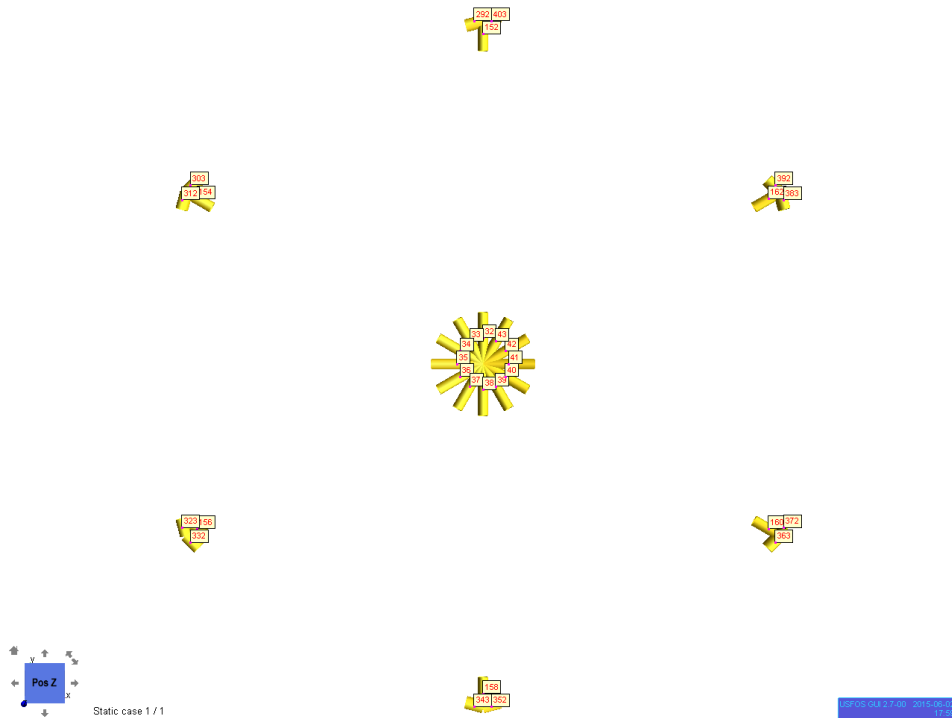


Figure 5.13: Numbering of the checked elements.

easy to find. As seen in **Fig. 5.14**, this implies using the free corrosion curve, even though the Ocean Farming concept in reality is to be equipped with cathodic protection. After running the analysis with the free corrosion S-N curve, a fatigue damage of approximately 4.0 was obtained at the most critical location with all SCFs equal to 1.0. This was way higher than expected. After investigating the magnitude of the recorded stress cycles, it was found that the stress ranges typically were around 5 MPa and that almost no stress ranges were larger than 10 MPa. An illustration of the stress range history for the most utilized element in the sea state with H_S equal to 1.0 meter and T_P equal to 8.8 seconds is seen in **Fig. 5.15**. For stress ranges of such limited magnitude, the free corrosion S-N curve estimates a fatigue damage that is around 10^4 times higher than if the cathodic protection curve is used, producing unrealistically conservative results. For this reason, and since all recorded stress ranges are way below the the fatigue limit where the cathodic protection curve changes slope, we have decided to use the cathodic protection S-N curve in our fatigue calculations.

The analysis procedure can be described by the following points, and is as previously mentioned, partly based on the work done by Jia [26]:

1. Establish the USFOS model.
2. Divide the scatter diagram into relevant blocks.

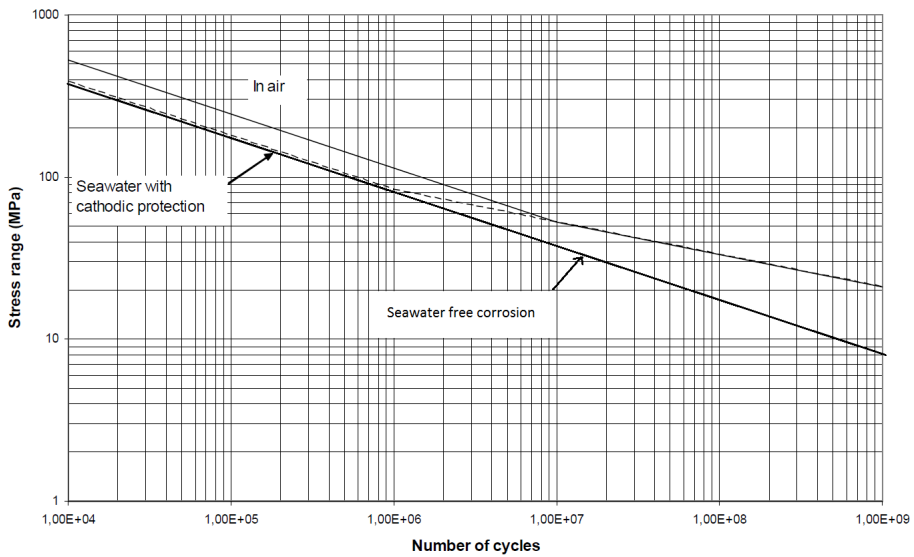


Figure 5.14: Design S-N curves in DNVGL-RP-0005, showing the transition from in-air to sea water conditions, based on figure in [15].

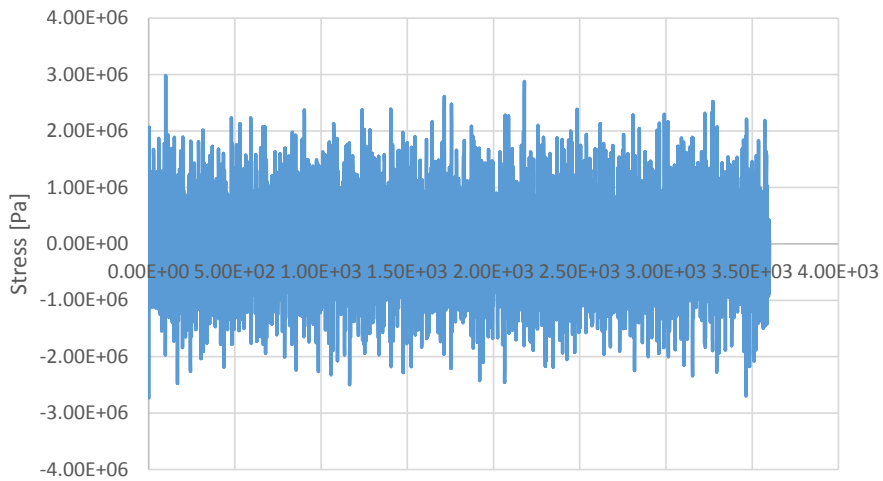


Figure 5.15: Obtained stress in the most utilized element, the plotted stress is taken as the real output minus the mean.

- 15 blocks with relevant probabilities.
- 8 wave directions with relevant probabilities.

3. Based on current measurements, a current velocity of 0.10 meters per second is applied in the same direction as the waves.
4. The damping model of the structure is set as described in section 4.3.5.
5. Assign appropriate hydrodynamic coefficients C_D and C_M to the members as described in chapter 4.
6. Run the dynamic analyses in USFOS. For computational reasons the sea state durations have been set to 1 hour and the timestep to 0.2 seconds.
 - Start with the first sea state and the first wave direction and proceed through the 120 analyses.
 - Time histories of the forces for the selected elements is dumped to file.
7. Choose a suitable S-N curve. In our case this means the T-curve for a structure in sea water with cathodic protection.
8. Calculate the fatigue damage for each sea state by using FATAL.
 - Calculate the stresses at 4 clock-positions at both the brace and chord side of the intersections based on the force time histories.
 - Number of cycles and stress ranges are calculated by a rainflow counting procedure.
9. Calculate the lifetime fatigue damage (25 years), D_{life} , at each position by multiplying the individual damages from each of the 120 analyses by the expected number of occurrences for the gives sea state and direction (during 25 years), and sum up all contributions.
10. Calculate the stress concentration factors that gives a Miner sum equal to 1, denoted SCF_{max}
 - All stress ranges are well within the part of the S-N curve with the inverse negative slope, m , equal to 5.0 (one can typically multiply the stress ranges by a SCF around 10 and still be on this part of the S-N curve).
 - The fatigue damages are then proportional to $(\Delta S)^5$. SCF_{max} can then be calculated according to Eq. (5.13).
$$SCF_{max} = \left(\frac{1}{D_{life}} \right)^{1/5} \quad (5.13)$$
 - These are seen as upper values of what the *real* SCFs can be, giving the criteria SCF_{real} must be lower than SCF_{max} .
11. Identify the most critical elements and clock-positions. This is the locations with the smallest obtained values of SCF_{max} .

5.2.3 Fatigue Limit State Results

The obtained lifetime fatigue damages, D_{life} , from the analyses are found in **Fig. 5.16**. The highest fatigue damage is found for element 154 with D_{life} equal to $6.13E-04$ at chord position 3, which is a crown point. As the highest fatigue damage is found at a crown point, this could indicate that in-plane bending is governing for this element, Berge [16].

| TOTAL FATIGUE DAMAGE | | | | | | | | | | |
|----------------------|------|-------|----------|----------|----------|----------|----------|----------|----------|----------|
| CON | NODE | BRACE | CPOS1 | CPOS2 | CPOS3 | CPOS4 | BPOS1 | BPOS2 | BPOS3 | BPOS4 |
| 1 | 1221 | 154 | 5.26E-04 | 1.29E-05 | 6.13E-04 | 2.38E-05 | 3.98E-04 | 9.78E-06 | 4.63E-04 | 1.80E-05 |
| 2 | 1221 | 303 | 1.99E-06 | 7.49E-07 | 1.12E-05 | 3.02E-07 | 1.50E-06 | 5.66E-07 | 8.51E-06 | 2.28E-07 |
| 3 | 1221 | 312 | 1.01E-05 | 3.89E-06 | 2.03E-05 | 2.16E-06 | 7.65E-06 | 2.94E-06 | 1.54E-05 | 1.63E-06 |
| 4 | 1241 | 156 | 2.50E-04 | 1.37E-04 | 3.50E-04 | 2.68E-04 | 1.89E-04 | 1.03E-04 | 2.65E-04 | 2.03E-04 |
| 5 | 1241 | 323 | 5.69E-06 | 5.84E-05 | 1.43E-05 | 4.83E-05 | 4.31E-06 | 4.42E-05 | 1.08E-05 | 3.66E-05 |
| 6 | 1241 | 332 | 5.24E-06 | 4.45E-06 | 1.99E-05 | 1.72E-05 | 3.97E-06 | 3.36E-06 | 1.50E-05 | 1.30E-05 |
| 7 | 1261 | 158 | 1.14E-04 | 5.37E-05 | 5.19E-05 | 5.44E-05 | 8.59E-05 | 4.06E-05 | 3.93E-05 | 4.12E-05 |
| 8 | 1261 | 343 | 4.91E-06 | 1.92E-05 | 2.07E-05 | 2.63E-05 | 3.72E-06 | 1.45E-05 | 1.56E-05 | 1.99E-05 |
| 9 | 1261 | 352 | 2.47E-06 | 7.14E-06 | 8.21E-06 | 1.49E-05 | 1.87E-06 | 5.41E-06 | 6.22E-06 | 1.13E-05 |
| 10 | 1281 | 160 | 1.05E-04 | 8.90E-05 | 7.56E-05 | 9.84E-05 | 7.91E-05 | 6.73E-05 | 5.72E-05 | 7.45E-05 |
| 11 | 1281 | 363 | 1.83E-06 | 3.38E-06 | 1.15E-05 | 1.38E-05 | 1.39E-06 | 2.56E-06 | 8.71E-06 | 1.05E-05 |
| 12 | 1281 | 372 | 8.67E-06 | 2.75E-05 | 2.38E-05 | 2.27E-05 | 6.56E-06 | 2.08E-05 | 1.80E-05 | 1.72E-05 |
| 13 | 1301 | 162 | 1.98E-04 | 4.44E-06 | 2.31E-04 | 2.79E-06 | 1.50E-04 | 3.36E-06 | 1.75E-04 | 2.11E-06 |
| 14 | 1301 | 383 | 4.31E-06 | 1.97E-07 | 1.10E-05 | 1.96E-07 | 3.26E-06 | 1.49E-07 | 8.34E-06 | 1.48E-07 |
| 15 | 1301 | 392 | 4.56E-06 | 1.67E-06 | 1.86E-05 | 8.63E-07 | 3.45E-06 | 1.26E-06 | 1.41E-05 | 6.53E-07 |
| 16 | 1201 | 152 | 1.21E-04 | 8.02E-07 | 5.95E-05 | 5.40E-07 | 9.13E-05 | 6.07E-07 | 4.50E-05 | 4.09E-07 |
| 17 | 1201 | 292 | 2.50E-06 | 1.50E-06 | 7.36E-06 | 6.65E-07 | 1.89E-06 | 1.13E-06 | 5.57E-06 | 5.03E-07 |
| 18 | 1201 | 403 | 4.22E-06 | 1.52E-07 | 1.66E-05 | 3.80E-07 | 3.19E-06 | 1.15E-07 | 1.26E-05 | 2.87E-07 |
| 19 | 2541 | 32 | 9.25E-05 | 2.45E-07 | 1.48E-04 | 2.60E-07 | 1.52E-05 | 4.02E-08 | 2.42E-05 | 4.25E-08 |
| 20 | 2541 | 33 | 1.19E-05 | 6.25E-08 | 1.05E-05 | 8.51E-08 | 1.96E-06 | 1.02E-08 | 1.71E-06 | 1.39E-08 |
| 21 | 2541 | 34 | 3.44E-05 | 9.64E-07 | 1.34E-05 | 6.43E-07 | 5.64E-06 | 1.58E-07 | 2.20E-06 | 1.05E-07 |
| 22 | 2541 | 35 | 1.28E-05 | 8.57E-08 | 4.45E-05 | 1.61E-07 | 2.09E-06 | 1.40E-08 | 7.30E-06 | 2.63E-08 |
| 23 | 2541 | 36 | 7.37E-06 | 4.86E-07 | 7.31E-06 | 3.18E-07 | 1.21E-06 | 7.97E-08 | 1.20E-06 | 5.21E-08 |
| 24 | 2541 | 37 | 9.93E-06 | 1.62E-07 | 1.37E-05 | 1.01E-07 | 1.63E-06 | 2.65E-08 | 2.25E-06 | 1.65E-08 |
| 25 | 2541 | 38 | 8.68E-05 | 4.25E-07 | 1.43E-04 | 3.13E-07 | 1.42E-05 | 6.96E-08 | 2.34E-05 | 5.13E-08 |
| 26 | 2541 | 39 | 1.24E-05 | 6.06E-08 | 1.83E-05 | 1.78E-07 | 2.04E-06 | 9.93E-09 | 3.01E-06 | 2.92E-08 |
| 27 | 2541 | 40 | 1.69E-05 | 8.89E-07 | 7.05E-06 | 4.12E-07 | 2.77E-06 | 1.46E-07 | 1.15E-06 | 6.75E-08 |
| 28 | 2541 | 41 | 1.08E-05 | 1.13E-07 | 6.47E-05 | 1.39E-07 | 1.77E-06 | 1.85E-08 | 1.06E-05 | 2.27E-08 |
| 29 | 2541 | 42 | 4.53E-05 | 2.31E-07 | 2.67E-05 | 3.68E-07 | 7.43E-06 | 3.78E-08 | 4.37E-06 | 6.04E-08 |
| 30 | 2541 | 43 | 6.83E-06 | 1.02E-07 | 1.76E-05 | 7.69E-08 | 1.12E-06 | 1.66E-08 | 2.89E-06 | 1.26E-08 |

Figure 5.16: Total damage summed up for all directions and sea states.

The resulting limiting stress concentration factors, SCF_{max} , calculated from the fatigue damages in **Fig. 5.16** using Eq. (5.13), are seen in **Fig. 5.17**. The lowest value of SCF_{max} is 4.39, and is obviously seen at the same location as the highest fatigue damage was observed, meaning element 154 at chord position 3.

An overview of the 10 most critical elements are seen in **Tab. 5.5**. For our analysis, the location of maximum damage is in general at a crown point on the chord side of the intersections. An illustration of the locations of these elements in the global model is found in **Fig. 5.18**. It is seen that the limiting stress concentration factors are in a range typical for tubular joints. This analysis can thus not rule out the possibility of fatigue failure during the Ocean Farming concepts lifetime.

| MAXIMUM SCF | | | | | | | | | | |
|-------------|------|-------|-------|-------|-------|-------|-------|-------|-------|-------|
| CON | NODE | BRACE | CPOS1 | CPOS2 | CPOS3 | CPOS4 | BPOS1 | BPOS2 | BPOS3 | BPOS4 |
| 1 | 1221 | 154 | 4.53 | 9.5 | 4.39 | 8.41 | 4.79 | 10.04 | 4.64 | 8.89 |
| 2 | 1221 | 303 | 13.82 | 16.79 | 9.77 | 20.14 | 14.61 | 17.76 | 10.33 | 21.29 |
| 3 | 1221 | 312 | 9.98 | 12.08 | 8.68 | 13.59 | 10.55 | 12.77 | 9.18 | 14.37 |
| 4 | 1241 | 156 | 5.25 | 5.93 | 4.91 | 5.18 | 5.55 | 6.27 | 5.19 | 5.48 |
| 5 | 1241 | 323 | 11.19 | 7.03 | 9.31 | 7.3 | 11.84 | 7.43 | 9.84 | 7.72 |
| 6 | 1241 | 332 | 11.38 | 11.76 | 8.72 | 8.98 | 12.03 | 12.43 | 9.22 | 9.49 |
| 7 | 1261 | 158 | 6.15 | 7.14 | 7.19 | 7.13 | 6.5 | 7.55 | 7.61 | 7.53 |
| 8 | 1261 | 343 | 11.53 | 8.78 | 8.65 | 8.24 | 12.19 | 9.28 | 9.14 | 8.71 |
| 9 | 1261 | 352 | 13.22 | 10.7 | 10.4 | 9.23 | 13.98 | 11.31 | 11 | 9.76 |
| 10 | 1281 | 160 | 6.25 | 6.46 | 6.67 | 6.33 | 6.61 | 6.83 | 7.06 | 6.69 |
| 11 | 1281 | 363 | 14.04 | 12.42 | 9.72 | 9.37 | 14.85 | 13.13 | 10.28 | 9.91 |
| 12 | 1281 | 372 | 10.29 | 8.17 | 8.41 | 8.49 | 10.88 | 8.64 | 8.89 | 8.98 |
| 13 | 1301 | 162 | 5.5 | 11.76 | 5.34 | 12.91 | 5.82 | 12.44 | 5.64 | 13.65 |
| 14 | 1301 | 383 | 11.83 | 21.94 | 9.81 | 21.96 | 12.51 | 23.2 | 10.37 | 23.22 |
| 15 | 1301 | 392 | 11.7 | 14.31 | 8.83 | 16.32 | 12.37 | 15.13 | 9.34 | 17.26 |
| 16 | 1201 | 152 | 6.08 | 16.56 | 7 | 17.93 | 6.43 | 17.51 | 7.4 | 18.96 |
| 17 | 1201 | 292 | 13.2 | 14.62 | 10.63 | 17.2 | 13.96 | 15.45 | 11.24 | 18.18 |
| 18 | 1201 | 403 | 11.88 | 23.1 | 9.03 | 19.23 | 12.56 | 24.42 | 9.55 | 20.34 |
| 19 | 2541 | 32 | 6.41 | 20.99 | 5.83 | 20.76 | 9.2 | 30.14 | 8.38 | 29.8 |
| 20 | 2541 | 33 | 9.65 | 27.6 | 9.91 | 25.94 | 13.86 | 39.62 | 14.23 | 37.25 |
| 21 | 2541 | 34 | 7.81 | 15.96 | 9.43 | 17.31 | 11.21 | 22.92 | 13.54 | 24.85 |
| 22 | 2541 | 35 | 9.53 | 25.91 | 7.42 | 22.85 | 13.68 | 37.2 | 10.65 | 32.8 |
| 23 | 2541 | 36 | 10.63 | 18.31 | 10.65 | 19.93 | 15.26 | 26.29 | 15.29 | 28.62 |
| 24 | 2541 | 37 | 10.01 | 22.81 | 9.39 | 25.08 | 14.38 | 32.75 | 13.48 | 36.01 |
| 25 | 2541 | 38 | 6.49 | 18.81 | 5.88 | 19.99 | 9.32 | 27 | 8.44 | 28.7 |
| 26 | 2541 | 39 | 9.58 | 27.77 | 8.86 | 22.38 | 13.75 | 39.87 | 12.72 | 32.13 |
| 27 | 2541 | 40 | 9 | 16.23 | 10.72 | 18.93 | 12.93 | 23.3 | 15.4 | 27.18 |
| 28 | 2541 | 41 | 9.85 | 24.52 | 6.88 | 23.53 | 14.14 | 35.21 | 9.88 | 33.78 |
| 29 | 2541 | 42 | 7.39 | 21.25 | 8.22 | 19.35 | 10.61 | 30.51 | 11.8 | 27.79 |
| 30 | 2541 | 43 | 10.79 | 25.04 | 8.93 | 26.47 | 15.5 | 35.95 | 12.82 | 38.01 |

Figure 5.17: The limiting SCF values for 25 years lifetime.

Table 5.5: Sorted list of the 10 most critical elements in the fatigue analysis.

| Element | Location of max damage | D_{life} | SCF_{max} |
|---------|------------------------|------------|-------------|
| 154 | CPOS3 | 6.13E-04 | 4.39 |
| 156 | CPOS3 | 3.50E-05 | 4.91 |
| 162 | CPOS3 | 2.31E-04 | 5.34 |
| 32 | CPOS3 | 1.48E-04 | 5.83 |
| 38 | CPOS3 | 1.43E-04 | 5.88 |
| 152 | CPOS1 | 1.21E-04 | 6.08 |
| 158 | CPOS1 | 1.14E-04 | 6.15 |
| 160 | CPOS1 | 1.05E-04 | 6.25 |
| 41 | CPOS3 | 6.47E-05 | 6.88 |
| 323 | CPOS2 | 5.84E-05 | 7.03 |

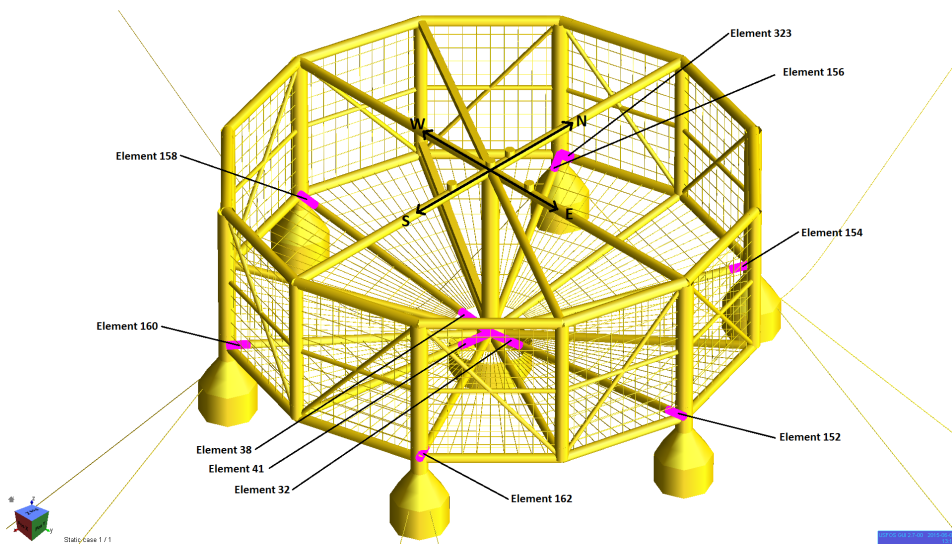


Figure 5.18: Top ten most damaged elements in the complete model along with directional definitions to be seen in connection with Fig. 5.11.

Qualitative Comparison and Final Remarks

In this chapter, we will discuss the results obtained in the ultimate- and fatigue limit state analyses and summarize with some concluding remarks. In addition, recommendations to further work will be given.

6.1 ULS: Results and Comparison

Our results from the ULS analysis is given in section 5.1, and shows that the Ocean Farming concept has the structural integrity needed to withstand the possible extreme environmental forces in Frohavet. Some simplifications and deviations are however present in the analysis which can affect the results to some extent. The most important are:

1. The analysis have been conducted using the *SpoolWave* option in USFOS, assuming that the highest loads will be seen for the highest waves. The results indicates that this in general is true, however, for such a new design, full 3-hour analyses would have been preferable.
2. Only one sea state have been considered. Other sea states along the 100-year contour line might give more violent and decisive responses.
3. Some deviations are present in our USFOS model, particularly when it comes to the distribution of masses from equipment, etcetera. This can lead to slightly different motion characteristics, and will also cause deviations in the static forces in the structural members.
4. Uncertainty in the chosen drag and inertia coefficients to be used in Morison's equation is present, leading to uncertainty in the calculated loads.

5. The net have been modelled with a coarser mesh and a larger structural diameter than in reality. In addition, both the net and the mooring lines have been modelled using beam elements, overestimating the axial compression and bending stiffness. This is however not expected to influence the results in any significant way.

It is particularly point 1. and 2. in the list above that introduces uncertainties to the validity of the obtained results. This means that our results do not necessarily represent the extreme 100-year response of the structure. Chances are that this extreme response can be seen for special wave trains passing the fish farm which is not captured by the SpoolWave option, or other sea states might be more critical. If we disregard this, our results are however expected to be of good quality.

Quite large deviations are seen in the obtained utilization values from our analyses if we compare them to what was found by Heiervang and Knutsen in their thesis. While our results shows that the fish farm is properly designed with respect to resisting extreme environmental forces, their results shows stress levels up to 50 percent above the allowable stress from the API-WSD standard. It is however difficult to conclude if this has to do with improvements in our modelling procedure, or if it is only the updated member dimensions from the structural drawings that are the cause to the deviations. The latter is however believed to be most decisive. A comparison of the results for the most severe wave and current direction are seen in **Fig. 6.1** and **6.2**. Note that their results are plotted for individual elements while we have plotted the global maxima. In addition, Heiervang and Knutsen have used wave and current directions for another quadrant than in our analyses.

It is seen that their obtained utilization values are significantly higher than ours. Our model is based on an updated design, and this is expected to be the main reason for the reduced utilizations. In addition, a negative vertical drift were detected in their analysis. It is likely that this has contributed to additional forces, and also increased the possibility of slamming loads on the top outer ring. It is also believed that the hydrodynamic damping is larger for our model as both the bottom net and the mooring lines are included, reducing the response.

6.1.1 Concluding Remarks

One of the goals of this thesis was to update and improve the USFOS model made by Heiervang and Knutsen. This showed to be very time-consuming as we had to model the fish farm from scratch. We are however very satisfied with the resulting model, and all major load effects seems to be properly accounted for (disregarding second order drift forces). The results from the ultimate limit state analysis shows that the Ocean Farming concept is properly designed with respect to structural strength criteria, and is within the requirements in the API-WSD standard. Further verification is however needed. Full 3-hour analyses combined with considering other sea states on the 100-year contour line would be preferable. The characteristic 100-year extreme elastic utilization values obtained from our analysis is presented in **Tab. 6.1**. It is seen that the results are symmetric about direction 315. This is as expected considering the structural layout.

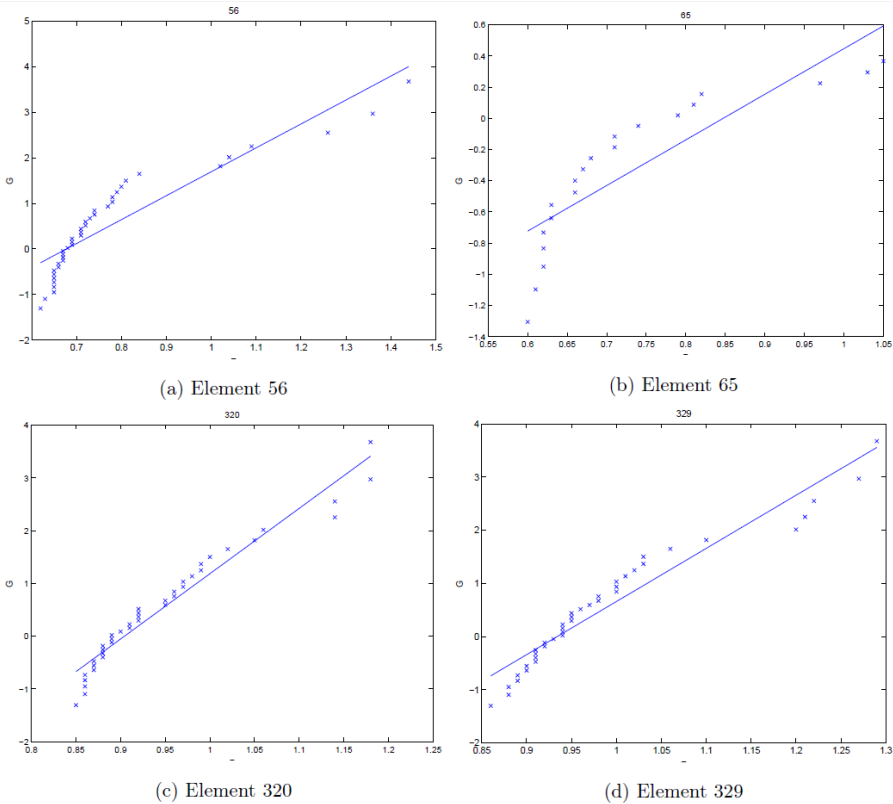


Figure 6.1: Utilizations found by Heiervang and Knutsen at the direction corresponding to our direction 315, but for another quadrant (dir 225). [24]

Table 6.1: Characteristic 100-year extreme API-WSD utilizations obtained in the ULS analysis.

| Wave and current direction | API-WSD utilization (90 percent fractile) |
|----------------------------|---|
| Dir 270 | 0.77 |
| Dir 285 | 0.78 |
| Dir 300 | 0.81 |
| Dir 315 | 0.82 |
| Dir 330 | 0.81 |
| Dir 345 | 0.78 |
| Dir 360 | 0.77 |

6.2 FLS: Results and Discussion

A simplified dynamic fatigue limit state analysis, based on a stochastic approach, has been carried out on the Ocean Farming concept, looking at the most critical joints. The results,

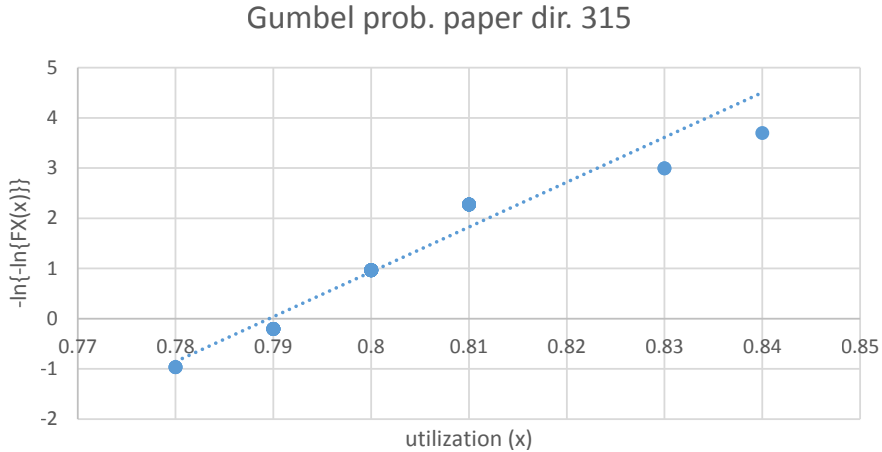


Figure 6.2: Gumbel probability paper for direction 315.

presented in section 5.2, indicates that the limiting stress concentration factors are in a range typical for tubular joints. The possibility of fatigue failure can thus not be ruled out. Some simplifications, partly due to lack of information, have however been introduced, affecting the validity of the results. The most important are:

1. All stress concentration factors used in the analyses have been set equal to 1.0.
2. In general, one will have different values of SCFs for axial forces, in-plane bending and out-of-plane bending. The effect of this is not captured in the analysis.
3. When estimating the limiting SCFs, SCF_{max} , it is assumed that all stress ranges are within the part of the S-N curve with inverse slope parameter m equal to 5.0, making the total fatigue damage proportional to $(\Delta S)^5$. This is true for the original analysis, but when introducing a SCF of a certain size, this will be a conservative assumption (for ΔS greater than 52.6 MPa, the damage is proportional to $(\Delta S)^3$).
4. Only 7 joints, giving a total of 30 chord-brace intersections, have been analysed. The possibility of other joints being more critical with respect to fatigue can not be ruled out.
5. In addition to inherent uncertainty in the received environmental data, the specific location of where the Ocean Farming concept shall be placed have not yet been decided. This gives additional uncertainty to the environmental data used in the fatigue analysis.
6. In NORSOK N-004 [47], it is stated that the number of load cycles shall be multiplied with the appropriate fatigue design factor in **Fig. 6.3** before the fatigue analysis is performed. This has not been done in our analyses, contributing to an underestimation of the calculated fatigue damage.

| Classification of structural components based on damage consequence | Access for inspection and repair | | |
|---|----------------------------------|-------------------|-------------------|
| | No access or in the splash zone | Accessible | |
| | | Below splash zone | Above splash zone |
| Substantial consequences | 10 | 3 | 2 |
| Without substantial consequences | 3 | 2 | 1 |

“Substantial consequences” in this context means that failure of the joint will entail danger of loss of human life; significant pollution; major financial consequences.

“Without substantial consequences” is understood failure where it can be demonstrated that the structure satisfy the requirement to damaged condition according to the ALSs with failure in the actual joint as the defined damage.

Figure 6.3: Fatigue design factors from NORSOK N-004. [47]

The basis of the entire analysis is point 1 in the list above. This will not be discussed further. It should however be mentioned that the analysis can be re-run when the real stress concentration factors are obtained. Implementation of these SCFs should be fairly easy.

Point 2 introduces some restrictions in the use of our obtained results. It has not been investigated what type of stress which is most governing for the fatigue life of the considered locations (axial, IPB, or OPB). Thus, if one is in a position where the the *real* SCFs are known and for example the axial SCF of a given location is larger than SCF_{max} , while the other SCFs are within the limit, it is uncertain if fatigue failure really will occur.

Quite a lot of work was invested in investigating the consequence of point 3. Assuming a constant negative inverse slope parameter, m , was necessary in order to find the limiting values of the SCFs. The chosen S-N curve was, as stated in section 5.2, the T-curve for structures with cathodic protection exposed to sea water. For this curve, m changes from 3.0 to 5.0 for ΔS less than 52.6 MPa (fatigue limit). When setting all SCFs equal to 1.0, all the recorded stress ranges was well below this limit, and the highest recorded stress range in the entire analysis was no more than 27 MPa. In connection with fatigue analyses, the Miner sum (fatigue damage) may be expressed in terms of an equivalent stress range, ΔS_{eq} . The main property of the equivalent stress range is that if one knows the value of ΔS_{eq} in addition to the total number of lifetime load cycles, the total fatigue damage can be estimated directly from the S-N curve by going in with this stress range value. The equivalent stress range is thus a very good indicator of the characteristic stress range during the lifetime of the structure. A quick and simplified estimate of ΔS_{eq} for the most utilized member of the analysis is performed below. The calculations are based on assuming a constant value of the inverse slope parameter and that the lifetime stress spectra can be described by the two-parameter Weibull distribution. The latter has shown to be true for many types of marine structures [1].

Based on the above assumptions, a closed form expression for ΔS_{eq} can be obtained, resulting in Eq. (6.1) [1].

$$\Delta S_{eq} = \frac{\Delta S_0}{(\ln(n_0))^{1/h}} \left[\Gamma \left(1 + \frac{m}{h} \right) \right]^{1/m} \quad (6.1)$$

where

- ΔS_0 maximum stress range during the load history
- n_0 total number of load cycles in the load history
- h Weibull shape parameter
- m negative inverse slope parameter of S-N curve
- Γ the complete Gamma function

n_0 can be found by dividing the total design life by the average zero-up-crossing period found from the scatter diagram ($\overline{T_Z} = 3.91$ seconds), giving $n_0 = 2.0 \cdot 10^8$. The largest stress range from the analysis was 27 MPa, however, somewhat larger stress ranges are expected to occur during the design life. A reasonable value of ΔS_0 is set to 45 MPa. The Weibull shape parameter depends on many factors such as wave climate, type of structure (drag versus inertia dominated), position of the joint in the structure, etcetera. Based on information found in *Fatigue Handbook* [1], h set to 1.0 is found to be suitable. As mentioned before, m is set equal to 5.0. The result is an equivalent stress range of $\Delta S_{eq} = 6.1$ MPa. By going into the S-N curve with this stress range, a lifetime fatigue damage of 5.72E-04 is obtained. This deviates by only 6 percent compared to what was found in our fatigue analysis. The obtained value of ΔS_{eq} is thus assumed to be a very good estimate of the characteristic stress of the most utilized member during the lifetime of the fish farm.

From the calculation above, it is seen that the equivalent stress range of the most utilized member in the fatigue analysis (element 154, chord position 3) is ΔS_{eq} approximately equal to 6 MPa. The limiting stress concentration factor for this particular location was found to be $SCF_{max} = 4.39$. If we simply multiply this SCF with ΔS_{eq} , we can get an estimate of the real equivalent stress, giving $\Delta S_{eq,real} = 27$ MPa. It is seen that this stress range is well below the fatigue limit where the negative inverse slope parameter m changes value. This means that even when the limiting SCF is implemented, most of the fatigue damage will occur for stress ranges below the fatigue limit (m equal to 5.0). The level of overestimation of the fatigue damage when assuming that the fatigue damage is proportional to $(\Delta S)^5$ for all stress ranges, even when introducing SCFs of a certain size, is thus assumed to be relatively small.

Point 4 about the limited amount of joints considered in the analysis, will have an unknown effect on the fatigue life of the fish farm. It is not possible to conclude that the most critical member is included in the fatigue analysis. We are however very confident that we have included *some* of the most critical elements.

It is hard to evaluate the effect of point 5. Fatigue in general is governed by the frequently occurring sea states, and even though some scatter is seen for the estimated extreme sea states, it is reasonable to believe that the observed sea state characteristics in general will be quite equal for the different possible locations. However, when, or if a final location

is chosen, it is obvious that the environmental data to be used in the fatigue analysis are chosen accordingly.

Point 6 can potentially have a significant effect on the calculated fatigue damage. Referring to **Fig. 6.3**, it is seen that the fatigue design factors to be multiplied with number of load cycles, ranges from 1-10. This means that potentially, the calculated fatigue damages have been underestimated by a factor of 10, depending on the structural component classification and accessibility for inspection and repair. For the considered joints, it is reasonable to believe that for most of the members, the classification of structural components based on damage consequence will be "without substantial consequences" combined with "accessible for inspection and repair", and "below splash zone". This will give a fatigue design factor of 2, doubling the total calculated fatigue damage, D_{life} . It should however be noted from Eq. (5.13), that the estimated limiting SCFs, SCF_{max} is proportional to $\sqrt[5]{D_{life}}$. This means that with a fatigue design factor equal to 2, the calculated values of SCF_{max} is only overestimated by about 15 percent.

6.2.1 Concluding Remarks

As discussed in section 6.2, the fatigue limit state analysis have been performed with some simplifications, introducing uncertainties, and thus affecting the validity of the results. Some of these affects the results in a conservative way, while others do not. The relative importance the simplifications are not known, and it is thus not possible to conclude if the final results are conservative or not. One should however remember that inherent uncertainty is always present when performing fatigue calculations, and prediction of fatigue failure is not an exact science. This has to do with for example, inherent uncertainty in the S-N data. In addition, the actual quality of the workmanship performed under construction will affect the actual fatigue life significantly. The so-called stress interaction effects (stress memory effects), briefly described in section 3.2, will also influence the actual fatigue crack growth.

By referring to **Tab. 5.5** and **Fig. 5.18**, one can see that it is in general the intersections between the bottom radial beams and the vertical columns that are most critical with respect to fatigue. If one considers the structural layout of the Ocean Farming concept, it is quite easy to imagine that the bottom radial beams will be the most dynamically loaded members. The fact that the results indicates that these beams are governing when it comes to the fatigue life of the structure this, is thus as anticipated. There is nevertheless no doubt that a more detailed fatigue analysis have to be performed, and it is highly recommended that the real stress concentration factors are obtained before performing this analysis. This will significantly reduce the uncertainty in the calculated fatigue damages. Our results are however not believed to be totally insignificant, and should be used as some first estimates in anticipation of more detailed results. The lowest obtained limiting stress concentration factor, including location and calculated lifetime fatigue damage is given in **Tab. 6.2**. It should be noted that this is within a range typical for tubular joints.

Table 6.2: Smallest obtained limiting stress concentration factors, including location and calculated lifetime fatigue damage, reference is made to Fig. 5.18.

| Element | Location of max damage | D_{life} | SCF_{max} |
|---------------------|------------------------|------------|-------------|
| 154 (bottom radial) | CPOS3 | 6.13E-04 | 4.39 |

6.3 Suggestions to Further Work

The work and results accomplished during this thesis should hopefully help further validate the Ocean Farming concept. However, much work remains, especially with respect to full 3-hour sea state simulations of a stochastic nature, more detailed fatigue limit state analyses as well as accidental limit state analyses. Below is an itemized list of suggestions to further validate the results in the next instance on this project.

- **Modelling**

- A better distribution of point masses representing deck loads should be applied to best match the center of gravity of the designed structure. This will affect the estimated natural periods of the fish farm.
- For investigating additional joints with respect to fatigue, modifications should be applied to the model. More specifically, dummy elements must be inserted at some locations, extending the chord, for FATAL to be able to check these joints with respect to fatigue.
- Further validation of the model should be performed. This includes for example checking mooring line and total drag forces against the model experiments.

- **Ultimate limit state**

- The global response analysis were conducted inside a quadrant, looking at only one sea state from the estimated 100-year contour line. To further validate the results, the complete contour line should be simulated to obtain a proper estimate for the largest ULS response. Full 3-hour sea state simulations should be run as the highest waves not necessarily will give the largest response.

- **Fatigue limit state**

- A more detailed fatigue assessment should be performed, investigating additional joints and considering 8 clock-positions along the intersections as recommended in DNVGL-RP-0005. It is highly recommended that the real stress concentration factors are obtained before performing this analysis. The fatigue design factors in **Fig. 6.3** should also be included.
- If a final location is chosen, this should be reflected in the chosen environmental conditions.

- **Miscellaneous**

- The analyses done here could also be run with completely different software packages to further validate the results.
- Accidental limit state (ALS) analyses, for instance investigating the effect of ship collisions, should be performed.
- The performance of USFOS and the employed utility tools (FATAL and Cod-Chk) should be further validated for use on floating structures like the Ocean Farming concept.

- ENDEX -

References

- [1] A. Almar-Næss. *Fatigue Handbook: Offshore Steel Structures*. Tapir, 1985.
- [2] J. Amdahl. *TMR4167 Marin Teknikk 2 - Del 2: Knekking*. NTNU - Department of Marine Technology, August 2009.
- [3] API-RP-2A-WSD. *Recommended Practice for Planning, Design and Constructing Fixed Offshore Platforms - Working Stress Design*, December 2000.
- [4] K.-J. Bathe and S. Bolourchi. Large displacement analysis of three-dimensional beam structures. *International Journal for Numerical Methods in Engineering*, 14(7):961–986, 1979.
- [5] S. Berge. *Fatigue and Fracture Design of Marine Structures - Fatigue Design of Welded Structures*. NTNU - Department of Marine Technology, September 2006.
- [6] P. T. Bore, H. Brandsegg, J. S. Folstad, M. K. Loe, C. Møgster, and K. Taraldsvik. Eksponert Havbruk - En Ny Æra? NTNU - Eksperter i Team, April 2014.
- [7] P. T. Bore and P. A. Fossan. *Rational Design of Offshore Aquaculture Structures*. NTNU - Project Thesis, December 2014.
- [8] P. T. Bore, P. A. Fossan, and K. Gregersen. USFOS Project. TMR4195 - Design of Offshore Structures, April 2014.
- [9] Y. Çengel and J. Cimbala. *Fluid Mechanics: Fundamentals and Applications*. Cengel series in engineering thermal-fluid sciences. McGraw-Hill Higher Education, 2010.
- [10] Directorate of Fisheries. *Aquaculture statistics*, July 2014. <http://www.fiskeridir.no/english/statistics/norwegian-aquaculture/aquaculture-statistics>.
- [11] Directorate of Fisheries. *Tildeling av grønne løyve 2013*, December 2014. <http://www.fiskeridir.no/akvakultur/groene-loeyve>.
- [12] DNV-OS-E301. *Position Mooring*, October 2010.
- [13] DNV-RP-C103. *Column-Stabilised Units*, October 2010.

-
- [14] DNV-RP-C205. Environmental Conditions and Environmental Loads, April 2014.
- [15] DNVGL-RP-0005. RP-C203: Fatigue design of offshore structures, June 2014.
- [16] W. Dover and A. M. Rao. *Fatigue in Offshore Structures*. New Delhi : Oxford & IBH Publ. Co., 1996.
- [17] P. C. Endresen, M. Fjøre, A. Fredheim, D. Kristiansen, and B. Enerhaug. Numerical modeling of wake effect on aquaculture nets. In *ASME 2013 32nd International Conference on Ocean, Offshore and Arctic Engineering*, pages V003T05A027–V003T05A027. American Society of Mechanical Engineers, 2013.
- [18] O. M. Faltinsen. *Sea loads on ships and offshore structures*. Cambridge University Press, Cambridge New York, 1993.
- [19] FAO. The State of World Fisheries and Aquaculture 2014 (SOFIA), 2014.
- [20] A. Fredheim. *Current Forces on Net Structure*. PhD thesis, Norwegian University of Science and Technology, Faculty of Engineering Science and Technology, 2005.
- [21] Global Maritime. Ocean Farming - Structural Drawings, 2014. Drawing no. 402-002-*
- [22] K. Hasselmann, T. Barnett, E. Bouws, H. Carlson, D. Cartwright, K. Enke, J. Ewing, H. Gienapp, D. Hasselmann, P. Kruseman, et al. Measurements of wind-wave growth and swell decay during the Joint North Sea Wave Project (JONSWAP). Technical report, Deutsches Hydrographisches Institut, 1973.
- [23] S. K. Haver. Prediction of Characteristic Response for Design Purposes. Preliminary version, Statoil internal, 2011.
- [24] M. F. Heiervang and M. F. Knutsen. Time Domain Analysis of Fish Farms Subjected to Extreme Environmental Conditions. Master’s thesis, Norwegian University of Science and Technology, 2014.
- [25] A. K. Imsland, P. Reynolds, G. Eliassen, T. A. Hangstad, A. Foss, E. Vikingstad, and T. A. Elvegård. The use of lumpfish (*Cyclopterus lumpus* L.) to control sea lice (*Lepeophtheirus salmonis* Krøyer) infestations in intensively farmed Atlantic salmon (*Salmo salar* L.). *Aquaculture*, 424–425(0):18 – 23, 2014.
- [26] J. Jia. An efficient nonlinear dynamic approach for calculating wave induced fatigue damage of offshore structures and its industrial applications for lifetime extension. *Applied Ocean Research*, 30(3):189 – 198, 2008.
- [27] J. Journée and W. Massie. *Offshore Hydromechanics - First Edition*. Delft University of Technology, January 2001.
- [28] D. Kristiansen. *Wave induced effects on floaters of aquaculture plants*. PhD thesis, Norwegian University of Science and Technology, Department of Marine Technology, Centre for Ships and Ocean Structures, 2010.
- [29] T. Kristiansen and O. M. Faltinsen. Modelling of current loads on aquaculture net cages. *Journal of Fluids and Structures*, 34(0):218 – 235, 2012.

-
- [30] P. Lader, T. Dempster, A. Fredheim, and Østen Jensen. Current induced net deformations in full-scale sea-cages for Atlantic salmon (*Salmo salar*). *Aquacultural Engineering*, 38(1):52 – 65, 2008.
- [31] I. Langen and R. Sigbjørnsson. *Dynamisk analyse av konstruksjoner*. Tapir, Trondheim, 1979.
- [32] C. M. Larsen. Vortex Induced Vibrations. A short and incomplete introduction to fundamental concepts, October 2011.
- [33] C. M. Larsen. *TMR4182 Marin Dynamikk*. NTNU - Department of Marine Technology, January 2012.
- [34] K. Larsen. Mooring and station keeping of floating structures. TMR4225 Marine Operations - Lecture Notes, February 2014.
- [35] F. Le Bris and D. Marichal. Numerical and experimental study of submerged supple nets: Applications to fish farms. *Journal of Marine Science and Technology*, 3(4):161–170, 1998.
- [36] G. Løland. *Current Forces on and Flow Through Fish Farms*. Doktor ingeniøravhandling / Norges Tekniske Høgskole, Universitetet i Trondheim. Division of Marine Hydrodynamics, the Norwegian Institute of Technology, 1991.
- [37] G. F. Loverich and L. Gace. The Effect of Currents and Wave on Several Classes of Offshore Sea Cages. In *Open Ocean Aquaculture '97 - Charting the Future of Ocean Farming*, pages 131–144, Maui, Hawaii, April 23-25 1997.
- [38] M. Matsuishi and T. Endo. Fatigue of metals subjected to varying stress. *Japan Society of Mechanical Engineers, Fukuoka, Japan*, pages 37–40, 1968.
- [39] Ministry of Fisheries and Coastal Affairs. Nye tiltak mot rømming og lakselus (Pressemelding), December 2011. <https://www.regjeringen.no/nb/aktuelt/nye-tiltak-mot-romming-og-lakselus--/id667455/>.
- [40] Ministry of Trade, Industry and Fisheries. Forskrift om krav til teknisk standard for flytende akvakulturanlegg (NYTEK-forskriften), FOR-2011-08-16-849 2015. <https://lovdata.no/dokument/SF/forskrift/2011-08-16-849?q=nytek>.
- [41] H. Moe, A. Fredheim, and O. Hopperstad. Structural analysis of aquaculture net cages in current. *Journal of Fluids and Structures*, 26(3):503 – 516, 2010.
- [42] B. O. Molberg. Derfor fikk Salmar nei, August 2014. <http://www.adressa.no/nyheter/okonomi/article10034650.ece>.
- [43] J. Morison, J. Johnson, S. Schaaf, et al. The force exerted by surface waves on piles. *Journal of Petroleum Technology*, 2(05):149–154, 1950.
- [44] G. Myrebøe. Havbasert Fiskeoppdrett - en viktig bidragsyter til verdens matproduksjon. Presented at NTNU Brohode Frøya, October 2014.
- [45] NORSOK-N-001. Integrity of offshore structures, September 2012.
-

-
- [46] NORSOK-N-003. Actions and actions effects, September 2007.
- [47] NORSOK-N-004. Design of steel structures, February 2014.
- [48] NS-9415. Marine fish farms - Requirements for site survey, risk analyses, design, dimensioning, production, installation and operation, 2009.
- [49] T. Olafsen, U. Winther, Y. Olsen, and J. Skjermo. Verdiskapning basert på produktive hav i 2050. Technical report, DKNVS and NTVA, 2012.
- [50] B. Pettersen. *TMR4247 Marin Teknikk 3 - Hydrodynamikk*. NTNU - Department of Marine Technology, January 2007.
- [51] M. Shainee, H. Ellingsen, B. Leira, and A. Fredheim. Design theory in offshore fish cage designing. *Aquaculture*, 392–395(0):134 – 141, 2013.
- [52] M. Shainee, B. J. Leira, H. Ellingsen, and A. Fredheim. An Optimum Design Concept for Offshore Cage Culture. In *ASME 2012 31st International Conference on Ocean, Offshore and Arctic Engineering*, pages 85–93. American Society of Mechanical Engineers, 2012.
- [53] Sjømat Norge. Om lakselus, June 2015. <http://lusedata.no/om-lakselus/>.
- [54] B. Skallerud. Efficient stress resultant plasticity formulation for thin shell applications: Implementation and numerical tests. USFOS Basic Theory, SINTEF Civil and Environmental Engineering, March 1998.
- [55] Statistics Norway. Aquaculture, 2013, final figures, October 2014. <http://ssb.no/en/jord-skog-jakt-og-fiskeri/statistikker/fiskeoppdrett>.
- [56] H. Strandenes. Usfos scripting, March 2012. <http://www.ivt.ntnu.no/imt/software/usfos:scripting>.
- [57] USFOS. *USFOS User's Manual - Modelling*. MARINTEK, February 1999.
- [58] USFOS. *USFOS User's Manual - Input Description USFOS Control Parameters*. USFOS, January 2014.
- [59] Vryhof Anchors BV. *Anchor Manual 2010 - The Guide to Anchoring*. Vryhof Anchors BV, 2900 AC Capelle aan den Yssel, The Netherlands, 2010. Provides technical details about anchors and mooring line components.

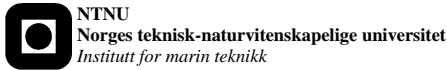
Appendix

A List of Acronyms

| | |
|----------------|---|
| ALS | Accidental limit state |
| AMOS | Center of Autonomous Marine Operations and Systems |
| API | American Petroleum Institute |
| CFD | Computational fluid dynamics |
| CoG | Center of gravity |
| DKNVS | Royal Norwegian Society of Sciences and Letters |
| FAO | Food and Agriculture Organization of the United Nations |
| FFT | Fast Fourier transform |
| FLS | Fatigue limit state |
| FORM | First order reliability method |
| GUI | Graphical user interface |
| HDPE | High density polyethylene |
| IPB | In-plane bending |
| JONSWAP | JOint North Sea WAve Project |
| MBL | Minimum breaking load |
| NTNU | Norwegian University of Science and Technology |
| NTVA | Norwegian Academy of Technological Sciences |
| OPB | Out-of-plane bending |

| | |
|-------------|-----------------------------|
| OS | Offshore standard |
| PET | Ethylene terephthalate |
| PM | Pierson-Moskowitz |
| RP | Recommended practice |
| SCF | Stress concentration factor |
| SWAN | Simulating WAves Nearshore |
| ULS | Ultimate limit state |
| VCG | Vertical center of gravity |
| VIV | Vortex induced vibrations |
| WSD | Working stress design |

B Master Thesis Problem Text



MASTER THESIS 2015

for

Stud. Techn. Pål Alexander Fossan/Pål Bore Takle

Rational design of offshore aquaculture structures
Rasjonelle dimensjoneringsmetoder for havbrukskonstruksjoner

Marine fish farming is in rapid development. Dimensions are expected to increase and locations are being moved to areas exposed to more energetic waves and stronger currents. This leads to several challenges: Strong currents can cause large net deformations and affect largely the hydroelastic behaviour of the cage. Wave overtopping may occur in during extreme waves, so nonlinear effects matter. Viscous effects are essential for the loading on the net structures, as well as the wake inside the cage. Another issue is the effect of biofouling on the net loading. Waves and currents are of concern for the volume within the fish cage and the design of mooring lines. Operations with a wellboat moored to the fish farm become challenging. For example the ship propeller can suck the net and this can partially break the net and cause fish escape.

Collapse of fish farms, with large-scale fish escape to the level experienced in the past, will not be tolerated by the society. New and extreme loading scenarios need to be properly designed for by means of “*first principles*” methods to meet required safety levels and performance.

Rational design requirements for aquaculture structures must be developed based on simulations of the governing physical phenomena, structural load effects and structural resistance. That is, the motion of the fish farm in irregular seas must be simulated, along with accurate assessment of load effects (stresses) in the load carrying structures. Fatigue, ultimate strength and accidental limit state conditions should be addressed. Simplified design oriented load cases, e.g. static load cases, should be developed and calibrated against fundamental numerical simulations.

The purpose of this work is to analyse Salmar’s steel cage concept for exposed areas in view of the functional and safety requirements. The starting point for the work is thesis conducted by Mads Heiervang and Mats Foss Knutsen in the spring of 2014.

The work is proposed carried out in the following steps:

- 1) Review of the model developed for simulations with USFOS. The adequacy of the model and need for improvements shall be addressed with respect to:
 - Modelling of catenary mooring lines
 - Added mass in heave for pontoons
 - Modelling of net, including pretension

- Modelling of drag forces
- Modelling of slamming forces, if relevant

To the extent needed evaluate the behaviour of subcomponents by simulations with simple sub-models

- 2) Perform comparative simulations with model tests carried out by Marintek with an updated model based on the work in pt 1)
- 3) Perform fatigue analysis of a tubular joint by time domain simulations with USFOS/FATAL. Verify that the calculations are correct and/or FATAL is correctly used by checking the results for simple, known cases. For the fatigue analysis stress concentration factors (SCF) will be needed (from beam forces to hot spot stresses). Preferably, this is obtained from Global Maritime. Alternatively, a detailed finite element model of the joint has or has to be established.
- 4) Conduct ultimate strength analysis based on the contour line method. Determine the characteristic load effects and elastic utilization for selected response variables for the cage and the mooring lines. Compare the results with previous investigations.
- 5) Investigate whether simplified methods can be used to check the compliance with FLS and ULS requirements. Can the design wave concept be used for ULS design?
- 6) Investigate the resistance of the concept with respect to abnormal waves and accidental ship collisions.
- 7) Conclusions and recommendation for further work

Literature studies of specific topics relevant to the thesis work may be included.

The work scope may prove to be larger than initially anticipated. Subject to approval from the supervisors, topics may be deleted from the list above or reduced in extent.

In the thesis the candidate shall present his personal contribution to the resolution of problems within the scope of the thesis work.

Theories and conclusions should be based on mathematical derivations and/or logic reasoning identifying the various steps in the deduction.

The candidate should utilise the existing possibilities for obtaining relevant literature.

Thesis format

The thesis should be organised in a rational manner to give a clear exposition of results, assessments, and conclusions. The text should be brief and to the point, with a clear language. Telegraphic language should be avoided.

The thesis shall contain the following elements: A text defining the scope, preface, list of contents, summary, main body of thesis, conclusions with recommendations for further work, list

of symbols and acronyms, references and (optional) appendices. All figures, tables and equations shall be numerated.

The supervisors may require that the candidate, in an early stage of the work, presents a written plan for the completion of the work. The plan should include a budget for the use of computer and laboratory resources, which will be charged to the department. Overruns shall be reported to the supervisors.

The original contribution of the candidate and material taken from other sources shall be clearly defined. Work from other sources shall be properly referenced using an acknowledged referencing system.

The report shall be submitted in two copies:

- Signed by the candidate
- The text defining the scope included
- In bound volume(s)
- Drawings and/or computer prints, which cannot be bound should be organised in a separate folder.
- The report shall also be submitted in pdf format along with essential input files for computer analysis, spreadsheets, MATLAB files etc in digital format.
-

Ownership

NTNU has according to the present rules the ownership of the thesis. Any use of the thesis has to be approved by NTNU (or external partner when this applies). The department has the right to use the thesis as if the work was carried out by a NTNU employee, if nothing else has been agreed in advance.

Thesis supervisor

Prof. Jørgen Amdahl

Contact person at Global Maritime: Roy Andre Erland

Deadline: June 10, 2015

Trondheim, January 14, 2015

Jørgen Amdahl

C Convergence Studies

A convergence study was conducted before the analyses were run in order to investigate properties of the numerical solution procedure in USFOS and correct possible instabilities that would lead to less reliable result. The study was focused on the parameters listed in **Tab. C.1** in which all the parameters were combined, resulting in 27 separate analyses. *Liter* is an USFOS-command used to switch on light iteration with the option of adjusting the max number of iterations in the calculations. *Phase seed* is the seed number input to the wave data, causing three different sea states.

Table C.1: The parameters combined for convergence study of the solution procedure.

| Timestep | Liter | Phase seed |
|----------|-------|------------|
| 0.2 | 1 | 10 |
| 0.5 | 2 | 20 |
| 1.0 | 3 | 30 |

At timestep 0.2, all the analyses were completed. However at timestep 0.5 and 1.0, only the analyses with *Liter* set to 1 were successful. In compliance with our limited understanding of this particular command, we are not able to explain why. From the studies it is clear that the analyses will run even at such large timestep as 1.0, but this may not be the best choice. In order to capture as many as possible of the peaks and bottoms in the sea state and accompanying response in the written result file, a smaller timestep were chosen. In regards to the convergence of the solution, they were surprisingly similar, suggesting that our significant investment in modelling had not been a waste of time. The results are summarized in **Fig. C.1, C.2, C.3, and C.4**. In the figure labels, *Liter* 1, 2, and 3, are in connection with timestep 0.2, while timestep 0.5 and 1.0 only show results for *Liter* 1. The three figures are from the sea state with seed 10.

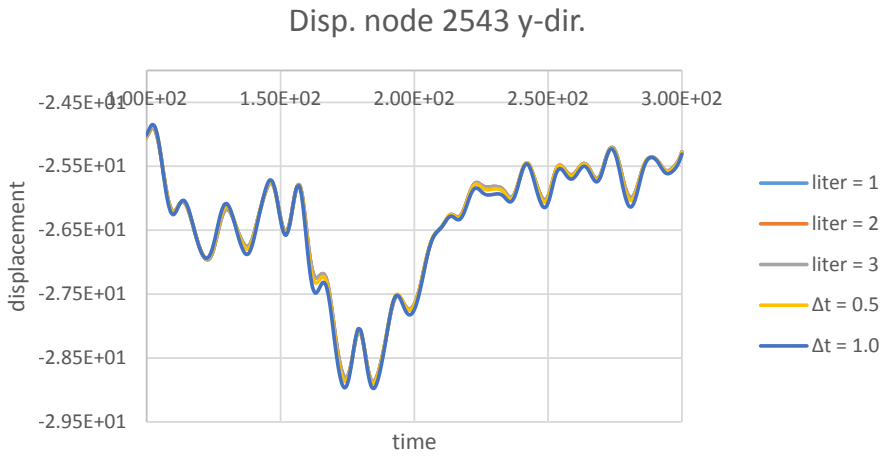


Figure C.1: Convergence study related to the LITER command, results are presented in the form of displacement of node 2543 in the y-direction.

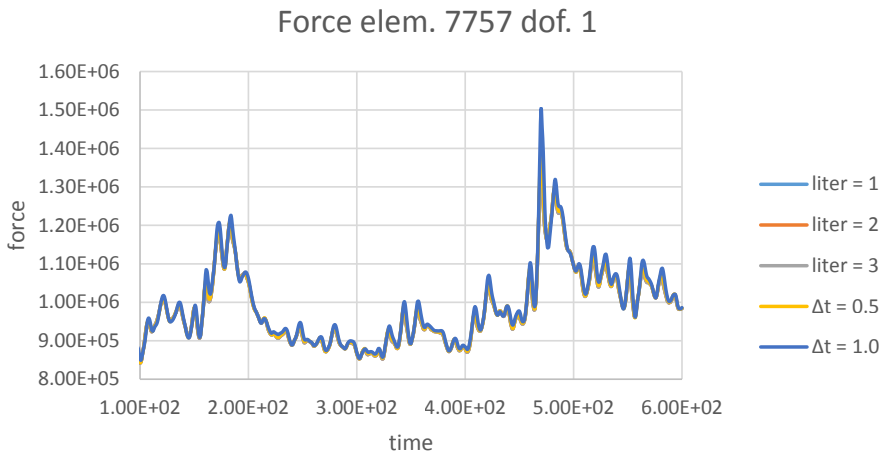


Figure C.2: Convergence study related to the LITER command, results are presented in the form of axial force in element 7757.

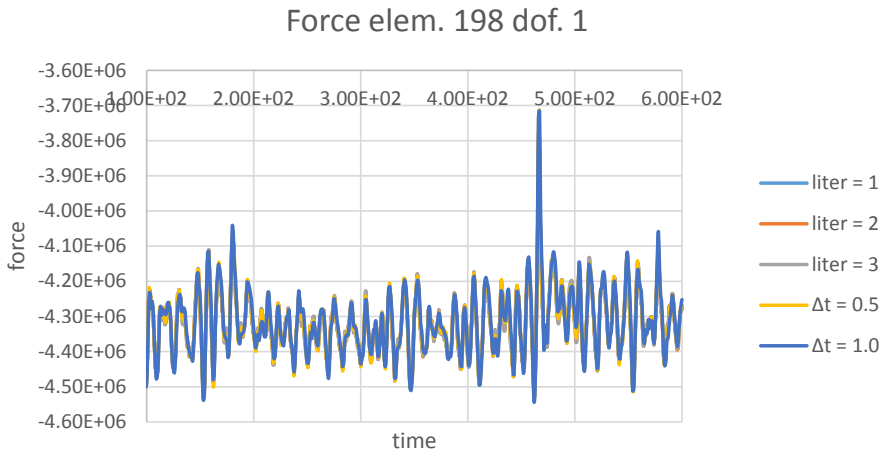


Figure C.3: Convergence study related to the Liter command, results are presented in the form of axial force in element 198.

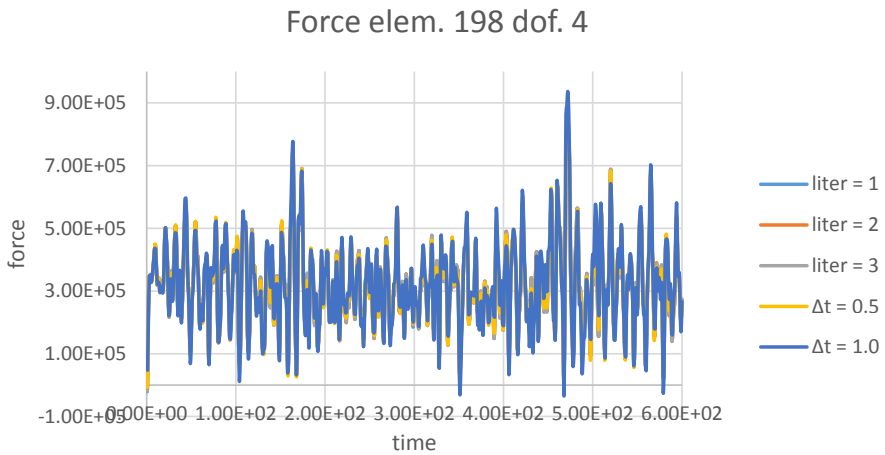


Figure C.4: Convergence study related to the Liter command, results are presented in the form of bending moment in element 198.

D Omitted Results

The Gumbel plots presented in the following were omitted in section 5.1 due to the very narrow spread in results/utilization. For these results, there are in reality no need for applying statistical distributions to arrive at an appropriate value for the characteristic ULS utilization. The omitted plots for these less critical directions are shown in **Fig. D.5, D.6, D.7, and D.8**. The complete and original scatter diagram which the environmental conditions used in the fatigue analysis is based upon is presented in **Fig. D.9**.

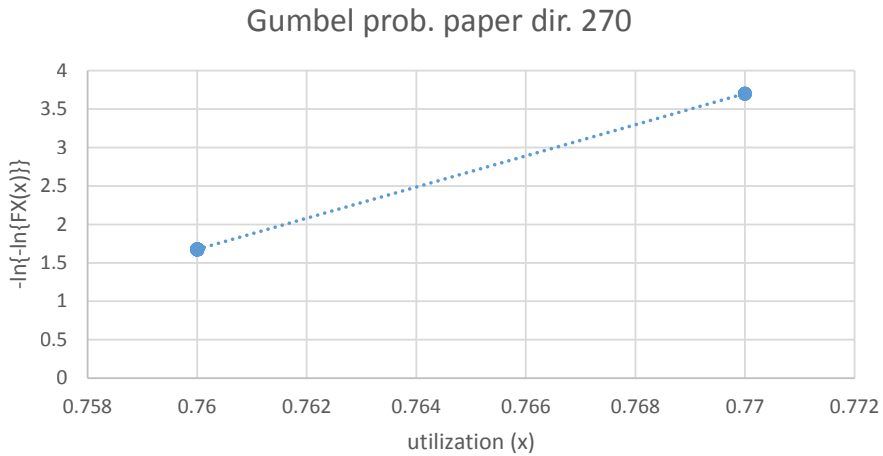


Figure D.5: Gumbel probability paper for direction 270.

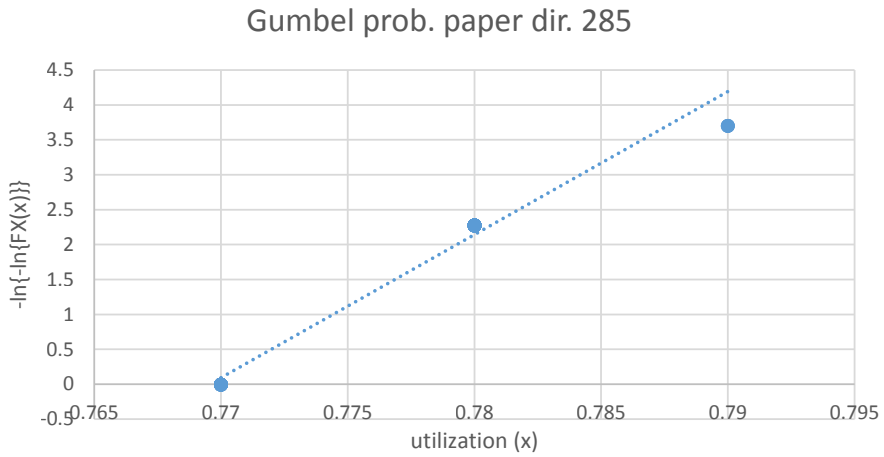


Figure D.6: Gumbel probability paper for direction 285.

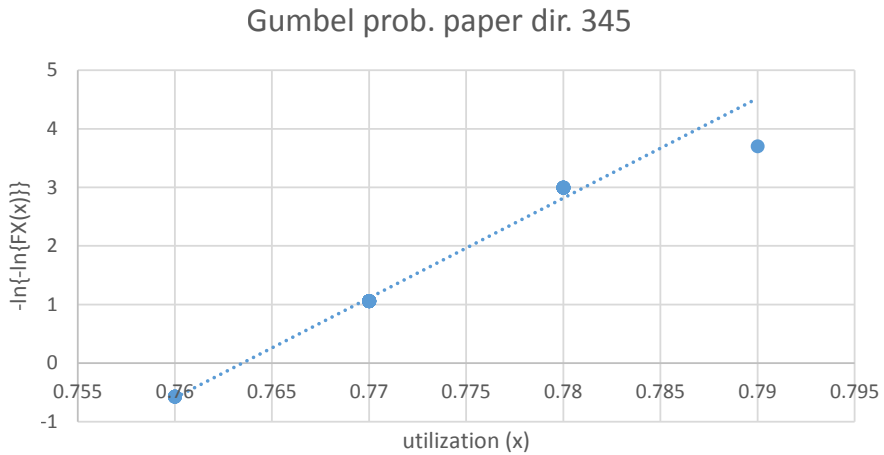


Figure D.7: Gumbel probability paper for direction 345.

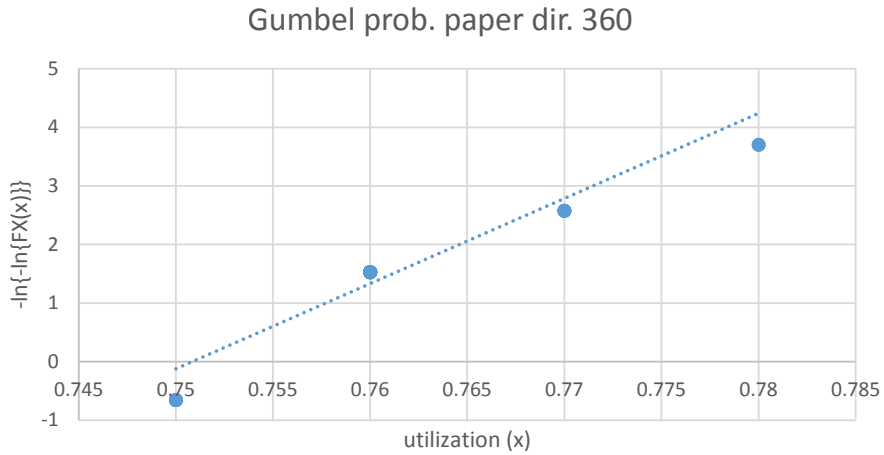


Figure D.8: Gumbel probability paper for direction 360.

| H_{m0} [m] \ T_{m02} [s] | 1 | 2 | 3 | 4 | 5 | 6 | 7 | 8 | 9 | 10 | 11 | 12 | 13 | 14 | 15 | 16 | 17 | 18 | 19 | 20 | Sum | |
|------------------------------|----|------|------|------|------|------|-----|-----|-----|-----|----|----|----|----|----|----|----|----|----|----|-----|-------|
| 0.5 | 18 | 2937 | 2346 | 1011 | 968 | 1000 | 764 | 595 | 314 | 135 | 26 | 3 | 2 | 1 | 0 | 0 | 0 | 0 | 0 | 0 | 0 | 10120 |
| 1.0 | 0 | 106 | 6960 | 1251 | 319 | 266 | 217 | 184 | 64 | 22 | 6 | 0 | 0 | 0 | 0 | 0 | 0 | 0 | 0 | 0 | 0 | 9395 |
| 1.5 | 0 | 0 | 369 | 2431 | 235 | 50 | 12 | 14 | 6 | 3 | 2 | 0 | 0 | 0 | 0 | 0 | 0 | 0 | 0 | 0 | 0 | 3122 |
| 2.0 | 0 | 0 | 0 | 503 | 89 | 20 | 0 | 1 | 0 | 0 | 0 | 0 | 0 | 0 | 0 | 0 | 0 | 0 | 0 | 0 | 0 | 613 |
| 2.5 | 0 | 0 | 0 | 35 | 53 | 7 | 1 | 0 | 0 | 0 | 0 | 0 | 0 | 0 | 0 | 0 | 0 | 0 | 0 | 0 | 0 | 96 |
| 3.0 | 0 | 0 | 0 | 0 | 18 | 5 | 1 | 0 | 0 | 0 | 0 | 0 | 0 | 0 | 0 | 0 | 0 | 0 | 0 | 0 | 0 | 24 |
| 3.5 | 0 | 0 | 0 | 0 | 3 | 2 | 0 | 0 | 0 | 0 | 0 | 0 | 0 | 0 | 0 | 0 | 0 | 0 | 0 | 0 | 0 | 5 |
| 4.0 | 0 | 0 | 0 | 0 | 0 | 0 | 0 | 0 | 0 | 0 | 0 | 0 | 0 | 0 | 0 | 0 | 0 | 0 | 0 | 0 | 0 | 0 |
| 4.5 | 0 | 0 | 0 | 0 | 0 | 0 | 1 | 0 | 0 | 0 | 0 | 0 | 0 | 0 | 0 | 0 | 0 | 0 | 0 | 0 | 0 | 1 |
| 5.0 | 0 | 0 | 0 | 0 | 0 | 0 | 0 | 0 | 0 | 0 | 0 | 0 | 0 | 0 | 0 | 0 | 0 | 0 | 0 | 0 | 0 | 0 |
| 5.5 | 0 | 0 | 0 | 0 | 0 | 0 | 0 | 0 | 0 | 0 | 0 | 0 | 0 | 0 | 0 | 0 | 0 | 0 | 0 | 0 | 0 | 0 |
| 6.0 | 0 | 0 | 0 | 0 | 0 | 0 | 0 | 0 | 0 | 0 | 0 | 0 | 0 | 0 | 0 | 0 | 0 | 0 | 0 | 0 | 0 | 0 |
| 6.5 | 0 | 0 | 0 | 0 | 0 | 0 | 0 | 0 | 0 | 0 | 0 | 0 | 0 | 0 | 0 | 0 | 0 | 0 | 0 | 0 | 0 | 0 |
| 7.0 | 0 | 0 | 0 | 0 | 0 | 0 | 0 | 0 | 0 | 0 | 0 | 0 | 0 | 0 | 0 | 0 | 0 | 0 | 0 | 0 | 0 | 0 |
| 7.5 | 0 | 0 | 0 | 0 | 0 | 0 | 0 | 0 | 0 | 0 | 0 | 0 | 0 | 0 | 0 | 0 | 0 | 0 | 0 | 0 | 0 | 0 |
| Sum | 18 | 3043 | 9675 | 5231 | 1685 | 1350 | 996 | 794 | 384 | 160 | 34 | 3 | 2 | 1 | 0 | 0 | 0 | 0 | 0 | 0 | 0 | 23376 |

Figure D.9: The original scatter diagram measured and simulated on location.

E Miscellaneous Figures

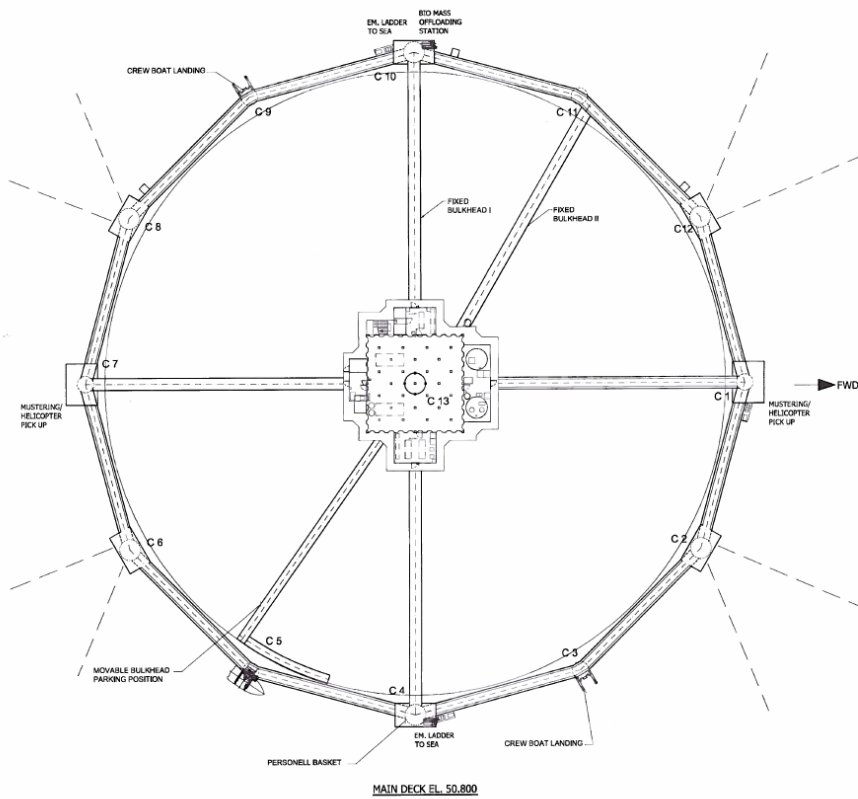
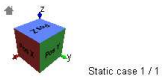
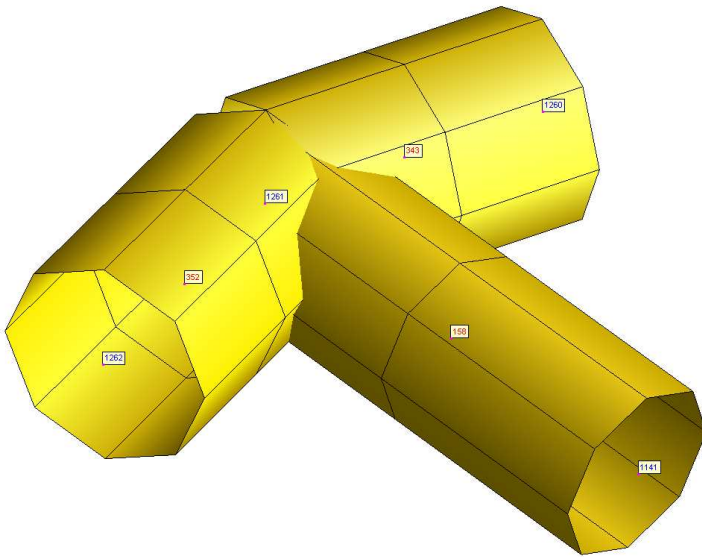


Figure E.10: Top view of the main deck, note the column names. (Global Maritime [21])



Static case 1 / 1

12/05/04 2:24:00 2016-05-10 24.12

Figure E.11: Screenshot of connection 7, 8, and 9, element numbers are in blue and node numbers are in red.

F Source Codes and Script Files

The source codes and script files presented here are for the most part abridged versions. The full files are found in the electronic appendix to this thesis.

F.1 Pre-Processing

The model.fem file to be read by USFOS is produced by a intricate MATLAB-script. The model is the same in ULS and FLS, but will be different depending on the direction of the incoming waves and current. The difference lies in which elements that gets assigned an current blockage factor. The abridged source code for the pre-processor is given in the listing below, and the "flowchart" of the process is shown in **Fig. F.12**.

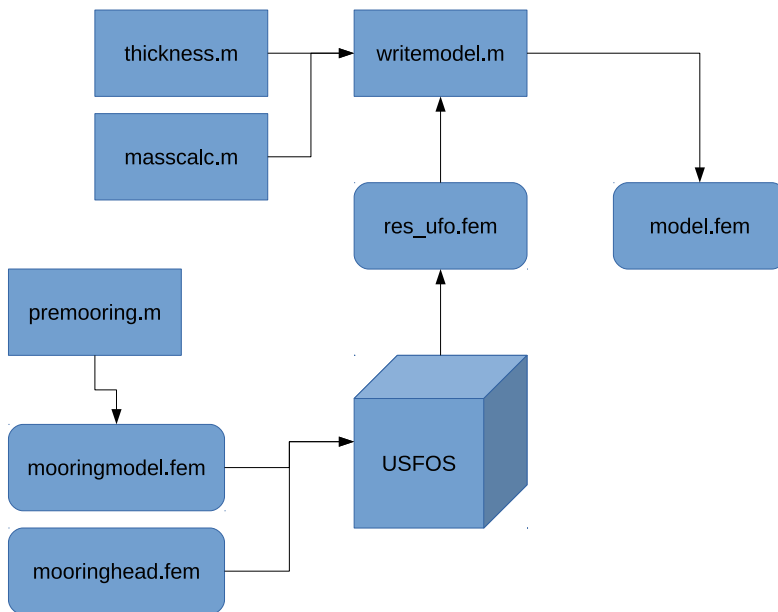


Figure F.12: A schematic flowchart of the preprocessor used to make the USFOS model file, .m denotes MATLAB-script file, and .fem denotes USFOS input/output.

code/premooring.m

```
close all
clear all
clc

% Making initial mooring line (lying on the bottom) to be stretched into its final
shape
```

```

g = 9.81;
rhoWater = 1025;
depth = 150;

% Top angle
phi = 49.1*pi/180;

% Top tension (force)
T = 20*g*10^3; % [N]
Ty = T*cos(phi);
Tz = T*sin(phi);

% Defining mooring line properties

% Chain
Lchain = 1000;
Dchain = sqrt(2)*0.088;
EAchain = 6.94*10^4*g*10^3;
wChain = 147; % [kg/m] (weight in water)
MBLchain = 718.8*g*10^3;
Achain = pi/4*Dchain^2;
yieldChain = MBLchain/Achain;
Echain = EAchain/Achain;
rhoChain = (wChain+(Achain*rhoWater))/Achain;

geoChain = 10;
matChain = 10;

% Fibre (polyester)
Lfibre = 100;
Dfibre = 0.16;
EAfibre = 2.40*10^4*g*10^3;
wFibre = 4; % [kg/m] (weight in water)
MBLfibre = 828*g*10^3;
Afibre = pi/4*Dfibre^2;
yieldFibre = MBLfibre/Afibre;
Efibre = EAfibre/Afibre;
rhoFibre = (wFibre+(Afibre*rhoWater))/Afibre;

geoFibre = 20;
matFibre = 20;

%-----Writing mooring line to file-----

Ltot = Lchain+Lfibre;

% Step size (length of beams)
Lstep = 5;

% Number of beams to split mooring line into
nBeams = Ltot/Lstep;

FID = fopen('premodelmooring.fem','w');

fprintf(FID,'HEAD           Mooring line premodel\n');
fprintf(FID,'           Test file\n');
fprintf(FID,'           PTB and PAF\n\n');

%-----NODES-----
startNODE = 10000;
NODE = [];
for i=1:(nBeams+1)
    NODE(i,1)=i+startNODE; % Node number
    NODE(i,2)=0; % x-coord
    NODE(i,3)=(i-1)*Lstep; % y-coord

```

```

NODE(i,4)=-depth; % z--coord
end

fprintf(FID,'NODE %i %.3f %.3f %.3f 1 1 1 0 0 0\n',NODE(1,1),NODE(1,2),NODE(1,3),
NODE(1,4));
for i=2:(nBeams+1)
fprintf(FID,'NODE %i %.3f %.3f %.3f\n',NODE(i,1),NODE(i,2),NODE(i,3),NODE(i,4));
end

%-----Spring to ground-----
materialS2G = 30;
startS2G = startNODE+1000;
for i=1:(nBeams+1)
fprintf(FID,'SPRNG2GR %i %i %i\n', i+startS2G,NODE(i,1),materialS2G);
end

%-----Beams-----
nChain = Lchain/Lstep;
nFibre = Lfibre/Lstep;

beamcounter = 10000;

% Chain
for i=1:nChain
fprintf(FID,'BEAM %i %i %i %i %i\n',beamcounter,i+startNODE,i+startNODE,
matChain,geoChain);
beamcounter = beamcounter+1;
end

%Fibre
for i=1+nChain:nBeams
fprintf(FID,'BEAM %i %i %i %i %i\n',beamcounter,i+startNODE,i+startNODE,
matFibre,geoFibre);
beamcounter = beamcounter+1;
end

% Material data

% Chain
fprintf(FID,'\n\n'
MatID E-mod poiss yield density\n');
fprintf(FID,'MISOIEP %10d %6u %6.1f %6u %6d\r\n', matChain,Echain,0.3,yieldChain,
rhoChain);

fprintf(FID,'\n\n'
GeoID Do Thick\n');
fprintf(FID,'PIPE %13d %6.3f %8.3f\r\n', geoChain,Dchain,Dchain/2-0.001);

% Fibre
fprintf(FID,'\n\n'
MatID E-mod poiss yield density\n');
fprintf(FID,'MISOIEP %10d %6u %6.1f %6u %6d\r\n', matFibre,Efibre,0.3,yieldFibre,
rhoFibre);

fprintf(FID,'\n\n'
GeoID Do Thick\n');
fprintf(FID,'PIPE %13d %6.2f %8.3f\r\n', geoFibre,Dfibre,Dfibre/2-0.001);

% Spring to ground
fprintf(FID,'\n\n'
MatID Typ SprTyp Coeff Stf DofCod
DofCod\n');
fprintf(FID,'MATERIAL %9d FRIC comp %8.2f %10u %6d %6d \r\n', materialS2G
,0.15,1E+4,12,3);

% Loads

fprintf(FID,'\n\n'
LCCase aX aY aZ\n');
fprintf(FID,'GRAVITY 1 0 0 -9.81\n');

fprintf(FID,'\n\n'
LCCase NodeID Fx Fy Fz\n');
fprintf(FID,'NODELOAD 1 %12d %10.2f %10.2f %10.2f\r\n', NODE(nBeams+1),0,Ty,Tz);

```

```
fclose(FID);
```

code/mooringmodel.fem

```
HEAD      Mooring line premodel
          Test file
          PTB and PAF

NODE 10001 0.000 0.000 -150.000  1 1 1 0 0 0
NODE 10002 0.000 5.000 -150.000
...
NODE 10219 0.000 1090.000 -150.000
NODE 10220 0.000 1095.000 -150.000
NODE 10221 0.000 1100.000 -150.000

SPRNG2GR 11001 10001 30
SPRNG2GR 11002 10002 30
...
SPRNG2GR 11219 10219 30
SPRNG2GR 11220 10220 30
SPRNG2GR 11221 10221 30

BEAM 10000 10001 10002 10 10
BEAM 10001 10002 10003 10 10
...
BEAM 10217 10218 10219 20 20
BEAM 10218 10219 10220 20 20
BEAM 10219 10220 10221 20 20

'
MatID      E-mod      poiss      yield      density
MISOIEP    10 5.596845e+10  0.3 5.796847e+08 1.310960e+04

'
GeoID      Do      Thick
PIPE       10 0.124  0.061

'
MatID      E-mod      poiss      yield      density
MISOIEP    20 1.170982e+10  0.3 4.039890e+08 1.223944e+03

'
GeoID      Do      Thick
PIPE       20 0.16   0.079

'
MatID      Typ      SprTyp      Coeff      Stf      DofCod      DofCod
MATERIAL   30  FRIC      comp      0.15      1000000      12      3

'
LCase      aX      aY      aZ
GRAVITY    1      0      0      -9.81

'
LCase      NodeID      Fx      Fy      Fz
NODELOAD   1      10221      0.00  128460.15  148298.45
```

code/mooringhead.fem

```
HEAD      Design Wave (regular wave)
          U S F O S progressive collapse analysis
          Usfos AS 2006
,
,
'In THIS FILE I HAVE SWITCHED OFF TRANSVERSE LOADING
```

```

'DUMP COORDINATES AT END OF ANALYSI
Switches Write FE_Model Time 60
liter 3

Dynres_E Force 10219 1 1
Dynres_E Force 10218 1 1
Dynres_E Force 10150 1 1
Dynres_E Force 10151 1 1
Dynres_E Force 11001 1 1
Dynres_E Force 11002 1 3
Dynres_E Force 11150 1 1
Dynres_E Force 11151 1 3

'
      End_Time   Delta_T   Dt_Res   Dt_Pri
Dynamic      60.0      0.002      0.1      0.1
'
-----
'      T i m e   H i s t o r i e s   e t c
-----
'
      ID <type>   T1      T2      Fac      Power
TIMEHIST      1   S_Curv   0.0    15.0    1        2
# TIMEHIST      3   S_Curv  10.0   70.0    0.1      2
'
      ID <type>   Dtime   Factor   Start_time
TIMEHIST      2   Switch   0.0     1.0     0.0
'
      Ildcs   Tim Hist
LOADHIST      1      1      ! Apply Grav and buoyancy
LOADHIST      2      2      ! Apply Wave
# LOADHIST      3      3      ! Apply transverse load
'
      Ildcs <type>   H      Period   Direction Phase   Surf_Lev Depth
WAVEDATA      2   Airy   0.01   20.0     0        0.0     0.0     150 ! Flat Sea
'
BUOYANCY      ! Switch ON Buoyancy
' Buoyform Panel Geo 1 2 3 4 5 6 7 8
' Buoyform Arc All
'REL_VELO      ! Account for Relative Velo (Drag Damp)
Wet_Elem All      ! Check All elements for wet/dry
'
=====
' Specify Gradually increasing Buoyancy. Let the buoyancy follow
' History no 1 (which also is used for the Gravity)
-----
'
'
      HistID ListTyp MatID
BuoyHist      1      All
'Hydropar BuDiam 0.01 Geo 7000 ! NB Minimum buoyancy because net weight is used
      in model
'
=====
' Specify "Panel" buoyancy formulation elements with mat=1
' Define the panel mesh with 20 elements in local X-direction of elem.
-----
Wave_Int 10      ! Use 20 sections along each element for
'
'
BeamType Riser All ! Switch ON riser elements for all beams
'
-----
'      Misc Parameters
-----
'
RAYLDAMP 0.05 0.05
DampRatio 0.5 0.5 0.02 100.0
'
'

```



```

close all
clear all
clc

%% RIGID OFFSHORE FISH-FARM CREATOR
% Based on Ocean Farming/Global Maritime design
% Code writes USFOS model file (model.fem)
% P.T.B. & P.A.F., NTNU

% MATERIAL DATA FOR THE NET IS MISSING
% ALL THICKNESSES MUST BE CHECKED AND CHANGED
% POINT MASSES MUST BE ADDED
% DRAG COEFFICIENTS AND SUCH...

%% Define overall cage geometry

radius = 55;           % radius [m]
Zside = -27;          % z-coordinate at bottom of side [m]
Zponton = -43;        % z-coordinate at bottom of pontoons [m]
height = 33;          % height outer columns [m]
heightcentre = 37;    % Height centre column

nSides = 12;           % number of sides
nCpontoons = 1;       % number of center pontoons
nSpontoons = 6;       % number of side pontoons

% Define direction of incoming current (and waves) for assigning
% currentblockage factors to correct members, 0 deg is in positive x-dir.

currdir = 270*pi/180;

%% Define material and elemental geometry

% Structural material
% Steel
strucmat = 1;
strucmod = 210E9;      % Young's modulus [MPa]
strucpoiss = 0.3;      % Poisson's ratio
strucyield = 355E6;    % yield strength [MPa]
strucdens = 7850;     % steel density [kg/m3]

% Net
strucmatnet = 2;
strucmodnet = 40E+9;
strucpoissnet = 0.3;
strucyieldnet = 355E7;
strucdensnet = 1025;
thermexpnet = 0.001;

% Include thicknesses from separate function
[betthick , cmidthick , obtthick , mcmidthick , scmidthick , tofmidthick , bofmidthick ,
rbmidthick , tfmidthick , scmidthickextra] = thickness(strucdens);

% ...geo is the geometric identifier
% ...dia is the diameter of the element [m]
% ...thick is the thickness of the element [m]

% Bottom outer ring
botringgeo = 2;
botringendgeo = 3;
botringdia = 2.049;
botringthick = bofmidthick; % Smearred avg. thickness
botringendthick = bofmidthick; % Thickness ends (one element on each side)

% Middle outer ring and diagonal supports
midsupgeo = 4;

```

```

midsupdiagendgeo = 5;
midsupdia = 1;
midsupthick = 0.015;
midsupdiagendthick = 0.03; % Thickness ends (one element on each side)

% Top outer ring
topsupgeo = 6;
topsupendgeo = 7;
topsupdia = 2.29;
topsupenddia = 2.33;
topsupthick = tofmidthick; % Smearred avg. thickness
topsupendthick = 0.04; % Thickness ends (one element on each side)

% Crossing wheelhouse supports
crosstopgeo = 8;
crosstopendgeo = 9;
crosstopdia = 2.05;
crosstopenddia = 2.08;
crosstopthick = tfmidthick; % Smearred avg. thickness
crosstopendthick = 0.04; % Thickness ends (one element on each side)

% Bottom radial elements
botradgeo = 10;
botradendgeo = 11;
botraddia = 1.75;
botradthick = rbmidthick; % Smearred avg. thickness
botradendthick = rbmidthick; % Thickness lateral end (one element)

% Outer verticals over pontoons
coloverpontgeo = 12;
coloverpontendgeo = 13;
coloverpontdia = 3.56;
coloverpontenddia = 3.58;
coloverpontthick = mcmidthick; % Smearred avg. thickness
coloverpontendthick = 0.04; % Thickness ends (one element on each side)

% Intermediate verticals
intvertgeo = 14;
intvertendgeo = 15;
intvertdia = 2.80;
intvertenddia = 2.83;
intvertthick = scmidthick; % Smearred avg. thickness
intvertendthick = 0.04; % Thickness ends (one element on each side)

% Center pontoon
centpontgeo = 16;
diapontoon = 17;
centpontthick = bccthick; % Smearred avg. thickness
stepconegeo = 17;
centconethick = bccthick; % Same thickness as cylinder part of the centre pontoon
stepconedia = 8;
centconegeo = 18;
h1cpontoon = 7; % heights starting from bottom and upwards [m]
h2cpontoon = 2; % bottom braces center joint at this point
h3cpontoon = 3;

% Outer pontoons
outpontgeo = 19;
dspontoon = 12;
outpontthick = double(obtthick); % Smearred avg. thickness of cone and bottom tank
outconegeo = 20;
h1spontoon = 7; % heights starting from bottom and upwards [m]
h2spontoon = 6;
h3spontoon = 3;

% Centre column
centcolgeo = 21;
centcolendgeo = 22;

```

```

centcoldia = 3.56;
centcolenddia = 3.58;
centcolthick = ccmidthick; % Smearred avg. thickness
centcolendthick = 0.04; % Thickness top element

% Movable bulkhead
movebulkgeo = 23;
movebulkwidth = 1.5;
movebulklengthtot = sqrt(55^2+7^2)+55;
movebulkweight = 299636;
movebulkthick = (movebulkwidth-(movebulkwidth^2-(movebulkweight/(movebulklengthtot*
strucedens)))^0.5)/2;

% Fixed bulkhead
fixedbulkgeo = 24;
fixedbulkdia = 2.05;
fixedbulklengthtot = 55;
fixedbulkweight = 172001;
fixedbulkthick = (fixedbulkdia-(fixedbulkdia^2-(fixedbulkweight*4/(pi*
fixedbulklengthtot*strucedens)))^0.5)/2;

% Intermediate vertical column C11
intvertextrageo = 25;
intvertextrathick = scmidthickextra; % Smearred avg. thickness
intvertendthick = 0.04; % Thickness ends (one element on each side)

% Tanks (equipment masses)
verttankgeo = 26;
horiztankgeo = 27;

% Net structure
netgeo = 28;
diathreads = 0.15; % diameter of threads [m], 0.0025 correct value
thickthreads = 0.074;

%% Mesh configuration

% Splitting number must be even to assure symmetry, and equal or above 4
% to create net connections, test model file by visual inspection before
% analysis.

nSplitSide = 10; % number of side splitting (vertical and horizontal)
nSplitBottom = 10; % number of bottom braces/columns splitting
zStep = height/nSplitSide; % vertical step size for side net

% Base node angles
deltaangle = 2*pi/nSides;
theta = [];
for i = 1:nSides
    theta(i) = deltaangle*(i-1);
end

% Bottom angle
thetaBottom = atan((h1spontoon+h2spontoon+h3spontoon-h1cpontoon-h2cpontoon)/radius);
% Radius step on bottom net
rStep = (radius-(diacpontoon/2))/nSplitBottom;

% Gathering all bottom nodes
NODE = [];
for k = 1:(nSplitBottom+1)
    % base nodes
    Radius = (diacpontoon/2)+((k-1)*rStep);
    zCoord = (Zpontoon+h1cpontoon+h2cpontoon)+(Radius*tan(thetaBottom));
    Bnode = [];
    for i = 1:nSides
        Bnode(i,1) = -Radius*sin(theta(i));
        Bnode(i,2) = Radius*cos(theta(i));
        Bnode(i,3) = zCoord;
    end
end

```

```

end
% nodes in 4-dim matrix where 3rd dim is side number and 4th dim is
% radius number
for i = 1:(nSides-1)
    for j = 1:nSplitSide
        NODE(j,1,i,k) = ((k-1)*nSplitSide*nSides)+((i-1)*nSplitSide)+j;
        xstep = (Bnode(i+1,1)-Bnode(i,1))/nSplitSide;
        ystep = (Bnode(i+1,2)-Bnode(i,2))/nSplitSide;
        NODE(j,2,i,k) = Bnode(i,1)+(j-1)*xstep;
        NODE(j,3,i,k) = Bnode(i,2)+(j-1)*ystep;
        NODE(j,4,i,k) = zCoord;
    end
end
% 12th side must be meshed separately
for j = 1:nSplitSide
    NODE(j,1,nSides,k) = ((k-1)*nSplitSide*nSides)+((nSides-1)*nSplitSide)+j;
    xstep = (Bnode(1,1)-Bnode(nSides,1))/nSplitSide;
    ystep = (Bnode(1,2)-Bnode(nSides,2))/nSplitSide;
    NODE(j,2,nSides,k) = Bnode(nSides,1)+(j-1)*xstep;
    NODE(j,3,nSides,k) = Bnode(nSides,2)+(j-1)*ystep;
    NODE(j,4,nSides,k) = zCoord;
end
end
%% Write nodes to file
FID1 = fopen('model.fem','w');

% Gathering all bottom nodes in 2-dim matrix
NODE2D = [];
for k = 1:(nSplitBottom+1)
    for i = 1:nSides
        for j = 1:nSplitSide
            NODE2D(((k-1)*nSplitSide*nSides)+((i-1)*nSplitSide)+j,1) = NODE(j,1,i,k);
            NODE2D(((k-1)*nSplitSide*nSides)+((i-1)*nSplitSide)+j,2) = NODE(j,2,i,k);
            NODE2D(((k-1)*nSplitSide*nSides)+((i-1)*nSplitSide)+j,3) = NODE(j,3,i,k);
            NODE2D(((k-1)*nSplitSide*nSides)+((i-1)*nSplitSide)+j,4) = NODE(j,4,i,k);
        end
    end
end
end
% Writing all bottom nodes
nNodesBottom = length(NODE2D);
for i = 1:nNodesBottom
    fprintf(FID1,'NODE %i %.3f %.3f %.3f\n',NODE2D(i,1),NODE2D(i,2),NODE2D(i,3),
        NODE2D(i,4));
end
end
% Gathering all outer nodes in 2-dim matrix
NODE2DSIDE = [];
for i = 1:nSides
    for j = 1:nSplitSide
        NODE2DSIDE(((i-1)*nSplitSide)+j,1) = NODE(j,1,i,nSplitBottom+1);
        NODE2DSIDE(((i-1)*nSplitSide)+j,2) = NODE(j,2,i,nSplitBottom+1);
        NODE2DSIDE(((i-1)*nSplitSide)+j,3) = NODE(j,3,i,nSplitBottom+1);
        NODE2DSIDE(((i-1)*nSplitSide)+j,4) = NODE(j,4,i,nSplitBottom+1);
    end
end
end
% Writing all side nodes
nNodesSide = length(NODE2DSIDE);
for j = 1:nSplitSide
    for i = 1:nNodesSide
        fprintf(FID1,'NODE %i %.3f %.3f %.3f\n',NODE2DSIDE(i,1)+(j*nNodesSide),
            NODE2DSIDE(i,2),NODE2DSIDE(i,3),NODE2DSIDE(i,4)+(j*zStep));
    end
end
end
nodecount = NODE2DSIDE(i,1)+(j*nNodesSide);

```

```

% Gathering structural nodes in matrices

% Bottom
bottomstrucnodes = [];
j=1;
for i = 1:nSplitSide:nNodesBottom-nNodesSide
    bottomstrucnodes(j) = NODE2D(i,1);
    j=j+1;
end
for i = nNodesBottom-nNodesSide+1:nNodesBottom
    bottomstrucnodes(j) = NODE2D(i,1);
    j=j+1;
end

% Side
NODE2DSIDEALL = [];
for j = 1:nSplitSide
    for i = 1:nNodesSide
        NODE2DSIDEALL(((j-1)*nNodesSide)+i) = NODE2DSIDE(i,1)+(j*nNodesSide);
    end
end

sidestrucnodes = [];
j=1;
for i = 1:nSplitSide:length(NODE2DSIDEALL)-nNodesSide
    sidestrucnodes(j) = NODE2DSIDEALL(i);
    j=j+1;
end

% Top ring
topringstrucnodes = [];
j=1;
for i = length(NODE2DSIDEALL)-nNodesSide+1:length(NODE2DSIDEALL)
    topringstrucnodes(j) = NODE2DSIDEALL(i);
    j=j+1;
end

% Define side pontoons by nodes and write to file
sidepontMat = Bnode;
for i = 2:2:nSides
    sidepontMat(i,:) = 0;
end
sidepontMat(all(~sidepontMat,2),:) = [];
nodecount = nodecount+1;
for i = 1:length(sidepontMat)
    fprintf(FID1,'NODE %i %.3f %.3f %.3f\n',nodecount,sidepontMat(i,1),sidepontMat(i,2),sidepontMat(i,3)-h3spontoon);
    nodecount = nodecount+1;
    fprintf(FID1,'NODE %i %.3f %.3f %.3f\n',nodecount,sidepontMat(i,1),sidepontMat(i,2),sidepontMat(i,3)-h3spontoon-h2spontoon);
    nodecount = nodecount+1;
    fprintf(FID1,'NODE %i %.3f %.3f %.3f\n',nodecount,sidepontMat(i,1),sidepontMat(i,2),sidepontMat(i,3)-h3spontoon-h2spontoon-h1spontoon);
    nodecount = nodecount+1;
end

% Write center nodes (starting at bottom)

% Centre pontoon plus small column on top of centre pontoon
fprintf(FID1,'NODE %i %.3f %.3f %.3f\n',nodecount,0,0,Zpontoon);
nodecount = nodecount+1;
fprintf(FID1,'NODE %i %.3f %.3f %.3f\n',nodecount,0,0,Zpontoon+h1cpontoon);
nodecount = nodecount+1;
fprintf(FID1,'NODE %i %.3f %.3f %.3f\n',nodecount,0,0,Zpontoon+h1cpontoon+h2cpontoon);
nodecount = nodecount+1;

```

```

%fprintf(FID1, 'NODE %i %.3f %.3f %.3f\n', nodecount, 0, 0, Zpontoon+h1cpontoon+h2cpontoon
+h3cpontoon);
%nodecount = nodecount+1;
% Centre column
centrestrucnodes = [];
for i = 1:nSplitSide+1
    fprintf(FID1, 'NODE %i %.3f %.3f %.3f\n', nodecount, 0, 0, Zpontoon+h1cpontoon+
h2cpontoon+h3cpontoon+(heightcentre/nSplitSide*(i-1)));
    centrestrucnodes(i) = nodecount;
    nodecount = nodecount+1;
end
topcentrenode = nodecount-1;

%fprintf(FID1, 'NODE %i %.3f %.3f %.3f\n', nodecount, 0, 0, Zpontoon+h1spontoon+h2spontoon
+h3spontoon+(height-5)/2);
%nodecount = nodecount+1;
%fprintf(FID1, 'NODE %i %.3f %.3f %.3f\n', nodecount, 0, 0, Zpontoon+h1spontoon+h2spontoon
+h3spontoon+height-5);
%nodecount = nodecount+1;
%fprintf(FID1, 'NODE %i %.3f %.3f %.3f\n', nodecount, 0, 0, Zpontoon+h1spontoon+h2spontoon
+h3spontoon+height);
%topcentrenode = nodecount;
%nodecount = nodecount+1;

%centrestrucnodes = [];
%for i = 1:4
%    centrestrucnodes(i) = topcentrenode-(i-1);
%end

% Write crossing wheelhouse support nodes
nCrossings = 4; % Problems in code if this number is not 2,4,6 or 12
nExtraCrossings = 1; % The extra fixed bulkhead (changes in code required if this
number is not 1)
nSplitCross = 10;
CrossStep = radius / nSplitCross;
thetaCross = [];
thetaCrossStep = 2*pi / nCrossings;
for i=1:nCrossings
    thetaCross(i) = (i-1)*thetaCrossStep;
end
thetaCross(nCrossings+nExtraCrossings) = theta(nSides); % The extra fixed bulkhead
angle

CrossNodes = [];
for i = 1:nCrossings+nExtraCrossings
    for j = 1:nSplitCross-1
        fprintf(FID1, 'NODE %i %.3f %.3f %.3f\n', nodecount, -CrossStep*j*sin(thetaCross
(i)), CrossStep*j*cos(thetaCross(i)), Zpontoon+h1spontoon+h2spontoon+
h3spontoon+height);
        CrossNodes(j, i) = nodecount;
        nodecount = nodecount+1;
    end
end

crosstopstrucnodes = [];
crosstopdim = size(CrossNodes);
for i = 1:crosstopdim(2)
    for j = 1:crosstopdim(1)
        crosstopstrucnodes(((i-1)*crosstopdim(1))+j) = CrossNodes(j, i);
    end
end

%% Write main element configuration

beamcount = 1;

% Write center column (starting from the top)

```

```

fprintf(FID1, 'BEAM %i %i %i %i\n', beamcount, topcentrenode, topcentrenode - 1, strucmat,
    centcolendgeo);
beamcount = beamcount + 1;
for i = 1:nSplitSide - 1
    fprintf(FID1, 'BEAM %i %i %i %i\n', beamcount, centrestrucnodes(nSplitSide + 1 - i),
        centrestrucnodes(nSplitSide - i), strucmat, centcolgeo);
    beamcount = beamcount + 1;
end

fprintf(FID1, 'BEAM %i %i %i %i\n', beamcount, topcentrenode - 1, topcentrenode - 2,
    strucmat, centcolgeo);
%beamcount = beamcount + 1;
fprintf(FID1, 'BEAM %i %i %i %i\n', beamcount, topcentrenode - 2, topcentrenode - 3,
    strucmat, centcolgeo);
%beamcount = beamcount + 1;

fprintf(FID1, 'BEAM %i %i %i %i\n', beamcount, topcentrenode - nSplitSide, topcentrenode
    - nSplitSide - 1, strucmat, centconegeo);
beamcount = beamcount + 1;
fprintf(FID1, 'BEAM %i %i %i %i\n', beamcount, topcentrenode - nSplitSide - 1,
    topcentrenode - nSplitSide - 2, strucmat, stepconegeo);
beamcount = beamcount + 1;
fprintf(FID1, 'BEAM %i %i %i %i\n', beamcount, topcentrenode - nSplitSide - 2,
    topcentrenode - nSplitSide - 3, strucmat, centpontgeo);
centpontelement = beamcount;
beamcount = beamcount + 1;

% Write side pontoons
sidepontcolelem = [];
for i = 1:nSpontoons
    fprintf(FID1, 'BEAM %i %i %i %i\n', beamcount, (nNodesSide * nSplitBottom) + ((i - 1)
        * 2 * nSplitSide) + 1, (nNodesSide * nSplitBottom) + (nNodesSide * (nSplitSide + 1)) + ((i
        - 1) * 3) + 1, strucmat, coloverpontendgeo);
    sidepontcolelem(i) = beamcount;
    beamcount = beamcount + 1;
    fprintf(FID1, 'BEAM %i %i %i %i\n', beamcount, (nNodesSide * nSplitBottom) + (
        nNodesSide * (nSplitSide + 1)) + ((i - 1) * 3) + 1, (nNodesSide * nSplitBottom) + (nNodesSide
        * (nSplitSide + 1)) + ((i - 1) * 3) + 2, strucmat, outconegeo);
    beamcount = beamcount + 1;
    fprintf(FID1, 'BEAM %i %i %i %i\n', beamcount, (nNodesSide * nSplitBottom) + (
        nNodesSide * (nSplitSide + 1)) + ((i - 1) * 3) + 2, (nNodesSide * nSplitBottom) + (nNodesSide
        * (nSplitSide + 1)) + ((i - 1) * 3) + 3, strucmat, outpontgeo);
    beamcount = beamcount + 1;
end

% Write bottom radial beams

% Inner radial elements (first "round" of elements)
for i = 1:nSplitSide:nSides*nSplitSide
    fprintf(FID1, 'BEAM %i %i %i %i\n', beamcount, topcentrenode - nSplitSide - 1, i,
        strucmat, botradgeo);
    beamcount = beamcount + 1;
end

% The rest
for i = 1:nSplitBottom - 1
    for j = 1:nSplitSide:nNodesSide
        fprintf(FID1, 'BEAM %i %i %i %i\n', beamcount, ((i - 1) * nNodesSide) + j, (i *
            nNodesSide) + j, strucmat, botradgeo);
        beamcount = beamcount + 1;
    end
end

% Lateral end elements
for j = 1:nSplitSide:nNodesSide
    fprintf(FID1, 'BEAM %i %i %i %i\n', beamcount, ((nSplitBottom - 1) * nNodesSide) + j, (
        nSplitBottom * nNodesSide) + j, strucmat, botradendgeo);
    beamcount = beamcount + 1;
end

```

```

% Outer vertical columns

% Columns over pontoons
k = 1;
vertcolpontelem = [];
for i = nSplitBottom+2:nSplitBottom+nSplitSide-1
    for j = 1:2*nSplitSide:nNodesSide
        fprintf(FID1, 'BEAM %i %i %i %i\n', beamcount, ((i-1)*nNodesSide)+j, (i*
            nNodesSide)+j, strucmat, coloverpontgeo);
        vertcolpontelem(k) = beamcount;
        beamcount = beamcount+1;
        k = k+1;
    end
end
% End elements
k = 1;
vertcolpontendelem = [];
for i = nSplitBottom+1:nSplitSide-1:nSplitBottom+nSplitSide
    for j = 1:2*nSplitSide:nNodesSide
        fprintf(FID1, 'BEAM %i %i %i %i %i\n', beamcount, ((i-1)*nNodesSide)+j, (i*
            nNodesSide)+j, strucmat, coloverpontendgeo);
        vertcolpontendelem(k) = beamcount;
        beamcount = beamcount+1;
        k = k+1;
    end
end

% Intermediate columns
k = 1;
vertcolintelem = [];
for i = nSplitBottom+2:nSplitBottom+nSplitSide-1
    for j = nSplitSide+1:2*nSplitSide:nNodesSide-nSplitSide
        fprintf(FID1, 'BEAM %i %i %i %i\n', beamcount, ((i-1)*nNodesSide)+j, (i*
            nNodesSide)+j, strucmat, intvertgeo);
        vertcolintelem(k) = beamcount;
        beamcount = beamcount+1;
        k = k+1;
    end
end
for i = nSplitBottom+2:nSplitBottom+nSplitSide-1
    fprintf(FID1, 'BEAM %i %i %i %i %i\n', beamcount, ((i-1)*nNodesSide)+nNodesSide+1-
        nSplitSide, (i*nNodesSide)+nNodesSide+1-nSplitSide, strucmat, intvertextrageo);
    vertcolintelem(k) = beamcount;
    beamcount = beamcount+1;
    k = k+1;
end

k = 1;
vertcolintendelem = [];
% End elements
for i = nSplitBottom+1:nSplitSide-1:nSplitBottom+nSplitSide
    for j = nSplitSide+1:2*nSplitSide:nNodesSide
        fprintf(FID1, 'BEAM %i %i %i %i %i\n', beamcount, ((i-1)*nNodesSide)+j, (i*
            nNodesSide)+j, strucmat, intvertendgeo);
        vertcolintendelem(k) = beamcount;
        beamcount = beamcount+1;
        k = k+1;
    end
end

% Write outer circular rings
% Bottom
botringelem = [];
botringendelem = [];
k = 1;
l = 1;
for i = 1:nSides-1
    for j = 2:nSplitSide-1

```

```

        fprintf(FID1, 'BEAM %i %i %i %i %i\n', beamcount, ((i-1)*nSplitSide)+j+
            nNodesSide*nSplitBottom, ((i-1)*nSplitSide)+j+nNodesSide*nSplitBottom+1,
            strucmat, botringgeo);
        botringelem(k) = beamcount;
        beamcount = beamcount+1;
        k = k+1;
    end
    for j = 1:nSplitSide-1:nSplitSide
        fprintf(FID1, 'BEAM %i %i %i %i %i\n', beamcount, ((i-1)*nSplitSide)+j+nNodesSide*
            nSplitBottom, ((i-1)*nSplitSide)+j+nNodesSide*nSplitBottom+1, strucmat,
            botringendgeo);
        botringendelem(1) = beamcount;
        beamcount = beamcount+1;
        l = l+1;
    end
end
for j = 2:nSplitSide-1
    fprintf(FID1, 'BEAM %i %i %i %i %i\n', beamcount, ((nSides-1)*nSplitSide)+j+
        nNodesSide*nSplitBottom, ((nSides-1)*nSplitSide)+j+nNodesSide*nSplitBottom+1,
        strucmat, botringgeo);
    botringelem(k) = beamcount;
    beamcount = beamcount+1;
    k = k+1;
end
fprintf(FID1, 'BEAM %i %i %i %i %i\n', beamcount, ((nSides-1)*nSplitSide)+1+nNodesSide*
    nSplitBottom, ((nSides-1)*nSplitSide)+1+nNodesSide*nSplitBottom+1, strucmat,
    botringendgeo);
botringendelem(1) = beamcount;
beamcount = beamcount+1;
l = l+1;
fprintf(FID1, 'BEAM %i %i %i %i %i\n', beamcount, nNodesSide+nNodesSide*nSplitBottom,
    nNodesSide*nSplitBottom+1, strucmat, botringendgeo);
botringendelem(1) = beamcount;
beamcount = beamcount+1;

% Middle
for i = 1:nNodesSide-1
    fprintf(FID1, 'BEAM %i %i %i %i %i\n', beamcount, i+(nNodesSide*nSplitBottom)+(
        nSplitSide/2*nNodesSide), i+(nNodesSide*nSplitBottom)+(nSplitSide/2*
        nNodesSide)+1, strucmat, midsupgeo);
    beamcount = beamcount+1;
end
fprintf(FID1, 'BEAM %i %i %i %i %i\n', beamcount, nNodesSide+(nNodesSide*nSplitBottom)+(
    nSplitSide/2*nNodesSide), (nNodesSide*nSplitBottom)+(nSplitSide/2*nNodesSide)+1,
    strucmat, midsupgeo);
beamcount = beamcount+1;

% Top
for i = 1:nSides-1
    for j = 2:nSplitSide-1
        fprintf(FID1, 'BEAM %i %i %i %i %i %i\n', beamcount, ((i-1)*nSplitSide)+j+(
            nNodesSide*nSplitBottom)+(nSplitSide*nNodesSide), ((i-1)*nSplitSide)+j+(
            nNodesSide*nSplitBottom)+(nSplitSide*nNodesSide)+1, strucmat, topsupgeo);
        beamcount = beamcount+1;
    end
    for j = 1:nSplitSide-1:nSplitSide
        fprintf(FID1, 'BEAM %i %i %i %i %i %i\n', beamcount, ((i-1)*nSplitSide)+j+(
            nNodesSide*nSplitBottom)+(nSplitSide*nNodesSide), ((i-1)*nSplitSide)+j+(
            nNodesSide*nSplitBottom)+(nSplitSide*nNodesSide)+1, strucmat, topsupendgeo
        );
        beamcount = beamcount+1;
    end
end
for j = 2:nSplitSide-1
    fprintf(FID1, 'BEAM %i %i %i %i %i %i\n', beamcount, ((nSides-1)*nSplitSide)+j+(
        nNodesSide*nSplitBottom)+(nSplitSide*nNodesSide), ((nSides-1)*nSplitSide)+j+(
        nNodesSide*nSplitBottom)+(nSplitSide*nNodesSide)+1, strucmat, topsupgeo);
    beamcount = beamcount+1;
end

```

```

end
fprintf(FID1, 'BEAM %i %i %i %i %i\n', beamcount, ((nSides-1)*nSplitSide)+1+(nNodesSide*
nSplitBottom)+(nSplitSide*nNodesSide), ((nSides-1)*nSplitSide)+1+(nNodesSide*
nSplitBottom)+(nSplitSide*nNodesSide)+1, strucmat, topsupendgeo);
beamcount = beamcount+1;
fprintf(FID1, 'BEAM %i %i %i %i %i\n', beamcount, nNodesSide+(nNodesSide*nSplitBottom)+(
nSplitSide*nNodesSide), (nNodesSide*nSplitBottom)+(nSplitSide*nNodesSide)+1,
strucmat, topsupendgeo);
beamcount = beamcount+1;

% Write crossing wheelhouse supports
for i = 1:nCrossings
sizeCross = size(CrossNodes);
for j = 1:sizeCross(1,1)-1
fprintf(FID1, 'BEAM %i %i %i %i %i\n', beamcount, CrossNodes(j, i), CrossNodes(j, i
)+1, strucmat, crosstopgeo);
beamcount = beamcount+1;
end

fprintf(FID1, 'BEAM %i %i %i %i %i\n', beamcount, topcentrenode, CrossNodes(1, i),
strucmat, crosstopendgeo);
beamcount = beamcount+1;

endCrossNodes = (nNodesSide*nSplitBottom)+(nSplitSide*nNodesSide)+1:nNodesSide/
nCROSSINGS:(nNodesSide*nSplitBottom)+(nSplitSide*nNodesSide)+nNodesSide;

fprintf(FID1, 'BEAM %i %i %i %i %i\n', beamcount, CrossNodes(sizeCross(1,1), i),
endCrossNodes(i), strucmat, crosstopendgeo);
beamcount = beamcount+1;
end

% Writing the extra fixed bulkhead crossing
for j = 1:sizeCross(1,1)-1
fprintf(FID1, 'BEAM %i %i %i %i %i\n', beamcount, CrossNodes(j, sizeCross(1,2)),
CrossNodes(j, sizeCross(1,2))+1, strucmat, fixedbulkgeo);
beamcount = beamcount+1;
end
fprintf(FID1, 'BEAM %i %i %i %i %i\n', beamcount, topcentrenode, CrossNodes(1, sizeCross
(1,2)), strucmat, fixedbulkgeo);
beamcount = beamcount+1;
fprintf(FID1, 'BEAM %i %i %i %i %i\n', beamcount, CrossNodes(sizeCross(1,1), sizeCross
(1,2)), endCrossNodes(nCrossings)+(2*nNodesSide/nSides), strucmat, fixedbulkgeo);
beamcount = beamcount+1;

% Writing movable bulkhead
fprintf(FID1, 'BEAM %i %i %i %i %i\n', beamcount, topcentrenode, endCrossNodes(nCrossings
)-(4*nNodesSide/nSides), strucmat, movebulkgeo);
topmovebulkelem = beamcount;
beamcount = beamcount+1;
fprintf(FID1, 'BEAM %i %i %i %i %i\n', beamcount, topcentrenode-nSplitSide, nNodesSide*
nSplitBottom+nNodesSide+1+(5*nSplitSide), strucmat, movebulkgeo);
bottommovebulkelem = beamcount;
beamcount = beamcount+1;

% Write diagonals

% Downwards
for i = 1:2*nSplitSide:nNodesSide-nSplitSide
for j = 2:nSplitSide-1
fprintf(FID1, 'BEAM %i %i %i %i %i %i\n', beamcount, i+(nNodesSide*nSplitBottom)+(
nNodesSide*(nSplitSide-(j-1)))+(j-1), i+(nNodesSide*nSplitBottom)+(
nNodesSide*(nSplitSide-j))+j, strucmat, midsupgeo);
beamcount = beamcount+1;
end
for j = 1:nSplitSide-1:nSplitSide
fprintf(FID1, 'BEAM %i %i %i %i %i\n', beamcount, i+(nNodesSide*nSplitBottom)+(
nNodesSide*(nSplitSide-(j-1)))+(j-1), i+(nNodesSide*nSplitBottom)+(nNodesSide
*(nSplitSide-j))+j, strucmat, midsupdiagendgeo);

```

```

        beamcount = beamcount+1;
    end
end
% Upwards
for i = 1+nSplitSide:2*nSplitSide:nNodesSide-nSplitSide
    for j = 2:nSplitSide-1
        fprintf(FID1,'BEAM %i %i %i %i %i\n', beamcount, i+(nNodesSide*nSplitBottom)+(
            nNodesSide*(j-1))+(j-1), i+(nNodesSide*nSplitBottom)+(nNodesSide*j)+j,
            strucmat, midsupgeo);
        beamcount = beamcount+1;
    end
    for j = 1:nSplitSide-1:nSplitSide
        fprintf(FID1,'BEAM %i %i %i %i %i\n', beamcount, i+(nNodesSide*nSplitBottom)+(
            nNodesSide*(j-1))+(j-1), i+(nNodesSide*nSplitBottom)+(nNodesSide*j)+j,
            strucmat, midsupdiagendgeo);
        beamcount = beamcount+1;
    end
end
for j = 2:nSplitSide-1
    fprintf(FID1,'BEAM %i %i %i %i %i %i\n', beamcount, (nNodesSide-(nSplitSide-1))+
        (nNodesSide*nSplitBottom)+(nNodesSide*(j-1))+(j-1), (nNodesSide-(nSplitSide-1))
        +(nNodesSide*nSplitBottom)+(nNodesSide*j)+j, strucmat, midsupgeo);
    beamcount = beamcount+1;
end
fprintf(FID1,'BEAM %i %i %i %i %i\n', beamcount, (nNodesSide-(nSplitSide-1))+
    (nNodesSide*nSplitBottom)+(nNodesSide*(1-1))+(1-1), (nNodesSide-(nSplitSide-1))+
    (nNodesSide*nSplitBottom)+(nNodesSide*1)+1, strucmat, midsupdiagendgeo);
beamcount = beamcount+1;
fprintf(FID1,'BEAM %i %i %i %i %i\n', beamcount, (nNodesSide-(nSplitSide-1))+
    (nNodesSide*nSplitBottom)+(nNodesSide*(nSplitSide-1))+(nSplitSide-1), 1+(
    nNodesSide*nSplitBottom)+(nSplitSide*nNodesSide), strucmat, midsupdiagendgeo);
beamcount = beamcount+1;

%% Write net configuration

netcount = beamcount+mod(-beamcount,1000);

% Bottom net

% Radial direction
BottomRadialNetElem = [];
for i = 1:nSides
    for j = 2:nSplitSide
        for k = 1:nSplitBottom
            fprintf(FID1,'BEAM %i %i %i %i %i %i %i\n', netcount, ((i-1)*nSplitSide)+j+((
                -1)*nNodesSide), ((i-1)*nSplitSide)+j+(k*nNodesSide), strucmatnet,
                netgeo, i);
            BottomRadialNetElem(k+((j-2)*nSplitBottom), i) = netcount;
            netcount = netcount+1;
        end
    end
end

% Circumferential direction
BottomCircumNetElem = [];
for i = 1:nSides-1
    for j = 1:nSplitBottom
        for k = 1:nSplitSide
            fprintf(FID1,'BEAM %i %i %i %i %i %i %i\n', netcount, ((i-1)*nSplitSide)+k+((
                -1)*nNodesSide), ((i-1)*nSplitSide)+k+1+((j-1)*nNodesSide),
                strucmatnet, netgeo, i);
            BottomCircumNetElem(k+((j-1)*nSplitSide), i) = netcount;
            netcount = netcount+1;
        end
    end
end
for j = 1:nSplitBottom
    for k = 1:nSplitSide-1

```

```

        fprintf(FID1, 'BEAM %i %i %i %i %i\n', netcount, ((nSides-1)*nSplitSide)+k+((
            j-1)*nNodesSide), ((nSides-1)*nSplitSide)+k+1+((j-1)*nNodesSide),
            strucmatnet, netgeo, nSides);
        BottomCircumNetElem(k+((j-1)*(nSplitSide-1)), nSides) = netcount;
        netcount = netcount+1;
    end
end
for j = 1:nSplitBottom
    fprintf(FID1, 'BEAM %i %i %i %i %i %i\n', netcount, ((nSides-1)*nSplitSide)+
        nSplitSide+((j-1)*nNodesSide), 1+((j-1)*nNodesSide), strucmatnet, netgeo, nSides
    );
    BottomCircumNetElem(j+(nSplitBottom*(nSplitSide-1)), nSides) = netcount;
    netcount = netcount+1;
end

% Side net

% Vertical direction
SideVerticalNetElem = [];
for i = 1:nSides
    for j = 2:nSplitSide
        for k = 1:nSplitSide
            fprintf(FID1, 'BEAM %i %i %i %i %i %i\n', netcount, (nNodesSide*nSplitBottom
                )+((i-1)*nSplitSide)+j+((k-1)*nNodesSide), (nNodesSide*nSplitBottom)
                +((i-1)*nSplitSide)+j+(k*nNodesSide), strucmatnet, netgeo, i+nSides);
            SideVerticalNetElem(k+((j-2)*nSplitSide), i) = netcount;
            netcount = netcount+1;
        end
    end
end
SideHorizontalNetElem = [];
% Horizontal direction
for i = 1:nSides-1
    for j = 2:nSplitSide
        for k = 1:nSplitSide
            fprintf(FID1, 'BEAM %i %i %i %i %i %i\n', netcount, (nNodesSide*nSplitBottom
                )+((i-1)*nSplitSide)+k+((j-1)*nNodesSide), (nNodesSide*nSplitBottom)
                +((i-1)*nSplitSide)+k+1+((j-1)*nNodesSide), strucmatnet, netgeo, i+
                nSides);
            SideHorizontalNetElem(k+((j-2)*nSplitSide), i) = netcount;
            netcount = netcount+1;
        end
    end
end
for j = 2:nSplitSide
    for k = 1:nSplitSide-1
        fprintf(FID1, 'BEAM %i %i %i %i %i %i\n', netcount, (nNodesSide*nSplitBottom)+((
            nSides-1)*nSplitSide)+k+((j-1)*nNodesSide), (nNodesSide*nSplitBottom)+((
            nSides-1)*nSplitSide)+k+1+((j-1)*nNodesSide), strucmatnet, netgeo, nSides+
            nSides);
        SideHorizontalNetElem(k+((j-2)*(nSplitSide-1)), nSides) = netcount;
        netcount = netcount+1;
    end
end
for j = 2:nSplitSide
    fprintf(FID1, 'BEAM %i %i %i %i %i %i\n', netcount, (nNodesSide*nSplitBottom)+((
        nSides-1)*nSplitSide)+nSplitSide+((j-1)*nNodesSide), (nNodesSide*nSplitBottom
        )+1+((j-1)*nNodesSide), strucmatnet, netgeo, nSides+nSides);
    SideHorizontalNetElem((j-1)+((nSplitSide-1)*(nSplitSide-1)), nSides) = netcount;
    netcount = netcount+1;
end

%% Write material data and elemental geometry

fprintf(FID1, 'MISOIEP %i %2e %2f %2e %2e\n', strucmat, strucmod, strucpoiss,
    strucyield, strucedens);
fprintf(FID1, 'MISOIEP %i %2e %2f %2e %2e %3f\n', strucmatnet, strucmodnet,
    strucpoissnet, strucyieldnet, strucedensnet, thermexpnet);

```



```

fprintf(FID1, 'PIPE %i %.3f %.3f\n', botringgeo, botringdia, botringthick); %
    Bottom outer ring
fprintf(FID1, 'PIPE %i %.3f %.3f\n', botringendgeo, botringdia, botringendthick); %
    Bottom outer ring end elements
fprintf(FID1, 'PIPE %i %.3f %.3f\n', midsupgeo, midsupdia, midsupthick); %
    Middle outer ring and diagonal supports
fprintf(FID1, 'PIPE %i %.3f %.3f\n', midsupdiagendgeo, midsupdia, midsupdiagendthick); %
    Diagonal supports end elements
fprintf(FID1, 'PIPE %i %.3f %.3f\n', topsupgeo, topsupdia, topsupthick); % Top
    outer ring
fprintf(FID1, 'PIPE %i %.3f %.3f\n', topsupendgeo, topsupenddia, topsupendthick); %
    Top outer ring end elements
fprintf(FID1, 'PIPE %i %.3f %.3f\n', crosstopgeo, crosstopdia, crosstopthick); %
    Crossing wheelhouse supports
fprintf(FID1, 'PIPE %i %.3f %.3f\n', crosstopendgeo, crosstopenddia, crosstopendthick); %
    Crossing wheelhouse supports end elements
fprintf(FID1, 'PIPE %i %.3f %.3f\n', botradgeo, botraddia, botradthick); %
    Bottom radial elements
fprintf(FID1, 'PIPE %i %.3f %.3f\n', botradendgeo, botraddia, botradendthick); %
    Bottom radial lateral end element
fprintf(FID1, 'PIPE %i %.3f %.3f\n', coloverpontgeo, coloverpontdia, coloverpontthick); %
    Outer columns over pontoons
fprintf(FID1, 'PIPE %i %.3f %.3f\n', coloverpontendgeo, coloverpontenddia,
    coloverpontendthick); % Outer columns over pontoons end elements
fprintf(FID1, 'PIPE %i %.3f %.3f\n', intvertgeo, intvertdia, intvertthick); %
    Intermediate vertical columns
fprintf(FID1, 'PIPE %i %.3f %.3f\n', intvertendgeo, intvertenddia, intvertendthick); %
    Intermediate vertical columns end elements
fprintf(FID1, 'PIPE %i %.3f %.3f\n', outpontgeo, dspontoon, outpontthick); %
    Outer pontoon, bottom tank
fprintf(FID1, 'PIPE %i %.3f %.3f %i %i %.3f\n', outconegeo, coloverpontenddia,
    outpontthick, 1, 1, dspontoon); % Outer pontoon, cone
fprintf(FID1, 'PIPE %i %.3f %.3f\n', centpontgeo, diacpontoon, centpontthick); %
    Centre pontoon, bottom tank
fprintf(FID1, 'PIPE %i %.3f %.3f\n', stepconegeo, stepconedia, centconethick); %
    Centre pontoon, intermediate tank
fprintf(FID1, 'PIPE %i %.3f %.3f %i %i %.3f\n', centconegeo, centcoldia, centconethick
    , 1, 1, stepconedia); % Centre pontoon, cone
fprintf(FID1, 'PIPE %i %.3f %.3f\n', centcolgeo, centcoldia, centcolthick); %
    Centre column
fprintf(FID1, 'PIPE %i %.3f %.3f\n', centcolendgeo, centcolenddia, centcolendthick); %
    Centre column top element
fprintf(FID1, 'BOX %i %.3f %.3f %.3f %.3f %.3f\n', movebulkgeo, movebulkwidth,
    movebulkthick, movebulkthick, movebulkthick, movebulkwidth); % Movable bulkhead
fprintf(FID1, 'PIPE %i %.3f %.3f\n', fixedbulkgeo, fixedbulkdia, fixedbulkthick); %
    Fixed bulkhead
fprintf(FID1, 'PIPE %i %.3f %.3f\n', intvertextrageo, intvertdia, intvertextrathick);
    % Intermediate vertical column C11

fprintf(FID1, 'PIPE %i %.3f %.3f\n', netgeo, diathreads, thickthreads); % Net

fprintf(FID1, 'Geometry %i TankVert 1\n', verttankgeo); %
    Vertical tank (equipment)
fprintf(FID1, 'Geometry %i TankHoriz 1\n', horiztankgeo); %
    Horizontal tank (equipment)

%% Writing groups for net

groupcount = 1;

% Bottom net
dummy = size(BottomRadialNetElem);
for i = 1:nSides
    fprintf(FID1, 'GROUPDEF %i Element\n', groupcount);
    groupcount = groupcount+1;
    for j = 1:floor(dummy(1,1)/4)

```

```

    fprintf(FID1,'%i %i %i %i\n',BottomRadialNetElem((j-1)*4+1,i),BottomRadialNetElem
        ((j-1)*4+2,i),BottomRadialNetElem((j-1)*4+3,i),BottomRadialNetElem((j-1)
            *4+4,i));
    end
    for k = (floor(dummy(1,1)/4)*4)+1:dummy(1,1)
        fprintf(FID1,'%i\n',BottomRadialNetElem(k,i));
    end
end
dummy = size(BottomCircumNetElem);
for i = 1:nSides
    fprintf(FID1,'GROUPDEF %i Element\n',groupcount);
    groupcount = groupcount+1;
    for j = 1:floor(dummy(1,1)/4)
        fprintf(FID1,'%i %i %i %i\n',BottomCircumNetElem((j-1)*4+1,i),BottomCircumNetElem
            ((j-1)*4+2,i),BottomCircumNetElem((j-1)*4+3,i),BottomCircumNetElem((j-1)
                *4+4,i));
    end
    for k = (floor(dummy(1,1)/4)*4)+1:dummy(1,1)
        fprintf(FID1,'%i\n',BottomCircumNetElem(k,i));
    end
end
bottomgroupcount = groupcount-1;

% Side Net
dummy = size(SideVerticalNetElem);
for i = 1:nSides
    fprintf(FID1,'GROUPDEF %i Element\n',groupcount);
    groupcount = groupcount+1;
    for j = 1:floor(dummy(1,1)/4)
        fprintf(FID1,'%i %i %i %i\n',SideVerticalNetElem((j-1)*4+1,i),SideVerticalNetElem
            ((j-1)*4+2,i),SideVerticalNetElem((j-1)*4+3,i),SideVerticalNetElem((j-1)
                *4+4,i));
    end
    for k = (floor(dummy(1,1)/4)*4)+1:dummy(1,1)
        fprintf(FID1,'%i\n',SideVerticalNetElem(k,i));
    end
end
dummy = size(SideHorizontalNetElem);
for i = 1:nSides
    fprintf(FID1,'GROUPDEF %i Element\n',groupcount);
    groupcount = groupcount+1;
    for j = 1:floor(dummy(1,1)/4)
        fprintf(FID1,'%i %i %i %i\n',SideHorizontalNetElem((j-1)*4+1,i),
            SideHorizontalNetElem((j-1)*4+2,i),SideHorizontalNetElem((j-1)*4+3,i),
            SideHorizontalNetElem((j-1)*4+4,i));
    end
    for k = (floor(dummy(1,1)/4)*4)+1:dummy(1,1)
        fprintf(FID1,'%i\n',SideHorizontalNetElem(k,i));
    end
end
sidegroupcount = groupcount-1;

%———— Gathering net———— groups————

% Entire bottom net
fprintf(FID1,'GROUPDEF %i Group\n',groupcount);
for i=1:bottomgroupcount
    fprintf(FID1,'%i\n',i);
end
entirebottomnetgroup = groupcount;
groupcount = groupcount+1;

% Entire side net
fprintf(FID1,'GROUPDEF %i Group\n',groupcount);
for i=bottomgroupcount+1:sidegroupcount
    fprintf(FID1,'%i\n',i);
end
entiresidenetgroup = groupcount;

```

```

groupcount = groupcount+1;

% Entire net
fprintf(FID1,'GROUPDEF %i Group %i %i\n',groupcount,entirebottomnetgroup,
entiresidenetgroup);
entirenetgroup = groupcount;
groupcount = groupcount+1;

% Pontoons
fprintf(FID1,'GROUPDEF %i Geom %i %i\n',groupcount,outpontgeo,outconegeo);
groupcount = groupcount+1;
fprintf(FID1,'GROUPDEF %i Geom %i\n',groupcount,centpontgeo);
centpontgroup = groupcount;
groupcount = groupcount+1;
fprintf(FID1,'GROUPDEF %i Elem %i %i %i %i %i\n',groupcount,sidepontcoelem);
fprintf(FID1,'FLOODED Group %i %i\n',groupcount-1,groupcount-2);
groupcount = groupcount+1;

% fprintf(FID1,'IntFluid %.1f TimeDep %i Element %i\n',1024,105,centpontelem);

%———— Making the movable bulkhead non-structural ————
fprintf(FID1,'NONSTRU Geom %i\n',movebulkgeo);

%———— Temperature field, net————

dummy1 = size(BottomRadialNetElem);
dummy2 = size(BottomCircumNetElem);
dummy3 = size(SideVerticalNetElem);
dummy4 = size(SideHorizontalNetElem);

fprintf(FID1,'ELEMTEMP 10 1 -1.0 0.0 0.0\n');
% Bottom net
for i = 1:dummy1(1,2)
    for j = 1:floor(dummy1(1,1)/4)
        fprintf(FID1,'%i %i %i %i\n',BottomRadialNetElem((j-1)*4+1,i),
            BottomRadialNetElem((j-1)*4+2,i),BottomRadialNetElem((j-1)*4+3,i),
            BottomRadialNetElem((j-1)*4+4,i));
    end
    for k = (floor(dummy1(1,1)/4)*4)+1:dummy1(1,1)
        fprintf(FID1,'%i\n',BottomRadialNetElem(k,i));
    end
end
for i = 1:dummy2(1,2)
    for j = 1:floor(dummy2(1,1)/4)
        fprintf(FID1,'%i %i %i %i\n',BottomCircumNetElem((j-1)*4+1,i),
            BottomCircumNetElem((j-1)*4+2,i),BottomCircumNetElem((j-1)*4+3,i),
            BottomCircumNetElem((j-1)*4+4,i));
    end
    for k = (floor(dummy2(1,1)/4)*4)+1:dummy2(1,1)
        fprintf(FID1,'%i\n',BottomCircumNetElem(k,i));
    end
end
% Side net
for i = 1:dummy3(1,2)
    for j = 1:floor(dummy3(1,1)/4)
        fprintf(FID1,'%i %i %i %i\n',SideVerticalNetElem((j-1)*4+1,i),
            SideVerticalNetElem((j-1)*4+2,i),SideVerticalNetElem((j-1)*4+3,i),
            SideVerticalNetElem((j-1)*4+4,i));
    end
    for k = (floor(dummy3(1,1)/4)*4)+1:dummy3(1,1)
        fprintf(FID1,'%i\n',SideVerticalNetElem(k,i));
    end
end
for i = 1:dummy4(1,2)
    for j = 1:floor(dummy4(1,1)/4)
        fprintf(FID1,'%i %i %i %i\n',SideHorizontalNetElem((j-1)*4+1,i),
            SideHorizontalNetElem((j-1)*4+2,i),SideHorizontalNetElem((j-1)*4+3,i),
            SideHorizontalNetElem((j-1)*4+4,i));
    end
end

```

```

end
for k = (floor(dummy4(1,1)/4)*4)+1:dummy4(1,1)
    fprintf(FID1,'%i\n',SideHorizontalNetElem(k,i));
end
end

%% Defining local z-axis of net

unitveccount = 1;
thetaNSide = [];
for i = 1:nSides-1
    thetaNSide(i) = theta(i)+((theta(i+1)-theta(i))/2);
end
thetaNSide(nSides) = theta(nSides)+((2*pi)-theta(nSides))/2);

% Bottom net
for i = 1:nSides
    fprintf(FID1,'UNITVEC %i %.3f %.3f %.3f\n',unitveccount,-sin(thetaBottom)*sin(
        thetaNSide(i)),sin(thetaBottom)*cos(thetaNSide(i)),-cos(thetaBottom));
    unitveccount = unitveccount+1;
end

% Side net
for i = 1:nSides
    fprintf(FID1,'UNITVEC %i %.3f %.3f 0.0\n',unitveccount,-sin(thetaNSide(i)),cos(
        thetaNSide(i)));
    unitveccount = unitveccount+1;
end

%% Node and element masses

fishfoodmass = 600000; % Apply at top centre node
marinegrowthmass = 50000; % Apply at all side columns nodes + bottom
icemass = 109000; % Apply at all side columns nodes
maindeckmass = 350496; % Apply at top centre node
equipmentmassaqua = 151141; % Apply at all top nodes + centre column + top
ring
equipmentmassmarine = 140163; % Apply at all side column nodes
walkwaymass = 150870; % Apply at all top crossing nodes + centre column
+ top ring
foundationmass = 129961; % Apply at top crossing nodes + top ring
platesdeckmass = 72138; % Apply at all side column nodes + centre column
bracketmass = 100000; % Apply at all side column nodes + bottom
anodemass = 15000; % Apply at all side column nodes
paintweldscorrosionmass = 329856; % Apply at all structural nodes
bulkheadmass = 172001+195706; % Apply at all top crossing nodes + top ring +
all side columns

oiltankmass = 18600; % At top crossings, specified node
watertankmass = 22000; % At top crossings, specified node
ensiletankmass = 50000; % At top crossings, specified node
fueloilmass = 3000; % At top crossings, specified node
extramass = 0; % Applied to get correct draught

sidecolumnmass = (icemass+equipmentmassmarine+anodemass)/length(sidestrucnodes); %
To be places at all side column nodes
centremass = fishfoodmass+maindeckmass; %
To be places at top node
sidecolumnbottommass = (marinegrowthmass+bracketmass)/(length(bottomstrucnodes)+
length(sidestrucnodes)); % To be placed at all side column and bottom nodes
topmass = foundationmass/(length(crosstopstrucnodes)+length(topringstrucnodes)); %
To be places at all top crossing and top ring nodes
topcentrecolumnmass = (equipmentmassaqua+walkwaymass)/(length(crosstopstrucnodes)+
length(centrestrucnodes)+length(topringstrucnodes)); % To be places at all top
crossing, top ring and centre column nodes
columnmass = bracketmass/(length(sidestrucnodes)+length(centrestrucnodes)); %
To be placed at all column nodes

```

```

topcrossingsidecolumnmass = bulkheadmass/(length(sidestrucnodes)+length(
    topringstrucnodes)+length(crosstopstrucnodes)); % To be places at all top
    crossing , top ring and side columns
allstrucnodesmass = paintweldscorrosionmass/(length(bottomstrucnodes)+length(
    sidestrucnodes)+length(topringstrucnodes)+length(centrestrucnodes)+length(
    crosstopstrucnodes)); % To be placed at all structural nodes

totnodemass = icemass+equipmentmassmarine+anodemass+fishfoodmass+maindeckmass+
    marinegrowthmass+bracketmass+foundationmass+equipmentmassaqua+walkwaymass+
    bracketmass+paintweldscorrosionmass+oiltankmass+watertankmass+ensiletankmass+
    fueloilmass+bulkheadmass;

% Equipment material
decktankmat = 100;
oiltankmat = 110;
watertankmat = 120;
ensiletankmat = 130;

% Centre node masses and other tanks
fprintf(FID1,' Material %i Equip %.1f\n',decktankmat,centremass+fueloilmass);
fprintf(FID1,' Material %i Equip %.1f\n',oiltankmat,oiltankmass);
fprintf(FID1,' Material %i Equip %.1f\n',watertankmat,watertankmass);
fprintf(FID1,' Material %i Equip %.1f\n',ensiletankmat,ensiletankmass);

% Fish food tank + centre node mass
fprintf(FID1,'Equip_1N %i %i %i %i\n',netcount,topcentrenode,decktankmat,verttankgeo)
;
netcount = netcount+1;
% Oil tank
fprintf(FID1,' Equip_1N %i %i %i %i\n',netcount,CrossNodes(2,1),oiltankmat,verttankgeo
);
netcount = netcount+1;
% Water tank
fprintf(FID1,' Equip_1N %i %i %i %i\n',netcount,CrossNodes(1,2),watertankmat,
    verttankgeo);
netcount = netcount+1;
fprintf(FID1,' Equip_1N %i %i %i %i\n',netcount,CrossNodes(2,4),ensiletankmat,
    verttankgeo);
netcount = netcount+1;

% Masses at side columns
for i = 1:length(sidestrucnodes)
    fprintf(FID1,'NODEMASS %i %.1f\n',sidestrucnodes(i),sidecolumnmass);
    fprintf(FID1,'NODEMASS %i %.1f\n',sidestrucnodes(i),sidecolumnbottommass);
    fprintf(FID1,'NODEMASS %i %.1f\n',sidestrucnodes(i),columnmass);
    fprintf(FID1,'NODEMASS %i %.1f\n',sidestrucnodes(i),allstrucnodesmass);
    fprintf(FID1,'NODEMASS %i %.1f\n',sidestrucnodes(i),topcrossingsidecolumnmass);
end

% Masses at top crossings
for i = 1:length(crosstopstrucnodes)
    fprintf(FID1,'NODEMASS %i %.1f\n',crosstopstrucnodes(i),topmass);
    fprintf(FID1,'NODEMASS %i %.1f\n',crosstopstrucnodes(i),topcentrecolumnmass);
    fprintf(FID1,'NODEMASS %i %.1f\n',crosstopstrucnodes(i),allstrucnodesmass);
    fprintf(FID1,'NODEMASS %i %.1f\n',crosstopstrucnodes(i),
        topcrossingsidecolumnmass);
end

% Masses at top ring
for i = 1:length(topringstrucnodes)
    fprintf(FID1,'NODEMASS %i %.1f\n',topringstrucnodes(i),topmass);
    fprintf(FID1,'NODEMASS %i %.1f\n',topringstrucnodes(i),topcentrecolumnmass);
    fprintf(FID1,'NODEMASS %i %.1f\n',topringstrucnodes(i),allstrucnodesmass);
    fprintf(FID1,'NODEMASS %i %.1f\n',topringstrucnodes(i),topcrossingsidecolumnmass
    );
end

% Masses as centre column

```

```

for i = 1:length(centrestrucnodes)
    fprintf(FID1,'NODEMASS %i %.1f\n',centrestrucnodes(i),topcentrecolumnmass);
    fprintf(FID1,'NODEMASS %i %.1f\n',centrestrucnodes(i),columnmass);
    fprintf(FID1,'NODEMASS %i %.1f\n',centrestrucnodes(i),allstrucnodesmass);
end

% Masses at bottom
for i = 1:length(bottomstrucnodes)
    fprintf(FID1,'NODEMASS %i %.1f\n',bottomstrucnodes(i),sidecolumnbottommass);
    fprintf(FID1,'NODEMASS %i %.1f\n',bottomstrucnodes(i),allstrucnodesmass);
end

%% Forces/moments applied to find natural periods

% Water plane stiffness
Atot = pi/4*(coloverpontdia^2+intvertdia^2)*6;
C33 = Atot*9.81*1025;

loadcount = 50;

% HEAVE
% Force to find natural period in heave
heaveload = 2*C33/nSides; %(will give a vertical displacement of two meter)
% Side mass (applied at top of all outer columns)
%for i = (nNodesSide*(nSplitBottom+nSplitSide))+1:nSplitSide:(nNodesSide*(
    nSplitBottom+nSplitSide))+nNodesSide
%    fprintf(FID1,'NODELOAD %i %i 0 0 %.1f\n',loadcount,i,-heaveload);
%end

% ROLL
rollload = C33/10;
rollmoment = C33*15;

outercolumnnoded = (nNodesSide*(nSplitBottom+nSplitSide))+1:nSplitSide:(nNodesSide
    *(nSplitBottom+nSplitSide))+nNodesSide;

%for i=1:3
%    fprintf(FID1,'NODELOAD %i %i 0 0 %.1f\n',loadcount,outercolumnnoded(i),-
    rollload);
%    fprintf(FID1,'NODELOAD %i %i 0 0 %.1f\n',loadcount,outercolumnnoded(i+4),
    rollload);
%end

%for i=1:2
%    fprintf(FID1,'NODELOAD %i %i 0 0 %.1f\n',loadcount,outercolumnnoded(nSides-(i
    -1)),rollload);
%    fprintf(FID1,'NODELOAD %i %i 0 0 %.1f\n',loadcount,outercolumnnoded(i+7),
    rollload);
%end

%fprintf(FID1,'NODELOAD %i %i 0 0 0 %.1f 0 0\n',loadcount,topcentrenode-(nSplitSide
    /2),rollmoment);

% PITCH
%fprintf(FID1,'NODELOAD %i %i 0 0 0 0 %.1f 0\n',loadcount,topcentrenode-(nSplitSide
    /2),rollmoment);

% SWAY
swayload = C33/(nSplitSide/2+1);

%for i = 1:nSplitSide/2+1
%    fprintf(FID1,'NODELOAD %i %i 0 %.1f 0 0 0\n',loadcount,((nSplitBottom*
    nNodesSide)+1)+((i-1)*nNodesSide),swayload);
%end

```

```

% SURGE
%for i = 1:nSplitSide/2+1
%   fprintf(FID1,'NODELOAD %i %i %.1f 0 0 0 0\n',loadcount,((nSplitBottom*
nNodesSide)+(3*nSplitSide)+1)+((i-1)*nNodesSide),swayload);
%end

% YAW
%fprintf(FID1,'NODELOAD %i %i 0 0 0 0 %.1f\n',loadcount, topcentrenode-2,2*
rollmoment);

loadcount = loadcount+1;

%% Current blockage
% Direction is defined at the top of the script.

deltanet = 30*pi/180;           % Angle between net sides
startangle = (270+15)*pi/180; % Net group 1 has normal direction 285 deg
nNetGroups = 4*nSides;        % Number of net groups
currblock = 0.9;

% The net

% All net groups must be associated with a direction (normal to the net, outwards)
netgroupdir = [];

for i = 1:4
    for j = 1:nSides
        netgroupdir((i-1)*nSides+j,1) = (i-1)*nSides+j;
        if j<=3
            netgroupdir((i-1)*nSides+j,2) = startangle+((j-1)*deltanet);
        else
            netgroupdir((i-1)*nSides+j,2) = startangle+((j-1)*deltanet)-(2*pi);
        end
    end
end

% Scanning through netgroupdir and assigning current blockage factor to
% correct groups

if (currrdir >= pi/2) && (currrdir <= 3*pi/2) % Between 90 and 270 deg
    for i = 1:nNetGroups
        if netgroupdir(i,2) < currrdir-(pi/2)-0.01
            fprintf(FID1,'HYDROPAR CurrBlock %.2f Group %i\n',currblock,netgroupdir(i
,1));
        elseif netgroupdir(i,2) > currrdir+(pi/2)+0.01
            fprintf(FID1,'HYDROPAR CurrBlock %.2f Group %i\n',currblock,netgroupdir(i
,1));
        end
    end
end

if (currrdir < pi/2) && (currrdir >= 0) % < 90 deg
    for i = 1:nNetGroups
        if (netgroupdir(i,2) > currrdir+(pi/2)) && (netgroupdir(i,2) < ((2*pi)-(pi/2)
-currrdir))
            fprintf(FID1,'HYDROPAR CurrBlock %.2f Group %i\n',currblock,netgroupdir(i
,1));
        end
    end
end

if (currrdir > 3*pi/2) && (currrdir <= 2*pi) % > 270 deg
    for i = 1:nNetGroups
        if (netgroupdir(i,2) < currrdir-(pi/2)) && (netgroupdir(i,2) > (currrdir-(3*pi
/2)))
            fprintf(FID1,'HYDROPAR CurrBlock %.2f Group %i\n',currblock,netgroupdir(i
,1));
        end
    end
end

```

```

end
end

% Centre column
fprintf(FID1,'HYDROPAR CurrBlock %.2f Geo %i\n',currblock,centcolgeo);
fprintf(FID1,'HYDROPAR CurrBlock %.2f Geo %i\n',currblock,centcolendgeo);
fprintf(FID1,'HYDROPAR CurrBlock %.2f Geo %i\n',currblock,centconegeo);

% Vertical columns
deltavertcol = 2*pi/6;
startanglepont = 3*pi/2; % Start angle, columns over pontoons
startangleint = (3*pi/2)+(deltavertcol/2); % Start angle, intermediate columns
vertcoldir = [];
% All elements must be associated with a direction (normal to the net, outwards)

% Columns over pontoons
k = 1;
dircolpont = startanglepont;
for i = 1:length(vertcolpontelem)
    vertcoldir(k,1) = vertcolpontelem(i);
    vertcoldir(k,2) = dircolpont;
    dircolpont = dircolpont + deltavertcol;
    if dircolpont >= 2*pi-0.01
        dircolpont = deltavertcol/2;
    end
    k = k+1;
end
dircolpont = startanglepont;
for i = 1:length(vertcolpontendelem)
    vertcoldir(k,1) = vertcolpontendelem(i);
    vertcoldir(k,2) = dircolpont;
    dircolpont = dircolpont + deltavertcol;
    if dircolpont >= 2*pi-0.01
        dircolpont = deltavertcol/2;
    end
    k = k+1;
end

dircolint = startangleint;
for i = 1:length(vertcolintelem)-(nSplitSide-2)
    vertcoldir(k,1) = vertcolintelem(i);
    vertcoldir(k,2) = dircolint;
    dircolint = dircolint + deltavertcol;
    if dircolint >= 2*pi-0.01
        dircolint = 0;
    end
    if (dircolint >= startangleint-(deltavertcol+0.01)) && (dircolint <=
        startangleint-0.01)
        dircolint = startangleint;
    end
    k = k+1;
end
for i = length(vertcolintelem)-(nSplitSide-2)+1:length(vertcolintelem)
    vertcoldir(k,1) = vertcolintelem(i);
    vertcoldir(k,2) = startangle-deltavertcol;
    k = k+1;
end
dircolint = startangleint;
for i = 1:length(vertcolintendelem)
    vertcoldir(k,1) = vertcolintendelem(i);
    vertcoldir(k,2) = dircolint;
    dircolint = dircolint + deltavertcol;
    if dircolint >= 2*pi-0.01
        dircolint = 0;
    end
    k = k+1;
end
end

```



```

nColElem = k-1;
% Scanning through vertcoldir and assigning current blockage factor to
% correct elements

if (currdir >= pi/2) && (currdir <= 3*pi/2) % Between 90 and 270 deg
    for i = 1:nColElem
        if vertcoldir(i,2) < currdir-(pi/2)-0.01
            fprintf(FID1,'HYDROPAR CurrBlock %.2f Elem %i\n',currblock,vertcoldir(i,1));
        elseif vertcoldir(i,2) > currdir+(pi/2)+0.01
            fprintf(FID1,'HYDROPAR CurrBlock %.2f Elem %i\n',currblock,vertcoldir(i,1));
        end
    end
end
if (currdir < pi/2) && (currdir >= 0) % < 90 deg
    for i = 1:nColElem
        if (vertcoldir(i,2) > currdir+(pi/2)) && (vertcoldir(i,2) < ((2*pi)-((pi/2)-currdir)))
            fprintf(FID1,'HYDROPAR CurrBlock %.2f Elem %i\n',currblock,vertcoldir(i,1));
        end
    end
end
if (currdir > 3*pi/2) && (currdir <= 2*pi) % > 270 deg
    for i = 1:nColElem
        if (vertcoldir(i,2) < currdir-(pi/2)) && (vertcoldir(i,2) > (currdir-(3*pi/2)))
            fprintf(FID1,'HYDROPAR CurrBlock %.2f Elem %i\n',currblock,vertcoldir(i,1));
        end
    end
end

% Bottom ring

deltabottomelem = 2*pi/nSides;
startanglebottom = (3*pi/2)+(deltabottomelem/2);
bottomdir = [];

k = 1;
dirbottom = startanglebottom;
for i = 1:nSides-1
    for j = 1:nSplitSide-2
        bottingelem(((i-1)*(nSplitSide-2))+j);
        bottomdir(k,2) = dirbottom;
        k = k+1;
    end
    dirbottom = dirbottom+deltabottomelem;
    if dirbottom >= 2*pi-0.01
        dirbottom = deltabottomelem/2;
    end
    if (dirbottom >= startanglebottom-(deltabottomelem+0.01)) && (dirbottom <= startanglebottom-0.01)
        dirbottom = startanglebottom;
    end
end
for i = length(bottingelem)-(nSplitSide-2)+1:length(bottingelem)
    bottomdir(k,1) = bottingelem(i);
    bottomdir(k,2) = startanglebottom-deltabottomelem;
    k = k+1;
end

dirbottom = startanglebottom;
for i = 1:nSides-1
    for j = 1:2
        bottingelem(((i-1)*2)+j);
        bottomdir(k,1) = bottingelem;
        bottomdir(k,2) = dirbottom;
    end
end

```

```

        k = k+1;
    end
    dirbottom = dirbottom+deltabottomelem;
    if dirbottom >= 2*pi-0.01
        dirbottom = deltabottomelem/2;
    end
    if (dirbottom >= startanglebottom-(deltabottomelem+0.01)) && (dirbottom <=
        startanglebottom-0.01)
        dirbottom = startanglebottom;
    end
end
for i = length(botringendelem)-2+1:length(botringendelem)
    bottomdir(k,1) = botringendelem(i);
    bottomdir(k,2) = startanglebottom-deltabottomelem;
    k = k+1;
end

nBotElem = k-1;
% Scanning through vertcoldir and assigning current blockage factor to
% correct elements

if (currdir >= pi/2) && (currdir <= 3*pi/2)    % Between 90 and 270 deg
    for i = 1:nBotElem
        if bottomdir(i,2) < currdir-(pi/2)-0.01
            fprintf(FID1,'HYDROPAR CurrBlock %.2f Elem %i\n',currblock ,bottomdir(i,1)
                );
        elseif bottomdir(i,2) > currdir+(pi/2)+0.01
            fprintf(FID1,'HYDROPAR CurrBlock %.2f Elem %i\n',currblock ,bottomdir(i,1))
                ;
        end
    end
end
if (currdir < pi/2) && (currdir >= 0)          % < 90 deg
    for i = 1:nBotElem
        if (bottomdir(i,2) > currdir+(pi/2)) && (bottomdir(i,2) < ((2*pi)-((pi/2)-
            currdir)))
            fprintf(FID1,'HYDROPAR CurrBlock %.2f Elem %i\n',currblock ,bottomdir(i,1)
                );
        end
    end
end
if (currdir > 3*pi/2) && (currdir <= 2*pi)    % > 270 deg
    for i = 1:nBotElem
        if (bottomdir(i,2) < currdir-(pi/2)) && (bottomdir(i,2) > (currdir-(3*pi/2)))
            fprintf(FID1,'HYDROPAR CurrBlock %.2f Elem %i\n',currblock ,bottomdir(i,1)
                );
        end
    end
end

%% Mooring line properties

g = 9.81;          % acceleration of gravity [m/s2]
rhowater = 1025;  % density of water [kg/m3]
depth = 150;      % water depth [m]
phi = 49.1*pi/180; % top angle at mooring point on cage

% Top tension [N]
T = 20*g*10^3;
Ty = T*cos(phi);
Tz = T*sin(phi);

% Mooring line is part chain (steel), part fibre (polyester)

% Chain
Lchain = 1000;
Dchain = sqrt(2)*0.088;
EAchain = 6.94*10^4*g*10^3;

```

```

wChain = 147; % weight in water [kg/m]
MBLchain = 718.8*g*10^3;
Achain = pi/4*Dchain^2;
yieldChain = MBLchain/Achain;
Echain = EAchain/Achain;
rhoChain = (wChain+(Achain*rhowater))/Achain;

geoChain = 30; % geometry ID
matChain = 30; % material ID

% Fibre
Lfibre = 100;
Dfibre = 0.16;
EAfibre = 2.40*10^4*g*10^3;
wFibre = 4; % weight in water [kg/m]
MBLfibre = 828*g*10^3;
Afibre = pi/4*Dfibre^2;
yieldFibre = MBLfibre/Afibre;
Efibre = EAfibre/Afibre;
rhoFibre = (wFibre+(Afibre*rhowater))/Afibre;

geoFibre = 40; % geometry ID
matFibre = 40; % material ID

Ltot = Lchain+Lfibre; % total length
Lstep = 5; % step size
nBeams = Ltot/Lstep; % number of splits
nl = 8; % number of lines
nN = nBeams+1; % number of nodes

% Number of springtground must be set manually, check output from
% mooring line stretch-up.
nS2G = 181;

%% Read mooringline coordinates
% Single line coordinates taken from file res_ufo.fem

FID2 = fopen('res_ufo.fem','r');
% Skip first 5 rows
for i = 1:5
    fgetl(FID2);
end
READNODE = textscan(FID2,'%s %d %f %f %f %d %d %d %d %d %d',nN);
fclose(FID2);

%% Copy mooring line, translate and rotate

% Node coordinates

NODEnumber = READNODE{2};
xNODEcord = READNODE{3};
yNODEcord = READNODE{4};
zNODEcord = READNODE{5};

% Figure for documentation

figure()
plot(yNODEcord,zNODEcord)
xlabel('Distance from anchor [m]')
ylabel('z [m]')
title('Mooring line profile')
xlim([700 1100])
ylim([-150 10])
grid on

figure()
plot(yNODEcord(1:201),zNODEcord(1:201),yNODEcord(201:end),zNODEcord(201:end),'r');
legend('Chain','Fibre');

```

```

xlabel('Distance from anchor [m]')
ylabel('z [m]')
title('Mooring line profile')
xlim([700 1100])
ylim([-150 10])
grid on

% Line angles
thetaLine = [];
anglestep = 2*pi/nl;
startAngle = 22.5*pi/180;
for i = 1:nl
    thetaLine(i) = (i-1)*anglestep+startAngle;
end

% Line 1 goes in positive y-direction and negative x-direction with an
% angle of 22.5 degrees, where 0 degrees is in positive y-direction.

Lhor = yNODEcord(nN); % horizontal length of line

% Coordinates in new system
xNODEcordNEW = [];
yNODEcordNEW = [];
zNODEcordNEW = [];

% Translating mooring line in z-direction to get to correct depth of
% mooring line top.
Ztrans =(Bnode(1,3)-zNODEcord(nN))-h3spontoon;

% Base mooring line
for i = 1:nN
    xNODEcordNEW(i) = 0;
    yNODEcordNEW(i) = Lhor-yNODEcord(i);
    zNODEcordNEW(i) = zNODEcord(i)+Ztrans;
end

% Rotating mooring lines to their respective angles
xNODErotation=[];
yNODErotation=[];
zNODErotation=[];
for i = 1:nl
    for j = 1:nN
        xNODErotation(j,i) = -yNODEcordNEW(j)*sin(thetaLine(i));
        yNODErotation(j,i) = yNODEcordNEW(j)*cos(thetaLine(i));
        zNODErotation(j,i) = zNODEcordNEW(j);
    end
end

% Translating mooring lines to their respective poontoons
xNODEmooring = [];
yNODEmooring = [];
zNODEmooring = [];
for j = 1:nN
    xNODEmooring(j,1) = xNODErotation(j,1)+(sidepontMat(2,1)-xNODErotation(nN,1));
    yNODEmooring(j,1) = yNODErotation(j,1)+(sidepontMat(2,2)-yNODErotation(nN,1));
    zNODEmooring(j,1) = zNODErotation(j,1);

    xNODEmooring(j,2) = xNODErotation(j,2)+(sidepontMat(2,1)-xNODErotation(nN,2));
    yNODEmooring(j,2) = yNODErotation(j,2)+(sidepontMat(2,2)-yNODErotation(nN,2));
    zNODEmooring(j,2) = zNODErotation(j,2);

    xNODEmooring(j,3) = xNODErotation(j,3)+(sidepontMat(3,1)-xNODErotation(nN,3));
    yNODEmooring(j,3) = yNODErotation(j,3)+(sidepontMat(3,2)-yNODErotation(nN,3));
    zNODEmooring(j,3) = zNODErotation(j,3);

    xNODEmooring(j,4) = xNODErotation(j,4)+(sidepontMat(3,1)-xNODErotation(nN,4));
    yNODEmooring(j,4) = yNODErotation(j,4)+(sidepontMat(3,2)-yNODErotation(nN,4));
    zNODEmooring(j,4) = zNODErotation(j,4);
end

```

```

xNODEmooring(j,5) = xNODErotation(j,5)+(sidepontMat(5,1)-xNODErotation(nN,5));
yNODEmooring(j,5) = yNODErotation(j,5)+(sidepontMat(5,2)-yNODErotation(nN,5));
zNODEmooring(j,5) = zNODErotation(j,5);

xNODEmooring(j,6) = xNODErotation(j,6)+(sidepontMat(5,1)-xNODErotation(nN,6));
yNODEmooring(j,6) = yNODErotation(j,6)+(sidepontMat(5,2)-yNODErotation(nN,6));
zNODEmooring(j,6) = zNODErotation(j,6);

xNODEmooring(j,7) = xNODErotation(j,7)+(sidepontMat(6,1)-xNODErotation(nN,7));
yNODEmooring(j,7) = yNODErotation(j,7)+(sidepontMat(6,2)-yNODErotation(nN,7));
zNODEmooring(j,7) = zNODErotation(j,7);

xNODEmooring(j,8) = xNODErotation(j,8)+(sidepontMat(6,1)-xNODErotation(nN,8));
yNODEmooring(j,8) = yNODErotation(j,8)+(sidepontMat(6,2)-yNODErotation(nN,8));
zNODEmooring(j,8) = zNODErotation(j,8);
end

% Making coordinates to each line
Line = [];
for i = 1:nI
    for j = 1:nN
        Line(j,1,i) = ((i-1)*nN)+NODEnumber(j);
        Line(j,2,i) = xNODEmooring(j,i);
        Line(j,3,i) = yNODEmooring(j,i);
        Line(j,4,i) = zNODEmooring(j,i);
    end
end

% Mooringline matrices on the following form , ID X Y Z
Line1 = Line(:, :, 1);
Line2 = Line(:, :, 2);
Line3 = Line(:, :, 3);
Line4 = Line(:, :, 4);
Line5 = Line(:, :, 5);
Line6 = Line(:, :, 6);
Line7 = Line(:, :, 7);
Line8 = Line(:, :, 8);

% Figures for documentation

figure()
plot(Line1(:,2),Line1(:,3),Line2(:,2),Line2(:,3),Line3(:,2),Line3(:,3),Line4(:,2),
      Line4(:,3),Line5(:,2),Line5(:,3),Line6(:,2),Line6(:,3),Line7(:,2),Line7(:,3),
      Line8(:,2),Line8(:,3))
legend('Line 1','Line 2','Line 3','Line 4','Line 5','Line 6','Line 7','Line 8')
xlabel('x [m]')
ylabel('y [m]')
title('Mooring spread')

figure()
plot(Line1(:,3),Line1(:,4))
xlabel('y [m]')
ylabel('z [m]')
title('Mooring line profile')

figure()
plot3(Line1(:,2),Line1(:,3),Line1(:,4),Line2(:,2),Line2(:,3),Line2(:,4),Line3(:,2),
      Line3(:,3),Line3(:,4),Line4(:,2),Line4(:,3),Line4(:,4),Line5(:,2),Line5(:,3),
      Line5(:,4),Line6(:,2),Line6(:,3),Line6(:,4),Line7(:,2),Line7(:,3),Line7(:,4),
      Line8(:,2),Line8(:,3),Line8(:,4))
legend('Line 1','Line 2','Line 3','Line 4','Line 5','Line 6','Line 7','Line 8')
xlabel('x [m]')
ylabel('y [m]')
zlabel('z [m]')
title('Mooring spread')

%% Writing mooring lines

```

```

% Nodes
for j = 1:n1
    fprintf(FID1,'NODE %i %.3f %.3f %.3f 1 1 1 1 1\n',Line(1, :, j));
    for i = 2:nN-1
        fprintf(FID1,'NODE %i %.3f %.3f %.3f\n', Line(i, 1, j), Line(i, 2, j), Line(i, 3, j),
            Line(i, 4, j));
    end
end

% Beams
nChain = Lchain/Lstep;
nFibre = Lfibre/Lstep;
beamcounter = netcount+mod(-netcount,1000);
for j = 1:n1
    % chain
    for i = 1:nChain
        fprintf(FID1,'BEAM %i %i %i %i %i\n', beamcounter, Line(i, 1, j), Line(i+1, 1, j),
            matChain, geoChain);
        beamcounter = beamcounter+1;
    end
    % fiber
    for i = 1+nChain:nBeams-1
        fprintf(FID1,'BEAM %i %i %i %i %i\n', beamcounter, Line(i, 1, j), Line(i+1, 1, j),
            matFibre, geoFibre);
        beamcounter = beamcounter+1;
    end
    if j <= 2
        fprintf(FID1,'BEAM %i %i %i %i %i\n', beamcounter, Line(nBeams, 1, j), (nNodesSide
            *nSplitBottom)+(nNodesSide*(nSplitSide+1))+((2-1)*3)+1, matFibre, geoFibre
        );
        beamcounter = beamcounter+1;
    elseif j>2 && j<=4
        fprintf(FID1,'BEAM %i %i %i %i %i\n', beamcounter, Line(nBeams, 1, j), (nNodesSide
            *nSplitBottom)+(nNodesSide*(nSplitSide+1))+((3-1)*3)+1, matFibre, geoFibre
        );
        beamcounter = beamcounter+1;
    elseif j>4 && j<=6
        fprintf(FID1,'BEAM %i %i %i %i %i\n', beamcounter, Line(nBeams, 1, j), (nNodesSide
            *nSplitBottom)+(nNodesSide*(nSplitSide+1))+((5-1)*3)+1, matFibre, geoFibre
        );
        beamcounter = beamcounter+1;
    else
        fprintf(FID1,'BEAM %i %i %i %i %i\n', beamcounter, Line(nBeams, 1, j), (nNodesSide
            *nSplitBottom)+(nNodesSide*(nSplitSide+1))+((6-1)*3)+1, matFibre, geoFibre
        );
        beamcounter = beamcounter+1;
    end
end

% Spring to ground
materialS2G = 50;
S2Gcount = beamcounter+mod(-beamcounter,1000);
for j = 1:n1
    for i = 1:nS2G
        fprintf(FID1,'SPRNG2GR %i %i %i\n', S2Gcount, Line(i, 1, j), materialS2G);
        S2Gcount = S2Gcount+1;
    end
end

%% Spring to ground for mooring line elements above sea bottom

seabottom = Line(1,4,1);

% Springs defined for all chain elements
% Spring material
for i=nS2G+1:nChain
    fprintf(FID1,'HYPELAST %i\n', materialS2G+i-nS2G);
end

```

```

fprintf(FID1, '%.2e %.2f\n', -1E6, seabottom-Line(i,4,1)-3);
fprintf(FID1, '%.2e %.2f\n', -2E5, seabottom-Line(i,4,1)-2);
fprintf(FID1, '%.2e %.2f\n', -1E5, seabottom-Line(i,4,1)-1);
fprintf(FID1, '%i %.2f\n', 0, seabottom-Line(i,4,1));
fprintf(FID1, '%i %.2f\n', 0, 0);
fprintf(FID1, '%i %.2f\n', 0, 10);
fprintf(FID1, '%i %.2f\n', 0, 20);
fprintf(FID1, 'MREF %i 0 0 %i 0 0 0\n', nChain+i-nS2G, materialS2G+i-nS2G);
end

% Writing springs
for i=1:n1
    for j=nS2G+1:nChain
        fprintf(FID1, 'SPRNG2GR %i %i %i\n', S2Gcount, Line(j,1,i), nChain+j-nS2G);
        S2Gcount = S2Gcount+1;
    end
end

%% Material, geometric, and loading data

fprintf(FID1, 'MISOIEP %i %.2e %.2f %.2e %.2e\n', matChain, Echain, 0.3, yieldChain, rhoChain);
fprintf(FID1, 'MISOIEP %i %.2e %.2f %.2e %.2e\n', matFibre, Efibre, 0.3, yieldFibre, rhoFibre);
fprintf(FID1, 'MATERIAL %i Fric Comp %.2f %.2e %i %i\n', materialS2G, 0.7, 1E5, 12, 3);

fprintf(FID1, 'PIPE %i %.3f %.3f\n', geoChain, Dchain, Dchain/2-0.001);
fprintf(FID1, 'PIPE %i %.3f %.3f\n', geoFibre, Dfibre, Dfibre/2-0.001);

fprintf(FID1, 'GRAVITY 1 0 0 -9.81\n');

% Groups by material
fprintf(FID1, 'GROUPDEF %i Mat %i\n', groupcount, strucmat);
structuregroup = groupcount;
groupcount = groupcount+1;
fprintf(FID1, 'GROUPDEF %i Mat %i\n', groupcount, matChain);
chaingroup = groupcount;
groupcount = groupcount+1;
fprintf(FID1, 'GROUPDEF %i Mat %i\n', groupcount, matFibre);
fibregroup = groupcount;
groupcount = groupcount+1;

%% Close file at end of creator

fclose(FID1);

```

code/thickness.m

```

function [bctthick, ccmidthick, obtthick, mcmidthick, scmidthick, tofmidthick, bofmidthick, rbmidthick, tfmidthick, scmidthickextra] = thickness(strucdens)

% Function calculates unknown thicknesses bases on geometry and total
% mass taken from structural drawings. Stiffeners and other internal
% details is smeared over thickness.

dens = strucdens; % [kg/m3]

% Buoyancy center tank
bctoutdia = 17; % [m]
bctlen = 7; % [m]
bctmass = 397228.95; % [kg]
bctinrad = sqrt(((bctoutdia/2)^2 - (bctmass/(pi*bctlen*dens)))); % [m]
bctthick = (bctoutdia/2) - bctinrad; % [m]

```

```

% Center column
ccoutdiatop = 3.58; % [m]
ccoutdiabot = 3.56; % [m]
cctopthick = 0.04; % [m]
cctoplen = 37/10; % [m]
cctopmass = masscalc(ccoutdiatop, cctopthick, cctoplen); % [kg]
ccrestmass = masscalc(ccoutdiabot, 0.03, 31.8)+masscalc(ccoutdiatop, 0.04, 5)+5300-
    cctopmass; % [kg]
ccrestlen = 37-cctoplen; % [m]
cmidthick = (ccoutdiabot-(ccoutdiabot^2-(ccrestmass*4/(pi*ccrestlen*dens)))^0.5)/2;

% Outer ballast tank
syms t
r1 = 12/2; % [m]
r2 = 3.5/2; % [m]
r3(t) = r1-t; % [m]
r4(t) = r2-t; % [m]
h1 = 7; % [m]
h2 = 6; % [m]
v1 = pi*(r1^2-r3^2)*h1; % [m3]
v2 = (1/3)*pi*(r1^2+(r1*r2)+r2^2)*h2; % [m3]
v3 = (1/3)*pi*(r3^2+(r3*r4)+r4^2)*h2; % [m3]
vtot = v1+v2-v3; % [m3]
mass = 199393.56; % [kg]
eqn = vtot*dens == mass; % [kg]
solt = vpasolve(eqn, t);
obtthick = solt(1);

% Main columns
mcoutdiatop = 3.58; % [m]
mcoutdiamid = 3.56; % [m]
mcbtthick = 0.04; % [m]
mcbtlen = 33/10; % [m]
mcovpontlen = 3; % [m]
mcbtmass = masscalc(mcoutdiatop, mcbtthick, mcbtlen)*2; % [kg]
mcovpontmass = masscalc(mcoutdiatop, mcbtthick, mcovpontlen); % [kg]
mcrestmass = masscalc(3.58, 0.04, 5.18+7)+masscalc(3.56, 0.03, 12+10)+masscalc
    (3.57, 0.033, 3)+(883+883+442+1325)-(mcbtmass)-mcovpontmass; % [kg]
mcrestlen = 33-(2*mcbtlen); % [m]
mcmidthick = (mcoutdiamid-(mcoutdiamid^2-(mcrestmass*4/(pi*mcrestlen*dens)))^0.5)/2;

% Secondary columns
scoutdiatop = 2.83; % [m]
scoutdiamid = 2.80; % [m]
scbtthick = 0.04; % [m]
scbtlen = 33/10; % [m]
scbtmass = masscalc(scoutdiatop, scbtthick, scbtlen)*2; % [kg]
screstmass = masscalc(scoutdiatop, 0.023, 25)+masscalc(scoutdiatop, 0.04, 5.18+5.05)
    +(333+333+2668)-(scbtmass); % [kg]
screstlen = 33-(2*scbtlen); % [m]
scmidthick = (scoutdiamid-(scoutdiamid^2-(screstmass*4/(pi*screstlen*dens)))^0.5)/2;

% Top of outer framework
tofdiaside = 2.33; % [m]
tofdiamid = 2.29; % [m]
toftthick = 0.04; % [m]
toflen = (2*14.235)/10; % [m]
tofmass = masscalc(tofdiaside, toftthick, toflen)*2; % [kg]
tofreftmass = masscalc(2.33, 0.04, 6)+masscalc(2.29, 0.019, 19.35)+(1568)-tofmass; % [kg]
tofreftlen = (2*14.235)-(2*toflen); % [m]
tofmidthick = (tofdiamid-(tofdiamid^2-(tofreftmass*4/(pi*tofreftlen*dens)))^0.5)/2;

% Bottom of outer framework
bofdia = 2.049; % [m]
bofthick = 0.025; % [m]

```

```

bofrestmass = masscalc(bofdia ,bofthick ,25.35)+2027; % [kg]
bofrestlen = (2*14.235); % [m]
bofmidthick = (bofdia-(bofdia^2-(bofrestmass*4/(pi*bofrestlen*dens)))^0.5)/2;

% Radial bottom structure
rbdia = 1.75; % [m]
rbthick = 0.024; % [m]
rbrestmass = masscalc(rbdia ,rbthick ,50)+2740; % [kg]
rbrestlen = sqrt(55^2+7^2); % [m]
rbmidthick = (rbdia-(rbdia^2-(rbrestmass*4/(pi*rbrestlen*dens)))^0.5)/2;

% Top framework
tfdiaside = 2.08; % [m]
tfdiamid = 2.05; % [m]
tfthick = 0.04; % [m]
tflen = 55/10; % [m]
tfmass = masscalc(tfdiaside ,tfthick ,tflen)*2; % [kg]
tfrestmass = masscalc(2.08,0.04,1.75+1.75)+masscalc(2.04,0.02,18.94+18.06)+masscalc
(2.05,0.025,3+2+2)+masscalc(2.06,0.028,4)+(1351+225+225+225+1351+451)-tfmass; %
[kg]
tfrestlen = 55-(2*tflen); % [m]
tfmidthick = (tfdiamid-(tfdiamid^2-(tfrestmass*4/(pi*tfrestlen*dens)))^0.5)/2;

% Secondary column C11
scmidthickextra = scmidthick; % [m]

end

```

code/masscalc.m

```

function [partmass] = masscalc(diameter ,thickness ,length)
% Calculates the mass of a pipe

densitypipe = 7850;

partmass = pi/4*(diameter^2-(diameter-(2*thickness))^2)*length*densitypipe;

end

```

code/model.fem

```

NODE 1 -0.000 8.500 -32.918
NODE 2 -0.425 8.386 -32.918
...
NODE 2595 19.250 33.342 6.000
NODE 2596 22.000 38.105 6.000
NODE 2597 24.750 42.868 6.000

BEAM 1 2552 2551 1 22
BEAM 2 2551 2550 1 21
...
BEAM 5437 2160 2041 2 28 24
BEAM 5438 2280 2161 2 28 24
BEAM 5439 2400 2281 2 28 24

MISOIEP 1 2.10e+11 0.30 3.55e+08 7.85e+03
MISOIEP 2 4.00e+10 0.30 3.55e+09 1.03e+03 0.001

PIPE 2 2.049 0.024
PIPE 3 2.049 0.024
...
PIPE 18 3.560 0.136 1 1 8.000
PIPE 21 3.560 0.032

```

```

PIPE 22 3.580 0.040

BOX 23 1.500 0.060 0.060 0.060 1.500

PIPE 24 2.050 0.064
PIPE 25 2.800 0.029
PIPE 28 0.150 0.074

Geometry 26 TankVert 1
Geometry 27 TankHoriz 1

GROUPDEF 1 Element
1000 1001 1002 1003
1004 1005 1006 1007
...
1076 1077 1078 1079
1080 1081 1082 1083
1084 1085 1086 1087
1088
1089
GROUPDEF 2 Element
1090 1091 1092 1093
1094 1095 1096 1097
1098 1099 1100 1101
...

GROUPDEF 51 Group 49 50
GROUPDEF 52 Geom 19 20
GROUPDEF 53 Geom 16
GROUPDEF 54 Elem 14 17 20 23 26 29

FLOODED Group 53 52

NONSTRU Geom 23

ELEMTEMP 10 1 -1.0 0.0 0.0
1000 1001 1002 1003
1004 1005 1006 1007
1008 1009 1010 1011
...

UNITVEC 1 -0.033 0.122 -0.992
UNITVEC 2 -0.089 0.089 -0.992
...
UNITVEC 22 0.966 0.259 0.0
UNITVEC 23 0.707 0.707 0.0
UNITVEC 24 0.259 0.966 0.0

Material 100 Equip 953496.0
Material 110 Equip 18600.0
Material 120 Equip 22000.0
Material 130 Equip 50000.0

Equip_1N 5440 2552 100 26
Equip_1N 5441 2554 110 26
Equip_1N 5442 2562 120 26
Equip_1N 5443 2581 130 26

NODEMASS 1321 2446.0
NODEMASS 1321 431.0
...
NODEMASS 1319 629.5
NODEMASS 1320 431.0
NODEMASS 1320 629.5

HYDROPAR CurrBlock 0.90 Group 4
HYDROPAR CurrBlock 0.90 Group 5
...

```

```

...
HYDROPAR CurrBlock 0.90 Elem 363
HYDROPAR CurrBlock 0.90 Elem 372
HYDROPAR CurrBlock 0.90 Elem 373

NODE 10001 -450.516 1000.149 -149.040 1 1 1 1 1 1
NODE 10002 -448.603 995.530 -149.048
...
NODE 11765 51.398 36.592 -41.337
NODE 11766 50.141 33.558 -37.561
NODE 11767 48.885 30.527 -33.782

BEAM 6000 10001 10002 30 30
BEAM 6001 10002 10003 30 30
...
BEAM 7757 11765 11766 40 40
BEAM 7758 11766 11767 40 40
BEAM 7759 11767 2536 40 40

SPRNG2GR 8000 10001 50
SPRNG2GR 8001 10002 50
...
SPRNG2GR 9445 11726 50
SPRNG2GR 9446 11727 50
SPRNG2GR 9447 11728 50

HYPELAST 51
-1.00e+06 -3.12
-2.00e+05 -2.12
-1.00e+05 -1.12
0 -0.12
0 0.00
0 10.00
0 20.00
MREF 201 0 0 51 0 0 0
HYPELAST 52
-1.00e+06 -3.49
-2.00e+05 -2.49
-1.00e+05 -1.49
...
MREF 219 0 0 69 0 0 0

SPRNG2GR 9448 10182 201
SPRNG2GR 9449 10183 202
...
SPRNG2GR 9597 11745 217
SPRNG2GR 9598 11746 218
SPRNG2GR 9599 11747 219

MISOIEP 30 5.60e+10 0.30 5.80e+08 1.31e+04
MISOIEP 40 1.17e+10 0.30 4.04e+08 1.22e+03

MATERIAL 50 Fric Comp 0.70 1.00e+05 12 3

PIPE 30 0.124 0.061
PIPE 40 0.160 0.079

GRAVITY 1 0 0 -9.81

GROUPDEF 55 Mat 1
GROUPDEF 56 Mat 30
GROUPDEF 57 Mat 40

```

F.2 Scripted Analysis

To utilize the full computational power, several analyses is run on different threads at the same time. A bash-script¹ has been constructed for this purpose. The script is heavily based on the code written by Strandenes [56], with a few minor alterations and additional modules. Source codes is given below accompanied by **Fig. F.13** and **F.14** for respectively ULS and FLS.

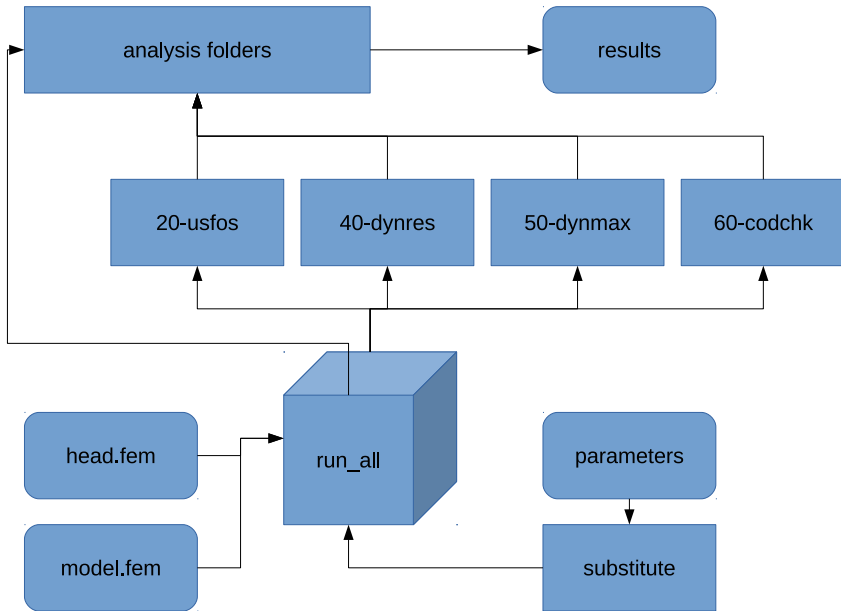


Figure F.13: A schematic flowchart of the bash-script used to run several ULS analyses on all threads available, the numbers before the modules assigns the sequence in which the modules is run.

ULS input

code/ulshead.fem

| code/ulshead.fem | | | | | |
|------------------|-------------------------------|-------|---------|-------|-----------------------------|
| HEAD | OCEAN FARMING RIGID FISH FARM | | | | |
| | TIME DOMAIN ANALYSIS | | | | |
| | P.T.B., P.A.F. – NTNU | | | | |
| | DataTyp | Value | ListTyp | ID's | |
| | HydroPar | Cm | 1.2 | All | ! Cm for all elements |
| | HydroPar | Cd | 1.05 | Group | ! Set Cd for all structural |
| | Elements | | | | |

¹born-again shell

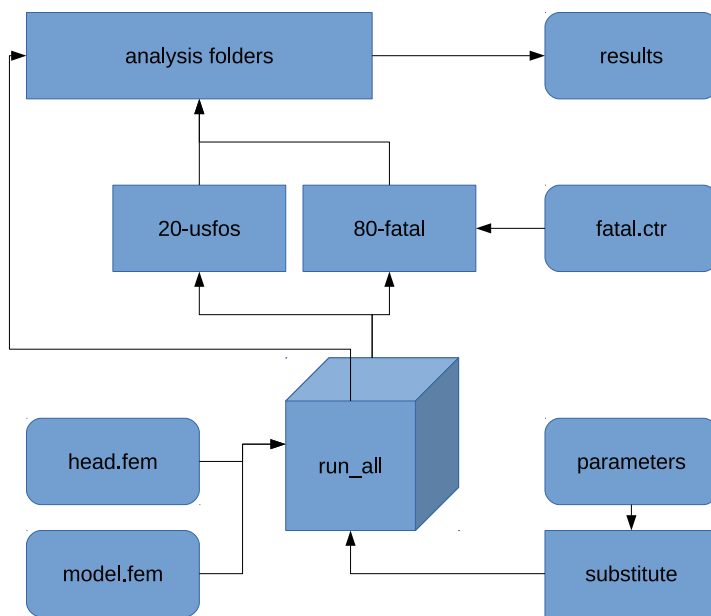


Figure F.14: A schematic flowchart of the bash-script used to run several FLS analyses on all threads available.

```

HydroPar Cd 2.4 Group 56 ! Set Cd for chain mooring
line parts
HydroPar Cd 1.6 Group 57 ! Set Cd for fibre mooring
line parts
HydroPar DirDepSW 1 Group 49 50 ! Specify DirDep for net
elements
HydroPar WaveInt 10 Group 55 51 ! Set number of IntP for
structure and net
HydroPar WaveInt 5 Group 56 57 ! Set number of IntP for
mooring lines
HydroPar WaveInt 20 Element 13 27 24 21 18 15 30 ! Set number of IntP
for all partly flooded members
HYDROPAR SlamCalc ON All
HYDROPAR Rel.Acc ON All
HYDROPAR Hydiam 0.0025 GROUP 49 50
HYDROPAR FillRatio 0.528 Elem 13 ! Centre pontoon
HYDROPAR FillRatio 0.598 Elem 27 24 21 ! C2, C4, C6 (cone part of side
pontoons)
HYDROPAR FillRatio 0.617 Elem 18 ! C8 (cone part of side pontoons)
HYDROPAR FillRatio 0.535 Elem 15 ! C10 (cone part of side pontoons)
HYDROPAR FillRatio 0.535 Elem 30 ! C12 (cone part of side pontoons)
,
,
--- Define General Coefficients ---
,
,
,
W_Coeffs ID typ alfa Cd
60 Drag -180 21.0763 ! Cd Bottom net elements

```

```

-165 42.0955
-150 61.6823
-135 78.5018
-120 91.4079
-105 99.5210
-90 102.2882
-75 99.5210
-60 91.4079
-45 78.5018
-30 61.6823
-15 42.0955
0 21.0763
15 42.0955
30 61.6823
45 78.5018
60 91.4079
75 99.5210
90 102.2882
105 99.5210
120 91.4079
135 78.5018
150 61.6823
165 42.0955
180 21.0763
,
*
W_Coeffs ID typ alfa Cd ! Cd Side net elements
61 Drag -180 26.6667
-165 53.2611
-150 78.0431
-135 99.3240
-120 115.6533
-105 125.9184
-90 129.4196
-75 125.9184
-60 115.6533
-45 99.3240
-30 78.0431
-15 53.2611
0 26.6667
15 53.2611
30 78.0431
45 99.3240
60 115.6533
75 125.9184
90 129.4196
105 125.9184
120 115.6533
135 99.3240
150 78.0431
165 53.2611
180 26.6667
,
,
----- Combine Drag/ Lift coeffs -----
,
,
W_Coeffs 1 Combine 60 ! Drag only
W_Coeffs 2 Combine 61 ! Drag only
,
,
----- Assign to Elements (through Group ID's) -----
,
,
Coeff ID List Type ID's
ElmCoeff 1 Group 49 ! Group 1 Elements gets actual Coeffs.
ElmCoeff 2 Group 50 ! Group 1 Elements gets actual Coeffs.
,
----- Analysis -----
,

```



```

'      ID Typ t1 f1 t2 f2 .....
TimeHist 102 points 0.0 10.0 15.0 10.0 20.0 1.0 3600.0 1.0      ! Initially
      increased damping
'
'      Damp ID      Type      Alpha 1  Alpha 2
' DampData      110      Rayl_All      0.12  1.24
DampData      111      Rayl_All      0.006  0.019      ! Damping for
      mooring lines
'
'      Damp ID
' ElemDamp      110      Mat      30
ElemDamp      111      Mat      40 30
'
CONSIMAS
' LumpMass 0.1
'
LITER
'      Type
Dynres_G      WaveElev
'
'      Type      Node_ID Dof      [Node_2 Dof_2]
DYNRES_N      Disp      2547  1
DYNRES_N      Disp      2547  2
DYNRES_N      Disp      2547  3
DYNRES_N      Disp      2547  4
DYNRES_N      Disp      2547  5
DYNRES_N      Disp      2547  6
'
'      ncnods
CNODES      1
'      nodex      idof      dfact
      2547      3      1.
'
' _____ E O F _____

```

code/ulsparam.txt

```

ORDR      SEED
1.00      9.00
1.00      18.00
...
1.00      351.00
1.00      360.00
2.00      9.00
2.00      18.00
...
2.00      351.00
2.00      360.00
3.00      9.00
3.00      18.00
...
3.00      351.00
3.00      360.00

```

FLS input

code/flshead.fem

```

HEAD      OCEAN FARMING RIGID FISH FARM
          TIME DOMAIN ANALYSIS
          P.T.B., P.A.F. — NTNU

```



```

,          DataType      Value  ListTyp  ID's
HydroPar   Cm          2.0     Group    55      ! Cm for all structural
elements
HydroPar   Cm          1.2     Group   56 57    ! Cm for all mooring and net
elements
HydroPar   Cd          0.8     Group    55      ! Set Cd for all structural
Elements
...
%-----%
%          ABRIDGED          %
%-----%
...
,
,          Type      Node.ID  Dof      [Node.2  Dof.2]
DYNRES_N    Disp      2547     1
DYNRES_N    Disp      2547     2
DYNRES_N    Disp      2547     3
DYNRES_N    Disp      2547     4
DYNRES_N    Disp      2547     5
DYNRES_N    Disp      2547     6
,
,          ncnods
CNODES      1
,          nodex      idof      dfact
,          2547      3         1.
,
FATIGUE      1      Joint      1221 1241 1261 1281 1301 1201 2541
,
_____      E O F      _____

```

code/flsparam.txt

| HEIGH | PERIO | PGAMM |
|-------|-------|-------|
| 0.50 | 3.50 | 3.3 |
| 0.50 | 8.80 | 1.0 |
| 0.50 | 13.3 | 1.0 |
| 1.00 | 4.00 | 3.3 |
| 1.00 | 8.80 | 1.0 |
| 1.00 | 13.2 | 1.0 |
| 1.50 | 5.10 | 3.3 |
| 1.50 | 9.20 | 1.0 |
| 1.50 | 13.5 | 1.0 |
| 2.00 | 5.30 | 3.3 |
| 2.00 | 8.60 | 1.0 |
| 2.50 | 5.90 | 3.3 |
| 2.50 | 7.90 | 3.3 |
| 3.00 | 6.80 | 3.3 |
| 3.67 | 7.30 | 3.3 |

code/fatal.ctr

```

HEAD _____
HEAD  ——— RIGID OFFSHORE FISH-FARM
HEAD _____
,
SkipStep  10
# ClockPos 44
,
,          JointID      D      T      .. Default ..
# ChordGeo      2      1.00  0.030  ! 1.000 0.020
,
,          JointID      BraceID      d      t      .. Default ..

```

```

# BraceGeo      2          3          0.500  0.025      !  0.500  0.015
,
JntClass      1
,
SCF      Print
,
SCF      All          JointID  BraceID  Scf_Ax_S  Scf_Ax_C  Scf_Mip_C  Scf_Mop_S
,
,
,
SN_Curve      Curve Definition          Specified
NORSOK T      SEA.CAT                    All
,
_____ E O F _____

```

Script modules

code/run_all.txt

```

#!/bin/bash
#
# Script that controls the execution of one or more analyses
# with parameter variation. The script calls different modules,
# each module doing it's own task.
#
# The file containing the parameters that are going to be substituted
# into the different data files are defined in the beginning of this
# script. The default (and recommended) filename is './input/parameters'
#
# This file is organized as a table, where the first line is a header
# line, one header per column. No spaces are allowed in the header. The
# column headers are the keys to look for in the files passed through the
# substitution process. The rest of the lines define each combination
# of parameters that is going to be executed, one execution per line.
#
# If your computer has more than one processor core, the analysis
# part will be run in parallel. The number of parallel processes
# is automatically determined, but can be overridden by setting the
# THREADS variable to the number of parallel threads. If this value is
# set to 0 or a negative value, the number of threads will default to
# the maximum possible number.
#
# Written by H. Strandenes, hakostra@stud.ntnu.no, 2011–2012.
#
# This file is licensed under the GNU General Public License,
# version 3, or later. Please see file LICENSE for details.
#

# _____ PARAMETERS _____ #
INPUTFILE="./input/parameters"      # The file containing the parameter data
THREADS=0                            # The number of parallel threads (0=auto)
# _____ #

# Define a function used to initialize modules
function initialize {
# Run all all scripts
for MOD in ./modules/*
do
if [ -f $MOD -a -x $MOD ]; then
$MOD init >> ./logs/init.log
fi
done

```

```

}

# Define function used to find what files that is going through substitution
function findfiles {
# Run all all scripts
for MOD in ./modules/*
do
if [ -f $MOD -a -x $MOD ]; then
$MOD files $1 | grep -v '^$' # The grep command is to remove empty lines
fi
done
}

# Do the postprocessing
function postp {
# Go through all scripts
for MOD in ./modules/*
do
if [ -f $MOD -a -x $MOD ]; then
$MOD postp2 >> ./logs/postp2.log
fi
done
}

# Make a folder for the contents of the terminal logs
if [ ! -d logs ]; then
mkdir logs
else
rm logs/*.log
fi

# Do the initialization
echo -n "Initializing folders..."
initialize

echo "Done."
echo -n "Assembling input files..."

# Reads the first line of the input file to get the column headers
read -r FIRSTLINE < $INPUTFILE

# Finds the number of columns
FIELDS='echo $FIRSTLINE | awk '{ print NF }''

# Make an array with the column/field names
for i in `seq 1 $FIELDS`
do
FIELD[$i]='echo $FIRSTLINE | awk '{ print $c }' c=$i'
done

# Reads the parameter file line by line
LINE=0
COMMAND=""
while read INPUTLINE
do
# Do not process the first line
LINE='expr $LINE + 1'
if [ $LINE -eq 1 ]; then
continue
fi

# Construct the case name/filename

```

```

CASENAME=""
for i in `seq 1 $FIELDS`
do
    VALUE=`echo $INPUTLINE | awk '{ print $c }' c=$i`
    CASENAME="$CASENAME"-${FIELD[$i]:0:2}=$VALUE"
done
CASENAME=${CASENAME:1}

# Do the substitution process for all files returned by the modules
while read INPOUT
do
    # If empty string, continue loop
    if [ ${#INPOUT} -lt 3 ]; then
        continue
    fi

    # Define file names
    INPUT=`echo -n $INPOUT | awk '{ print $1; }'`
    OUTPUT=`echo -n $INPOUT | awk '{ print $2; }'`

    # Create folder for output file if it not exist
    OUTDIR=`dirname $OUTPUT`
    if [ ! -d $OUTDIR ]; then
        mkdir $OUTDIR
    fi

    # Copy original file to destination
    cp $INPUT $OUTPUT

    # Substitution process for each field
    for i in `seq 1 $FIELDS`
    do
        VALUE=`echo $INPUTLINE | awk '{ print $c }' c=$i`

        # Substitute in header and model file
        ./substitute ${FIELD[$i]} $VALUE $OUTPUT
    done
done <<< "`findfiles $CASENAME`"

# Putting the job in the command string
COMMAND="$COMMAND}${CASENAME}\0"
done < "${INPUTFILE}"

# Find the number of threads your computer can run
if [ $THREADS -lt 1 ]; then
    THREADS=`cat /proc/cpuinfo | grep processor | wc -l`
fi

# Executing the commands in parallel
echo "Done."
echo "Running multiple analyses with $THREADS threads in parallel..."
echo -e $COMMAND | xargs -0 -n 1 -P $THREADS ./runone analyze

# Running postprocessing
echo "Parallel processing done."
echo "Running postprocessing tasks..."

# No parallel run of postprocessing
echo -e $COMMAND | xargs -0 -n 1 -P 1 ./runone postp1

# Final postprocessing
echo -n "Running final postprocessing..."
postp

```

```
echo "Done."
echo "Finished!"
```

code/substitute.txt

```
#!/bin/bash

sed "1,$ s/$1/$2/g" $3 > subst_string.temp
mv subst_string.temp $3
```

code/20-usfos.txt

```
#!/bin/bash
#
# Script that executes Usfos. The execution is divided into parts:
# - Initialization: Folder for analysis files are created
# - Files to pass through substitution: head.fem, model.fem, and fatal.ctr
# - Analysis: USFOS is run in the case subfolder
# - Postprocessing: Nothing special at the moment
#
# This script takes one or two arguments. The first is the task to do
# (must always be present), the second is the case name/description.
# This can (and will) be omitted for the initialization and postprocessing
# tasks.
#
# The action argument can be one of the following:
# - init      (no name/description required)
# - files     (require case name as second argument)
# - analyze   (require case name as second argument)
# - postpl    (require case name as second argument)
# - postp2    (no name/description required)
#
# Written by H. Strandenes, hakostra@stud.ntnu.no, 2011–2012.
# Modified by P.A. Fossan, palalexa@stud.ntnu.no, 2014–2015.
#
# This file is licensed under the GNU General Public License,
# version 3, or later. Please see file LICENSE for details.
#

# Define the input variables
if [ $# -eq 1 ]; then
    ACTION=$1
elif [ $# -eq 2 ]; then
    ACTION=$1
    CASENAME=$2
else
    echo "20-usfos: Invalid number of argumens supplied."
    exit
fi

# The initialization
if [ $ACTION == "init" ]; then
    # Make a folder for USFOS analysis files
    echo "20-usfos: Creating analysis folders."
    if [ ! -d analysis ]; then
        mkdir analysis
    fi

# Return the files to look for substitutions in
elif [ $ACTION == "files" -a $# -eq 2 ]; then
    echo "input/head.fem analysis/$CASENAME/head.fem"
    echo "input/model.fem analysis/$CASENAME/model.fem"
```

```

echo "input/fatal.ctr analysis/$CASENAME/fatal.ctr"

# Do the individual analyzes
elif [ $ACTION == "analyze" -a $# -eq 2 ]; then
    echo "20-usfos: Running analysis in USFOS."

    # Go to analysis folder
    cd ./analysis/$CASENAME

    # Run the USFOS program
    usfos <<EndIn
    head
    model

    result
    EndIn

    # Return to base folder (previous folder)
    cd -

# Do postprocessing after individual run (for example to extract results)
elif [ $ACTION == "postp1" -a $# -eq 2 ]; then
    echo "20-usfos: No postprocessing tasks done."
    exit

# Do postprocessing after all individual runs (for example to do statistics)
elif [ $ACTION == "postp2" ]; then
    echo "20-usfos: No postprocessing tasks done."
    exit

# Else, do nothing
else
    echo "20-usfos: Invalid action argument supplied, or missing case name."
    exit
fi

```

code/40-dynres.txt

```

...
% ABRIDGED %
...

# Run dynres on the USFOS uoutput
dynres <<EndIn
result
2
1
1
1
history
0
0
EndIn

# Return to base folder (previous folder)
cd -

...
% ABRIDGED %
% ABRIDGED %

```

...

code/50-dynmax.txt

```
...
%*****%
%      ABRIDGED      %
%*****%
...

# Run dynmax on the USFOS uoutput
dynmax <<EndIn
1
0
result.dyn
dynmax

1
0
EndIn

# Return to base folder (previous folder)
cd -

...
%*****%
%      ABRIDGED      %
%*****%
...
```

code/60-codchk.txt

```
...
%*****%
%      ABRIDGED      %
%*****%
...

# Run codchk on the USFOS uoutput
codchk <<EndIn
result
codecheck
100
5000
0.2
202
N
0.8
1.2
Yes
1.0
EndIn

# Delete .raf file for storage purposes
# rm result.raf

# Return to base folder (previous folder)
cd -

...
%*****%
%      ABRIDGED      %
%*****%
...
```

code/80-fatal.txt

```
...
%%%%%%%%%%%%%%%%%%%%%%%%%%%%%%%%%%%%%%%%%%%%%%%%%%%%%%%%%%%%%%%%%%%%%%%%
%          ABRIDGED          %
%%%%%%%%%%%%%%%%%%%%%%%%%%%%%%%%%%%%%%%%%%%%%%%%%%%%%%%%%%%%%%%%%%%%%%%%
...

# Run fatal on the USFOS uoutput
fatal <<EndIn
result
fatal.ctr

fatigue
EndIn

# Return to base folder (previous folder)
cd -

...
%%%%%%%%%%%%%%%%%%%%%%%%%%%%%%%%%%%%%%%%%%%%%%%%%%%%%%%%%%%%%%%%%%%%%%%%
%          ABRIDGED          %
%%%%%%%%%%%%%%%%%%%%%%%%%%%%%%%%%%%%%%%%%%%%%%%%%%%%%%%%%%%%%%%%%%%%%%%%
...

```

F.3 Post-Processing

Each analysis produces result-files in their respective folders. A simple but repetitive scripting technique is therefore used to gather all these and extract the wanted results. The summarized results is then written for further post-processing. The title of the script are listed above the code segment and should be descriptive enough to explain the purpose. The codes are heavily abridged due to the fact that they are repetitive, it should thus be easy to recognize the pattern.

Ultimate limit state

ULSpostAPI.m reads the most utilized member in each analysis and collects these for each direction. The script writes result-files for each direction to be further processed. ULSpostELEM.m simply lists the ten most utilized members for all directions.

code/ULSpostAPI.m

```
close all
clear all
clc

tic

%% Direction = 270

disp(_____);
disp('Processing direction = 270');

% Read from several api-results in subfolders
cd('ULS270Run/analysis ');
apimat = zeros(120,4);

```



```

count = 1;
for i = 1:3
    for j = 9:9:360
        foldername = ['OR=', num2str(i), '.00_SE=', num2str(j), '.00'];
        cd(foldername);
        file1 = fopen('apicheck ');
        for k = 1:42
            line = fgetl(file1);
        end
        resrow = textscan(line, '%f');
        numbers = [resrow{:}, 1];
        element = numbers(1);
        if element >= 1000
            line = fgetl(file9);
            resrow = textscan(line, '%f');
        end
        numbers = [resrow{:}, 1];
        element = numbers(1);
        utilization = numbers(2);
        fclose(file1);
        apimat(count, 1) = i;
        apimat(count, 2) = j;
        apimat(count, 3) = element;
        apimat(count, 4) = utilization;
        count = count+1;
        cd('../');
    end
end
cd('../');

% Check what order maximum lies within
apimat1ord = apimat(1:40,:);
apimat2ord = apimat(41:80,:);
apimat3ord = apimat(81:120,:);
apimat270complete = apimat1ord;
for i = 1:40
    if apimat1ord(i,4) < apimat2ord(i,4)
        apimat270complete(i,:) = apimat2ord(i,:);
        disp('2. order larger than 1. order for seed');
        disp(apimat1ord(i,2));
    elseif apimat1ord(i,4) < apimat3ord(i,4)
        apimat270complete(i,:) = apimat3ord(i,:);
        disp('3. order larger than 1. order for seed');
        disp(apimat1ord(i,2));
    elseif apimat2ord(i,4) < apimat3ord(i,4)
        disp('3. order larger than 2. order for seed');
        disp(apimat1ord(i,2));
    end
end

% Write summary to single file
file2 = fopen('270api', 'w');
fprintf(file2, '%8s %8s %8s %8s\n', 'ORDR', 'SEED', 'ELEM', 'UTIL');
for i = 1:40
    fprintf(file2, '%8d %8d %8d %8d\n', apimat270complete(i,:));
end
fclose(file2);

disp('Finished with direction = 270');

%% Direction = 285

disp(_____')
disp('Processing direction = 285');

% Read from several api-results in subfolders
cd('ULS285Run/analysis ');

```

```

...
%  

%  

%  

...
%%  

disp(_____)
toc

```

code/ULSpstELEM.m

```

close all
clear all
clc

tic
totmat = zeros(10,14);

%% Direction = 270

disp(_____)
disp('Processing direction = 270');

% Read from several api-results in subfolders

cd('ULS270Run/analysis ');
elemmat = [];
count = 1;
for i = 1:3
    for j = 9:9:360
        foldername = ['OR=', num2str(i), '.00_SE=', num2str(j), '.00'];
        cd(foldername);
        file = fopen('fort.88');
        for k = 1:10
            line = fgetl(file);

        end
        for m = 1:10
            line2 = fgetl(file);
            dummy = textscan(line2, '%f');
            dummy2 = [dummy{:}, 1];
            element = dummy2(1);
            if element >= 1000
                line2 = fgetl(file);
                dummy = textscan(line2, '%f');
            end
            dummy2 = [dummy{:}, 1];
            element = dummy2(1);
            utiliza = dummy2(2);
            elemmat(count,1) = element;
            elemmat(count,2) = utiliza;
            count = count+1;
        end
        fclose(file);
        cd(' ../ ');
    end
end
cd(' ../ ');

sorted = sortrows(unique(elemmat, 'rows'), 2);
[a,b] = size(sorted);
cutoff = sorted(a-9:a,:);
totmat(:,1:2) = cutoff;

disp('Finished with direction = 270');

```

```

%% Direction = 285

disp('-----')
disp('Processing direction = 285');

% Read from several api-results in subfolders

cd('ULS285Run/analysis ');

...
%%%%%%%%%%%%%%%%%%%%%%%%%%%%%%%%%%%%%%%%%%%%%%%%%%%%%%%%%%%%%%%%%%%%%%%%%%%%%%
% ABRIDGED %
%%%%%%%%%%%%%%%%%%%%%%%%%%%%%%%%%%%%%%%%%%%%%%%%%%%%%%%%%%%%%%%%%%%%%%%%%%%%%%
...

%% Write to file

file = fopen('elemlist','w');
fprintf(file,'%10s %10s %10s %10s %10s %10s %10s %10s %10s %10s %10s %10s %10s\n',
        '270ELEM','270UTIL','285ELEM','285UTIL','300ELEM','300UTIL','315ELEM','315UTIL',
        '330ELEM','330UTIL','345ELEM','345UTIL','360ELEM','360UTIL');
for i = 10:-1:1
    fprintf(file,'%10d %10.2f %10d %10.2f %10d %10.2f %10d %10.2f %10d %10.2f %10d',
            totmat(i,:));
end
fclose(file);

elemlist = zeros(70,1);
elemlist(1:10) = totmat(:,1);
elemlist(11:20) = totmat(:,3);
elemlist(21:30) = totmat(:,5);
elemlist(31:40) = totmat(:,7);
elemlist(41:50) = totmat(:,9);
elemlist(51:60) = totmat(:,11);
elemlist(61:70) = totmat(:,13);
uniquelist = unique(elemlist);

file = fopen('uniqueelements','w');
fprintf(file,'%10s\n','ELEMENT');
for i = 1:length(uniquelist)
    fprintf(file,'%10d\n',uniquelist(i));
end
fclose(file);

%%

disp('-----')
toc

```

Fatigue limit state

FLSpostpro.m gathers fatigue damage from all sea states and directions in a matrix. All individual damages are multiplied by the expected number of occurrences for the given sea states and directions. All contributions are then summed up, giving the lifetime fatigue damage at each position. The resulting matrix is then read by FLSscfmax.m which calculates what the SCF at the 4 clock-positions (brace and chord) around the intersection must be in order to accumulate to damage 1 during the lifetime.

code/FLSpostpro.m

```
close all
```

```

clear all
clc

tic

numseastates = dlmread('numseastates.txt');

%% Direction = 45

disp('-----')
disp(' Processing direction = 45');

cd('FLS45Run/analysis ');

%-----

cd('HE=0.50_PE=3.50_PG=3.3 ');
matrix1 = zeros(30,3);
count = 1;
file1 = fopen('fatigue_scf.txt');
for i = 1:6
    line = fgetl(file1);
end
for j = 1:30
    line2 = fgetl(file1);
    dummy = textscan(line2,'%d');
    dummy2 = [dummy{:},1];
    connec = dummy2(1);
    node = dummy2(2);
    brace = dummy2(3);
    matrix1(count,1) = connec;
    matrix1(count,2) = node;
    matrix1(count,3) = brace;
    count = count+1;
end
count = 1;
file2 = fopen('fatigue.dam');
for k = 1:16
    line = fgetl(file2);
end
for m = 1:30
    line2 = fgetl(file2);
    dummy = textscan(line2,'%*d %f %f %f %f %f %f %f %f');
    dummy2 = [dummy{1,:}];
    cpos1 = dummy2(1);
    cpos2 = dummy2(2);
    cpos3 = dummy2(3);
    cpos4 = dummy2(4);
    bpos1 = dummy2(5);
    bpos2 = dummy2(6);
    bpos3 = dummy2(7);
    bpos4 = dummy2(8);
    matrix1(count,4) = cpos1;
    matrix1(count,5) = cpos2;
    matrix1(count,6) = cpos3;
    matrix1(count,7) = cpos4;
    matrix1(count,8) = bpos1;
    matrix1(count,9) = bpos2;
    matrix1(count,10) = bpos3;
    matrix1(count,11) = bpos4;
    count = count+1;
end
for n = 4:11
    matrix1(:,n) = matrix1(:,n)*numseastates(1,1);
end
file3 = fopen('totalfatigue ','w');
fprintf(file3,'%8s %8s %8s %15s %15s %15s %15s %15s %15s %15s\n','CON','NODE','
BRACE','CPOS1','CPOS2','CPOS3','CPOS4','BPOS1','BPOS2','BPOS3','BPOS4');

```

```

for p = 1:30
    fprintf(file3,'%8d %8d %8d %15E %15E %15E %15E %15E %15E %15E %15E\n',matrix1(p
        ,:));
end
fclose('all');
cd('..');

%-----
cd('HE=0.50_PE=8.80_PG=1.0');
matrix2 = zeros(30,3);
count = 1;
file1 = fopen('fatigue_scf.txt');
for i = 1:6
    line = fgetl(file1);
end
for j = 1:30
    line2 = fgetl(file1);
    dummy = textscan(line2,'%d');
    dummy2 = [dummy{:},1];
    connec = dummy2(1);
    node = dummy2(2);
    brace = dummy2(3);
    matrix2(count,1) = connec;
    matrix2(count,2) = node;
    matrix2(count,3) = brace;
    count = count+1;
end
count = 1;
file2 = fopen('fatigue.dam');
for k = 1:16
    line = fgetl(file2);
end
for m = 1:30
    line2 = fgetl(file2);
    dummy = textscan(line2,'%*d %f %f %f %f %f %f %f %f');
    dummy2 = [dummy{1,:}];
    cpos1 = dummy2(1);
    cpos2 = dummy2(2);
    cpos3 = dummy2(3);
    cpos4 = dummy2(4);
    bpos1 = dummy2(5);
    bpos2 = dummy2(6);
    bpos3 = dummy2(7);
    bpos4 = dummy2(8);
    matrix2(count,4) = cpos1;
    matrix2(count,5) = cpos2;
    matrix2(count,6) = cpos3;
    matrix2(count,7) = cpos4;
    matrix2(count,8) = bpos1;
    matrix2(count,9) = bpos2;
    matrix2(count,10) = bpos3;
    matrix2(count,11) = bpos4;
    count = count+1;
end
for n = 4:11
    matrix2(:,n) = matrix2(:,n)*numseastates(2,1);
end
file3 = fopen('totalfatigue','w');
fprintf(file3,'%8s %8s %8s %15s %15s %15s %15s %15s %15s %15s\n','CON','NODE','
    BRACE','CPOS1','CPOS2','CPOS3','CPOS4','BPOS1','BPOS2','BPOS3','BPOS4');
for p = 1:30
    fprintf(file3,'%8d %8d %8d %15E %15E %15E %15E %15E %15E %15E %15E\n',matrix2(p
        ,:));
end
fclose('all');
cd('..');

```

```

%-----
cd('HE=0.50_PE=13.3_PG=1.0');
matrix3 = zeros(30,3);

...
%%%%%%%%%%%%%%%%%%%%%%%%%%%%%%%%%%%%%%%%%%%%%%%%%%%%%%%%%%%%%%%%%%%%%%%%
%           ABRIDGED                               %
%%%%%%%%%%%%%%%%%%%%%%%%%%%%%%%%%%%%%%%%%%%%%%%%%%%%%%%%%%%%%%%%%%%%%%%%
...

%% Write summary to file

totalfatigue = matrix45;
totalfatigue(:,4:11) = matrix45(:,4:11)+matrix90(:,4:11)+matrix135(:,4:11)+matrix180
(:,4:11)+matrix225(:,4:11)+matrix270(:,4:11)+matrix315(:,4:11)+matrix360(:,4:11)
;

file1 = fopen('totfatiguedamage','w');
fprintf(file1,'%154s\n','TOTAL FATIGUE DAMAGE');
fprintf(file1,'%144s\n','-----');
fprintf(file1,'%8s %8s %8s %15s %15s %15s %15s %15s %15s %15s\n','CON','NODE','
BRACE','CPOS1','CPOS2','CPOS3','CPOS4','BPOS1','BPOS2','BPOS3','BPOS4');
for p = 1:30
    fprintf(file1,'%8d %8d %8d %15f %15f %15f %15f %15f %15f %15f %15f\n',
        totalfatigue(p,:));
end
fprintf(file1,'%144s\n','-----');
fprintf(file1,'%154s\n','DIRECTION 45');
fprintf(file1,'%144s\n','-----');
fprintf(file1,'%8s %8s %8s %15s %15s %15s %15s %15s %15s %15s\n','CON','NODE','
BRACE','CPOS1','CPOS2','CPOS3','CPOS4','BPOS1','BPOS2','BPOS3','BPOS4');
for p = 1:30
    fprintf(file1,'%8d %8d %8d %15f %15f %15f %15f %15f %15f %15f %15f\n',matrix45(p
,:));
end

...
%%%%%%%%%%%%%%%%%%%%%%%%%%%%%%%%%%%%%%%%%%%%%%%%%%%%%%%%%%%%%%%%%%%%%%%%
%           ABRIDGED                               %
%%%%%%%%%%%%%%%%%%%%%%%%%%%%%%%%%%%%%%%%%%%%%%%%%%%%%%%%%%%%%%%%%%%%%%%%
...

fclose('all');

save totmatrix.mat totalfatigue

disp(-----)
onlydam = totalfatigue(:,4:11);
[val,loc] = max(onlydam(:));
disp('Maximum value is')
disp(val)
disp(-----)
toc

```

code/FLSscfmax.m

```

close all
clear all
clc

load totmatrix.mat totalfatigue
[m,n] = size(totalfatigue);
scfmatrix = totalfatigue;

for i = 1:m
    for j = 4:n

```

```

        scfmatrix(i,j) = (1/scfmatrix(i,j))^(1/5);
    end
end

file = fopen('maximumscf','w');
fprintf(file,'%154s\n','MAXIMUM SCF');
fprintf(file,'%144s\n';
fprintf(file,'%8s %8s %8s %15s %15s %15s %15s %15s %15s %15s %15s\n','CON','NODE','
    BRACE','CPOS1','CPOS2','CPOS3','CPOS4','BPOS1','BPOS2','BPOS3','BPOS4');
for k = 1:30
    fprintf(file,'%8d %8d %8d %15.2f %15.2f %15.2f %15.2f %15.2f %15.2f %15.2f\n',scfmatrix(k,:));
end
fclose('all');

onlyscf = scfmatrix(:,4:11);
[val,loc] = max(onlyscf(:));
disp('Maximum value is ')
disp(val)
disp('-----')
[val,loc] = min(onlyscf(:));
disp('Minimum value is ')
disp(val)

```

- EOF -
